INVESTIGATIONS ON CARBON COMPOSITE FOAMS FROM BIOMASS BY FILTER-PRESSING FOR THERMAL INSULATION AND EMI SHIELDING APPLICATIONS

A Thesis submitted
in partial fulfillment for the Degree of

Doctor of Philosophy

by

CHITHRA A

SC16 D044

DEPARTMENT OF CHEMISTRY
INDIAN INSTITUTE OF SPACE SCIENCE AND TECHNOLOGY
THIRUVANANTHAPURAM
February 2022

Dedicated to my beloved father, mother, sister, brother,

husband, daughter, and teachers……………

सत्यमेव जयते

भारतीय अंतरिक्ष विज्ञान एवं प्रौद्योगिकी संस्थान
(वि.अ.आयोग अधिनियम 1956 की धारा-3 के अधीन मानित विश्वविद्यालय घोषित)
भारत सरकार, अंतरिक्ष विभाग, वलियमला पोस्ट, तिरुवनंतपुरम 695 547 भारत

INDIAN INSTITUTE OF SPACE SCIENCE AND TECHNOLOGY
(A Deemed to be University u/s 3 of the UGC Act, 1956)
Government of India, Department of Space
Valiamala P. O, Thiruvananthapuram 695 547 India

www.iist.ac.in

CERTIFICATE

This is to certify that the thesis entitled '**Investigations on carbon composite foams from biomass by filter-pressing for thermal insulation and EMI shielding applications**', submitted by Chithra A to the Indian Institute of Space Science and Technology, Thiruvananthapuram, in partial fullfilment for the award of the degree of Doctor of Philosophy, is a *bona fide* record of research work carried out by her under our supervision. The contents of this thesis, in full or in parts, have not been submitted to any other Institution or University for the award of any degree or diploma.

Dr. R Rajeev
Head (Retired)
Analytical and Spectroscopy Division
Thiruvananthapuram

Dr. K Prabhakaran
Professor
Dept. of Chemistry, IIST
Thiruvananthapuram

Thiruvananthapuram
February 2022

Counter signature of HOD with seal

डॉ. संध्या के वाई / Dr. Sandhya K Y
आचार्य एवं अध्यक्ष / Professor & Head
रसायन विभाग / Department of Chemistry
भारतीय अंतरिक्ष विज्ञान एवं प्रौद्योगिकी संस्थान
Indian Institute of Space Science and Technology
अंतरिक्ष विभाग, भारत सरकार / Dept. of Space, Govt. of India
तिरुवनंतपुरम / Thiruvananthapuram - 695 547

DECLARATION

I declare that this thesis entitled **'Investigations on carbon composite foams from biomass by filter-pressing for thermal insulation and EMI shielding applications'**, submitted in partial fulfillment of the degree of **Doctor of Philosophy** is a record of original work carried out by me under the supervision of **Dr K. Prabhakaran and Dr Rajeev R** and has not formed the basis for the award of any other degree or diploma, in this or any other Institution or University. In keeping with the ethical practice in reporting scientific information, due acknowledgements have been made wherever the findings of others have been cited.

Chithra A

SC16 D044

Thiruvananthapuram

February 2022

ACKNOWLEDGEMENTS

I express my sincere gratitude to my guide, Prof. K. Prabhakaran, for allowing me to work in his group. His guidance and encouragement were the foundations of this thesis work. His wealth of knowledge, passion for research and work ethic have been sources of great inspiration to me and which I sincerely wish to emulate in my professional career. I also express heartful gratitude to my guide Dr Rajeev R, for allowing me to permit to do PhD and to work under his guidance. My research supervisors had spent enough time discussing the experiments, data analysis and paper writing and gave me a lot of suggestions and support to overcome the difficulties during my PhD tenure.

I also take this opportunity to thank S. Somanath Director, VSSC & IIST, for providing all facilities to carry out my research. I also take this opportunity to thank Dr V. K. Dadhwal, former Director, IIST, for providing all facilities to carry out my research. It is also a pleasure to extend my heartfelt gratitude to Prof. Kuruvilla Joseph, Dean (Student Activities, Student Welfare and Outreach) for his support throughout my research tenure. I am also thanks to Dr. S A Illogovan, Deputy Director of VSSC, R. Sadhana, Dr. Benny K George, Group Director, Analytical, Spectroscopy and Ceramic group of VSSC for permitting me to do part-time PhD and support during my PhD time. I am also thanks to the all members in Ceramic matrix Products Division of VSSC to give their facility to do my PhD work. I would like to thank all my doctoral committee members, Dr. U.S Hareesh (NIIST), Dr. C. Gowri (VSSC), Prof. Nirmala R. James (IIST) and Dr. K. Y. Sandhya (IIST) and Dr. Sooraj(IIST) for their valuable suggestions and encouragement in improving the quality of the thesis work. I thank the faculty members of the Department of Chemistry for their support. I thank my colleagues and section Heads, Ms. Roopa Dimple, Dr. Deepthi L Sivadas, Ms Deepthi Thomas and Dr. Vijayalekshmi K P in the Analytical and Spectroscopy Division, VSSC for encouragement and characterization support. I am grateful to the members of NIIST, SCTIMST, SAIF, Kerala University and Cochin University for helping in the characterization of my samples. I also thank Mrs. Aparna and Dr. Surendran (NIIST) for helping me with characterization. I am grateful to my friends, Dr. Sujith Vijayan, Dr. Praveen Wilson and Dr. Linsha Vazhayal for their help in my experimental work and for their fruitful discussions in writing this thesis. I am also thankful to Mr. Rakesh Krishnan P.P., Govind Kumar Sharma, Dr. R. Narasimman, and Mr. Neeraj V.S., former and current members of my group, for their support during my tenure in IIST. I thank all my fellow research scholars for their love and support. I am thankful to have received assistance from valued members of the staff, Mr. Loveson Albert, Mrs. Bindu J.M., Mrs. Jayasree R, Mrs. Jayasree L and Mrs. Bindhu P.C. I am forever thanks to parents, husband and sister for their endless love and encouragement. Words cannot express my love and affection towards my daughter for her patience through the journey of my research work. I am also thanks to my friends and colleagues, Mrs. Suchithra C, Mr. SanuVarghese, Mr. Augustus, Mrs. Kasturi K, Mr. Pramood V Bhaskar and Mrs. Jayalakeshmi Babu who have been a constant encouragement and support. I thank each and every one who helped and inspired me in the last five years.

CHITHRA A

ABSTRACT

Carbon foams are new generation materials having an interconnected three-dimensional cellular structure. They exhibit unique properties such as lightweight, tailorable thermal and electrical conductivity, high-temperature tolerance, and good sound and electromagnetic wave absorption. Hence, they have been widely used in various applications such as thermal management, fire-resistant lightweight structures, thermal protection system in aircraft, electromagnetic interference shielding for electronic and telecommunication devices, electrode in energy storage devices, acoustic damping, adsorbent for gases and toxic chemicals and substrate for catalysts. Carbon foams are generally prepared from fossil fuel-based synthetic polymers and pitches. Due to the depletion of fossil fuels and other environmental concerns, the researchers are focused on alternative precursors for carbon foams. Biomass is a good candidate raw material for valuable carbon products because it is available in large quantities at low cost, naturally renewable and environment-friendly. Biomasses such as tannin, lignin and sucrose are extensively researched for the preparation of carbon foams. However, natural cotton, sawdust, rice husk and newspaper waste are not explored for the preparation of carbon foams even though available in large quantities at a very low cost. The development of an environmentally friendly processing route for the production of carbon foam monoliths from these biomasses would not only generate wealth but also help the management of solid wastes. The main objective of this thesis is to develop an eco-friendly processing method for carbon composite foams from agricultural residues such as rice husk, sawdust, cotton and newspaper and their characterization for possible applications in high-temperature thermal insulation and EMI shielding.

A filter-pressing set was fabricated in-house from a PVC pipe, a Buchner funnel and a filter flask for consolidation of the biomasses. Cotton-sucrose composites were prepared by consolidating natural cotton fiber dispersed in aqueous sucrose solution by filter-pressing followed by freeze-drying. The caramelization of the sucrose in the cotton-sucrose composite followed by carbonization produced carbon composite foams. The XRD and Raman spectrum analysis indicated the amorphous (turbostratic graphite) nature of the carbon composite foams. The compressive strength (5 kPa to 1.4 MPa) and thermal conductivity (0.069 to 0.185 W m^{-1}K^{-1}) were depended on the foam density (0.06 to 0.31 g cm^{-3}) which was modulated by varying the sucrose solution concentration (100 to 700 g L^{-1}). The tubular carbon fiber formed from cotton was welded at their contact points by the amorphous carbon produced from sucrose leading to partial flexibility at low sucrose solution concentrations (100 & 200 g L^{-1}). The advancement of fiber- to- fiber bonding area at higher sucrose solution concentrations (300 to 700 g L^{-1}) resulted in rigid carbon composite foams. The porosity in the inter-fiber space and lumen of the carbonized cotton

fiber contributed to the low thermal conductivity. The carbon composite foams prepared at a sucrose solution concentration at 500 g L^{-1} and above were amenable to machining using conventional machines and tools. The carbon composite foams exhibited absorption dominated EMI shielding. The carbon composite foams showed EMI shielding effectiveness in the range of 21.5 to 38.9 dB.

Sawdust, a waste generated in the wood industry was used for the preparation of carbon composite foams due to its unique cellular structure. Filter-pressing of sawdust powder dispersed in sucrose solution followed by freeze-drying produced sawdust-sucrose composites in which the sawdust particles were cemented together by sucrose. The caramelization of sucrose in the sawdust-sucrose composite followed by carbonization produced amorphous carbon composite foams. The density of the carbon composite foams was modulated in the range of 0.17 to 0.35 g cm^{-3} by using the sucrose solution of concentrations in the range of 200 to 700 g L^{-1}. The compressive strength of carbon composites foams in the transverse direction (0.24 to 3.2 MPa) is higher than that in the filter-pressing direction (0.22 to 1.76 MPa) due to the preferential orientation of elongated sawdust particles transverse to the filter-pressing direction. The electrical conductivity increases from 18.2 to 33.8 S cm^{-1} when the foam density increases from 0.15 to 0.35 g cm^{-3}. The carbon composite foams exhibited excellent fire resistance with low thermal conductivity in the range of 0.12 to 0.20 W $m^{-1}K^{-1}$. The carbon composite foams showed absorption dominated EMI shielding with total shielding effectiveness in the range of 25 to 53 dB.

Rice husk, an agro-waste produced in large quantity during rice processing was used for the preparation of carbon-silica (**C/SiO$_2$**) and carbon-silicon carbide (**C/SiC**) composite foams due to its inherent pore structure and presence of silica. Sucrose-rice husk composites were prepared by filter-pressing rice husk powder dispersions in sucrose solution followed by freeze-drying. The caramelization of sucrose in sucrose-rice husk composites followed by carbonization produced **C/SiO$_2$** composite foams. Carbothermal reduction of silica in the **C/SiO$_2$** composite for 1600 ^{o}C produced **C/SiC** composite foams. The formation of β-SiC and micro-graphite during carbothermal reduction was confirmed by XRD, TEM and Raman analysis. The density of **C/SiO$_2$** and **C/SiC** composite foams were modulated in the ranges of 0.26 to 0.37 and 0.18 to 0.29 g cm^{-3} using sucrose solution concentrations in the range of 300 to 600 g L^{-1}. The compressive strength, thermal conductivity and EMI shielding effectiveness of the **C/SiO$_2$** composite foams were in the ranges of 0.32 to 1.67 MPa, 0.150 to 0.205 W $m^{-1}K^{-1}$ and 18 to 38.5 dB, respectively. The compressive strength was decreased to the range of 0.19 to 1.19 MPa and thermal conductivity and EMI shielding effectiveness were increased to the ranges of 0.165-0.431 W $m^{-1}K^{-1}$ and 20 to 43.7 dB, respectively, by carbothermal reduction of silica in the **C/SiO$_2$** composite foam to SiC. The electrical conductivity of **C/SiO$_2$** composite foams increased from 19 to 94 S cm^{-1} when sucrose solution concentration increased from

300 to 600 g L^{-1}. The **C/SiC** composite foams showed higher electrical conductivity in the range of 102 to 371 S cm^{-1} due to the graphitization of carbon during heat-treatment at 1600 °C for carbothermal reduction. The electrically conducting carbon, dielectric SiO_2 and SiC and the inherent pore channels in rice husk contributed to the EMI shielding.

The waste newspaper was successfully used for the preparation of mechanically robust carbon-gehlenite composite foams. The pulp prepared by mixing newspaper and sucrose solution was subjected to filter-pressing followed by drying produced newspaper-sucrose composites. The caramelization of sucrose in the newspaper-sucrose composite followed by carbonization produced carbon-gehlenite composite foams. The amorphous nature of carbon and the presence of gehlenite in the carbon composite foams were confirmed by XRD analysis. The gehlenite content estimated using thermogravimetric analysis decreased from 41.8 to 13.6 wt.% when the sucrose solution concentration increased from 0 to 700 g L^{-1}. The carbon composite foam density increased from 0.18 to 0.39 g cm^{-3} when the sucrose solution concentration increased from 0 to 700 g L^{-1}. The porosity of the carbon composite foams, calculated from their bulk and skeletal densities, decreased from 92.8 to 82.7 % when the sucrose solution concentration increased from 0 to 700 g L^{-1}. The carbon-gehlenite composite foams showed compressive strength and Young's modulus in the ranges of 0.2 to 1.7 MPa and 3.4 to 69.9 MPa, respectively. The carbon-gehlenite composite foams exhibited excellent fire resistance. The carbon-gehlenite composite foams of density in the range of 0.18 to 0.39 g cm^{-3} showed a room temperature thermal conductivity in the range of 0.1 to 0.2 Wm^{-1} K^{-1}. The carbon-gehlenite composite foams exhibited absorption dominated EMI shielding. The total EMI shielding effectiveness increased from 15.9 to 44.9 dB when sucrose solution concentration increased from 0 to 700 g L^{-1}.

The prepared carbon composite foams from various biomasses could be good candidates for high-temperature thermal protection in aerospace, lightweight fire-resistant structure for building compartments in ships and absorption dominated EMI shielding in the electronic and telecommunication industry.

TABLE OF CONTENTS

2. MATERIALS AND METHODS

3. CARBON COMPOSITE FOAMS FROM NATURAL COTTON

4. **CARBON COMPOSITE FOAMS FROM SAWDUST**

5. **CARBON- SILICA AND CARBON-SILICON CARBIDE COMPOSITE FOAMS FROM RICE HUSK**

6. CARBON-GEHLENITE COMPOSITE FOAMS FROM NEWSPAPER

7. CONCLUSIONS AND FUTURE SCOPE

LIST OF TABLES

LIST OF FIGURES

ABBREVIATIONS

AC	Activated Carbon
ASTM	American Society for Testing and Materials
BET	Brunauer-Emmett-Teller
BMI	Bismaleimide
CF	Carbon foam
CMB	Carbon Micro Belt
CNT	Carbon Nanotube
DFT	Density Functional Theory
DHW	Domestic Hot water
EDAX	Energy Dispersive X-ray Analysis
EM	Electromagnetic
EMI	Electromagnetic Interference
GO	Graphene Oxide
HOPG	Highly Oriented Pyrolytic Graphite
ICP-AES	Inductively Coupled Plasma Resonance- Atomic Emission Spectroscopy
MWCNT	Multi-walled Carbon Nanotube
MCM	Mobil Composition of matter
MCMB	Mesocarbon Micro Beads
PA	Paraffin
PAA	Palmitic acid
PEG	Polyethylene glycol
PCM	Phase change material
PEO106-PPO70- PEO106	Poly(ethylene oxide)- block-poly polystyrene-block-poly(4-vinyl pyridine
PF	Phenol- formaldehyde
PSD	Pore Size Distributions
PSeP4VP	Polystyrene-block-poly(4-vinyl

	Pyridine
PVC	Polyvinylchloride
r-GO	Reduced graphene oxide
RVC	Reticulated Vitreous Carbon Foam
SBA	Santa Barbara Amorphous
SDC	Sawdust derived carbon foam
SE	Secondary electron
SE_R	Shielding Effectiveness due to Reflection
SE_M	Shielding Effectiveness due to Multiple internal Reflection
SE_T	Total shielding effectiveness
SEM	Scanning Electron Microscope
TEM	Transmission Electron Microscope
TGA	Thermogravimetric analysis
XRD	X-ray Diffraction Analysis
CCF	Cotton derived Carbon Foam

NOTATIONS

ρ	Density
ρ^*	Relative density
ρb	Bulk density
ρs	Skeletal density
κ	Thermal conductivity
α	Thermal diffusivity
cp	Specific heat
R_f	Resistivity of foam
Rs	Resistivity of solid
λ	Wavelength
θ	Angle of diffraction
V	Voltage drop
I	Current
S	Distance between the pin

NOMENCLATURE

$C_{125}H_{188}O_{80}$	Caramelin
$C_{24}H_{36}O_{18}$	Caramelan
$C_{36}H_{50}O_{25}$	Caramelen
K_2CO_3	Potassium carbonate
KOH	Potassium hydroxide
K_2TiO_3	Potassium titanate
OH^-	Hydroxyl ion
SiC	Silicon carbide
SiO_2	Silicon dioxide
$ZnCl_2$	Zinc chloride

CHAPTER 1

INTRODUCTION

This chapter intends to give an overview of carbon foams, their precursors and processing methods with the state-of-the-art literature survey. The properties and applications of carbon foams are briefly presented. The development of carbon foams from biomasses is also reviewed. Further, this chapter introduces the motivation and objectives of the research work. At the end of the chapter, the organization of the whole thesis and a brief introduction for each chapter is mentioned.

1.1 Carbon

Carbon is the most important element on the earth. It is positioned in 6th place in the periodic table. The carbon atoms possess the electronic configuration of $1s^2 2s^2 2p^2$. By the utilization of s and p- electrons, it has been able to hybridize to form sp, sp^2 and sp^3 states to produce strong single and multiple covalent bonds with other carbon atoms and atoms of other elements(Burchell, 1999). Because of its unique hybridization capacity, carbon can exist in different forms. The versatile bonding of carbon allows a very large number of possible allotropes. Nearly 522 possible allotropes have been reported for pure carbon(Sundqvist, 2021). The carbon allotropes exist in one-dimensional, two-dimensional and three-dimensional forms. **Fig. 1.1** shows some of the important allotropes of carbon. They include bulk crystalline forms such as diamond, graphite and nanocrystalline forms such as fullerene, graphene and carbon nanotube. Many rarer varieties of carbon nanostructures such as nanodumbbells, nanoflowers, nanorice, nanolines, nanotowers, nanoshuttles, nanobowling, nanowheels, nanofans, nanopencils, nanotrees, nanoarrows and nanonails are reported recently. These nanoforms with unusual shapes exhibit properties suitable for application in various fields such as catalysis, medical, and electronics(Kharisov & Kharissova, 2019).

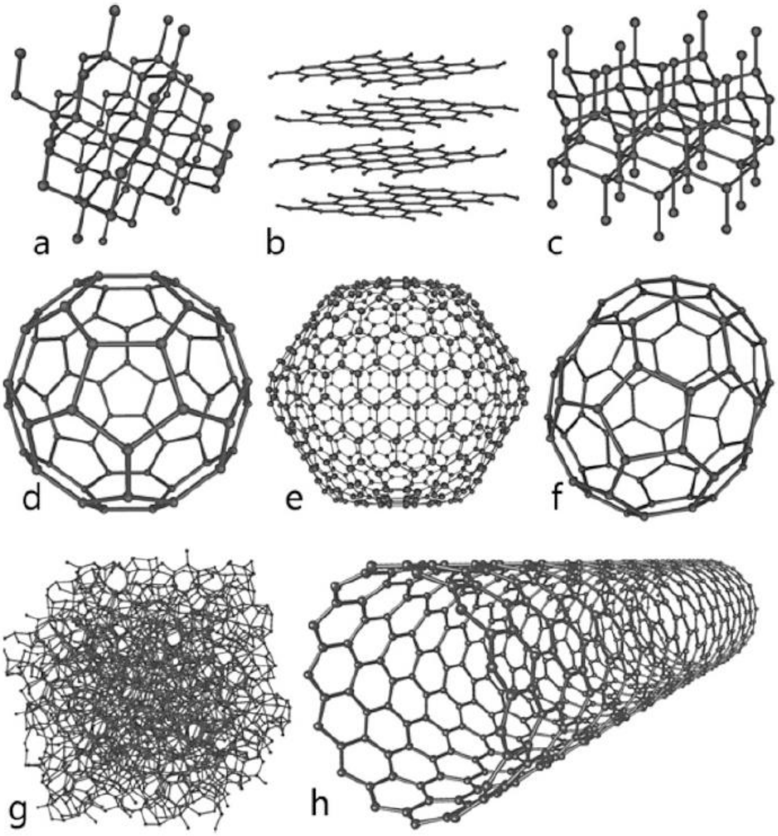

Fig. 1.1 Different allotropes of carbon (a) diamond (b) graphite (c) lonsdaleite (d) C60 (e) C540 (f) C70 (g) amorphous carbon and (h) single walled carbon nanotube (Kharisov & Kharissova, 2019)

In nature, carbon mainly exists in two crystalline forms viz. diamond and graphite. Most commonly, diamond is found in a cubic structure in which each carbon atom is covalently bonded to other immediate neighbours by $Sp^3\sigma$ bonds in a tetrahedral array. Diamond has the highest hardness (10,000 $kgmm^{-2}$), poor electrical conductivity, wide bandgap (5.47 eV), high melting point (4500 K at 10 GPa pressure) and good thermal conductivity (Changle Chen & Chen, 2008; Graebner, 1995). Besides the cubic structure, diamond rarely exists in a hexagonal form called lonsdaleite. Lonsdaleite is formed by the transformation of graphite to diamond by its hexagonal lattice on the application of high temperature and pressure. It is reported to be harder than a cubic diamond(Kharisov & Kharissova, 2019).

Graphite is another crystalline form of carbon, in which atoms are arranged in a hexagonal manner. It is composed of a series of graphene layers having a hexagonal array of carbon atoms in the x-y plane which are stacked in the z-direction by weak Vander Waals interactions. Each carbon atom has three σ-bonds leading along the hexagonal edges which correspond to sp^2 hybridization. The remaining electron in the pz orbital form a π- electron cloud that is delocalized over the entire layer. The π- electrons thus behave like a 2-dimensional electron gas and their mobility leads to electrical conductivity(Pierson, 1993). The spacing between the stacked layers is quite large (~0.335 nm). Graphite has a high melting point of 4250 K at 16.2 GPa pressure(Pierson, 2012). It has the highest electrical conductivity of 10^4 S cm^{-1} and possesses a zero bandgap(Pierson, 2012). The thermal conductivity of graphite ranges from 25-470 $Wm^{-1}K^{-1}$(Teboho et al., 2018). Highly oriented pyrolytic graphite (HOPG) is the highest-quality synthetic form of graphite(Inagaki, 2013). Graphite is highly stable in an inert atmosphere but oxidizes in an air atmosphere above 700 °C(Kharisov & Kharissova, 2019).

Amorphous or glassy carbon is another important form of carbon. The amorphous form of carbon includes carbon black, charcoal, lampblack and coke which are possessing a low degree of crystallinity. They are formed by the thermal decomposition or pyrolysis of organic compounds, synthetic polymers and biomasses(Kouchi, 2011). They have a turbostratic structure in which poorly organized graphitic planes are arranged in ribbons as in polymers. They are brittle. They exhibit properties such as low density (~1.5 g cm^{-3}), high-temperature stability, resistance to chemical attack and high oxidation resistance compared to other types of carbon. Their electrical resistivity is in the range of $\sim 3–8 \times 10^{-4}\ \Omega$ cm(Serp, 2013). The carbon materials used in various applications are bulk crystalline or amorphous forms, carbon-carbon composites and porous carbon. A brief description of porous carbon materials is given in the following section.

1.2 Porous Carbon

Porous carbon materials are solid carbon matrices composed of an interconnected network of pores filled with a gas(White, Budarin, et al., 2009). Porous carbon materials can be classified into microporous(pore size <2 nm), mesoporous (pore size 2-50 nm) and macroporous(pore size >50 nm) according to their pore diameter. **Fig. 1.2** displays three dimensional and 2-dimensional structure of porous carbon.

They possess high surface area, permeability, better chemical resistance, excellent thermal stability, low density, high-temperature tolerance and tailorable electrical and thermal conductivity(De et al., 2015; Libin & Hu, 2018). Hence, they are used in many potential applications such as electrode materials for batteries, fuel cells, supercapacitors, as a sorbent for separation processes, gas storage and as catalyst support(Estevez et al., 2018; Kaur et al., 2019; K. Wang et al., 2017; Xiang, Wang, et al., 2017; Xiao et al., 2017; B. Zhang et al., 2014; X. Zhang et al., 2015). Conventionally porous carbon materials are synthesised from organic precursors such as coal, pitches, wood, fruit shells and synthetic polymers by various methods(S. Gao et al., 2018; Hu et al., 2021; Ren et al., 2016; H. Wang et al., 2020; Q. Wei et al., 2019; White, Antonietti, et al., 2009; White, Budarin, et al., 2009; C. Wu et al., 2016; Zheng et al., 2020).

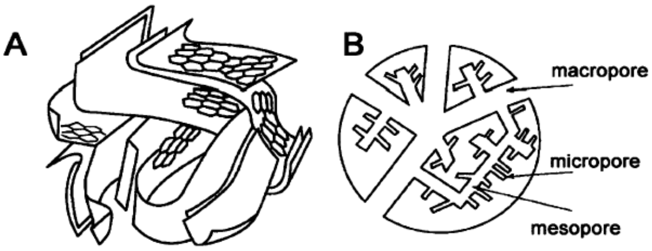

Fig. 1.2 Three dimensional (a) and two-dimensional structure (b) of the porous carbon(White, Budarin, et al., 2009)

1.2.1 Microporous carbon

Microporous carbon materials primarily include carbon molecular sieves and activated carbons, which contain microporous channels with a pore diameter below 2 nm(Kyotani, 2003). Molecular sieve carbons are a special type of microporous carbons that possess uniform micropores of several angstroms in diameter. These molecular sieve carbons have been used in various fields such as the separation of gas molecules, shape-selective catalysis and electrodes for electrochemical double-layer capacitors(B. J. Lee et al., 2006). Molecular sieve carbons are prepared by the pyrolysis of a mixture of coal, biomass and organic additives (Jüntgen et al., 1981; Mohamed et al., 2010; Prasetyo et al., 2017; Vyas et al., 1992; Jinhua Zhang et al., 2018). By changing the pyrolysis temperature and precursor ratio, one can tune the pore size of the molecular sieve carbons. Miura group synthesised molecular sieve carbon from ion-exchange resins. In this, spherical polystyrene-based resins with a sulphonic acid group are first ion-exchanged with cations. The resultant ion-exchanged resins are carbonized at 900 °C under a nitrogen atmosphere to produce a molecular sieve with sharp pore size distributions(Nakagawa et al., 1999).

The ordered microporous carbon can be synthesised by the template-assisted method(B. J. Lee et al., 2006). In order to make microporous carbon with uniform pore as well as the ordered regular pore array, rigid inorganic templates such as zeolites are being used(Su et al., 2005). Zeolites are aluminosilicate materials with ordered structures and they possess uniform sub-nanometer sized pores. A carbon precursor infiltrated into the pore channels of the zeolite is stabilized by cross-linking and subsequently carbonized. After the carbonization, the templates are removed by etching with HF solution. The resulting material exhibited the highest surface area and uniform ordered micropores(B. J. Lee et al., 2006; Ma et al., 2000).

Activated carbon (AC) is getting good attention in various fields due to its low cost, easy processing, well-developed porosity, high surface area and good chemical stability. AC is an amorphous carbon that exhibits a turbostratic structure(Marsh & Reinoso, 2006). AC is synthesised by both the chemical activation and physical activation of polymers and biomasses(Deng et al., 2010; Shijie Li et al., 2017; Tian et al., 2019; Zhu et al., 2008). The physical activation is a two-stage process in which the first step is the carbonization of the raw materials in the absence of oxygen followed by the activation with the support of an oxidizing gas such as O_2, CO_2 and steam in the temperature range of 800-1200 °C(Marsh & Reinoso, 2006). The physical activation is the green process that does not evolve any harmful chemicals at the time of activation. However, the process has some disadvantages such as high processing time, low carbon yield and relatively low surface area. Chemical activation involves impregnation of the precursor with the activation agent (KOH, phosphoric acid, K_2CO_3, $ZnCl_2$ etc) followed by heating under an inert gas atmosphere at the temperature between 400 to 850°C(Deng et al., 2010; Girgis & El-Hendawy, 2002; Hayashi et al., 2002; K. Li et al., 2010; Shijie Li et al., 2017; Maneechakr & Karnjanakom, 2017; Mohanty et al., 2005; Otowa et al., 1997; Ozdemir et al., 2014; Yue et al., 2018). Another type of microporous carbon is carbide-derived carbon. Here metal carbides are the carbon precursor. The metal in the metal carbide precursor is selectively removed by reaction with chlorine at high temperatures (Gudavalli & Dhakal, 2018). This method generates narrow micropore size distribution, high specific surface area and large pore volume. A typical TEM microstructure of carbide-derived microporous carbon is shown in **Fig. 1.3**

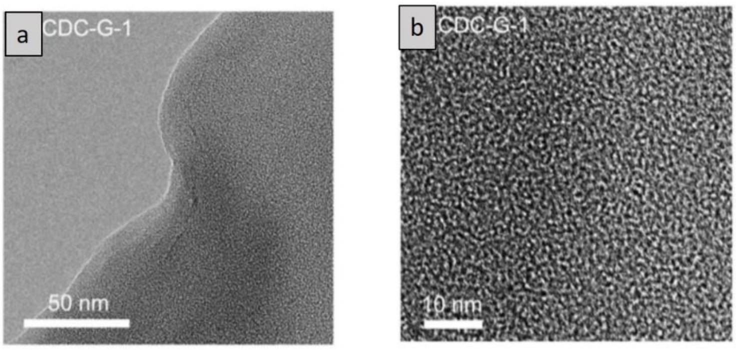

Fig. 1.3 TEM image of carbide-derived microporous carbon at Low (a) and high magnification(b) (P.C. Gao et al., 2015)

1.2.2 Mesoporous carbon

Mesoporous carbon contains pores of size between 2-50 nm. Mesoporous carbon materials include the ordered mesoporous carbon, disordered mesoporous carbon, carbon aerogel and mesoporous carbon film. The following methods are employed for the synthesis of mesoporous carbon:

(i) Hard templating methods
(ii) Direct carbonization of polymer blends
(iii) Carbonization of the polymer aerogels

Ordered mesoporous carbon is primarily prepared through the hard templating method for which mesoporous silica such as MCM-48, MCM-41, SBA-15 etc., MgO and zeolite of suitable pore size are used as templates(Lee et al., 2006; Xin & Song, 2015). This approach includes (i) impregnation of porous templates with the organic precursors (ii) cross-linking and carbonization of the impregnated organic precursor and (iii) removal of the template(Inagaki et al., 2016). A typical schematic diagram of mesoporous carbon preparation by a hard template method is given in **Fig. 1.4**. Amphiphilic molecules, such as surfactant and block copolymers, have been extensively employed as soft templates in the synthesis of ordered mesoporous carbon. Block copolymer surfactants such as poly(ethylene oxide)- block-poly(propylene oxide)-block-poly(ethylene oxide) (PEO106-PPO70- PEO106) (Pluronic F127), PEO20-PPO70-PEO20 (Pluronic P123), polystyrene-block-poly(4-vinyl pyridine) (PSeP4VP), etc. are used as soft template for the preparation of ordered mesoporous carbon(Liang et al., 2008; Libbrecht et al., 2017). TEM image of a typical ordered mesoporous carbon is shown in **Fig. 1.5**

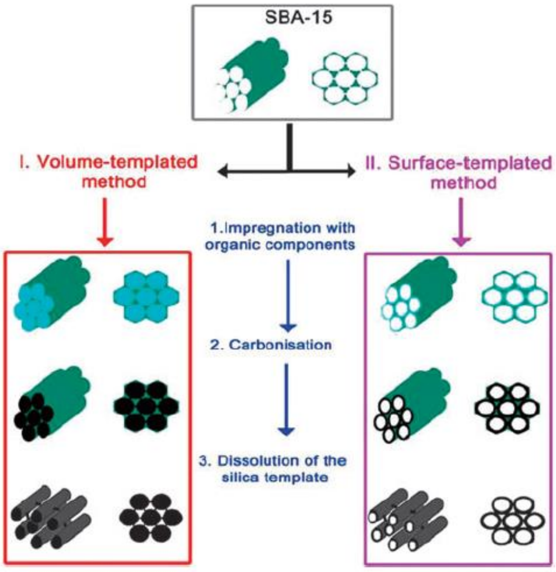

Fig. 1.4 Schematic representation of the preparation of mesoporous carbon by hard template method(White, Budarin, et al., 2009)

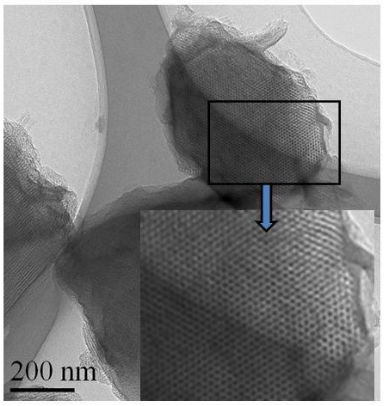

Fig. 1.5 TEM image of a typical ordered mesoporous carbon(Abdul et al., 2015)

Besides the ordered mesoporous carbon, various methods have been developed for the synthesis of disordered mesoporous carbon with uniform pore size. These carbon materials are prepared from various approaches which include templating with silica nanoparticles or silica gel, anodic alumina, aluminosilicate gel and polymer beads and copolymerization of carbon precursors with inorganic precursors such as tetraethyl orthosilicate(Liang et al., 2008). Carbon aerogels are another type of mesoporous carbon material which are prepared by the carbonization of polymer aerogels. The polymer aerogels are obtained by sol-gel polycondensation of phenolic compounds and formaldehyde followed by supercritical drying(Sarathchandran & Ilangovan, 2021; Worsley & Baumann, 2016). Carbon aerogel has unique properties such as lightweight, very low thermal conductivity, high surface area and good mechanical strength(X. Gao et al., 2020; F. Li et al., 2019). Hence these materials can be used in various fields such as energy storage, contaminant removal and gas separation and high-temperature thermal insulation(Du et al., 2018; Geng et al., 2020; Wiener et al., 2009). A photograph of a carbon aerogel monolith showing its lightweight is given in **Fig. 1.6**.

Fig.1.6 Photograph of a carbon aerogel monolith (*Carbon Aerogel - Bing Images*, n.d.)

1.2.3 Macroporous carbon

In macroporous carbon materials, the pore dimension is greater than 50 nm. They include porous carbon monolith, 3D- ordered carbon framework and carbon foam. Macroporous carbon materials are primarily synthesised through three approaches such as (i) foaming and setting of precursors (ii) polymer foam replication and (iii) template-assisted synthesis(Kim et al., 2017; Lee et al., 2006; Nagel et al., 2014). Based on the synthesis approaches, carbon precursor and heat treatment temperature one can control the porosity, pore morphology, pore interconnectivity and crystallinity of the macroporous carbon materials. The lightweight macroporous carbon materials with porosity greater than 70 vol% are called carbon foams. The following section gives a detailed description of carbon foams, their synthesis, properties and applications.

1.3 Carbon Foam

Carbon foams are macroporous carbon materials. Carbon foam is defined by Klett as a porous product containing regularly shaped, predominately concave, homogeneously dispersed cells which interact to form a three-dimensional array throughout a continuum material of carbon, predominately in the non-graphitic state(J. Klett, 2005). Carbon foam exists in the cellular and reticulated structure. Normally two types of cellular structures are available: open cellular and closed cellular. In an open cellular structure, the neighbouring cells are inter-connected through openings called cell windows. Therefore, the open cellular foams exhibit high permeability. In closed cellular foams, the cells are isolated. This type of carbon foam possesses lower porosity, higher mechanical strength and lower thermal conductivity. Carbon foams are also available in the reticulated structure. The reticulated foams consist of net-work like struts and ligaments(H. Liu et al., 2020). The SEM images of typical open cellular, closed cellular and reticulated carbon foams are given in **Fig.1.7**. The carbon foams are also classified into graphitic and amorphous depending on the crystallinity(Nagel et al., 2014). The crystalline nature of carbon foam depends on the carbon precursor and heat treatment temperature. Various precursors used for the preparation of carbon foams are described in the following section.

Fig. 1.7 SEM micrographs of open cellular(a), closed cellular(b) and reticulated (c) carbon foams (Narasimman et al., 2015; *Reticulated Carbon Foam - Bing Images*, n.d.)

1.3.1 Carbon foam precursors

Carbon foam can be prepared from different precursors such as thermoplastics, thermosetting polymers and biomasses. The thermoplastic precursors such as coal-tar pitch, petroleum pitch and synthetic mesophase pitch produce soft carbon which can be graphitized by high-temperature heat treatment(Chen et al., 2006; Li et al., 2011). On the other hand, the thermosetting polymers and biomasses produce hard carbon which is difficult to graphitize even by high-temperature heat treatment(Nagel et al., 2014).

1.3.1.1 Thermoplastic precursors

Thermoplastic precursors used for the preparation of carbon foam are pitches which include coal tar pitch, petroleum pitch, asphaltite and naphthalene or anthracene-based pitches. They are carbonaceous viscoelastic materials that are derived from fossil fuels. Pitches are a complex mixture of molecules with average molecular weight ranges from 300 to 400 depending on the source and the pre-treatment condition(Kershaw & Black, 1993). Coal tar pitches are obtained by the distillation of coal tar around 400 °C(Kuznetsov et al., 2015). Petroleum pitches are generated from the high aromatic content feedstock in petroleum refining. The pitches mainly contain a mixture of condensed polycyclic aromatic and alicyclic hydrocarbons. The coal tar pitch contains more aromatic fractions than the petroleum pitch. The structure of some of the molecules present in pitch is shown in **Fig. 1.8**. The molecules in pitch are further condensed and then stack through π-π interaction to produce an anisotropic (liquid crystalline) structure on heating at temperatures nearly 400 ^{o}C. The resulting pitch is called the mesophase pitch. Mesophase pitch is also synthesized directly from pure polycyclic aromatic compounds such as naphthalene and anthracene. **Fig. 1.9** shows the schematic diagram of the mesophase particle in pitch.

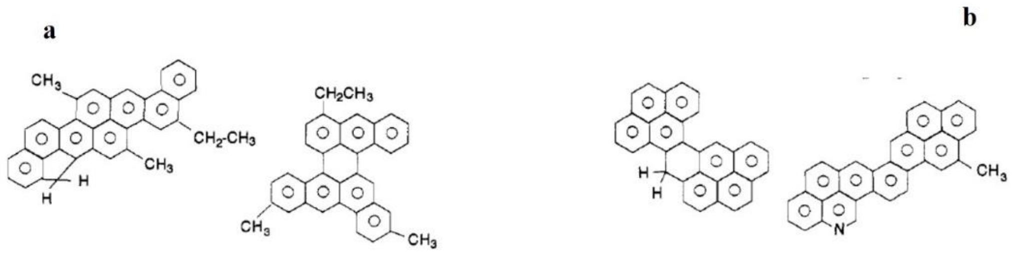

Fig.1.8 Structures of representative molecules in coal tar pitches (a) and petroleum pitches(b) (Kershaw and black 1993)

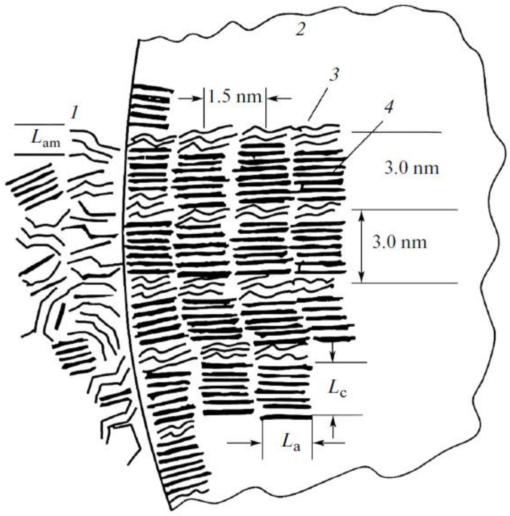

Fig. 1.9 Schematic diagram of a mesophase particle in pitch isotropic phase(1), mesophase particle fragment(2), amorphous phase(3) and crystallites(4) (Kuznetsov et al., 2015)

In general, thermoplastic raw materials pass through a plastic stage during the carbonization heat treatment. Under sufficient temperature, crystallites tend to order parallel to one another and are clustered into the mesophase. With the increase in the temperature above 2000 °C, mesophase domains can grow to very large sizes and form graphitic structures(Ogale et al., 2002). Carbon derived from the mesophase pitches is highly graphitizable compared to the coal tar and petroleum pitches.

1.3.1.2 Thermosetting polymers

Thermosetting polymers are available in the low molecular weight form with low viscosity called resins. These resins get hardened on heating under elevated temperature as a result of further polymerization and cross-linking. Thermosetting polymers such as phenol-formaldehyde, polyimide, polyurethane, polybenzoxazine and polyfurfuryl alcohol are widely studied for the preparation of carbon foams(Farhan et al., 2016; Inagaki et al., 2004; Lorjai et al., 2009; Qu et al., 2017). The structure of different thermosetting precursors is given in **Fig. 1.10**. The solid polymeric foams prepared from the precursor resins are subsequently carbonized to produce the carbon foams. The cross-linked thermosetting polymers do not pass through a plastic stage on heating. Hence, the carbon derived from these polymers are hard and therefore not easily graphitizable. That is, they are rigid in structure and the graphene layers are randomly oriented(Nagel et al., 2014).

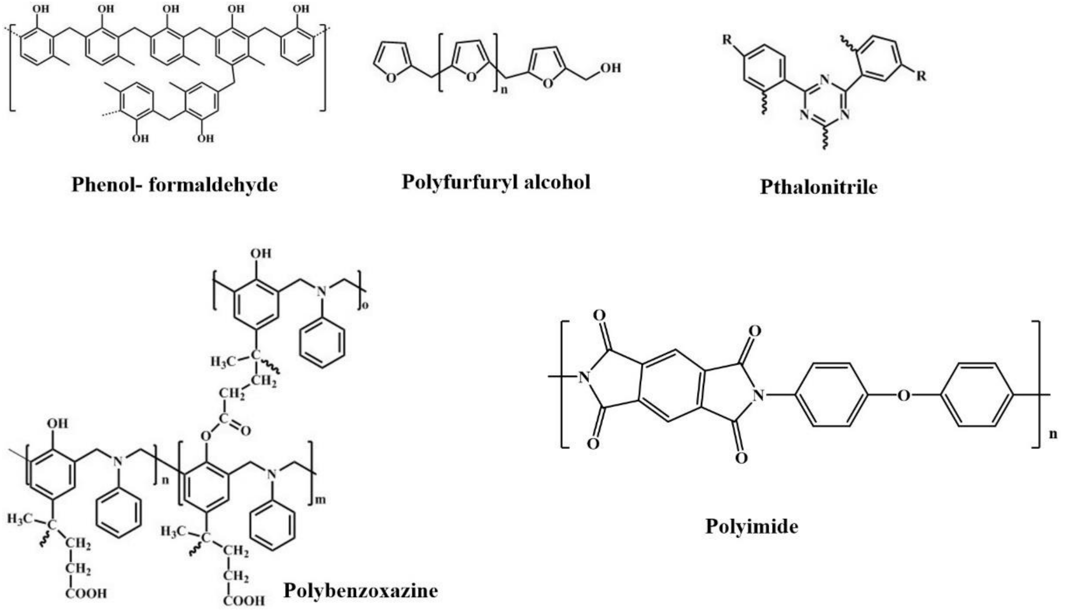

Fig. 1.10 Structures of thermosetting polymer used for carbon foam processing(Gowariker et al., 1986)

1.3.1.3 Biomasses

Large scale exploitation due to the population boom and the resultant industrialization led to the fast depletion of fossil fuels. Therefore, the researches focus on the replacement of fossil fuel-based carbon precursors with renewable resources such as biomass. Though a large number of biomass-based precursors are used for the preparation of activated carbon, only a few are studied for the preparation of carbon foams due to the difficulty in processing. Lignin, tannin, sucrose and cellulose are widely studied for the preparation of carbon foams and aerogel monoliths(Prabhakaran et al., 2007; Seo, Park, Shin, Baeck, et al., 2014;

Sheng et al., 2019; Tondi et al., 2009; Wilson et al., 2018a; Zhuo et al., 2016). The structure of biomass-based precursors used for carbon foam preparation is given in **Fig. 1.11.** Cellulose and lignin are polymers whereas tannin and sucrose are simple molecules. These biomasses leave a considerable amount of carbon residue during pyrolysis. However, the carbon yield of these biomasses is less than that of the thermoplastic and thermosetting carbon precursors. On the other hand, they possess advantages such as large availability at low cost, eco-friendly nature and do not produce harmful products during pyrolysis. The carbon produced from these biomasses is hard and therefore difficult to graphitize.

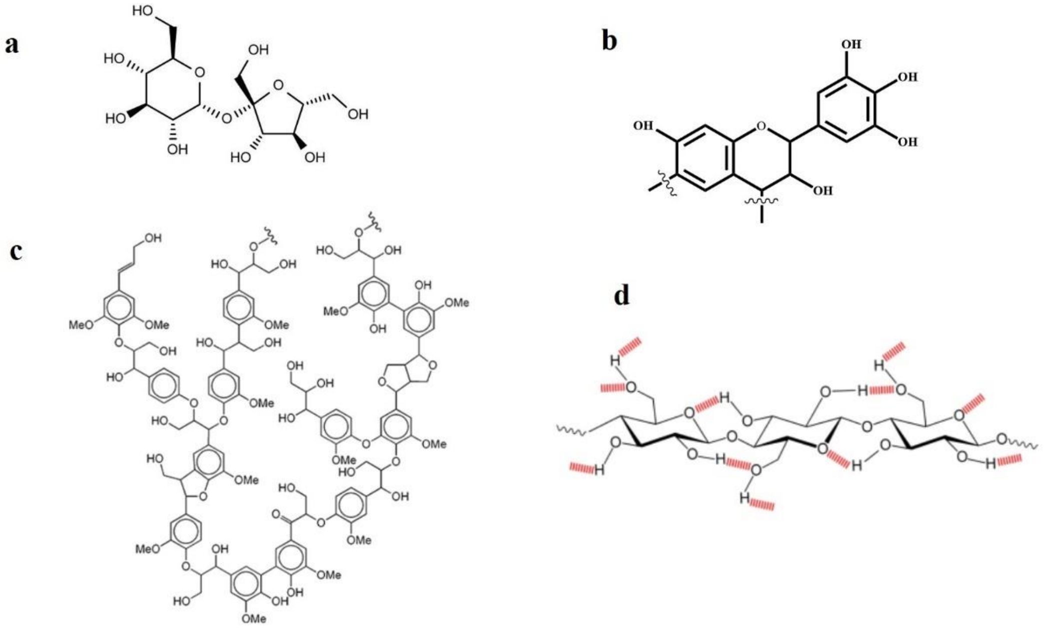

Fig. 1.11 Structures of biomass-based carbon foam precursors. sucrose(a) tannin(b) lignin (c) and cellulose(d) (Jana et al., 2014; *Lignin - American Chemical Society*, n.d.; Tursi, 2019)

1.3.2 Processing of carbon foam

There are mainly three general methods reported for the synthesis of carbon foams. They are foaming by a blowing agent, polymer foam replication and using a suitable pore template. The foaming method uses organic polymer resins and pitches as precursors for the preparation of carbon foams. In this method, the precursors containing the blowing agent are heated under controlled pressure condition. The foaming occurs by the formation of bubbles due to the evolution of gases. These gases are produced as a result of the decomposition or evaporation of the blowing agent or the partial decomposition of the precursor. The foaming accompanies an increase of viscosity due to further polymerization and cross-linking reactions. This increase of viscosity stabilizes the bubble and finally set the foam into a solid. Surfactants are also often used to stabilize the bubbles. The parameters such as temperature, pressure, heating rate and pressure drop have to be controlled for the formation of foam with the desired cell size and structure. The obtained organic foam is further carbonized to produce carbon foam (Inagaki et al., 2015). Blowing agents such as diethyl ether, pentane, aluminium nitrate, sodium bicarbonate and azodicarbonamide are used for the preparation of carbon foams(Liu et al., 2007; Narasimman & Prabhakaran, 2012; Tondi et al., 2009; Wu et al., 2011). The disadvantage of this method is that the formation of the bubbles could not be controlled precisely. Hence this method gives carbon foams with inhomogeneous distribution of cells.

Albert et.al first demonstrated a process for the production of carbon foam from petroleum pitch. In this process, petroleum pitch was heated with a blowing agent in a mould under pressure. At the high temperature and pressure, gas evolved by the decomposition of the blowing agent dissolved into the molten pitch. After that, the pressure was lowered to nucleate bubbles and produce foam. The temperature was also decreased to modify the viscosity to control the growth rate of bubbles and finally to set the foamed pitch into a solid body. The resulting foam body was subjected to oxidative stabilization and carbonization heat-treatments to form carbon foam(Albert et al., 1981). In the 1990's Stiller et.al in Virginia University developed a method for the preparation of carbon foam from the coal- tar pitch. In this, coal- tar pitch was heated at about 325- 500 °C and pressure up to 100 MPa under inert conditions in a mould. The volatile products obtained by the pyrolysis of the pitch at this condition foam the pitch. The bubbles were stabilized by the increase in viscosity due to polymerization. The foamed pitch was cocked to make it infusible and subsequently carbonized at 1200 °C. After that, the resultant was graphitized at 2600 °C(Stiller et al., 2005). **Fig. 1.12** shows the SEM image of carbon foam derived from the coal tar pitch.

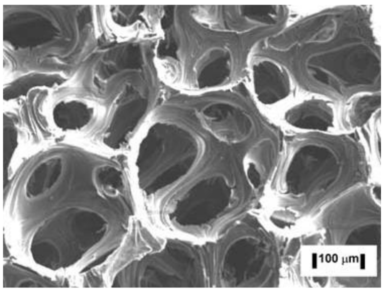

Fig. 1.12 SEM image of carbon foam derived from the coal tar pitch(Scheffler & Colombo, 2006)

There are several techniques available for the production of graphitic carbon foam from mesophase pitch. Hager et.al and Kernas have established a traditional blowing technique for carbon foam preparation from mesophase pitch(Kernas Kristen, 1999; J. Klett, 2005) In this, mesophase pitch is softened by thermal treatment under inert gas pressure followed by saturated with a blowing agent and then depressurized. The solid foam thus obtained is then subjected to oxidative stabilization and subsequent carbonization and graphitization to form carbon foam. **Fig. 1.13** is SEM image of graphite foam developed from mesophase pitch. Several modified techniques are reported for the carbon foam preparation from mesophase pitch in order to avoid the blowing agent and oxidative stabilization(J. Klett, 2005; Klett et al., 2000; Sizhong Li et al., 2011). Generally, the mesophase pitch-based carbon foams exhibit high mechanical strength, thermal conductivity and electrical conductivities due to the well-oriented mesophase layer within the bubble walls leading to a well-crystallized graphite structure(J W Klett et al., 2004).

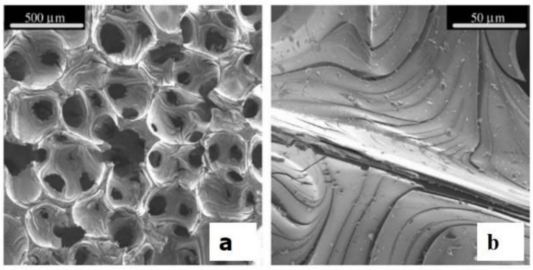

Fig. 1.13 Low (a) and high magnification(b) SEM images of mesophase pitch-derived carbon foam(J W Klett et al., 2004)

Foaming using a blowing agent is widely used for the preparation of carbon foams from synthetic polymers such as phenol-formaldehyde (PF), poly(aryl acetylene), poly(benzoxazine) etc.(Lei et al., 2010; M. Liu et al., 2007; Lorjai et al., 2009; Sharma et al., 2020) Carbon foams are prepared from PF resins by blowing their ethanol solution at various concentrations at 170 °C under the pressure of 4 MPa, followed by carbonization at 800 °C. The bulk density and compressive strength of the carbon foam varies with the concentration of PF- solutions. The bulk density and compressive strength of the carbon foam varies from 0.24 to 0.73 g mL^{-1} and 13.1 to 98.3 MPa, respectively, when the concentration of PF solution changes from 0.13 to 0.36 g mL^{-1}(Lei et al., 2010). Foaming of poly(aryl acetylene) using pentane as a blowing agent followed by setting and carbonization produces cellular carbon foam with high compressive strength of 25.8 MPa(Liu et al., 2007).

The replication method produces reticulated carbon foams. In this method, foams of polymers such as polyurethane and melamine-formaldehyde of desired cell size are used as the templates(S. Chen et al., 2013; da Silva et al., 2020; Inagaki et al., 2004, 2015; Jana et al., 2013; Sharma et al., 2020). The polymer foam template is impregnated with the carbon precursor resin followed by squeezing by rolling to remove the excess resin present in the pores. The precursor resin coated on the surface of webs and struts of the polymer foam template is subsequently stabilized by cross-linking and then heated in an inert atmosphere furnace for carbonization and graphitization. The synthetic polymers, pitches and sucrose are used as a precursor for the preparation of reticulated carbon foams by the replication method. Unlike the blowing method, the replication technique gives foams of well-controlled porosity and cell structures(Inagaki et al., 2015).

Particles are also used as a template for the preparation of macroporous carbon materials. Spherical submicrometer sized particles such as colloidal nanosilica and polystyrene which can self-organize themselves into a colloidal crystal (opal) are used as pore templates(Yi et al., 2001). These are the excellent endotemplate to prepare the ordered macroporous carbon. The synthesis step involves filling the carbon precursor into the interstitial space of colloidal crystals followed by the carbonization and finally removal of templates to generate a carbon skeleton. Before the infiltration of the carbon precursor, sintering is usually performed to create the neck between the spherical silica particles. It provides the interconnections between the spherical pores in the resulting macroporous carbon materials. Infiltration of liquid precursors such as phenolic resin and sucrose solution and chemical vapour deposition from gaseous precursors such propylene, benzene and divinylbenzene are used to fill the interstitial space in the colloidal crystal. Three-dimensional macroporous carbon material was first synthesised by Zakhidov and group through the colloidal - template method(Anvar et al., 1998). Baumann et al utilized a polymer microsphere as a template for the synthesis of the ordered macroporous carbon materials(Baumann & Satcher, 2003). Chai et.al developed a dual template method using polystyrene sphere and silica particles as templates for the preparation of the ordered macroporous carbon materials(Chai et al., 2004). The SEM photomicrograph of ordered macroporous carbon is shown in **Fig. 1.14**.

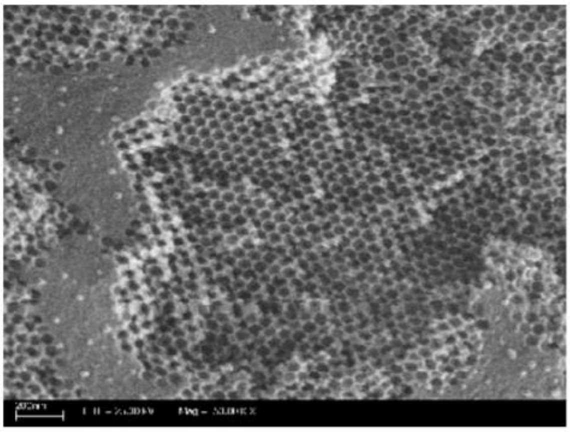

Fig. 1.14 SEM image of the ordered macroporous carbon with 62 nm pores(Kang et al., 2002)

1.3.3 Carbon foams from biomasses

Biomasses are generally used for the preparation of activated carbons. A variety of biomasses such as wood, coconut shell, orange peel, almond shell, banana peel, corncob, shrimp shell, fish waste, soybean, cotton and starch are studied for the preparation of activated carbon(El-Sayed et al., 2014; El Nemr et al., 2009; Mohammad et al., 2015; Mondal et al., 2017; M. M. Rahman et al., 2014; Ren et al., 2016; Sevilla & Fuertes, 2011; Sivadas et al., 2015; T. Wang et al., 2009; Wilson et al., 2018c; C. Wu et al., 2016) However, there is a limited number of reports using biomasses as precursors for the preparation of carbon foams. Preparation of carbon foams from biomasses such as wood, lignin, tannin, cellulose and sucrose is well reported(Prabhakaran et al., 2007; Seo, Park, Shin, Hyeon, et al., 2014; Z. Shen et al., 2021; Tondi et al., 2009). Nagle et al. prepared cellular carbon materials from wood by carbonization under controlled temperature and atmosphere(Byrne & Nagle, 1997). The cellular carbon produced exhibited 25% higher compressive strength than the corresponding wood. Klett at the Sandia National Laboratories first produced carbon foam from cork, a natural cellular precursor(Klett, 2000). Rios et al. prepared carbon foam from olive stone by swelling and subsequent carbonization. The obtained carbon foam exhibited a low density in the range of 0.2–0.3 g cm^{-3}(Rios et al., 2006). Wang et.al synthesised carbon foam from birch sawdust through liquefaction, activation and carbonization processes. The prepared carbon foam exhibited a low density in the range of 0.021–0.023 g cm^{-3} and a surface area in the range of 534-555 m^{2}g^{-1}(R. Wang et al., 2012). Seo et al reported a PMMA template-based method for the preparation of macroporous carbon from lignin(Seo et al., 2014).

Celzard and co-workers developed carbon foams and aerogels from tannin by different processing routes. The reaction of phenolic nuclei in tannin with formaldehyde was used for the polymerization as in the phenol-formaldehyde system (Tondi et al., 2009). The foaming of the tannin-based resins was accomplished by blowing using low volatile liquids such as diethyl ether, whipping followed by setting and emulsion templating (Celzard et al., 2015; Szczurek et al., 2014, 2015; Tondi et al., 2009). These methods produced interconnected cellular carbon foams of a range of densities and cell sizes. The tannin derived glassy carbon foams were evaluated for thermal insulation, fire resistance, acoustic absorption and EMI shielding applications(Amaral-Labat et al., 2013; Celzard et al., 2011, 2012; Letellier, Macutkevic, Paddubskaya, Plyushch, et al., 2015). The tannin derived carbon foam exhibited good compressive strength ranges from 0.31-0.82 MPa when density ranges from 0.035 to 0.06 g cm^{-3}(A Celzard et al., 2010). Carbon foams with improved thermal conductivity and mechanical properties were achieved by the addition of the exfoliated graphite as a filler in the carbon foam matrix(Jana et al., 2014). The composite foam exhibited a thermal conductivity of 3.65 Wm^{-1}K^{-1} and compressive strength of 6.9 MPa.

Cellulose-based materials have been widely used to prepare carbon foam and aerogel monoliths. Bi.et.al processed twisted carbon aerogel from raw cotton by carbonization at 800 °C. The prepared aerogel exhibited an oil absorption capacity of 50–190 times of its weight(Bi et al., 2013). Sheng et.al prepared a carbon sponge by the direct carbonization of cotton and used the same as a host for form-stabilized wax-based composite phase change materials. The carbon sponges consist of cotton-derived hollow carbon fibres with an interconnected network structure (Sheng et al., 2019). Men et al. prepared carbonaceous foams from cotton using poly (ionic liquid) as an activating agent. Poly (ionic liquid) is reported to promote carbonization, increase microporosity, improve oxidation stability and flame resistance of the resulting carbon foam(Men et al., 2013).

Waste paper is the abundantly available cheap cellulose-based precursor for the production of carbon foams and aerogel monoliths. Paham et al. processed carbon aerogel from the waste paper for adsorptive removal of the contaminant from wastewater. The prepared carbon aerogel exhibited a high surface area of 892 m^2g^{-1} which facilitate the adsorption of organic compounds such as phenol and 2-chlorophenol from wastewater (Pham et al., 2021). Vazhayal et.al prepared carbon aerogel from waste tissue paper and polyvinyl alcohol which exhibited a high CO_2 adsorption capacity and EMI shielding effectiveness. The prepared carbon aerogel exhibited an interconnected three-dimensional porous structure with low density (0.057 g cm^{-3}), high porosity (~97%), high specific surface area (1384 m^2 g^{-1}) and low thermal conductivity (0.087 W m^{-1} K^{-1})(Vazhayal et al., 2019). The microstructure of carbon aerogel prepared from tissue paper and PVA is shown in **Fig. 1.15**.

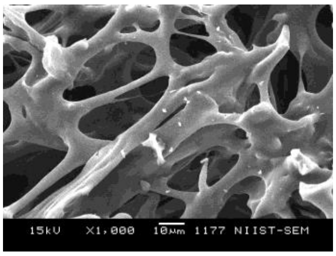

Fig.1.15 SEM microstructure of carbon aerogel prepared from tissue paper and PVA(Vazhayal et al., 2019)

Bi et al. synthesized a hydrophobic carbon microbelt aerogel (CMB) from waste paper. The CMB aerogel exhibited a low density of 5.8 mg cm^{-3} and a specific surface area of 178 m^2 g^{-1}. The CMB aerogel showed a high sorption capacity (56-188 mg g^{-1}) for oils with good recyclability(Bi et al., 2014). The microstructure of carbon microbelt aerogel is shown in **Fig. 1.16**.

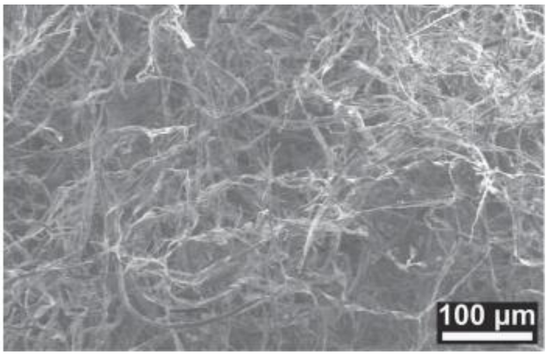

Fig. 1.16 SEM images of the belts in CMB aerogels(Bi et al., 2014)

Sucrose is a widely studied precursor for the production of carbon foams. Prabhakaran et al. first reported a process for the preparation of low-density carbon foams from sucrose(Prabhakaran et al., 2007). In this work, a resin prepared by heating acidic aqueous sucrose solution was foamed in a glass tray in an air oven to produce solid organic foam. The carbonization of solid organic foam results in cellular amorphous carbon foams. The obtained carbon foams showed low density (0.115 to 0.145 g cm^{-3}) and compressive strength (~0.89 MPa). Narasimman et al. reported a faster process for the preparation of low-density carbon foams (0.053–0.085 g cm^{-3}) from molten sucrose using aluminium nitrate as a blowing agent(R Narasimman & Prabhakaran, 2012). Herein, the water vapour generated by –OH condensation is responsible for the nucleation and growth of bubbles. The aluminium nitrate helps in the generation and stabilization of gas bubbles in molten sucrose and enables the faster setting of the foam by producing H^+ ions which catalyze the –OH condensation. The carbon foams with improved oxidation resistance are produced from molten sucrose using boric acid instead of aluminium nitrate as a blowing agent(R Narasimman & Prabhakaran, 2013). The compressive strength of carbon foams produced from molten sucrose is improved by incorporating milled carbon fibre and activated carbon particles(Rajaram Narasimman et al., 2015; Rajaram et al., 2015). **Fig.1.17** shows the SEM image of the carbon composite foam prepared from sucrose and carbon fibre. The incorporation of MWCNT and graphene oxide enhanced the electrical conductivity and compressive strength of carbon foams produced from molten sucrose by thermo-foaming. These carbon foams exhibited high EMI shielding effectiveness(R Narasimman et al., 2016).

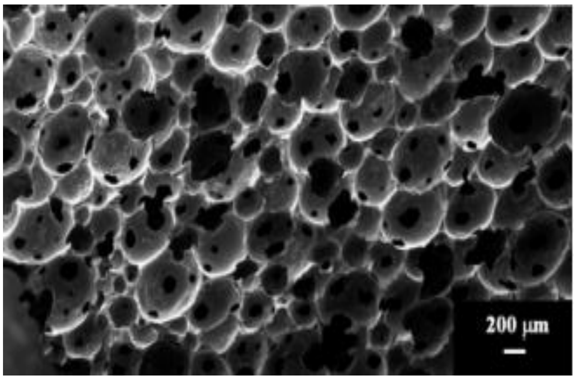

Fig. 1.17 SEM image of carbon composite foam prepared from sucrose and carbon fibre(Rajaram et al., 2015)

The cellular carbon foams produced from sucrose are brittle and produce debris during storage, transportation and further processing due to the large cell size. Wilson et.al prepared microcellular carbon foams from sucrose and NaCl powder by compression of a molding process(Wilson et al., 2017). In this, pastes of NaCl powder in molten sucrose are prepared by hot blending of the sucrose-NaCl mixtures. The pastes are set in a steel mould by hot pressing at 160 °C. The NaCl templates are removed by extraction with water after carbonization. The microstructure, compressive strength, foam density and thermal conductivity are controlled by changing NaCl to sucrose weight ratios in the range of 0.7 to 1.2. The uniform pore size distribution and a low density are achieved by using glycerol as a plasticizing additive(Wilson et al., 2018). The cell sizes of microcellular carbon foams are observed in the range of 3 to 6 μm. The prepared microcellular carbon foam exhibited low density (0.214 to 0.096 g cm^{-3}) and thermal conductivity (0.235-0.087 W $m^{-1}K^{-1}$). The photograph of a microcellular carbon foam body and its SEM microstructure is shown in **Fig. 1.18**. The thermal conductivity of the microcellular carbon foams is improved by the addition of graphite filler and the same is used as a host for form-stable wax-based phase change material for thermal energy storage (Wilson et al., 2019). Jana et al. also prepared composite carbon foams from sucrose and graphite powder by a foaming method. The prepared carbon composite foam exhibited high compressive strength (5 MPa) and thermal conductivity (7 Wm^{-1} K^{-1}) for storing wax-based phase change material(Jana et al., 2016).

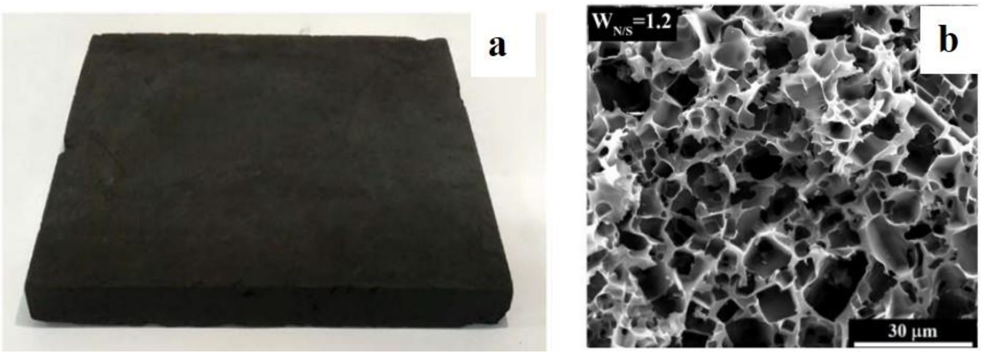

Fig.1.18 Photograph (a) and SEM image (b) of microcellular carbon foam (Wilson et al., 2017)

1.3.4 Properties of carbon foam

The properties of the carbon foam depend on the cell size, cell interconnectivity and crystallinity of the carbon. The cell size, cell interconnectivity and crystallinity of carbon foams depends on the precursors, processing method and heat-treatment temperature. The following section discusses the properties of the carbon foam such as density, compressive strength, thermal conductivity, electrical conductivity, fire resistance and EMI shielding effectiveness.

1.3.4.1 Density and porosity

Bulk density (ρb) is the ratio of the mass of the solid matrix to the volume of the foam body. The volume of the specimen is determined by measuring the dimension of a regular shaped specimen (commonly rectangular body) using vernier callipers. The bulk density of the foam is an important parameter as properties such as compressive strength, electrical conductivity, thermal conductivity and EMI shielding effectiveness depends on the bulk density.

The skeletal density of the material (ρs) is the ratio of mass to volume of the material, excluding the volume of the voids. It is determined by using a gas pycnometer with gas displacement. The relative density is the ratio of bulk density to the skeletal density of the material. Materials with a relative density below 0.3

are considered foams. If the relative density is greater than 0.3, the pores become isolated and the material is called porous solid(Gibson & Ashby, 1997).
The porosity is the percentage of the voids within the material. It is calculated from the relative density of the foam using the following formula (Equation 1.1):

$$\text{Porosity} = (1-\rho b/\rho s)*100 \qquad \text{(Equation 1.1)}$$

where ρb is the bulk density of the specimen, ρs is the skeletal density of the specimen

1.3.4.2 Compressive strength

The compressive strength of carbon foams depends on bulk density, cell size, cell interconnectivity and strut and ligament thickness. The strength of carbon foams is commonly evaluated in compressive mode. The compressive strength and Young's modulus are obtained from the compressive stress-strain measurements made on rectangular carbon foam bodies using a Universal Testing Machine. The carbon foams show brittle failure under compression. The typical stress-strain curve of a brittle carbon foam is shown in **Fig. 1.19**. The stress-strain curve shows an initial linear elastic region followed by a serrated plateau and a strain hardening region(Gibson & Ashby, 1997). The stress corresponding to the plateau region is taken as the compressive strength and the slope of the initial linear region is taken as Young's modulus.

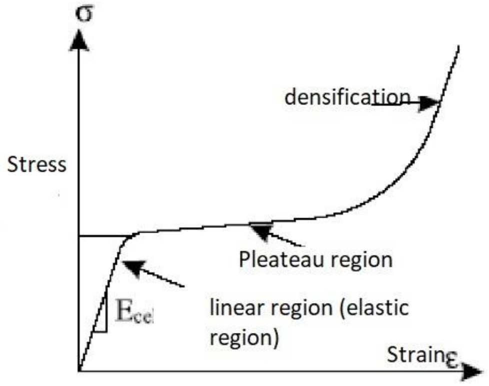

Fig. 1.19 Typical compressive stress-strain curve of a carbon foam(Sadighi & Salami, 2012)

The compressive strength of carbon foams depends on the nature of the precursors, processing method and heat treatment temperature. These parameters affect the density, pore size, pore interconnectivity and crystallinity of the carbon foam which in turn affect the compressive strength. Specifically, the mechanical strength is influenced by the combined effect of its relative density, percentage of open or closed cells, and the shape anisotropy ratios of cells. The closed-cell carbon foam normally exhibits better mechanical strength than open-cell carbon foams of the same density. Thermoplastic (pitch) derived carbon foams exhibit comparatively higher compressive strength than synthetic polymer and biomass-derived carbon foams(Baran et al., 2013; Chong Chen et al., 2006; Sizhong Li et al., 2007). The compressive strength of carbon foams is further improved by incorporating reinforcing additives. The reinforcing additives such as MWCNT, graphite powder, carbon powder, clay, carbon fibre and mesocarbon microbeads have been used for the improvement of the compressive strength of the carbon foams(Jana et al., 2014; R Narasimman et al., 2014, 2016; Sharma et al., 2020; X. Wang et al., 2006). Li et al. fabricated carbon foam with high compressive strength from mixtures of mesocarbon microbeads and mesophase pitch by foaming, carbonization and graphitization. The resultant carbon foam exhibited compressive strength of 23.7 MPa(Sizhong Li et al., 2007). Carbon foam derived from thermosetting plastics such as phenol-formaldehyde resin, polyimide, melamine, cyanate ester and polyarylacetylene, exhibited the compressive strength of 3.1-12.5 MPa, 0.25 MPa, 19.0 kPa, 3.15 MPa, 25.8 MPa, respectively(Ye et al., 2019). Luo et.al prepared carbon foam reinforced with $K_2Ti_{16}O_{13}$ whiskers from phenolic resin. The carbon foam produced exhibited a compressive strength of 7.43 MPa at 2 wt.% $K_2Ti_{16}O_{13}$ whiskers(Luo et al., 2011). On the other hand, the carbon foams derived from biomasses such as tannin, bread and sucrose exhibited a compressive strength of 3.6 to 6.9 MPa, 3.6 MPa, 0.115-0.145 MPa, (Jana et al., 2014; Prabhakaran et al., 2007a; Tondi et al., 2009; Y. Yuan et al., 2016b). Narasimman et al. used carbon fibre, carbon powder, MWCNT and graphene as reinforcing additives to improve the compressive strength of sucrose based carbon foams(R Narasimman et al., 2014, 2015, 2016; Rajaram Narasimman et al., 2015; Rajaram et al., 2015). The compressive strength of carbon foams prepared from various precursors is summarised in **Table 1.1**.

Table 1.1 Compressive strength of carbon foams derived from various precursors

Sl.No.	Precursor	Compressive strength (MPa)	Density (g cm^{-3})	Reference
1	Petroleum pitch	3.9	0.34	(Chong Chen et al., 2006)
2	Coal	2.9	0.32	(Chong Chen et al., 2004)
3	Coal tar pitch	18.7	0.67	(Chong Chen et al., 2006)
4	Asphaltene	18.7	0.83	(Baran et al., 2013)
5	Mesophase AR pitch	3.35	0.77	(Yu et al., 2014)
6	Mesophase with microbeads	23.7	0.78	(Sizhong Li et al., 2007)
7	Mesophase pitch with clay reinforcement	6.2-12.8	0.71-0.61	(X. Wang et al., 2006)
8	Phenolic-resin with $K_2Ti_{16}O_{13}$ whiskers	7.43	0.32	(Luo et al., 2011)
9	Phenolic resin with coal tar	13.1	0.74	(Farhan et al., 2014)
10	Cyanate ester	3.25-9.6	0.23-0.59	(T. Chen et al., 2015)
11	Polybenzoxazine	9.5	0.48	(Lorjai et al., 2009)
12	Phthalonitrile	1.86	0.152	(L. Zhang et al., 2016)
13	Polyarylacetylene	25.8	0.6	(M. Liu et al., 2007)

14	Bread	3.6	0.29	(Y. Yuan et al., 2016b)
15	Mimosa Tannin	3.6-6.9	0.13-0.51	(Jana et al., 2014)
16	Tannin	0.62	0.067	(Tondi et al., 2009)
17	Spruce sawdust	0.40-1.97	0.21-0.26	(Yargic & Ozbay, 2019)
18	sucrose	0.145	0.85	(Prabhakaran et al., 2007b)
19	Sucrose with carbon powder	0.42-3.4	0.138–0.22	(Rajaram Narasimman et al., 2015)
20	Sucrose with boric acid as a blowing agent	0.08-1.6	0.1-0.16	(R Narasimman & Prabhakaran, 2013)
21	Sucrose with kaolinite	0.08-0.21	0.072–0.108	(Ji et al., 2014)

1.3.4.3 Thermal conductivity

Thermal conductivity is the ability of a material to transfer heat under steady-state conditions. It is the measure of heat transfer within the material. Heat transfer within highly porous cellular material in the absence of forced fluid flow is due to conductive, convective and radiative mechanisms. The convective heat transfer within the fluid phase can be neglected since the smaller size of pores. The conductive heat transfer may occur through the solid network, lattice vibration, movement of the electron, fluid and molecular interactions(Gibson & Ashby, 1997). The radiative heat transfer is by electromagnetic radiation exchanged between solid walls or struts. The combined conductive and radiative heat transfers in cellular materials for most thermal applications can be characterized by an overall thermal conductivity. The thermal conductivity of carbon foam is typically calculated from the thermal diffusivity, specific heat and foam density using the following equation (Equation 1.2):

$$\kappa = \alpha \cdot \rho \cdot Cp \qquad \text{(Equation 1.2)}$$

where, κ = Thermal conductivity (W $m^{-1} \cdot K^{-1}$), α = Thermal diffusivity (cm^2 s^{-1}), Cp =Specific heat (J g^{-1} K^{-1}), and ρ = Density (g cm^{-3}).

The thermal conductivity of the carbon foam depends upon the crystalline structure, density, cell size and cell interconnectivity. Therefore, thermal conductivity depends on the type of carbon precursors, processing method and heat treatment temperature used for the preparation of carbon foams. The graphitic carbon foams prepared from mesophase pitch generally exhibit higher thermal conductivity than the amorphous/turbostratic carbon foams prepared from synthetic polymers or biomasses. The thermal conductivity of carbon foams decreases with the increase of porosity and decrease of pore size. The closed-cell foam exhibits lower thermal conductivity than the open cell foams of the same density. The thermal conductivity of carbon foams is further modulated by incorporating fillers such as graphite powder, graphene, clay, CNT, carbon fibres and $K_2Ti_6O_{13}$ whiskers (Kumar, Dhakate, Gupta, et al., 2013; Luo et al., 2011; R Narasimman et al., 2015; X. Wang et al., 2006; Wilson et al., 2019; K. Zhang et al., 2016). The thermal conductivity values of carbon foams prepared from various precursors are tabulated in Table **1.2**.

Table 1.2 Thermal conductivity of carbon foam from various precursors

Sl.No.	**Precursors**	**Thermal conductivity ($Wm^{-1}K^{-1}$)**	**Density (g cm^{-3})**	**Reference**
1	Coke and mesocarbon microbeads	0.24-0.26 (100 °C)	0.38-0.45	(He et al., 2013)
2	SiO_2 aerogel and pitch	0.1-0.2	0.18-0.39	(H. Liu et al., 2019)

3	Coal tar pitch and montmorillonite clay	0.25-2	0.67-0.727	(X. Wang et al., 2006)
4	Phenolic resole resin and $K_2Ti_6O_{13}$	0.24-0.4	0.23-0.25	(Luo et al., 2011)
5	Phenolic resin and cenospheres	0.02-0.21	0.3-0.45	(Kumar et al., 2018a)
6	Tannin	0.44	0.067	(Tondi et al., 2009)
7	Sucrose with aluminium nitrate blowing agent	0.05-0.15	0.04 to 0.07	(R Narasimman & Prabhakaran, 2012a)
8	Sucrose with aluminium nitrate and boric acid as blowing agent	0.043 to 0.057	0.103–0.16	(R Narasimman & Prabhakaran, 2013)
9	Bismaleimide (BMI) resin and montmorillonite clay	0.1-0.46	0.26-0.32	(Y. Wang et al., 2017)

1.3.4.4 Fire resistance

Fire-resistant materials are designed to resist burning and withstand heat. These are one of the major components in the manufacturing of ships, buildings and automobiles. Usually, polymer-based fire-retardant coatings are applied to protect core structures. These coatings exhibit poor oxidation resistance, poor chemical resistance to strong acidic/alkaline reagents and organic solvents as well as release toxic gases. Though carbon materials undergo oxidation at high temperatures, they do not catch fire and support a sustainable flame. Therefore, carbon foams are candidate materials for lightweight thermally insulating fire-resistant structural material. Carbon foams derived from pitches, synthetic organic polymers and biomasses exhibit excellent fire resistance and do not catch fire even when exposed to oxyacetylene flame(Kumar et al., 2019; Tondi et al., 2009). A photograph of a carbon foam body prepared from sucrose exposed to oxyacetylene flame showing its fire resistance is shown in Fig.**1.20 (a)**. Though the carbon foam body does not catch fire the oxyacetylene flame pierce through due to the oxidation of carbon. A Photograph of the carbon foam body after exposure to oxyacetylene flame is shown in **Fig.1.20 (b)**.

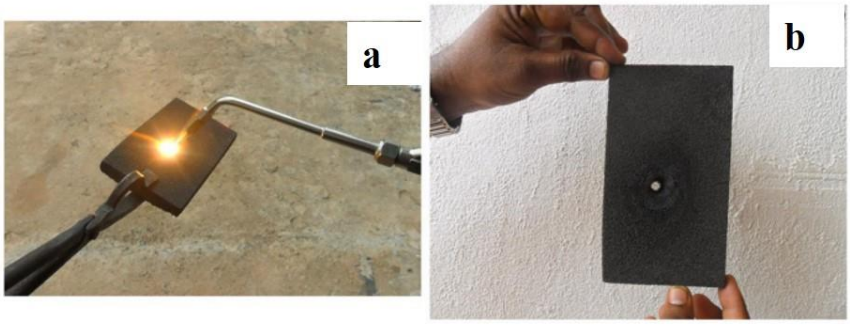

Fig.1.20 A photograph of carbon foam during exposure to oxyacetylene flame(a) and after flame exposure(b) (Rajaram Narasimman et al., 2015)

1.3.4.5 Electrical conductivity

The carbon foams are electrically conducting due to the presence of conjugated π-electron in the aromatic carbon (graphene layer). The electrical conductivity of the carbon foam mainly depends on the crystallinity and bulk density(Gibson & Ashby, 1997). The electrical conductivity generally increases linearly with an increase in the density of the carbon foams. The resistivity of solid foam is directly related to relative density as per the following formula **(**Equation 1.3):

$$R_f \propto Rs / (\rho^*/\rho_s) \qquad \text{(Equation 1.3)}$$

where R_f is the resistivity of the foam, Rs is the resistivity of the solid, ρ^*/ρ_s is the relative density

As the density falls, the average cross-section available for conduction decreases and the tortuosity of the current path increases. Both of them raises resistivity.

The electrical conductivity of the carbon foam depends on the type of carbon precursors and processing conditions such as heat-treatment temperature. Normally, pitch derived carbon foams exhibit fairly high electrical conductivity than synthetic polymer and biomass-derived carbon foams. The pitch derived carbon foams have a graphitic structure compared to the amorphous nature of carbon foams produced from synthetic polymers and biomasses. The heat-treatment temperature above 1500 °C improve the degree of crystallinity and thereby increase the electrical conductivity of carbon foams. Thermosetting polymer and biomass-derived turbostratic carbon foams do not promote the easy movement of electrons in the foam body and therefore exhibit lower electrical conductivity. The carbon foams derived from thermosetting polymers such as phenolic resin and polyimide exhibited electrical conductivity in the range of 1.0- 250 S cm^{-1}(Agrawal et al., 2019; Kumar, Dhakate, Gupta, et al., 2013; Patle et al., 2020; Tang et al., 2018). On the other hand, the biomass-derived carbon foam exhibited an electrical conductivity in the range of 0.05-70 S cm^{-1}(Letellier, Macutkevic, Paddubskaya, Klochkov, et al., 2015). The electrical conductivity of the carbon foam is further improved by the addition of fillers such as CNT, graphene and graphite powders (Agrawal et al., 2019; Amini et al., 2011; R Narasimman et al., 2015; Patle et al., 2020).

1.3.4.6 EMI shielding Effectiveness

Electromagnetic interference (EMI) is the disruption of the operation of an electronic device when it is in the vicinity of an electromagnetic field (EM field) that is caused by another electronic device. The materials used to shield the electromagnetic interference are called EMI shielding materials(Kuruvilla et al., 2019). Electromagnetic interference shielding refers to the reflection and absorption of electromagnetic radiation by a material that acts as a shield against the penetration of the radiation(Jaroszewski et al., 2018). In recent years, EMI shielding materials have been of great interest due to the tremendous increase in the number of electronic devices which generate severe electromagnetic radiations. The traditionally used metallic materials shield EM waves mainly by reflection. In addition, they are heavy and prone to corrosion. The development of lightweight and corrosion-resistant materials with absorption dominated high shielding effectiveness is of utmost importance(Sankaran et al., 2018). In this connection, carbon-based materials have gained increasing attention owing to their high electrical conductivity, and good corrosion resistance(Geetha et al., 2009). The creation of porosity in carbon materials make them lighter and improves their EMI shielding effectiveness by reducing the impedance mismatch with air, creating more interfaces for polarization and promoting reflections back and forth within the pores. That is, carbon foams are superior to the metal-based EMI shields currently in use. The incorporation of dielectric and magnetic particles in the carbon framework provides an additional enhancement in EMI shielding due to relaxation losses by the interaction of EM waves with the electric and magnetic dipoles, respectively.

The attenuation of EM waves by the shielding material has a contribution from reflection at the surface and absorption throughout the material due to conduction and polarization losses. The multiple internal reflections within the pores present in the material facilitate absorption of EM waves preventing their early transmission. The sum of the contributions of reflection (S_R), absorption (S_A) and multiple internal reflections (S_M) is termed as total shielding effectiveness, SE_T.

$$S_T\ (\mathrm{dB}) = S_R + S_A + S_M = -10 \log\left(P_t/P_i\right) \qquad \text{(Equation 1.4)}$$

where P_i and P_t are the incident and transmitted power, respectively(Kuruvilla et al., 2019). The mechanism of EMI shielding is schematically represented in Fig. **1.21**. When the total shielding effectiveness of the materials is more than 10 dB, the losses related to total internal multiple reflections can be neglected and the total shielding effectiveness (S_T) will be written as (Equation 1.5):

$$S_T = S_R + S_A \qquad \text{(Equation 1.5)}$$

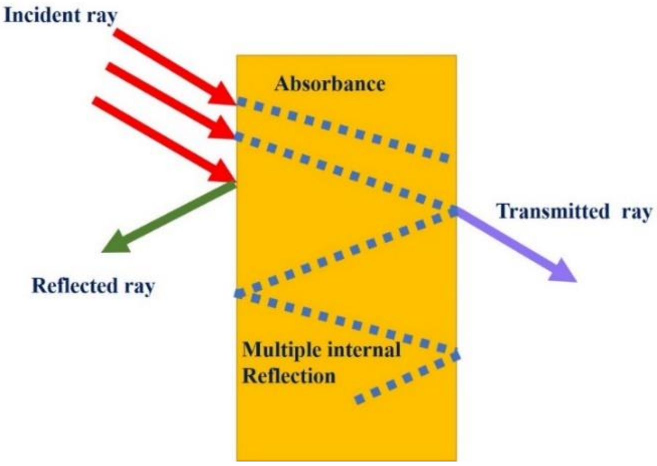

Fig. 1.21 Schematic representation of EMI shielding mechanism

The carbon foams and carbon foam composites usually exhibit an absorption dominated electromagnetic interference shielding. An effective method to enhance the EMI shielding performance is the incorporation of a secondary phase with high electrical conductivity or magnetic permeability. Rajeev Kumar and co-workers synthesized carbon foams of high EMI shielding effectiveness from coal tar pitch and ferrocene(Kumar, Dhakate, & Mathur, 2013). Ni-Zn ferrite is investigated as fillers in carbon composite foams for EMI shielding due to its high magnetic permeability and magnetic loss(H. Liu et al., 2016). The resultant carbon composite foam exhibited absorption dominated superior EMI shielding effectiveness. Incorporation of multiwalled carbon nanotube, graphene, and reduced graphene oxide exhibited improved mechanical strength and electrical conductivities as well as high EMI shielding effectiveness in carbon foams derived from sucrose and phenolic resin(Agrawal et al., 2019; Kumar, Dhakate, Gupta, et al., 2013; Q. Li et al., 2016a; R Narasimman et al., 2016). The EMI shielding effectiveness of the carbon foams prepared from various precursors reported in the literature is summarized in **Table 1. 3**.

Table 1.3 EMI shielding effectiveness of carbon foams reported in the literature

Sl. No.	**Absorbing material**	**EMI shielding effectiveness (dB)**	**Reference**
1	Shape-memory carbon foam composites	25.3–44.7	(Jia et al., 2021)
2	rGO/sugarcane derived hybrid carbon foams	39-53	(L. Wang et al., 2020)
3	Carbon-rGO composites foam	−23.2 to −50.7	(Agrawal et al., 2019)
4	Phenolic-based carbon foam modified with	8-32	(Y. Zeng et al., 2019)

	GO/SiO$_2$ hybrid nanomaterials		
5	Carbon foam from bread	17.2	(Y. Yuan et al., 2016a)
6	Carbon foam from Platanus Orientalis	~25-38	(FARHAN et al., 2018)
7	carbon-cenosphere composite foams	−25.2 to −48.6	(Kumar et al., 2018b)
8	Phenol-formaldehyde resin derived carbon-MCMB composite foams	-27.5 to -62.4	(Sharma et al., 2020)
9	Carbon foam from melamine	23	(H.-G. Shi et al., 2021)
10	Ultrathin carbon foam from polyimide/graphene composite	18-24	(Y. Li et al., 2016)
11	Microcellular carbon foam from sucrose by NaCl particle templating	24.7 to 41.7	(Wilson et al., 2018a)
12	Carbon composite foam from sucrose and multi-walled carbon nanotube	26 to 39	(R Narasimman et al., 2016)
13	Carbon foam from cotton with	36	(Gu et al., 2020)

	reduced graphene oxide		
14	Open-cell carbon foam from phenolic composite consisting of nanoferric oxide and MWCNT	~62	(Q. Li et al., 2016b)
15	Carbon foam derived from polyimide	39 - 54	(Jia et al., 2020)

1.3.4.7 Acoustic properties

Carbon foams are scarcely studied for their acoustic properties compared to other applications such as thermal management, energy storage and EMI shielding. In this regard, Celzard et al. investigated the acoustic properties of carbon foams with reticulated and cellular structures(A Celzard & Cedex, 2013). Carbon foams prepared from tannin exhibit high air flow resistance potential but low sound absorption due to the high density. The high sound absorption coefficient is achieved by improving the porosity of the carbon foams. The studies indicated that the cellular carbon foams show better sound absorption properties at lower frequencies and vice versa for the reticulated carbon foams (Amaral-Labat et al., 2013; Letellier et al., 2017). Mesophase pitch-based carbon foams and composite graphite foams are also studied for acoustic insulation. The highly porous and low-density carbon foam obtained from naphthyl-synthesized mesophase pitch showed good absorption properties even at low frequencies(N. Gao et al., 2018).

1.3.5 Applications of Carbon foams

Carbon foams find a large number of applications in industrial and strategic sectors owing to their excellent properties. The properties can be tuned by selecting suitable precursors and processing methods. The following section briefly describes some of the important applications of carbon foams.

1.3.5.1 Thermal insulation and thermal protection

Due to the unique properties such as high thermal stability, low thermal conductivity ablative property and lightweight, carbon foams can be used as high-temperature thermal insulation and ablative structures in thermal protection systems in aerospace. Synthetic polymers and biomass-derived amorphous carbon foams are preferred for thermal protection applications due to their low thermal conductivity. **Fig. 1.22** is showing carbon foam exposed to thermal protection test. The limitations of carbon foams are their brittle nature and oxidation in the air atmosphere at high temperatures. Therefore, the thermal protection and ablative structure based on carbon foams are fabricated in the form of sandwich structures in which the carbon foam forms the core and carbon-carbon composites form the facing sheets. A photograph of a sandwich composite structure using carbon foam as a core is shown in **Fig. 1.23**.

Fig. 1.22 A photograph of carbon foams during thermal protection test(*www. Cofoam/Tps*, n.d.)

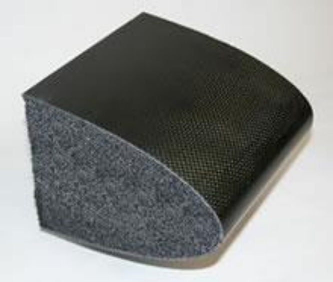

Fig. 1.23 Sandwich composite with carbon foam core(*www. Cfoam/Thermalprotection.Jpg*, n.d.)

1.3.5.2 Host for phase change materials

Sustainable development demands conservation of energy as the conventional resources of energy such as petroleum is rapidly depleting. Solar thermal energy is one of the options. A large amount of solar energy is wasted during the daytime. If this solar energy is stored and used during demand, the consumption of fossil fuels can be reduced, alleviating energy shortage and environmental issues. Thermal energy storage systems using phase change materials (PCMs) are used for solar thermal energy storage. PCMs are substances that, when going through a change in their physical state, can absorb or release large amounts of latent heat. Among the various possible phase transitions, the solid-liquid transition is widely used for solar thermal energy storage. However, the low thermal conductivity and weak photo-absorption of pure PCMs hinder their efficient usage. To overcome these issues the phase change materials are stored in porous media made of thermally conducting materials. Carbon foams are candidate materials for hosting the phase change materials for thermal energy storage due to their interconnected porous structure and high thermal conductivity. The main advantage of carbon foams as a host matrix is that it permits a high PCM-to-carbon foam volume ratio and enhanced thermal conductivity, which increases the energy storage capacity of the device(Khan et al., 2018). Maleki et al. used commercially available melamine derived carbon foam (CF) as a host for three different organic phase change materials (PCMs), including polyethylene glycol (PEG), paraffin (PA), and palmitic acid (PAA). The prepared CF/PEG, CF/PA, and CF/PAA composite PCM exhibited a considerable latent thermal storage capacity of 145.7, 124 and 198.2 J g^{-1}, respectively. The CF/PA system showed a better cycle ability than other composites after 200 frequent heating/cooling cycles. The black coloured CF/PA composite exhibited a significant increase in light absorbance and thereby a high light-to-thermal energy conversion efficiency (95%). The CF/PA composite could provide domestic hot water (DHW) for a building with an efficiency of 88.1%(Maleki et al., 2020). The photograph of carbon foam-paraffin composites showing their form-stability (**Fig.1.24a**) and the schematic of the water heating system using phase change materials **(Fig.1.24b**) are shown in **Fig. 1.24**.

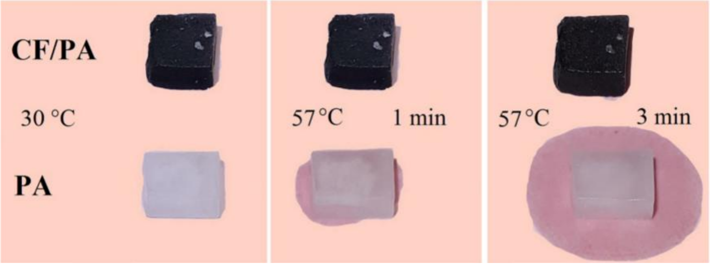

Fig. 1.24a Photographs of the pure PCMs and their composite stability at different temperatures(Maleki et al., 2020)

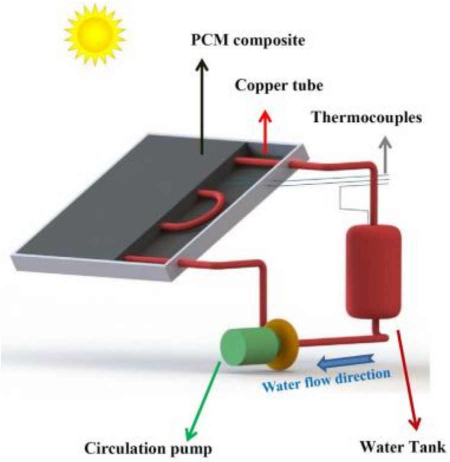

Fig. 1.24b Schematic diagram of solar heating system(Maleki et al., 2020)

1.3.5.3 Thermal management

A large amount of heat energy is produced in various electronic types of equipment during their operation. This heat generated is detrimental to their long-term function. Therefore, heat sinks are used to absorb and dissipate this heat energy and thereby protect the device. Conventionally, metal-based fin structures and foams are used as heat sinks in electronic systems due to their high thermal conductivity. ORNL's graphite foam developed by Klett et al. has a high thermal conductivity in the range of 50-150 W $m^{-1}K^{-1}$. The specific thermal conductivity of > 300 W $m^{-1}K^{-1}g^{-1}cm^{3}$ observed is significantly higher than that of the conventional metal foams (Gallego & Klett, 2003). The heat sink application tested by replacing a standard aluminium heat sink from a Pentium 133 microprocessor with a graphite foam showed superior performance(J. Klett & Conway, 2000). Wu et.al investigated a V-shaped corrugated carbon foam heat sink for thermal management of electronics with forced air convection. The carbon foam (PocoFoam) of 51 mm Length, 51 mm width,19 mm height was used for the study. The performance of the carbon foam heat sink was characterized in terms of heat transfer coefficient and flow resistance. A heat transfer coefficient of 2210 Wm^{-2} K^{-1} was achieved at airflow speed of 7.8 m s^{-1} and at a pressure drop of 1320 Pa, which is higher than the performance target for the next generation advanced heat sink material(W. Wu et al., 2011). **Fig. 1.25** shows a photograph of a corrugated structure of carbon foam for heat sink application.

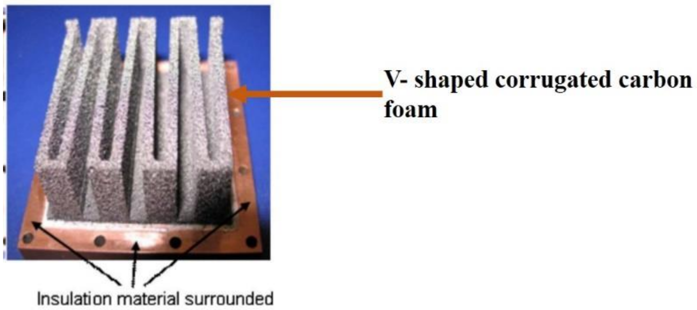

Fig. 1.25 Photograph of V-shaped corrugated heat sink (W. Wu et al., 2011)

1.3.5.4 Adsorbent for toxic chemicals and Oil absorber

The carbon foams are used as monolithic adsorbents due to their high surface area and interconnected pore structure. The thermosetting material derived carbon foam with an open-cell structure can achieve high surface area and excellent hydrophobicity. The carbon foam has been extensively reported as absorbents for organic pesticides, toxic gases, oil, organic solvent etc. Narasimman et al. prepared carbon composite foam from molten sucrose and activated carbon powder which exhibited a good CO_2 adsorption capacity of 3.04 mmol g^{-1} and selectively absorbed oil from the oil-water emulsion(Narasimman et al., 2014b). Lee et al. used carbon foam derived from phenolic resin for the removal of copper and lead from aqueous solutions. The maximum adsorption capacity of lead and copper determined was 91 mg g^{-1} and 247 mg g^{-1}, respectively(C.G. Lee et al., 2015). Lightweight carbon foams of high hydrophobicity synthesized from cotton and graphene oxide by Gu et.al exhibited high oil absorption capacity in the range of 16-27 times of their weight(Gu et al., 2020). The hydrophobic carbon foams synthesized from lignin–resorcinol–glyoxal (LRG) by Rao et.al absorbed 24 times its weight of oils and organic solvents(Rao et al., 2020).

1.3.5.5 Energy storage

Carbon foams find applications in electrochemical energy storage systems as electrodes due to their interconnected pore structure, high porosity, large surface area, high electrical conductivities and excellent corrosion resistance. These unique features endow easier and faster ion and electron transport throughout the electrode. Their structural stability improves the life cycle of the energy storage device. Besides these, the electrochemically active material can be loaded into the porous structure of the carbon foam which enables high capacity with enhanced energy and power densities(Khan et al., 2018). Mainly, carbon composite foams with CNT and graphene are used for energy storage applications(Qiu et al., 2020; Rodríguez-García et al., 2018; Tjandra et al., 2018; Vazquez-Samperio et al., 2020; Yuhang Zhang et al., 2021).

Wei and co-workers reported 3D nitrogen-doped carbon foam-CNT hybrids hosting TiO_2 nanoparticles as a free-standing electrode for Li-ion batteries. The doping of nitrogen endows carbon foam with enhanced electron transfer and excellent wettability, hence nitrogen-doped carbon foam is widely used for the application of energy storage(W. Yuan et al., 2018).

Lithium-sulphur (Li-S) battery research is drawn attention due to its high theoretical capacity and energy density. But the fabrication and utilization of Li-S batteries are limited by the volume expansion during the charge-discharge process and poor conductivity of sulphur. Carbon foams provide a conductive framework and improve sulphur loading. Xiang and group fabricated a 3D flexible multifunctional hybrid of nitrogen-doped carbon foam@CNTs decorated with ultrafine MgO nanoparticles for use as a current collector in Li-S batteries. The dense carbon nanotubes wrapped on the carbon foam matrix enhance flexibility and build an interconnected conductive network for rapid ionic/electronic transport. Synergistic action of MgO nanoparticles and *in situ* N-doping significantly suppresses enhanced chemisorption of lithium polysulfides. Hence, it acts as a good electrode with a high sulphur loading of 14.4 mg cm^{-2}, a high gravimetric capacity of 612 mAh g^{-1} and an areal capacity of 8.8 mAh cm^{-2} after 50 cycles at 0.05 C(Xiang, Wu, et al., 2017).

Carbon foams are also used in supercapacitors of high energy density and high specific capacitance. Park et.al fabricated a porous carbon foam by polycondensation of resorcinol and formaldehyde by PMMA as a pore generator. In order to improve wettability with electrolyte and surface activity, carbon foam is doped with nitrogen. Nitrogen-doped carbon foam to improve the energy density of the supercapacitor. N-doped carbon foam exhibited the specific capacitance (137.8 F/g at a 10 mV/s scan rate with 6 M KOH electrolyte) and exhibited good cyclic stability(Park et al., 2015).

1.3.5.6 EMI shielding

The lightweight, relatively high strength, high thermal stability, excellent corrosion resistance and high EMI shielding effectiveness made the carbon foams attractive for EMI shielding applications in the strategic sector. The shortcomings of metal-based EMI shields currently used can be overcome by using carbon foams. The carbon foam-based EMI shielding improve the stealth of defence systems as the mechanisms of EMI shielding is absorption dominated which reduce the chance of detection by the radars of the enemy. The electronic enclosures made of CFOAM $^{(R)}$ were reported to provide greater than 60 dB shielding effectiveness for RF waves of frequency in the range of 100 to 20 GHz(*EMI Shielding - CFOAM® Carbon Foam*, n.d.). A photograph of EMI shielding enclosures made from CFOAM is shown in **Fig. 1.26.**

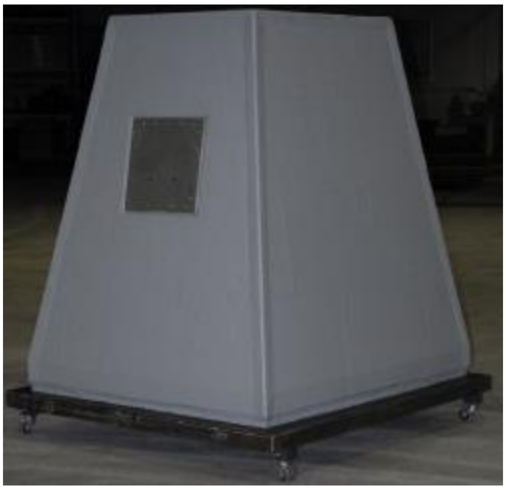

Fig.1.26 A photograph of EMI shielding enclosures made from CFOAM(*www.Cfoam.Com/Emi Shielding*, n.d.)

1.4 The Objective and Scope of the thesis

Generally, carbon foams are processed from coal, pitches and synthetic polymers prepared from petroleum-derived monomers. Fossil fuels which are the sources of the above precursors are depleting fast because of rapid industrialization. Therefore, the researchers are searching for alternative and renewable carbon precursors. Biomass is a renewable resource of carbon which is available in large volumes at a relatively low cost. A large number of biomasses are studied for the preparation of undoped and hetero-atom doped activated carbons for applications in energy storage, adsorption and catalysis. On the other hand, biomasses such as tannin, sucrose, olive stone and lignin are studied as precursors for the preparation of carbon foams. However, large quantities of biomasses such as rice husk, sawdust, natural cotton and newspaper are either wasted or underutilized. There is no report on the preparation of monolithic structural carbon foams from the above biomasses. The conversion of these biomasses into monolithic carbon foams generate wealth from waste. In addition, the utilization of newspaper waste for carbon foam preparation helps the management of municipal solid waste. The present thesis focus on the eco-friendly and cost-effective processing of these biomasses to monolithic carbon-composite foams.

The specific objectives of the thesis are as below:

(i) To prepare monolithic carbon composite foams from biomasses
(ii) To study biomasses such as natural cotton, sawdust, rice husk and newspaper waste as a precursor for carbon composite foams.
(iii) To develop an eco-friendly processing method for carbon composite foam monolith from the biomasses
(iv) To characterize the carbon composite foams prepared from the biomasses
(v) To study the carbon composite foams for thermal insulation and EMI shielding applications

1.5 Organization of the thesis

This thesis describes the methodology for the preparation of carbon composite foams from biomasses such as natural cotton, sawdust, rice husk, and newspaper waste using sucrose as a binder. The thesis focus on the development of an eco-friendly and simple processing method for the preparation of carbon composite foams from the biomasses. The carbon composite foams are characterized in detail using spectroscopic and microstructure analysis and mechanical property evaluation. The thermal conductivity and EMI shielding effectiveness of the carbon composite foams are evaluated for possible applications in thermal protection and EMI shielding. The thesis is organized into six chapters.

Chapter 1 provides a state-of-the-art literature survey on porous carbon and carbon foams with a special focus on biomass-derived carbon. This chapter provides a brief description of the properties and potential applications of carbon foams along with the research problem and objectives of the thesis.

The details of materials used for the preparation of carbon composite foams is presented in **Chapter 2.** The processing of biomasses into carbon composite foams is described in this chapter. The characterization methods used for the evaluation of carbon composite foam are also described.

In **chapter 3**, the characterization of the carbon composite foams by XRD, Raman spectra, microstructure and textural property analysis is presented. The density, compressive strength, electrical conductivity, thermal conductivity and EMI shielding effectiveness of carbon composite foams are discussed as a function of the concentration of sucrose solution used for their preparation by filter-pressing.

In **Chapter 4**, the characterization of these carbon composite foams for crystallinity, textural properties and pore structure is presented. The effects of sucrose concentration on density, compressive strength, electrical conductivity, thermal conductivity and EMI shielding effectiveness of the carbon composite foams are discussed.

Chapter 5 The C/SiO_2 and C/SiC composite foams are characterized for SiO_2 and SiC content, crystallinity, pore structure and the results are discussed. The effects of sucrose solution concentration and high-temperature heat-treatment for carbothermal reduction of silica to SiC on density, compressive strength, thermal conductivity and EMI shielding effectiveness of carbon composite foams are presented.

The carbon-gehlenite composite foams are characterized for gehlenite content, crystallinity, textural properties and the results are presented in chapter 6. The density, compressive strength, thermal conductivity and EMI shielding effectiveness evaluated for the carbon composite foams are discussed as a function of sucrose solution concentration.

The outcome of the study is summarized in **Chapter 7**. This chapter also briefs on the scope for future research on this subject.

CHAPTER-2

MATERIALS AND METHODS

2.1 Materials

Biomass such as cotton, sawdust, rice husk and waste newspaper were used for the preparation of carbon composite foams. The cotton fibre was procured from a local market. Sawdust of *Artocarpus hirsutus* wood was collected from a local sawmill. Rice husk was collected from a local rice mill. The waste newspaper was from the author's house. The food-grade sucrose was procured from a local market. The distilled water was used for the preparation of the sucrose solution.

2.2 Methods preparation of carbon composite foams

2.2.1 Processing of carbon composite foam using cotton

The solution of concentrations in the range of 100 to 700 g L^{-1} were prepared by dissolving the sucrose in the distilled water at room temperature. 40 g of cotton fibre was dispersed in 3 litres of the sucrose solution by agitating with a glass rod. The dispersed carbon fibre was consolidated by using a set-up fabricated in-house from a PVC pipe, Buchner funnel filter-flask and mild steel piston. A photograph of the filter-pressing set is shown in **Fig. 2.1**. The cotton fibre dispersed in the sucrose solution was poured into the PVC pipe of the filter-pressing setup and consolidated by filtration of sucrose solution through a carbon cloth placed on the Buchner funnel. A gentle hand pressing with the piston was given towards the end of the consolidation process. The sucrose solution collected in the filter flask was reused for the preparation of subsequent samples of the same composition. The sucrose solution retained in the filter-pressed bodies was frozen by keeping in a freezer at -70 °C for 24 hours. The frozen bodies were freeze-dried in a lyophilizer (Lyodel 85, Lyodel pumps, India) to produce sucrose bonded cotton composite bodies.

The sucrose bonded cotton composite bodies were heated in an air atmosphere at 160 °C for 2 h to caramelize the sucrose. The heating rate was 1 °C min^{-1}. The caramel bonded cotton bodies were carbonized by heating in an inert atmosphere furnace at 900 °C for 2 h at a heating rate of 1 °C min^{-1}. Ultrapure (99.99%) argon was used for creating the inert atmosphere. The samples were unloaded after the natural cooling of the furnace to room temperature. The argon atmosphere was maintained during cooling. The preparation of carbon composite foam is schematically represented in **Fig. 2.2**.

Fig. 2.1 Photograph showing the filtration set-up

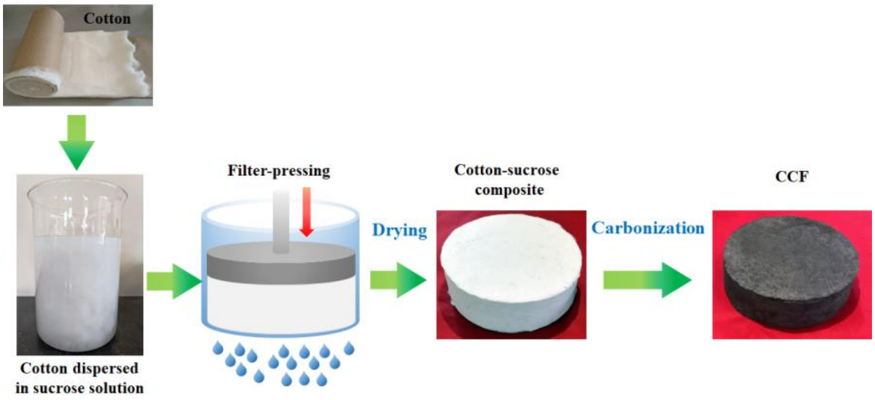

Fig. 2.2 Schematic representation for the processing of carbon composite foams

2.2.2 Processing of carbon composite foams using sawdust

The sawdust collected from a local sawmill was dried in an air oven at 100 °C for 24 hours. The dried sawdust was ground in a kitchen grinder mixer and sieved through a mesh of size 1 mm. The sucrose solution of concentrations in the range of 100 to 700 g L^{-1} was prepared. 40 g of the sawdust powder was mixed with 500 ml sucrose solution of various concentrations to produce slurries. The slurries were stirred for 15 minutes using a mechanical stirrer for proper wetting of the sawdust particles with the sucrose solution. The sawdust slurry was poured into the PVC pipe of the filter-pressing setup and the sucrose solution was allowed to filter out through the Buchner funnel to consolidate the particles. A plastic mesh was placed on the Buchner funnel to avoid the loss of sawdust particles through the filtrate. Towards the completion of natural filtration, a gentle hand pressing with the mild steel piston was applied for proper consolidation to produce a cylindrical body. The consolidated bodies removed from the filter-pressing setup were cooled in a freezer at -70 °C and then freeze-dried. The freeze-dried bodies were heated in an air oven at 160 °C for 4 hours. The heating rate was 20 °C hr^{-1}. The heat-treated bodies were carbonized in an inert atmosphere furnace at 900 °C for 2 hours. Ultrapure argon was used to create the inert atmosphere. The heating rate was 0.5 °C min^{-1} up to 600 °C and then 1°C min^{-1}. The flow chart for the preparation of carbon composite foams from sawdust is shown in **Fig.2.3**.

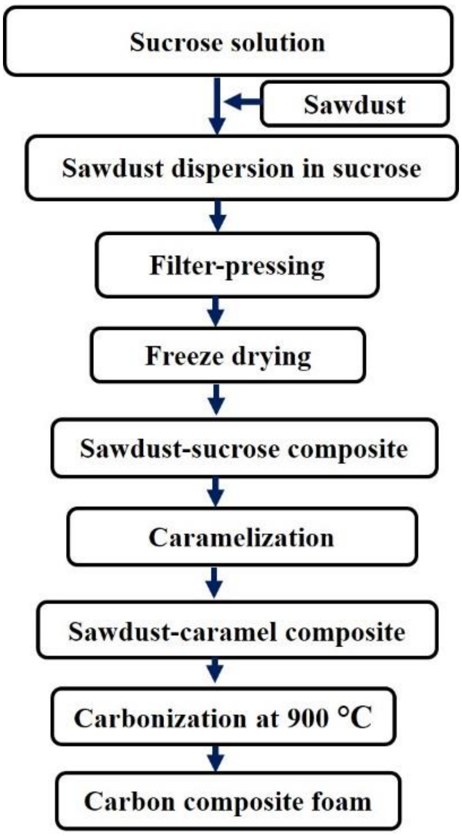

Fig. 2.3 Flow chart of the processing step for carbon composite foam

2.2.3 Processing of C/SiO_2 and C/SiC composite foams

The rice husk collected from the rice mill was washed with distilled water and dried in an air oven at 100 ^{o}C. The dried rice husk was ground to a powder using a flour mill. Solution of concentrations in the range of 100 to 700 g L^{-1} was prepared by dissolving sucrose in distilled water. Nearly 60 g of rice husk powder was dispersed in 500 ml of the sucrose solution by stirring using a mechanical stirrer. The rice husk powder dispersion in the sucrose solution was poured into the PVC pipe of the filter-pressing set-up and particles were consolidated into cylindrical bodies by filtration through the Buchner funnel. The consolidated body was gently hand pressed using the stainless-steel piston before removal from the PVC pipe. The filter-pressed bodies were frozen in a deep freezer at -50°C and then freeze-dried to produce rice husk-sucrose composites. The rice husk-sucrose composite bodies were annealed at 160 °C for 2 hours in an air oven. The annealed bodies placed into a furnace were heat-treated at 900 °C for 2 hours in an ultrapure argon atmosphere at a heating rate of 1°C min^{-1}. The carbonized bodies were further heat-treated in a high-temperature sintering furnace at 1600 °C for 2 hours under the ultrapure argon atmosphere. The heat-treated bodies were removed from the furnaces after cooling to room temperature. The same inert atmosphere was maintained during cooling. The flow chart for the processing of composite foams is shown in **Fig. 2.4**.

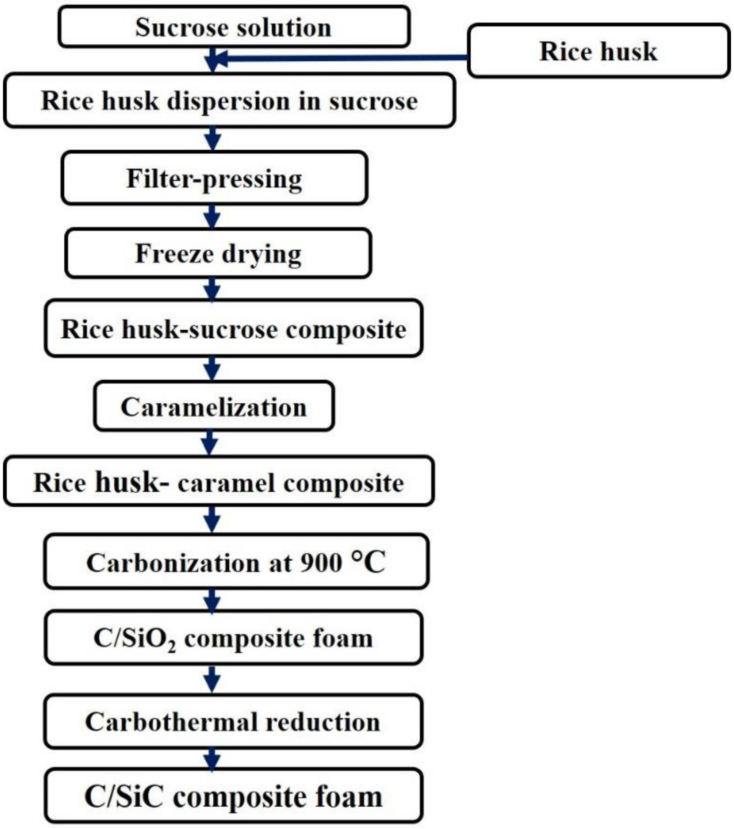

Fig. 2.4 Flow chart for the preparation of **C/SiO$_2$** and **C/SiC** composite foams

2.2.4 Processing of carbon composite foams using newspaper

The solution of various concentrations in the range of 100 to 700 g L^{-1} were prepared by dissolving the sucrose in distilled water. 50 g of the shredded newspaper was soaked in 1.5 L of sucrose solution for 1 hour. The newspaper soaked in the sucrose solution was thoroughly mixed using a kitchen mixture for 5 minutes to form a newspaper pulp. The photograph of newspaper pulp is displayed in **Fig. 2.5**. The newspaper pulp was poured into the PVC pipe of the filter-pressing setup and consolidated to a cylindrical body of 3 cm height and 10 cm diameter by vacuum filtration using a vacuum pump. A gentle pressing was applied towards the end of the consolidation by inserting a mild steel piston to prevent the lateral shrinkage at the top of the body. The consolidated wet bodies removed from the filter-pressing setup was dried in an air oven at 70 °C to a constant weight and then at 100 °C for 4 hours to form newspaper-sucrose composites. The newspaper-sucrose composites were annealed at 160 °C for 12 hours in an air oven. The heating rate of 1 °C min^{-1} was used from 100 to 160 °C. The annealed newspaper-sucrose composites were heated in an inert atmosphere furnace at 900 °C for 2 hours at a heating rate of 1 °C min^{-1}. Ultrahigh pure (99.99 %) argon was used to create the inert atmosphere. The same inert atmosphere was maintained during the cooling of the furnace. The schematic representation of the processing of carbon composite foam from newspaper waste is given in **Fig. 2.6**.

Fig. 2.5 A photograph of newspaper pulp

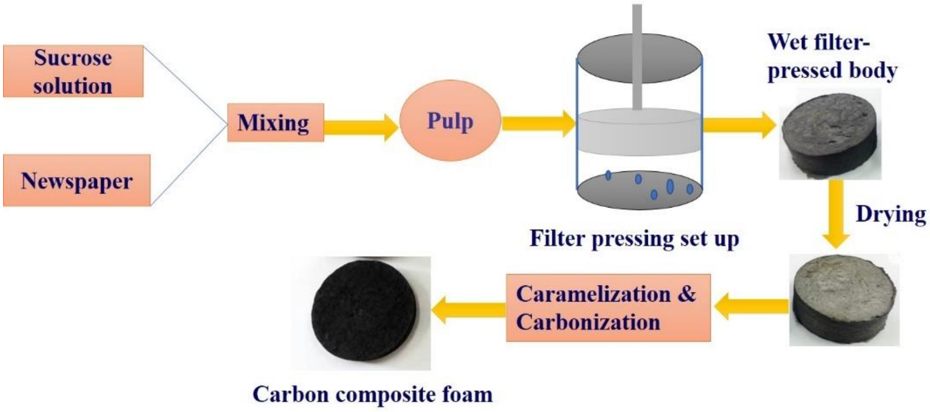

Fig. 2.6 Schematic representation of processing of carbon - gehlenite composite foam

2.3 Characterization

2.3.1 Inductively coupled plasma-atomic emission spectral (ICP-AES) analysis

Impurities present in the sucrose was determined by Perkin Elmer optima 4000 V ICP-AES. The calibration curves of the elements to be analysed were prepared by aspirating their standard solutions and measuring the emission intensities at the selected emission lines. The sample solutions were aspirated into the plasma of the ICP-AES and emission intensities were measured. Using the calibration graphs, the concentration of each element was calculated.

2.3.2 Particle size evaluation

The particle size of the ash obtained by the heating newspaper at 900 °C in an air atmosphere was evaluated using a particle size analyzer (Malvern Matersizer2000, UK). The ash sample dispersed in water was used. 632 nm He-Ne laser was used for the measurement.

2.3.3 Viscosity measurement of pulp

The viscosity of the newspaper pulp was measured using a Brookfield RVT model rotational viscometer (Brookfield Engineering Inc., Middleboro, MA) with the help of a small sample adapter and a cylindrical spindle (SC21).

2.3.4 Morphology analysis of rice husk powder

The morphology of rice husk powder was analysed using an optical microscope (Leica M205).

2.3.5 Thermogravimetric analysis (TGA)

Thermogravimetric analysis (TGA) was carried out using a thermogravimetric analyser (TA instruments, Q-50 USA). A known weight of the sample was heated in an air atmosphere at a heating rate of 5 ºC/minute for the estimation of inorganic residue.

2.3.6 Carbon yield

The carbon yield was estimated by heating a known weight of the sample in a nickel crucible in an inert atmosphere furnace at 900 °C for 2 h. Ultrapure (99.99%) argon was used to create the inert atmosphere and the heating rate was 1 °C min^{-1}. The carbon yield was calculated using the following formula (Equation 2.1):

$$\text{Carbon yield} = \frac{\text{Weight of carbon obtained at 900 °C}}{\text{Weight of precursor}} \text{X}100 \qquad \text{(Equation 2.1)}$$

2.3.7 Carbonization shrinkage

The shrinkage during carbonization was calculated from the dimensions of the respective bodies before and after carbonization. The dimensions of the samples were measured using a vernier calliper.

2.3.8 Density and porosity measurement

The density of the carbon composite foams was calculated from their weight and dimensions. Rectangular bodies of 50 mm x 40 mm x 15 mm size were used for density measurement. The samples were prepared by cutting the carbonized bodies using a hacksaw blade and polishing using emery paper. The skeletal density of the carbon composite foam samples was analysed using a helium pycnometer (Micromeritics AccuPyc II 1340). The porosity of the carbon composite foam was calculated from its bulk density (ρ_b) and skeletal density(ρ_s). The porosity was calculated from **Equation 2.2**

$$\text{Porosity} = (1- \rho b/\rho s)*100 \qquad \text{Equation 2.2}$$

2.3.9 X-ray diffraction (XRD) analysis

X-ray diffraction patterns were recorded using Bruker D8 Discover diffractometer with Cu Kα radiation of wavelength 1.5406 A° at a scanning rate of 2.4° min^{-1}. The carbon composite foam was crushed using a motor and pestle and the resultant powders were used for the XRD analysis. The XRD patterns were recorded at 2θ in the range of 10 to 90 ° with a step size of 0.02°. The d-spacing was calculated from Bragg's equation (**Equation 2.3**)

$$n\lambda=2d\ \sin\theta \qquad \text{Equation (2.3)}$$

where λ is the wavelength of the X-ray, d is the d-spacing and θ is the angle of diffraction

2.3.10 Raman spectra analysis

The Raman spectra were recorded with a confocal Raman microscope (WITec alpha 300R). A 532 nm laser source was used for excitation and five spectra with an integration time of 1 sec were recorded. The spectra were collected using Peltier cooled CCD array detector at a spectral resolution of 1 cm^{-1}.

2.3.11 Scanning electron microscopy (SEM) analysis

The microstructure was observed using a scanning electron microscope (Carl Zeiss EVO18 SEM). Fractured surfaces of the carbon composite foams were used for the analysis. The samples were sputter-coated with gold before the microstructure analysis. The images were recorded using secondary electron (SE) detectors.

2.3.12 Textural properties measurement

The textural properties of the carbon composite foams were obtained from N_2 adsorption-desorption measurements. The samples were degassed at 300 °C for 16 h in a flowing nitrogen atmosphere before the adsorption-desorption measurements. The surface area was calculated using the BET (Brunauer-Emmett-Teller) equation. The amount of N_2 adsorbed at a relative pressure of 0.99 was used to calculate the total pore volume. The micropore volume was estimated by using the t-plot method. The pore size distribution was computed from the N_2 adsorption isotherm using density functional theory.

2.3.13 Compressive strength measurement

Compressive strength and Young's modulus of the carbon composite foams were obtained from the stress-strain measurements carried out using a Universal Testing Machine (INSTRON 5050, USA) at a crosshead speed of 0.5 mm min^{-1}. Rectangular samples of 24mm x 24 mm x 12 mm size were used for the measurements. The test was carried out according to ASTM C 395 M-05.

2.3.14 Machinability

The machinability of the carbon composite foams was qualitatively tested by drilling holes and cutting slots on carbon composite foam bodies using conventional drilling and milling machines and high-speed steel tools.

2.3.15 Thermal conductivity measurements

The thermal conductivity of the carbon composite foams was measured using the transient plane source method (Hot Disk, TPS 2500S, Sweden). Rectangular samples of 40 mm x 40 mm x 15 mm size were used. The samples were cut using a hacksaw blade and the faces were polished to flat surfaces to ensure seamless contact when the planar sensor was sandwiched for the measurement. The Kapton sensor of the instrument was sandwiched between the identical foam samples with perfect contact. The schematic representation of the thermal conductivity measurement is shown in **Fig. 2.7**.

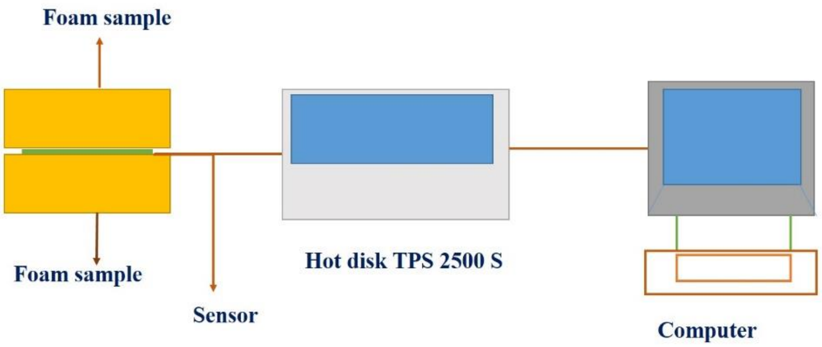

Fig. 2.7 Schematic representation of the thermal conductivity measurement

2.3.16 Fire resistance

The fire resistance of the samples was tested by exposing 20 mm thick carbon composite foams to oxyacetylene flame.

2.3.17 Electrical conductivity measurement

The electrical conductivity measurement of the carbon composite foams was carried out by the four-probe method using a programmable current source (Keithley 6221) and a digital voltmeter. The probes used were the spring-loaded type and a minimum pressure was applied to ensure proper electrical contact between the sample and the probes. The voltage between the two pins was separated by a distance (S) of 2 mm. The schematic representation of electrical conductivity measurement of carbon composite foam is given in **Fig. 2.8**. The bulk resistivity

(R_f) was calculated from the current (I) and voltage (V) reading using the equation given below (equation 2.2):

$$R_f = 2\pi S \frac{V}{I} \qquad \text{(Equation 2.2)}$$

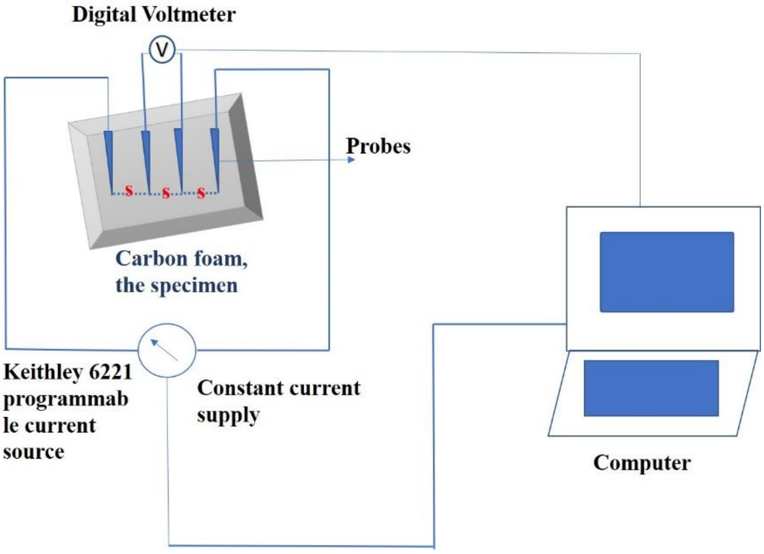

Fig. 2.8 Schematic representation of electrical conductivity measurement of carbon composite foam

2.3.18 Electromagnetic interference (EMI) shielding effectiveness measurement

The electromagnetic interference (EMI) shielding effectiveness of the carbon composite foams was measured in the X-band (8.2 to 12.4 GHz) region of microwave spectra with the help of a network analyser (E5071E) using a corresponding waveguide. The rectangular carbon composite foam samples of size 22.7 mm x 10.2 mm x 5 mm were used. The samples were prepared by cutting the foam bodies and finishing with fine emery paper to the dimensions of the cavity of the shim. The samples were then push fitted to establish proper electrical contact with the internal walls and thereby minimize the spurious leakage of the microwave.

CHAPTER-3

CARBON COMPOSITE FOAMS FROM NATURAL COTTON

3.1 Introduction

Natural cotton is an abundant, tubular fibrous cellulosic material obtained from cotton plants (Dochia et al., 2012). It contains ~44 wt.% carbon. Natural cotton is used for the synthesis of a large number of amorphous carbon materials such as carbon aerogels, carbon composites, and activated carbon for various applications(Cao & Ma, 2020; H. Chen et al., 2015; Long Chen et al., 2017; Du et al., 2018; Ziyu Li et al., 2017; Sartova et al., 2019; Sheng et al., 2019; Y. Wei et al., 2018; Yin et al., 2021). Carbon materials produced from cotton possess superior flexibility, textural properties, electrical conductivity and hydrophobicity(Long Chen et al., 2017; Ziyu Li et al., 2017; Sivadas et al., 2015). They are employed as an adsorbent for toxic chemicals and heavy metal ions, absorbent for oils to clean up oil spillage, host for phase change materials, catalyst support for hydrogen evolution reaction and electrode for batteries and supercapacitors(H. Chen et al., 2015; Du et al., 2018; Gu et al., 2020; Sheng et al., 2019; Youfang Zhang et al., 2016). Bi et al. prepared carbon fibre aerogel by simple carbonization of raw cotton and demonstrated an oil absorption capability as high as 192 times of its weight(Bi et al., 2013). Flexible carbon aerogels in diverse shapes are prepared from natural cotton by Zhang et al. by sodium chlorite treatment followed by filtration, drying and carbonization. The prepared flexible carbon aerogels were employed for oil absorption(Junping Zhang et al., 2016). The cotton-based carbon aerogels reported in the literature have poor structural integrity as well as very low strength to use in any thermo-structural applications(B. Wang et al., 2013; C. Wang et al., 2015). Structural integrity and improved mechanical strength can be achieved by bonding the tubular fibrous carbon obtained from cotton with amorphous carbon derived from molecular/polymer precursors. The present chapter reports the preparation of robust composite carbon foam from natural cotton by filter-pressing. Sucrose, a naturally renewable molecule obtained from sugarcane, is used to bind the natural cotton fibres to produce a green composite body. The high-temperature carbonization of the cotton-sucrose composite produces carbon composite foams. The carbon produced from sucrose binds the cotton-derived tubular fibrous carbon during carbonization. In this chapter, the density, compressive strength, thermal conductivity and electromagnetic interference (EMI) shielding effectiveness of the carbon composite foams as a function sucrose solution concentration used for their preparation are discussed,

3.2 Results and discussion

3.2.1 Determination of the impurities in sucrose

The impurities present in the sucrose were determined by ICP-AES analysis. The sucrose solution contains 30, 40,10 and 80 ppm of Na, K, Mg and Ca, respectively as impurities.

3.2.2 Morphology of cotton fibre

Morphology of cotton fibre was measured using a field emission scanning electron microscope. FESEM image of the cotton fibres is shown in **Fig 3.1**. Cotton fibres are found to be curly and ribbon-like. Most of the fibres are exhibiting a diameter in the range of 18 -30 μm with a length in the range of 2-3 cm.

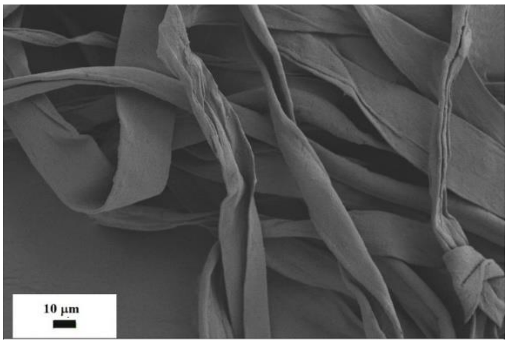

Fig.3.1 FESEM image of cotton fibre

3.2.3 Carbon yield and ash content of cotton and sucrose

The carbon yield estimated by heating sucrose and natural cotton in an argon atmosphere at 900 °C for 2 hr is 11.1 and 24.2 wt.%, respectively. Ash content at 900 °C was estimated by thermogravimetric analysis in the air atmosphere. The ash content of cotton and sucrose is 0.03 and 0.57 wt.%, respectively.

3.2.4 Processing of carbon composite foam

The natural cotton being hydrophilic disperses in water and aqueous sucrose solution when agitated with a glass rod. The natural cotton fibres dispersed in water medium consolidate to a compact body up on filter-pressing. The cohesive forces between the wet cotton fibres hold them together as an integral body. However, on drying, the body expands to a large volume as the cohesive forces between the resilient cotton fibres vanish upon drying. A photograph showing a body consolidated by filter-pressing of an aqueous dispersion of cotton fibre before and after freeze-drying is given in **Fig. 3.2**. On the other hand, the cotton fibre dispersed in sucrose solution of concentration in the range of 100 to 700 g L^{-1} retains the shape upon drying as the sucrose present in the solution binds the cotton fibres. Our attempts to dry the filter-pressed bodies by conventional ambient drying result in a higher concentration of sucrose on the surface compared to the interior. This is due to the migration of sucrose to the surface along with water during the drying. On the other hand, the freeze-drying produce sucrose bonded cotton a body containing a uniform concentration of sucrose throughout as the water from the bodies is removed by sublimation. The amount of sucrose in the cotton-sucrose composite body depends on the sucrose solution concentration. The sucrose in the cotton-sucrose composite body increases from 29 to 74 wt.%, when the sucrose solution concentration increases from 100 to 700 g L^{-1}. The concentration of sucrose retained in the body as a function of sucrose solution concentration is shown in **Fig. 3.3**.

Fig. 3.2 Photograph of filter-pressed cotton at zero sucrose concentration before (left) and after freeze-drying (right)

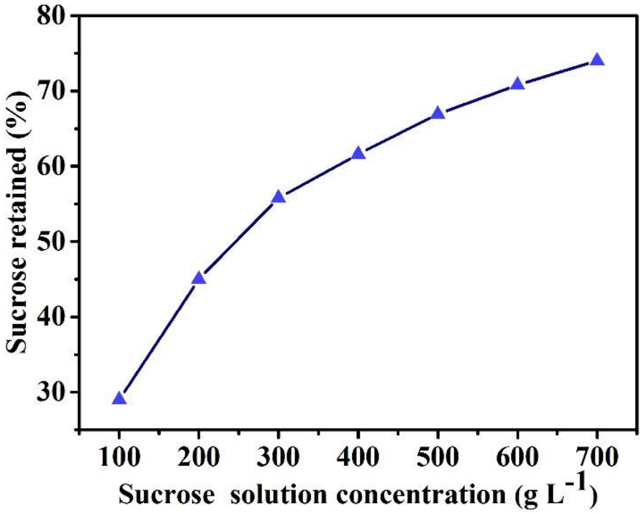

Fig. 3.3 Concentration of sucrose retained in the body as a function of sucrose solution concentration

On heating at 160 °C, the sucrose in the composite body undergoes caramelization. The caramelization involves the decomposition of sucrose to glucose and fructose anhydride and their subsequent condensation polymerization to a high molecular weight infusible structure. This infusible polymeric structure is called humin or caramelin with an average molecular formula, $C_{125}H_{188}O_{80}$(Darder & Ruiz-Hitzky, 2005; R Narasimman & Prabhakaran, 2012). The cotton and the caramel in the cotton-caramel composites undergo carbonization on heating in an inert atmosphere furnace to form carbon-carbon composite foams. In this, the carbon produced from the caramel binds the tubular fibrous carbon produced from cotton. The carbon composite foams thus obtained are designated as **CCF-X**, where **X** stands for the concentration of sucrose solution used for their preparation.

3.2.5 Carbonization shrinkage

The caramelization of sucrose in the sucrose-cotton composite does not produce any measurable shrinkage to the body. On the other hand, the cotton-caramel composites underwent considerable shrinkage in the filter-pressing and transverse directions during carbonization, except the one prepared at a sucrose solution concentration of 100 g L^{-1}. The cotton-caramel composite prepared at 100 g L^{-1} underwent a considerable expansion in the filter pressing direction instead of contraction. Here, the carbon produced from the small amount of sucrose retained in the filter-pressed body is not sufficient to properly hold the resilient tubular carbon fibres produced from cotton. **Fig. 3.4** is the photograph of a cotton -sucrose composite (left) and carbon composite foam bodies at a sucrose solution concentration of 100 g L^{-1} showing expansion in the filter-pressing direction during carbonization (right).

Fig. 3.4 Photograph of the cotton-sucrose composite body (left) and carbon composite foam (right) prepared at a sucrose solution concentration of 100 g L^{-1}

The observed diametrical carbonization shrinkage is in a narrow range of 23.6 to 25.1 % at sucrose solution concentrations in the range of 100 to 700 g L^{-1}. During filter-pressing, the majority of the cotton fibres align perpendicular to the filter-pressing direction. Therefore, carbonization shrinkage transverse to the filter-pressing direction is governed by the linear shrinkage of cotton fibre. On other hand, the shrinkage in the filter-pressing direction increases from 15.5 to 32 % when the sucrose solution concentration increases from 200 to 700 g L^{-1}. The carbonization shrinkage in the filter-pressing direction as a function of sucrose solution concentration is given in **Fig. 3.5**.

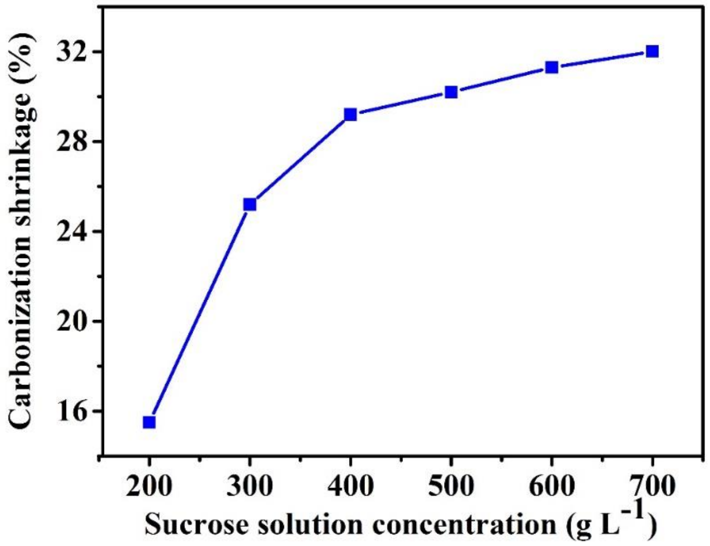

Fig. 3.5 Variation of carbonization shrinkage in the filter-pressing direction as a function of sucrose solution concentration

The shrinkage in the filter-pressing direction is mainly due to the shrinkage of caramel and diametrical shrinkage of cotton fibre during carbonization. The contribution from the diametrical shrinkage of cotton fibre is more or less the same in samples prepared at various sucrose concentrations. The increase in shrinkage in the filter-pressing direction with an increase in sucrose solution concentration is contributed by the caramel matrix. That is, shrinkage of the caramel matrix during carbonization brings the carbonized cotton fibres close to each other. Photograph showing a cotton-sucrose composite, a cotton-caramel composite and a carbon composite foam demonstrating shrinkage in the filter-pressing and transverse direction during carbonization is given **Fig. 3.6**.

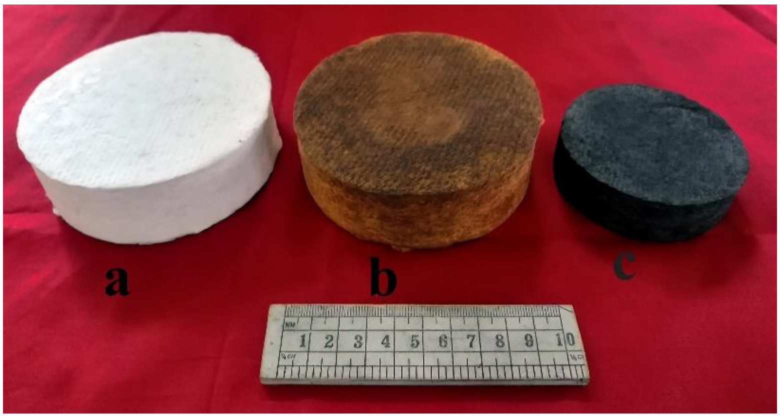

Fig. 3.6 Photograph showing (a) cotton-sucrose composite (b) caramel-cotton composite (c) carbon composite foam

The cotton-caramel composite prepared using sucrose solution of concentration 100 g L^{-1} produced 15.2 wt. % carbon during pyrolysis at 900 °C. The carbon yield of cotton-caramel composites increases from 15.2 to 21.4 wt.% when the sucrose solution concentration increases from 100 to 700 g L^{-1}. This is due to the increase in the concentration of sucrose in the body possessing a higher carbon yield.

3.2.6 Density and porosity of carbon composite foam

The density of the carbon foam body depends on the sucrose retained in the filter-pressed body which in turn is decided by the solution concentration. The density of the carbon composite foam was calculated from the mass and volume of rectangular bodies. The foam density increases from 0.06 to 0.31 g cm^{-3} when the sucrose solution concentration increases from 100 to 700 g L^{-1}. The increase in foam density is due to an increase in the concentration of carbon produced from caramel and an increase in shrinkage in the filter-pressing direction. **Fig. 3.7** shows the effect of sucrose solution concentration on the carbon foam density.

The total porosities were calculated from the bulk densities of the carbon composite foam and skeletal density of the carbon composite foam obtained from the gas pycnometer (1.95 g cm^{-3}). The porosity of the carbon composite foams is in the range of 84 to 97 %. The porosity of the carbon composite foams decreases with increases in the sucrose solution concentration.

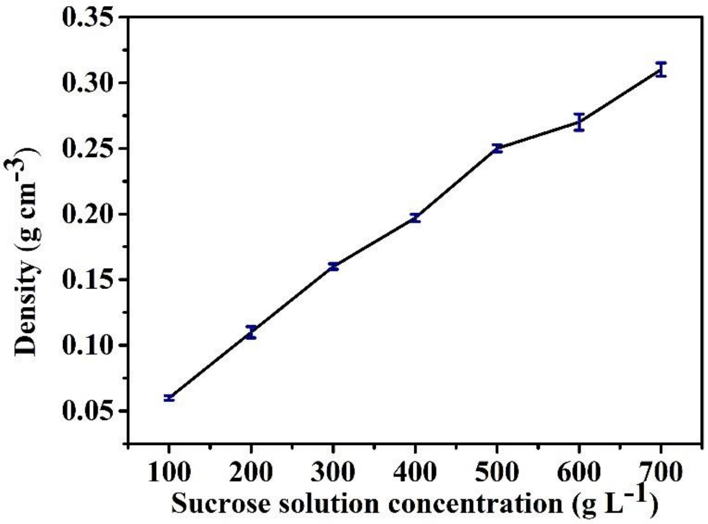

Fig. 3.7 Effect of sucrose solution concentration on carbon composite foam density

3.2.7 XRD analysis

To study the crystalline/amorphous nature of the carbon in the **CCF-X**, XRD analysis was done in three representative samples **CCF-100, CCF-400** and **CCF-700**. The XRD spectrum of the carbon composite foams shows two broad peaks at 2θ values of 23.7° and 44° corresponding to the reflections from (002) and (101) planes of turbostratic carbon(Barnakov et al., 2015; R Narasimman & Prabhakaran, 2012). The XRD patterns of carbon foams prepared at various sucrose solution concentrations are shown in **Fig. 3.8**. The peaks in the XRD spectrum of carbonized cotton fibre are broader than that of carbonized sucrose. This indicates a more amorphous nature of cotton derived carbon than sucrose derived carbon due to poor stacking of graphene layers. The carbon composite foams exhibit sharper peaks due to the sucrose derived carbon. The inter-planar distance (d_{002}) for the sucrose derived and cotton derived carbon are 0.367 and 0.390 nm, respectively. The d_{002} values of carbon composite foams are observed in between that of sucrose derived carbon and cotton derived carbon as expected.

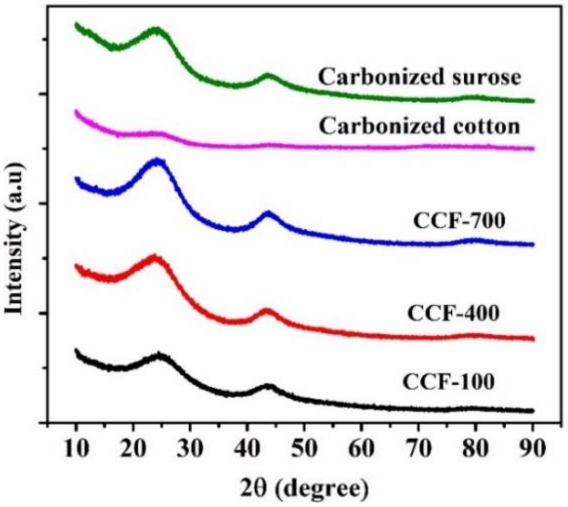

Fig. 3.8 XRD patterns of carbonized cotton, carbonized sucrose and carbon composite Foams

3.2.8 Raman spectra analysis

The disordered nature of the carbon is further confirmed by the fact that the Raman spectrum of carbon composite foams shows intense D-band at 1345 cm^{-1} corresponding to sp^3 carbon in addition to the G-band at 1580 cm^{-1} corresponding to graphitic carbon(Dychalska et al., 2015; Marton et al., 2013). The Raman spectra of carbon composite foam, carbonized sucrose and carbonized cotton are given in **Fig. 3.9**. The ratio of the intensity of the D-band to the G-band (I_D/I_G) calculated from the full-width half maximum of the respective peaks is given in **Table 3.1**. The carbonized cotton shows a higher I_D/I_G ratio of 2.34 due to its more disordered nature however the carbon obtained from sucrose shows a lower value of 1.57. A decrease in I_D/I_G ratio from 2.32 to 2.06 is observed from **CCF-100** to **CCF-700** due to an increase in the concentration of more ordered sucrose derived carbon in the composite.

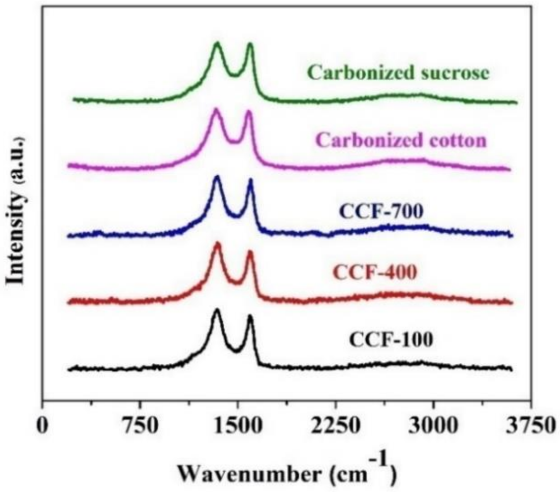

Fig. 3.9 Raman spectra of carbonized cotton, carbonized sucrose and carbon composite foams

Table 3.1 I_D/I_G ratio of **CCF-X** samples, carbonized cotton and sucrose

Sample Name	**I_D/I_G**
CCF-100	2.32
CCF-400	2.13
CCF-700	2.06
Carbonized cotton	2.34
Carbonized sucrose	1.57

3.2.9 Foam microstructure

The SEM microstructures of the **CCFs** observed from the filter-pressing direction clearly shows the web-like random arrangement of tubular carbonized cotton fibres perpendicular to the filter-pressing direction. The carbonized cotton fibres are welded together at their contact points by the carbon produced from sucrose. The welding of carbonized cotton fibres at their contact points by the carbon produced from sucrose is evidenced in the SEM image of **CCF-200** shown in **Fig. 3.10a**. The enhancement in bonding between the carbonized cotton fibres with carbon produced from sucrose achieved by the advancement of contact area between the fibres with an increase in sucrose concentration is evidenced from the SEM image of **CCF-500** observed from the filter pressing direction as shown in **Fig**. **3.10b**. The

SEM images of **CCF-500** and **CCF-700** observed transverse to the filter-pressing direction is as shown in **Fig. 3.10c** and **Fig. 3.10d**, respectively. These images further confirm transverse orientation and enhancement in bonding between the carbonized cotton fibres with an increase of sucrose concentration. The SEM analysis indicates two types of macropores in the **CCFs**. One type is the inter-fibre porosity created due to the web-like random arrangement of carbonized cotton fibre perpendicular to the filter-pressing direction and the stacking of the webs in the Z-direction. The second type is the lumen of the tubular carbonized cotton fibre.

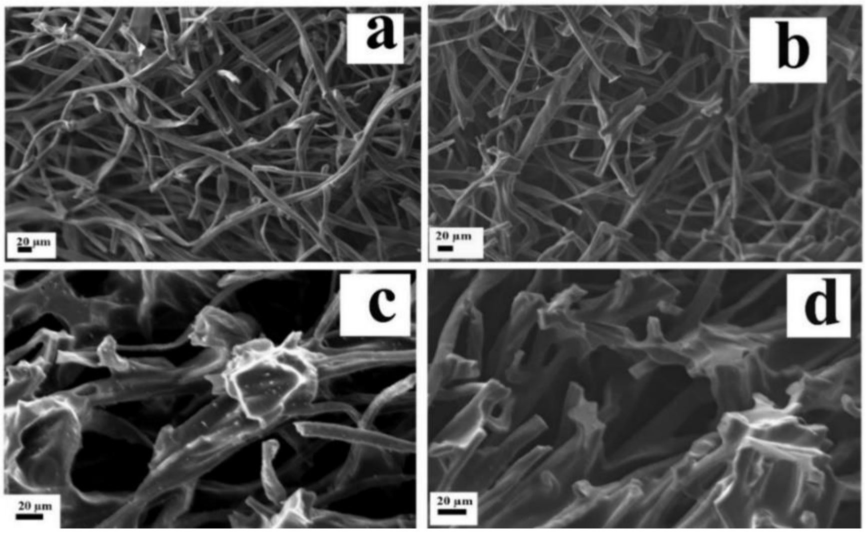

Fig. 3.10 SEM images of **CCF-200** (a) & **CCF-500** (b) in the filter pressing direction and **CCF-500** (c) & **CCF-700** (d) in the transverse direction

3.2.10 Textural properties

The textural properties of **CCFs** were evaluated by N_2 adsorption-desorption studies at 77 K. The N_2 adsorption-desorption of carbonized cotton and carbon composite foams show a combination of type I and type IV isotherms with a sharp increase in the extent of adsorption at lower relative pressure and a prominent hysteresis loop at relative pressures in the range of 0.4-0.9. This indicates the presence of micro, meso and macropores in the **CCFs**. On the other hand, the carbonized sucrose shows type I isotherm indicating its microporous nature. The micropores in carbonized cotton and sucrose are generated by an *in situ* activation. That is, during carbonization of cotton and sucrose, the oxygen retained in the carbon structure by –OH condensation reacts with the carbon at higher temperatures to form carbon monoxide which resulted in the formation of micropores(R. Narasimman et al., 2014). The broad hysteresis observed in adsorption-desorption isotherms of carbon composite foams may be due to the partial blocking of the mouth of mesopores in carbonized cotton by microporous carbon produced from sucrose. This makes the mesopores in the carbonized cotton ink-bottle type. The N_2 adsorption-desorption isotherm of **CCFs** is shown in **Fig. 3.11a**. The carbonized cotton fibre (**CCF-0**) exhibits the highest surface area, micropore volume and total pore volume of 897 m^2g^{-1}, 0.321 cm^3g^{-1} and 0.486 cm^3g^{-1}, respectively. The corresponding values of carbon obtained by carbonization of sucrose at 900 °C are 394 m^2g^{-1}, 0.144 cm^3g^{-1} and 0.183 cm^3g^{-1}, respectively. The surface area, micropore volume and total pore volume of **CCFs** show a decreasing trend with an increase in sucrose concentration. This is due to the increase in the concentration of sucrose-derived carbon possessing lower surface area and pore volume. The textural properties of **CCFs** are given in **Table 3.2.** Pore size distribution derived from the density functional theory (DFT) method is displayed in **Fig. 3.11b**. The DFT pore size distribution curves exhibit multiple peaks. Three major peaks are observed at 1.23, 1.55 and 1.82 nm.

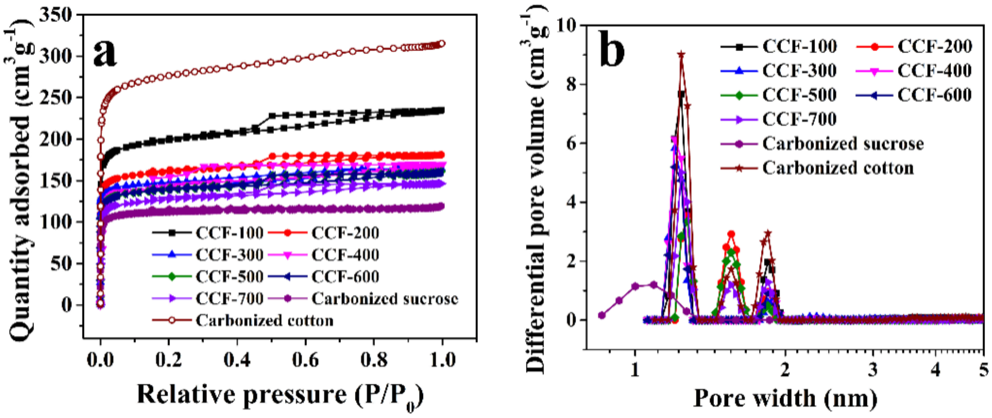

Fig. 3.11 (a) N_2 adsorption-desorption isotherms and (b) DFT pore size distribution of **CCFs**

Table 3.2 Textural properties of carbon composite foams

Sample name	BET surface area (m^2g^{-1})	Micropore area (m^2g^{-1})	Micropore volume (cm^3g^{-1})	Total pore volume (cm^3g^{-1})
Cotton carbonized	897	703	0.321	0.486
Sucrose carbonized	394	339	0.144	0.183
CCF-100	773	644	0.232	0.36
CCF-200	637	541	0.196	0.279
CCF-300	583	497	0.180	0.245
CCF-400	576	490	0.178	0.235
CCF-500	574	481	0174	0263
CCF-600	550	470	0.170	0.248
CCF-700	503	420	0.151	0.226

3.2.11 Compressive strength

Thermo-structural and EMI shielding applications demand good strength for the carbon foams. The carbon aerogels prepared from sodium chlorite-treated natural cotton reportedly exhibit very high and reversible compressibility. However, the compressive strength (stress at 10% strain) reported was very feeble (less than 0.1 kPa) to use for any thermo-structural applications. The **CCFs** prepared by filter-pressing at sucrose solution concentrations of 100 and 200 g L^{-1} exhibit reversible compressibility to limited strain values. The cyclic compression test indicates perfect reversibility up to strain values of 30 % and 20 % for **CCF-100** and **CCF-200**, respectively. The stress-strain graph of **CCF-100** and **CCF-200** demonstrating their reversible compressibility limit is shown in **Fig. 3.12**. Within the strain level, the reversibility in compression persists in **CCF-100** and **CCF-200** over a large number of loading and unloading cycles. The stress-strain graph of **CCF-100** and **CCF-200** demonstrating their reversible compressibility over a large number of compression cycles is shown in **Fig. 3.13**. The compressive strength (stress at 10% strain) of **CCF-100** and **CCF-200** are 5 and 41.6 kPa, respectively.

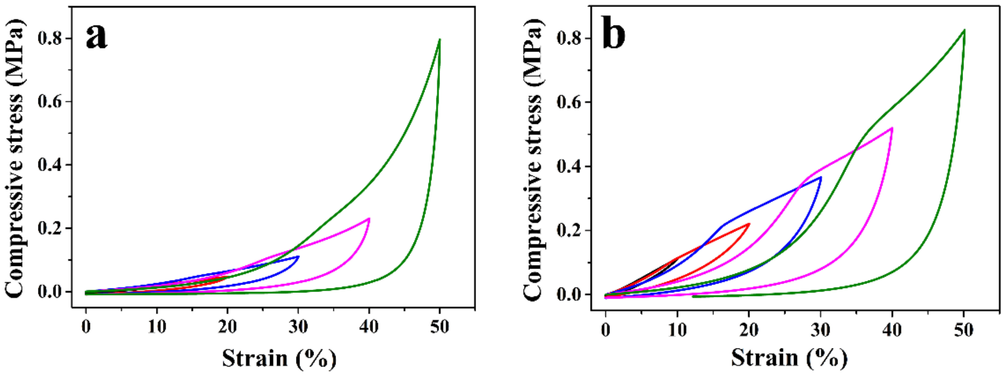

Fig. 3.12 Cyclic compression of **CCF-100**(a) and **CCF-200**(b) showing their reversibility limit

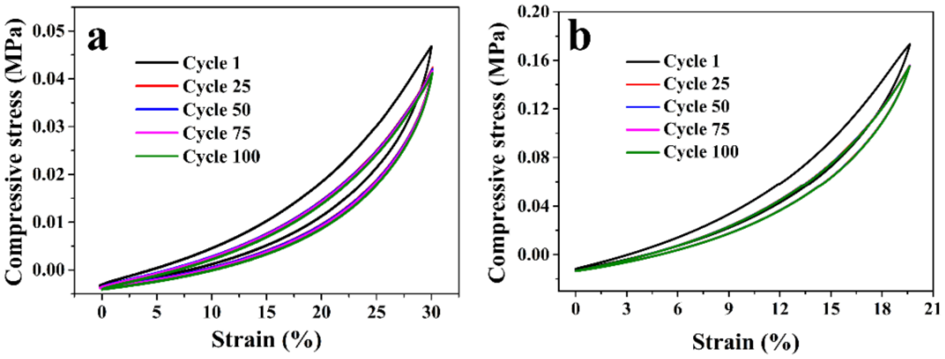

Fig. 3.13 Stress-strain graphs of **CCF-100**(a) and **CCF-200** (b) showing their reversibility over a large number of compression cycles

The compressive strength of **CCFs** prepared at sucrose concentrations in the range of 300 to 700 g L^{-1} are measured in the filter-pressing and transverse directions. The **CCF-300 to CCF-700** exhibit irreversible compression. Their stress-strain behaviour is similar to that of any other brittle foam material. That is, the stress-strain graph has an initial linear region followed by a plateau and a final region of densification. The stress-strain graph of **CCFs** prepared at sucrose solution concentrations in the range of 300 to 700 g L^{-1} is shown in **Fig. 3.14a**. The slope of the initial linear region is taken as Young's modulus and stress corresponding to the 10% strain is considered as the compressive strength. The **CCF-300** shows a compressive strength of 0.34 MPa when measured in the filter-pressing direction. The compressive strength in the filter-pressing direction increases with an increase in sucrose solution concentration and reaches a value of 1.4 MPa for **CCF-700**. The corresponding increase in Young's modulus is from 3 to 39 MPa. On the other hand, **CCF-300** shows a compressive strength of 0.65 MPa, when tested in transverse to the filter-pressing direction. The compressive strength in the transverse direction increases from 0.65 to 2.26 MPa when the sucrose solution concentration increases from 300 to 700 g L^{-1}. The corresponding increase in Young's modulus ranges from 12 to 182 MPa. The observed increase in compressive strength and Young's modulus with an increase in sucrose solution concentration is due to an increase in foam density. The higher compressive strength and Young's modulus of carbon composite foam measured in the transverse direction compared to the filter pressing direction is due to the preferential orientation of the carbonized cotton fibres in the transverse direction. **Fig. 3.14b** shows the compressive strength and Young's modulus of carbon composite foams as a function of their density.

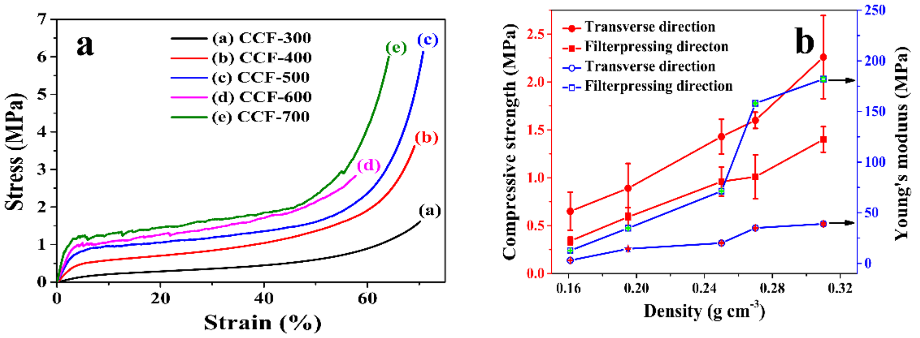

Fig. 3.14 Stress-strain graph (a) and the compressive strength and Young's modulus (b) as a function of sucrose solution concentration of rigid carbon composite foams

During consolidation, the cotton fibres are randomly assembled perpendicular to the filter-pressing direction to form a web-like structure. The stacking of the web-like structure in the filter-pressing direction produces bodies of more or less the same fibre compaction, irrespective of the sucrose solution concentration. In the filter-pressed body, the inter-fibre space is filled with the sucrose solution. During freeze-drying, the sucrose present in the solution retained in the body either deposits on the cotton fibre surface or remains in the inter-fibre space. The inter-fibre space is progressively filled by the sucrose as the solution concentration increases. During heat treatment at 160 °C, the sucrose melts before setting by caramelization. At low sucrose concentrations, the molten sucrose recedes to the fibre-to-fibre contact points and welds them during setting by caramelization. That is, in carbon-carbon composite foams prepared at low sucrose solution concentrations, the carbonized cotton fibres in the web are welded together only at their contact points. It has been demonstrated that the carbon foam produced by the carbonization of non-woven cotton fibre felt exhibit complete flexibility with very poor strength. However, welding of the fibres together at the contact points provides limited flexibility with reasonable improvement in compressive strength from 0.1 to 5 kPa. Partial flexibility of the carbon composite foams prepared at sucrose solution concentrations of 100 and 200 g L^{-1} is due to the welding of the carbonized cotton fibre in the web, only at the contact points. During compression, to a limited extent, the carbon fibre between the contact point bends without disrupting the weld. This reversible bending of carbon fibre is responsible for the reversible compression to a limited strain value. Compression beyond this strain value either disrupts the weld at contact points or breaks the carbonized cotton fibres that lead to failure. The fibre-to-fibre bonding area advances beyond the contact points with an increase in sucrose concentration. This transforms partially flexible carbon composite foam to a rigid one when the sucrose solution concentration increases from 200 to 300 g L^{-1} and above. The welding of the carbonized cotton fibres at contacts points at low sucrose concentration and enhancement in the bonding of carbonized cotton fibres by filling the inter-fibre space with carbon produced from sucrose at higher concentrations is illustrated in **Fig. 3.15**.

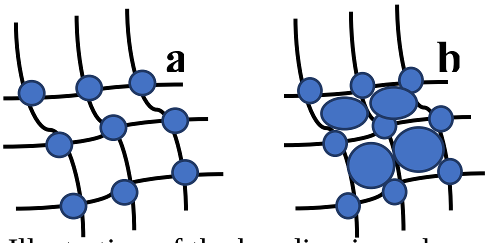

Fig. 3.15 Illustration of the bonding in carbon composite foam at low (a) and high (b) sucrose concentrations

3.2.12 Machinability

Machinability is a desirable characteristic of foam materials for thermal protection, lightweight structure, acoustic absorption and EMI shielding applications. The foam materials prepared in simple shapes can be machined to desired contours provided they withstand stresses during the machining operations. The **CCF-100** to **CCF-400** set of foams cannot be mounted in conventional milling and drilling machines for machining as they are either partially flexible or do not have sufficient strength to resist damages while gripping in the machines. On the other hand, **CCF-500**, **CCF-600** and **CCF-700** have sufficient strength and rigidity to be mounted in machines for machining. Photographs of a **CCF-500** body gripped on a milling machine and the body after machining showing slots made by milling and a hole made by drilling are presented in **Fig. 3.16**.

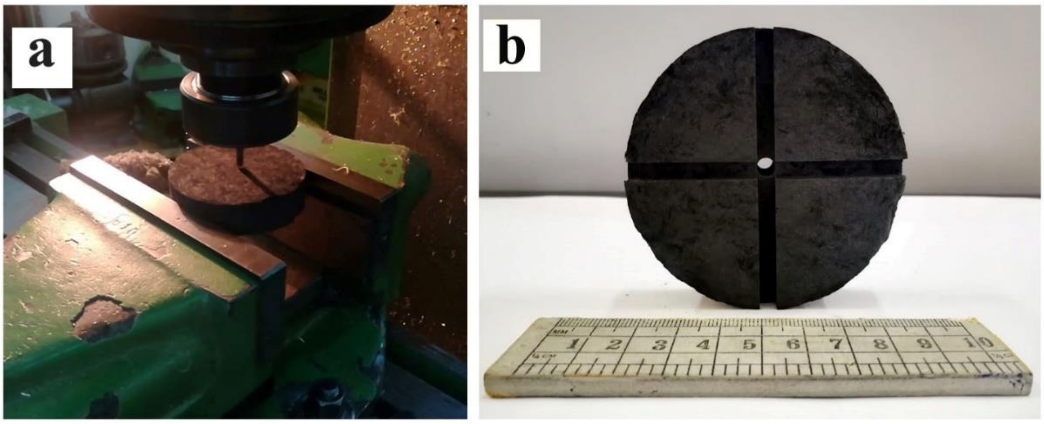

Fig. 3.16 Photograph of (a) **CCF-500** body gripped on a milling machine and (b) the body after machining showing slots made by milling and a hole made by drilling

3.2.13 Thermal conductivity

The high-temperature thermal protection materials demand low thermal conductivity and stability at high temperatures. The **CCF-100** exhibited a low thermal conductivity of 0.069 W $m^{-1}K^{-1}$ at room temperature. The thermal conductivity increases with an increase in sucrose solution concentration and reaches a value of 0.185 W $m^{-1}K^{-1}$ for **CCF-700**. The observed increase in thermal conductivity is due to an increase in the density of **CCFs**. The density and thermal conductivity of the **CCF**s exhibits a near-linear relationship. A plot of thermal conductivity of **CCFs** as a function of density is shown in **Fig. 3.17**. The observed thermal conductivity of **CCFs** is comparable to or lower than that of amorphous carbon foams of similar densities reported in the literature(R Narasimman & Prabhakaran, 2012; Wilson et al., 2018b). The carbon composite foams contain two types of macropores in addition to the micro and mesopores as evidenced by the SEM analysis and N_2 adsorption-desorption studies. The macropores are due to the inter-fibre space of the web-like arrangement as well as the lumen of the carbonized cotton fibre. The lumen in the flattened carbonized cotton fibre can be considered as closed pore channels as the sucrose-derived carbon may close the mouth of the lumen, especially at higher sucrose concentrations. It is well known that foams with closed pores show lower thermal conductivity compared to the ones with open pores having the same porosity. The lower thermal conductivity is attributed to the factors such as the amorphous nature of the sucrose and cotton-derived carbon, high porosity and the presence of closed porosity due to the lumen of the carbonized cotton fibre. The thermal conductivity measured in the transverse direction does not show a significant difference from the one measured in the filter-pressing direction.

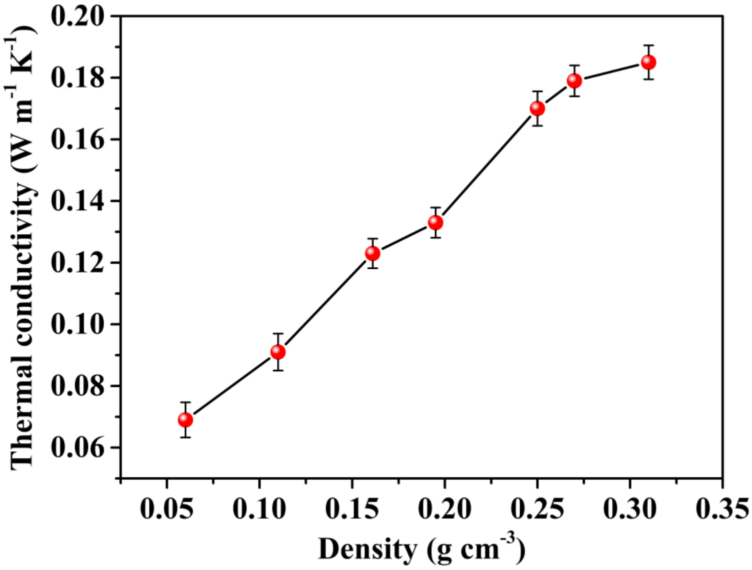

Fig. 3.17 Thermal conductivity of **CCFs** as a function of foam density

3.2.14 Electrical conductivity

Carbon foams are electrically conducting due to the extended conjugated double bonds present in the graphene layers. The electrical conductivity depends on the crystalline nature of the carbon foam which in turn depends on the carbon precursor and heat treatment temperature. The amorphous carbon foams produced from synthetic polymers and biomasses show lower electrical conductivities compared to the graphitic foams produced from mesophase pitch. The electrical conductivity of **CCF-X** as a function of foam density is shown in **Fig. 3.18**. The electrical conductivity increases from 3.8 to 54.2 S cm^{-1} when the foam density increases from 0.16 to 0.31 g cm^{-3}. As the density increases, inter-fibre bonding increases which leads to the improved electrical conductivity of the carbon composite foam. That is, an increase in inter-fibre bonding enhances the path for the movement of electrons.

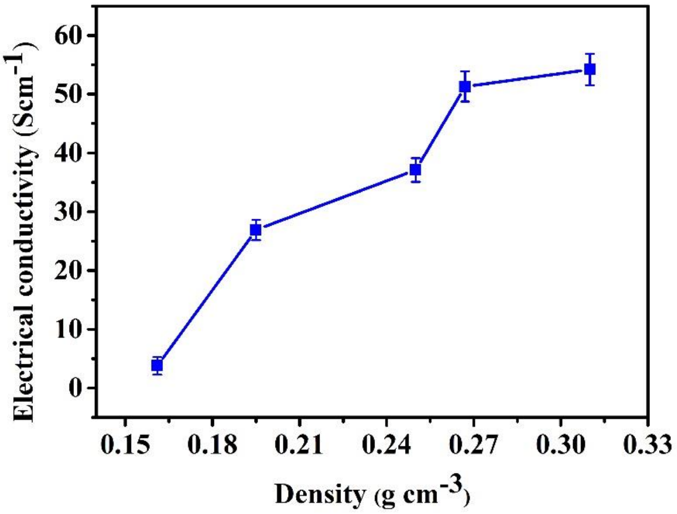

Fig. 3.18 Electrical conductivity of carbon composite foams as a function of density

3.2.15 Oxidation resistance

The drawback of carbon-based materials is that they undergo oxidation when exposed to air or oxygen atmosphere at higher temperatures. Generally, carbon-based materials start oxidation at a temperature of ~ 400 °C. The carbonized cotton fibre and carbon produced from sucrose are stable up to 550 °C as evidenced from the thermogram. The thermograms of carbonized cotton fibre and **CCF-700** in an air atmosphere are shown in **Fig. 3.19**. Further, an increase in temperature results in rapid weight loss due to their oxidation.

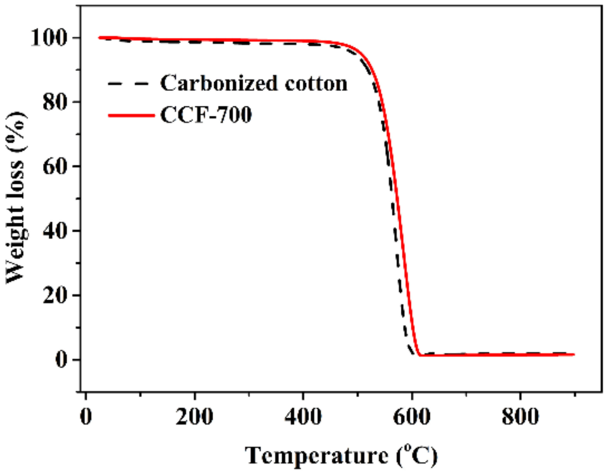

Fig. 3.19 TGA of carbonized cotton and carbon composite foam

3.2.16 Fire resistance

Though **CCF-X** is are prone to oxidation at temperatures above 550 °C, they exhibit excellent fire resistance. They do not combust even when exposed to oxyacetylene flame. However, the portion in contact with the oxyacetylene flame undergoes oxidation which results in the formation of a hole. The time required for the flame to pierce through the foam depends on its density. The time for the flame to pierce through 2 cm thick **CCF-100** of density 0.06 g cm^{-3} is 10 s. The flame penetration time increases to 128 s when the foam density increases to 0.31g cm^{-3}. Photographs of a **CCF-X** body exposed to oxyacetylene flame demonstrating its fire resistance and hole formed due to oxidation are shown in **Fig. 3.20**.

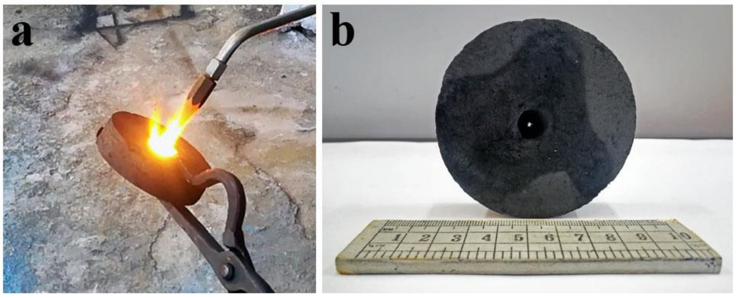

Fig. 3.20 Photographs of **CCF** body exposed to oxyacetylene flame demonstrating its fire resistance (a) and a hole formed due to oxidation

3.2.17 Electromagnetic Interference Shielding

Electromagnetic interference shielding refers to the protection of electronic and telecommunication devices against the penetration of interfering electromagnetic radiation. The fast-growing electronic and telecommunication industry demands the development of lighter materials with high EMI shielding effectiveness to combat this problem. Materials capable of reflecting and or absorbing the EM radiations are used for this purpose. In this connection, carbon foams and reduced graphene oxide have gained increasing attention owing to their high electrical conductivity, lightweight, porous structure and corrosion resistance. Herein, we study the EMI shielding effectiveness of rigid **CCF-x** materials (**CCF-300** to **CCF-700**) as we are unable to prepare thin samples from flexible foam bodies of low mechanical strength for EMI shielding measurements.

When the incident electromagnetic wave falls on the carbon composite foams, three phenomena take place i.e. losses due to reflection (SE_R), absorption (SE_A) and multiple internal reflections (SE_M) within pores(Kumar et al., 2018c)(Kuruvilla et al., 2019).

Fig. 3.21 is a typical graph showing the SE_R, SE_A and SE_T of the **CCF-700** in the X- band region. It is observed that the SE_T of all the samples is almost constant over the entire X-band range. The constant shielding effectiveness values observed are attributed to the homogenous and regular web-like conductive network. The effect of sucrose concentration on the EMI SE of rigid **CCF** samples at a frequency of 11GHz is shown in **Fig. 3.22**. The rigid **CCFs** exhibit absorption dominated EMI shielding behaviour. The EMI SE_T of **CCF** materials increases from 21.5 to 38.9 dB when the sucrose concentration increases from 300 to 700 g L^{-1}. The absorption contribution to total EMI SE observed is in the ranges of 11.9 to 31.0 dB whereas the reflection contribution is in the narrow ranges of 9.6 to 7.8 dB. The absorption of EM waves is mainly due to dielectric and magnetic losses. Since **CCFs** are non-magnetic, the EM absorption is primarily from the dielectric losses. The dielectric loss involves both relaxation and conduction losses. The relaxation loss is mainly due to the polarization which is caused by defects and functional groups present in the shielding materials. On the other hand, the reflection loss is due to the impedance mismatch at the carbon foam-air interface.

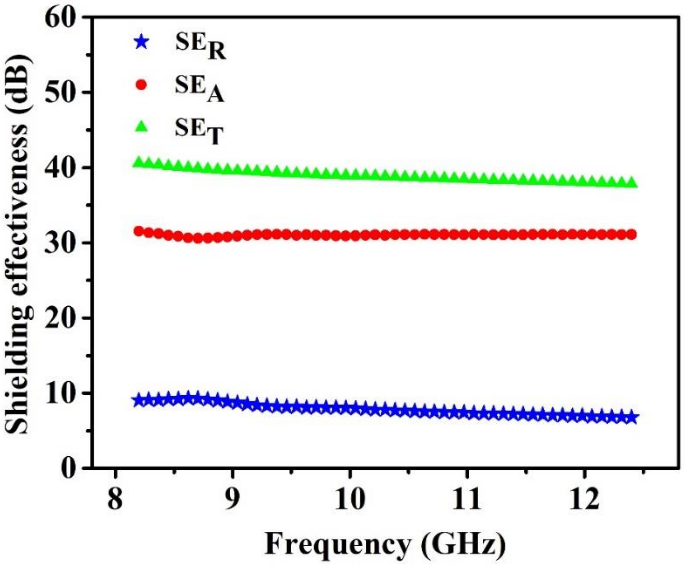

Fig. 3.21 EMI shielding effectiveness of **CCF-700** as a function of frequency

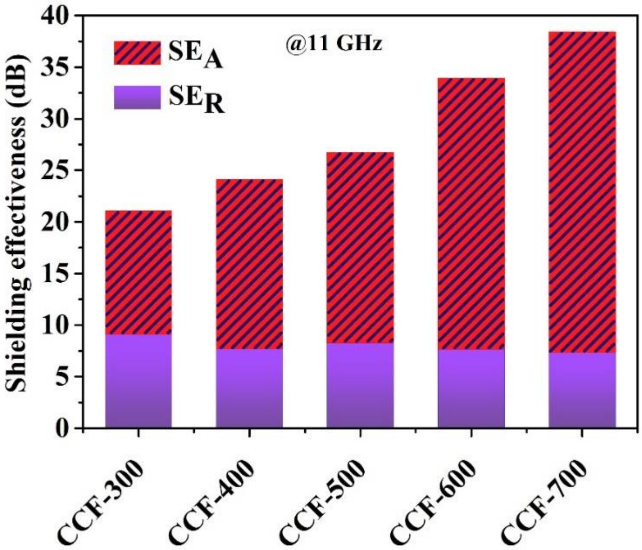

Fig. 3.22 EMI shielding effectiveness of carbon composite foams at 11 GHz frequency

The relatively high surface area and porosities support impedance matching and permit the incident EM waves to enter the **CCF** with nominal surface reflection. The EM waves enter the carbon composite foams reflect back and forth within the pores resulting in enhanced absorption due to relaxation (due to oxygen-containing functional groups in carbon material) and conductive losses. The mechanism of EMI shielding is schematically represented in **Fig. 3.23**.

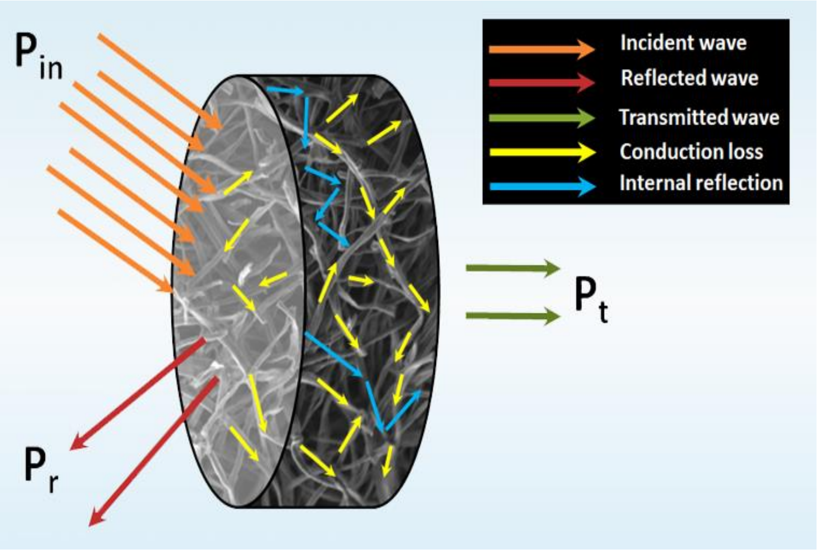

Fig. 3.23 Schematic representation of EMI shielding mechanism

The increase in EMI SE_T of **CCF** with an increase in sucrose solution concentration is due to an increase in relaxation and conductive losses because of the increase in bulk density. The increase in conductive loss is supported by the fact that the electrical conductivity of the **CCFs** increases with an increase in sucrose solution concentration. This is due to the increase in foam density as well as an increase in the concentration of sucrose derived carbon having more crystalline nature. Specific shielding effectiveness is defined as the ratio of shielding effectiveness to the bulk density of the foam materials. The specific shielding effectiveness of **CCF** materials is in the range of 108-138 dB cm^3g^{-1} which is comparable with other porous carbon materials reported in the literature. It has been reported that a minimum EMI SE of 20 dB is required for materials to be considered for practical EMI shielding applications. In this regard, all the studied **CCF-X** qualify for practical applications. Moreover, the EMI SE of the **CCF-X** materials is comparable with the carbon foams derived from some of the other biomass precursors such as sucrose, tannin, bread, coconut shell, tissue paper and sugarcane(Letellier, Macutkevic, Paddubskaya, Plyushch, et al., 2015; R Narasimman et al., 2016; Vazhayal et al., 2019; L. Wang et al., 2020; Y. Yuan et al., 2016).

The observed low thermal conductivity, high fire-resistance and EMI shielding effectiveness coupled with reasonably high compressive strength make the **CCFs** a candidate material for high-temperature thermal protection in aerospace, lightweight fire-resistant structure for shipbuilding and EMI shielding.

3.3 Conclusions

A filter-pressing method was studied for the preparation of robust carbon composite foams from natural cotton and sucrose. Natural cotton fibres dispersed in the sucrose solution was consolidated by filter-pressing followed by freeze-drying produce cotton fibre-sucrose composite bodies. The carbon composite foams produced by carbonization of cotton–sucrose composites show flexible to rigid transition at sucrose concentration above 200 g L^{-1}. The limited flexibility observed up to a sucrose solution concentration of 200 g L^{-1} is due to the welding of carbonized cotton fibres at their contact points by the carbon produced from sucrose. The advancement of the fibre-to-fibre bonding area at higher sucrose concentration makes the carbon composite foams rigid. The carbon composite foam exhibited an increase in density from 0.06 to 0.31 g cm^{-3} with an increase in the sucrose concentration from 100 to 700 g L^{-1}. The increased density is responsible for the observed increase in compressive strength and thermal conductivity of carbon composite foams. The compressive strength and thermal conductivity of the carbon composite foams increases from 5 kPa to 1.4 kPa and 0.07 to 0.185 W $m^{-1}K^{-1}$, respectively, when the density increase from 0.06 to 0.31 gcm^{-3}. The higher compressive strength measured transverse to the filter-pressing direction is due to the preferential transverse orientation of cotton fibre during filter-pressing. Both inter-fibre porosity and porosity due to the lumen of the carbonized cotton fibre are responsible for the low thermal conductivity of the carbon composite foams. The carbon composite foams show excellent fire resistance as they do not catch fire when exposed to oxyacetylene flame. The carbon composite foams obtained at sucrose solution concentration in the range of 500 to 700 g L^{-1} are amenable to machining such as milling and drilling using conventional machines and tools. The **CCFs** exhibit absorption dominated EMI shielding with shielding effectiveness and specific shielding effectiveness in the ranges of 21.5 to 38.9 dB and 108-138 dB cm^3 g^{-1}, respectively. The prepared carbon composite foam can be a candidate material for high-temperature thermal protection in aerospace, lightweight fire-resistant structure for building compartments in ships and EMI shielding materials in electronic equipment.

CHAPTER-4

CARBON COMPOSITE FOAM FROM SAWDUST

4.1 Introduction

Wood is a naturally renewable lignocellulosic material with a unidirectional aligned cellular pore structure. Pyrolysis of wood results in cellular carbon materials with unidirectionally aligned pores(Byrne & Nagle, 1997). The cellular carbon with unidirectionally aligned pores obtained by pyrolysis of wood gives rise to anisotropic thermal, electrical, mechanical and acoustic properties(Byrne & Nagle, 1997; Li Chen et al., 2018; F. Shen et al., 2016; Xue et al., 2017; Y. Yuan et al., 2017). However, the carbonization of large wood pieces results in cracking and warpage. Ultrasonic impregnation of wood with phenolic resin before carbonization is used to suppress the warpage and formation of crack during carbonization(Okabe et al., 1996). However, the dependence on wood for the production of cellular carbon materials leads to excessive deforestation. Sawdust is a powder form of wood generated as waste in the wood industry. The sawdust is utilized for the preparation of carbon foams through a liquefaction process(W. Li et al., 2015; R. Wang et al., 2012). In this, liquefied sawdust is polymerized using formaldehyde and the resulting polymer is subjected to foaming, setting and carbonization to produce carbon foams. Nevertheless, the liquefaction and further polymerization of the liquefied sawdust uses phenol and formaldehyde, respectively. Ozbay et al reported carbon foam by high-pressure foaming of bio-pitch prepared from pyrolytic oil of spruce sawdust(Ozbay & Yargic, 2019).

The microstructure examination of sawdust indicates that the cellular pore structure of wood is preserved in the particles. Therefore, bodies with randomly oriented cellular pores can be fabricated by consolidating the sawdust particles dispersed in a liquid medium and cementing them with a carbonaceous material. The subsequent carbonization results in a carbon foam body with randomly oriented pores. The present chapter reports the preparation of carbon composite foams from sawdust by filter-pressing using sucrose as a carbonaceous binder. The density, compressive strength, thermal conductivity and EMI shielding effectiveness of the carbon composite foams are evaluated as a function of sucrose solution concentration and discussed.

4.2 Results and discussion

4.2.1 Characterization of sawdust

The grinding and sieving of the sawdust collected from the sawmill produce elongated particles of length and width in the ranges of 0.26 to 0.9 and 0.07 to 0.55 mm, respectively, as evidenced by the SEM photomicrograph shown in **Fig. 4.1.** The grinding does not affect the pore channels present in the sawdust particles. The pore channels in sawdust particles are visible in the high magnification SEM image is shown in **Fig. 4.2**. The sawdust powder on carbonization at 900 ^{o}C yield 27.5 wt.% carbon.

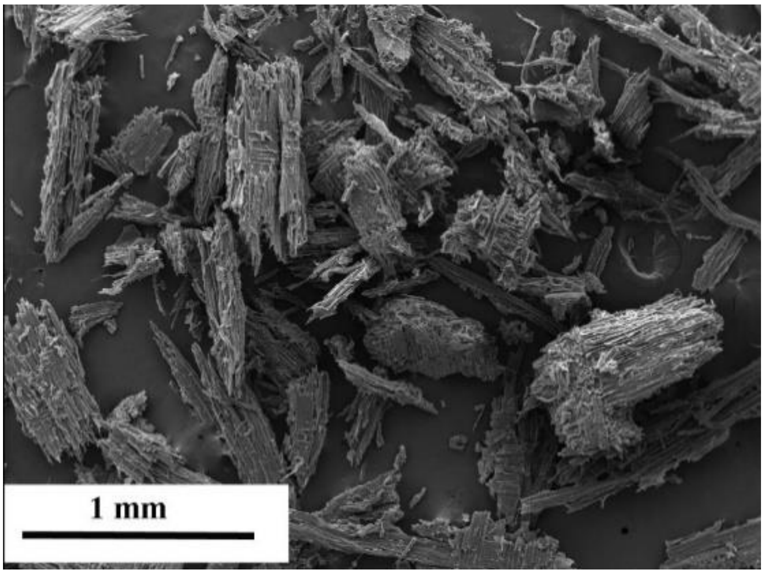

Fig. 4.1 SEM photograph of sawdust particle

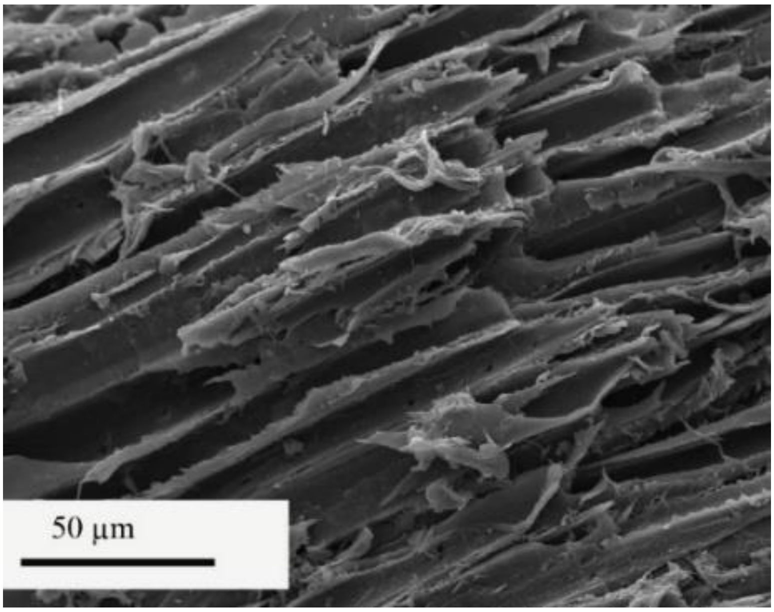

Fig. 4.2 High magnification SEM image of sawdust

4.2.2 Processing of carbon composite foam

The sawdust particles easily disperse in sucrose solution when mixing using a mechanical stirrer. Filter-pressing of the sawdust powder slurries in sucrose solution consolidates the particles into bodies. The cohesive strength of particles in wet filter-pressed bodies provides adequate robustness for easy removal from the filter-pressing set-up and further handling. The conventional drying of filter-pressed sawdust body at room temperature and in an air oven produces a non-uniform distribution of sucrose. During drying, the sucrose solution moves to the surface by capillary action and water evaporates from the surface depositing the sucrose. This leads to a concentration gradient of sucrose in the dried body with a very low concentration at the centre and a high concentration at the periphery. However, freeze-drying produces sucrose bonded sawdust bodies containing a uniform concentration of sucrose throughout. The concentration of sucrose in the body increases from 16 to 58 wt% when the sucrose solution concentration increases from 100 to 700 g L^{-1}. The concentration of sucrose retained in the body as a function of sucrose solution concentrations is shown in **Fig. 4.3**. On heating at 160 °C, the sucrose in the sucrose bonded sawdust body undergoes caramelization. The caramelization involves the decomposition of sucrose to glucose and fructose anhydride and their subsequent polymerization through –OH condensation to produce infusible products such as humin or caramelin of average molecular formula $C_{125}H_{188}O_{80}$(Darder & Ruiz-Hitzky, 2005; R Narasimman & Prabhakaran, 2012). These polymeric structures strongly bind the sawdust particles. On heating at 900 °C, the sawdust and caramel in the caramel bonded sawdust undergo carbonization and the carbon produced from caramel binds the porous carbon obtained from the sawdust particle. The sawdust derived carbon composite foams are designated as **SDC-X**, where **X** stands for the sucrose solution concentration in g L^{-1}.

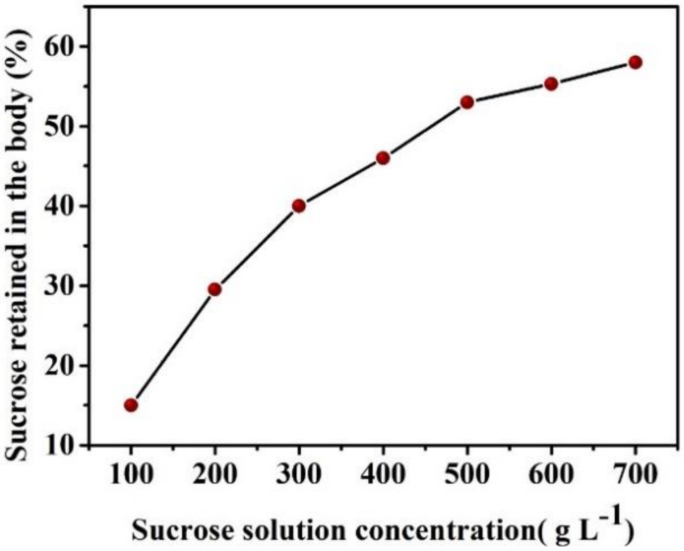

Fig. 4.3 Concentration of sucrose retained in the body as a function of sucrose solution concentration

4.2.3 Shrinkage of the carbon composite foam

The bodies does not undergo any significant shrinkage during caramelization whereas a remarkable shrinkage is observed during carbonization. The shrinkage marginally increases with an increase in sucrose solution concentration. The diametrical shrinkage of the bodies increases from 23.7 to 24.9% when the sucrose solution concentration increases from 100 to 700 g L^{-1}. On the other hand, the bodies exhibit slightly higher shrinkage in the filter pressing direction. The shrinkage in the filter pressing direction increases from 26.5 to 30.4 % when the sucrose solution concentration increases from 100 to 700 g L^{-1}. A photograph containing the filter-pressed sawdust body, caramel bonded sawdust body and carbon foam showing their relative sizes is shown in **Fig. 4.4.**

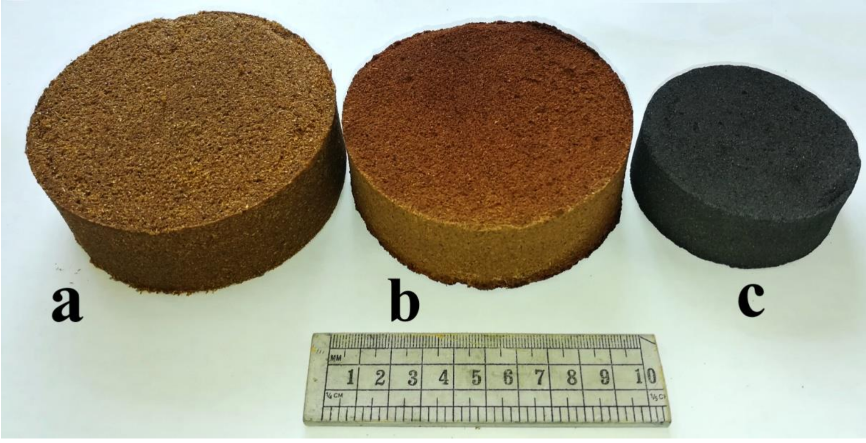

Fig. 4.4 Photograph of filter pressed sawdust(a), caramel bonded sawdust(b) and carbon foam bodies (c)

4.2.4 Density and porosity

The density of the **SDC-X** depends on the amount of sucrose in the sucrose bonded sawdust body which is in turn decided by the sucrose solution concentration. The density of the **SDC-X** increases from 0.15 to 0.35 g cm^{-3} when the sucrose solution concentration increases from 100 to 700 g L^{-1}. **Fig. 4.5** shows the effect of sucrose solution concentration on the density of the resulting carbon composite foam. The carbon produced from the sucrose deposits in the inter-particle region binds the macroporous carbon particles produced from sawdust. As the sucrose concentration increases, more sucrose derived carbon deposits in the inter-particle region result in a decrease of inter-particle porosity. This leads to an increase in foam density. The skeletal density of the carbon foams measured using a helium pycnometer is in the range of 2.01 to 2.08 g cm^{-3}, with an average value of 2.04 g cm^{-3}. The porosity calculated from the average skeletal density and bulk density of the carbon composite foam is in the range of 82.8 to 92.6 %.

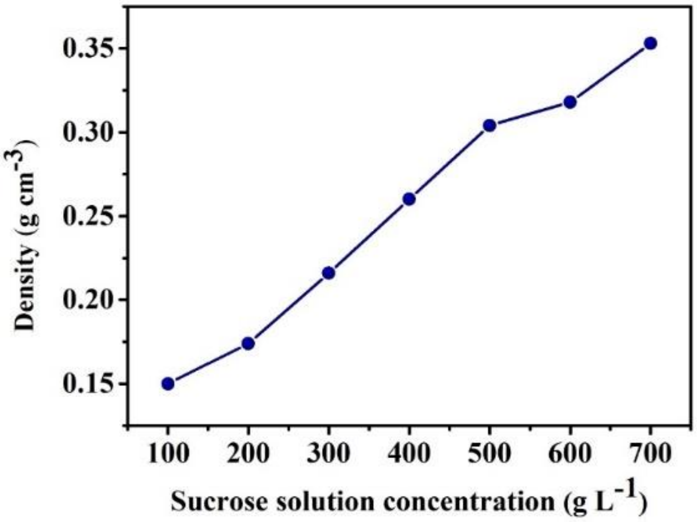

Fig. 4.5 Effect of sucrose solution concentration on carbon foam density

4.2.5 Microstructure

The SEM microstructure of the carbon composite foam bodies shows the random orientation of the carbonized sawdust particles. **Fig. 4.6a-d** shows the low magnification SEM microstructures of carbon composite foams prepared at various sucrose solution concentrations. The decrease in inter-particle porosity with an increase in sucrose solution concentration is evidenced in the microstructures.

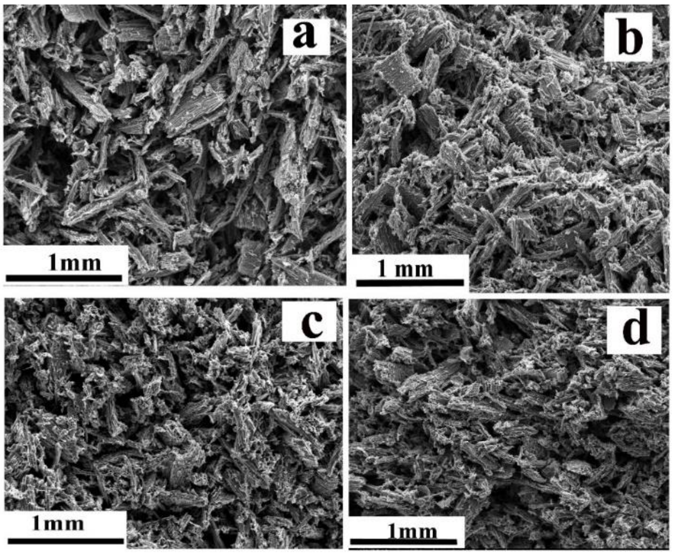

Fig. 4.6 Low magnification SEM photomicrograph of carbon foam prepared at a sucrose solution concentration of 200 g L^{-1} (a), 400 g L^{-1} (b), 600 g L^{-1} (c) and 700 g L^{-1}

The orientation of the carbonized sawdust particles in different directions is evidenced in the high magnification SEM image shown in **Fig. 4.7a**. Although the random orientation of carbonized sawdust particles is evident in the microstructure, a slight preference in an orientation transverse to the filter-pressing direction exists due to the elongated nature of the particle. The random orientation of the particles leads to the orientation of pore channels in all possible directions. The high magnification SEM microstructure shown in **Fig. 4.7b** clearly shows that the pore channels are perfectly preserved in the carbonized sawdust particles even at the highest sucrose solution concentration of 700 g L^{-1}. The pore channels have close to a rectangular shape. The average breadth and width of the rectangular pore channels calculated from the SEM microstructures are 15 and 10 μm, respectively.

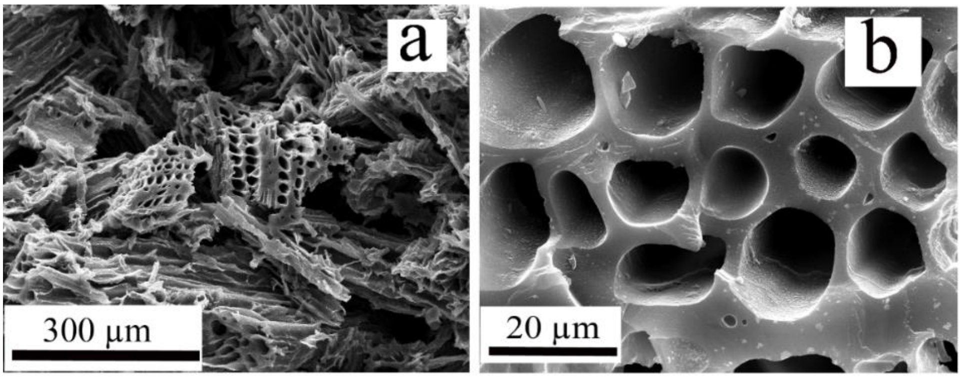

Fig. 4.7 High magnification SEM images of carbon foam at 700 g L^{-1} showing the orientation of carbonized particles in different directions(a) and pore channel(b)

The high magnification SEM analysis was conducted to understand the seeping of sucrose solution into the pore channels of sawdust. **Fig. 4.8** shows the SEM microstructure of a pore channel in carbon composite foams prepared at a sucrose solution concentration of 400 g L^{-1}. Fine island-like deposits of carbon, probably produced from sucrose is observed on the pore channel surfaces. This indicates that the sucrose solution seeps into the pore channels of sawdust. To study the effect of sucrose concentration on the thickness of the fine island-like deposit, a high magnification image of pore channel surface SEM was analysed.

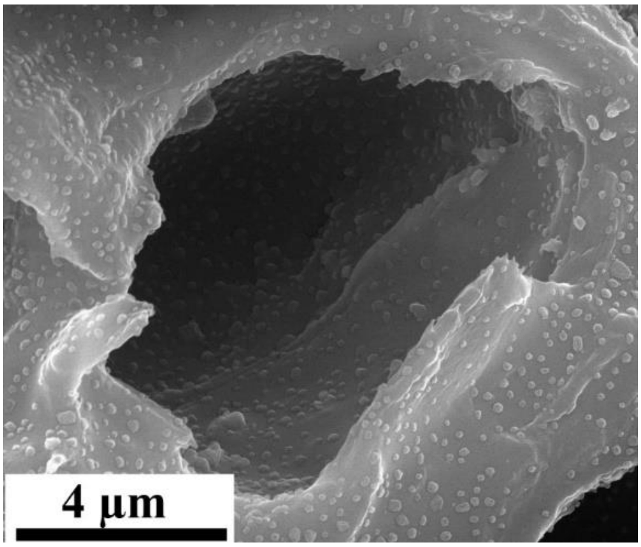

Fig. 4.8 SEM microstructure of pore channel in carbon foam prepared at a sucrose solution concentration of 400 g L^{-1}

The pore channel surface of the carbonized sawdust particles is smooth (**Fig. 4.9a**). On the other hand, island-like carbon deposits of nearly 50 nm thickness are observed on the pore channel surface of carbon foam prepared at a lower sucrose solution concentration. These carbon deposits spread over the whole pore channel surface when the sucrose solution concentration increases to 700 g L^{-1} as evidenced from the high magnification SEM images. The high magnification SEM microstructures of pore channel surfaces of carbon composite foams prepared at various sucrose solution concentrations are shown in **Fig. 4.9b-d**. However, the amount of sucrose solution that seeps into the pore channels is only sufficient to make a ~50 nm coating of carbon on the pore channel surface even at a sucrose solution concentration of 700 g L^{-1}. This further confirms the fact that the majority of the carbon produced from sucrose is present in the inter-particle region and bind the carbonized sawdust particles.

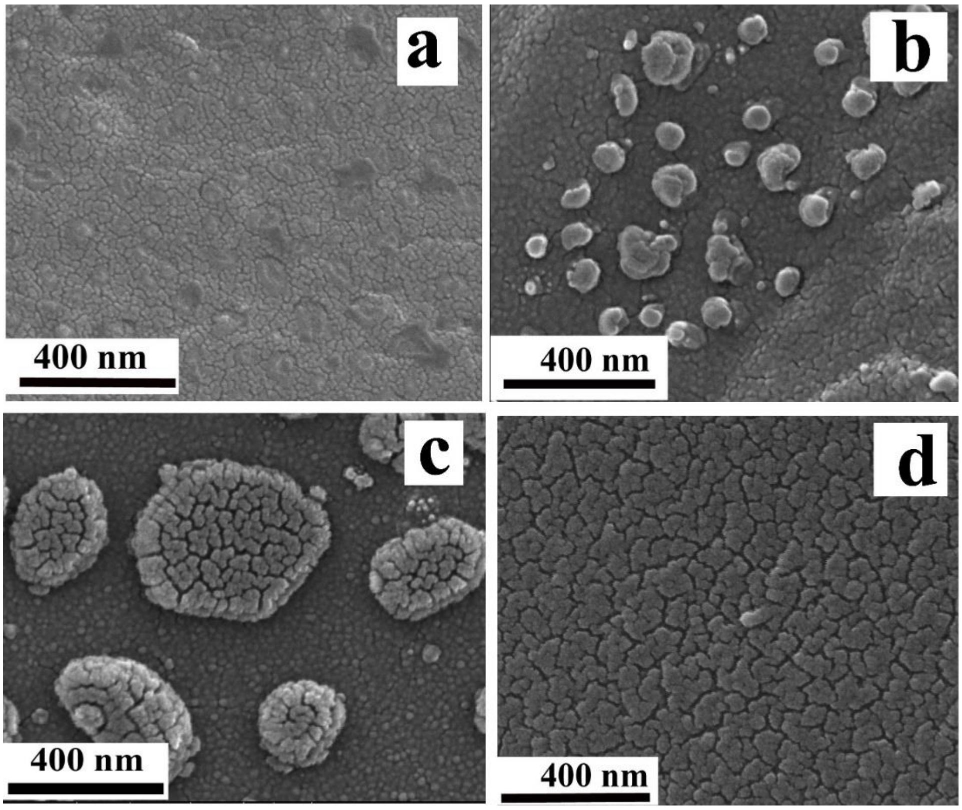

Fig. 4.9 High magnification SEM microstructure of a pore channel surface in carbon foam prepared at sucrose solution concentrations of 0 g L^{-1}(a), 200 g L^{-1}(b), 400 g L^{-1}(c) and 700 g L^{-1}(d)

4.2.6 XRD analysis

The crystallinity in carbon composite foam was studied by XRD analysis. The XRD spectra of the carbon composite foams show two broad peaks at 2θ values of 24.2° and 43.3° corresponding to the reflections from (002) and (101) planes of turbostratic carbon(Barnakov et al., 2015). The XRD patterns of carbonized sawdust and carbon composite foams are displayed in **Fig. 4.10**. The carbonized sawdust shows very broad peaks indicating the presence of a more disordered graphene layer. On the other hand, sharper and more intense (002) and (101) peaks are observed for carbon composite foams prepared at higher sucrose solution concentrations. This indicates that the carbon produced from sucrose has a more ordered structure compared to that obtained from sawdust. The d-spacing values are calculated from (002) reflections using Bragg's equation. The observed d- spacing of the carbon composite foams is 0.38 nm. The observed high d-spacing value indicates poor stacking of graphene layers in the turbostratic carbon.

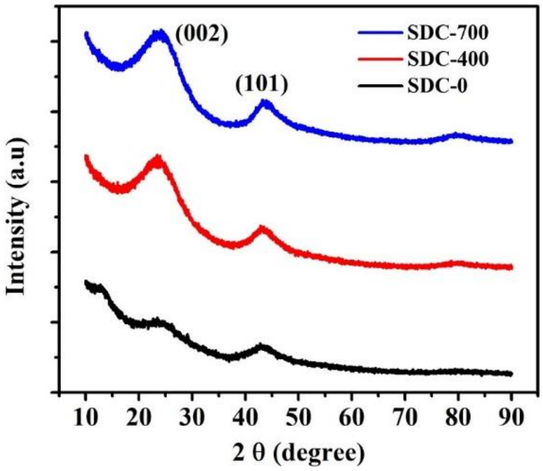

Fig. 4.10 XRD patterns of carbon composite foams derived from sawdust

4.2.7 Raman spectra analysis

The turbostratic nature of the carbon is further confirmed by the fact that the Raman spectra of carbon composite foams show intense D-band at 1345 cm^{-1} corresponding to sp^3 carbon in addition to the G-band at 1580 cm^{-1} corresponding to graphitic carbon(Konstantin et al., 2008). Raman spectra of composite foams are displayed in **Fig. 4.11**. The ratio of the intensity of the D-band to the intensity of the G band (I_D/I_G) was calculated from the full-width half maxima. The observed I_D/I_G of the carbon composite foams decreases from 2.64 to 1.74 when the sucrose solution concentration increases from 0 to 700 g L^{-1}. **Table 4.1** shows the I_D/I_G ratio of carbon composite foams.

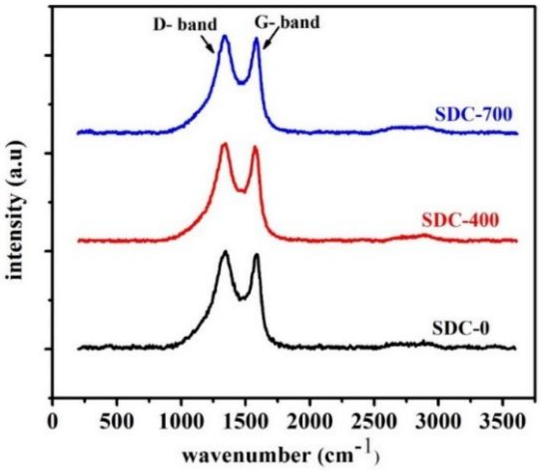

Fig. 4.11 Raman spectra of carbon foams prepared at various sucrose solution concentrations

Table 4.1 I_D/I_G ratio of carbon composite foams

Sample Name	**I_D/I_G ratio**
SDC-0	2.65
SDC-400	2.45
SDC-700	1.74

4.2.8 Compressive strength

The practical utility of the carbon foams in thermo-structural applications demands reasonably good mechanical strength. The carbon foams prepared without sucrose does not have any integrity and crumple into powder while handling. On the other hand, the carbon composite foam prepared at a sucrose solution concentration of 100 g L^{-1} has adequate handling strength. However, it fails while cutting and finishing samples for compressive strength measurements. The carbon composite foams prepared at sucrose solution concentrations in the range of 200 to 700 g L^{-1} exhibits robustness. The compressive stress-strain graph of carbon composite foams prepared at various sucrose solution concentrations is shown in **Fig. 4.12**. The stress-strain graphs obtained are typical of brittle foam materials. The compressive stress-strain of carbon composite foams have an initial linear region followed by a plateau and a region of densification. The stress corresponding to the plateau region is considered as compressive strength and the slope of the initial linear region is taken as Young's modulus.

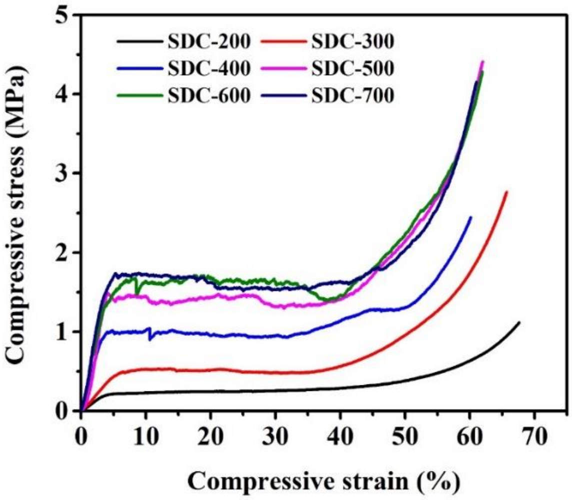

Fig. 4.12 Compressive stress-strain graph of carbon foams prepared at a various sucrose solution concentration

The carbon composite foams show slight anisotropy in the compressive strength and Young's modulus. The compressive strength and Young's modulus measured in the filter-pressing direction is lower than those measured in the transverse direction. The carbon composite foam prepared at a sucrose solution concentration of 200 g L^{-1} shows nearly the same compressive strength values in both filter-pressing and transverse directions. The compressive strength in the filter pressing direction increases from 0.22 to 1.76 MPa when the sucrose solution concentration increases from 200 to 700 g L^{-1}. On the other hand, in the transverse direction, the compressive strength increases from 0.24 to 3.2 MPa when the sucrose solution concentration increases from 200 to 600 °C. Further increase in sucrose solution concentration to 700 g L^{-1} decreases the compressive strength value to 2.8 MPa. Young's modulus in the filter-pressing direction increases from 5.5 to 81.5 MPa when the sucrose solution concentration increases from 200 to 700 g L^{-1}. On the other hand, Young's modulus in the transverse direction increases from 6 to 80.5 MPa when the sucrose solution concentration increases from 200 to 600 g L^{-1}. Further, an increase in sucrose solution concentration to 700 g L^{-1} decreases

Young's modulus value to 66.6 MPa. The compressive strength and Young's modulus of carbon composite foams are presented as a function of sucrose solution concentration and measurement direction in **Fig. 4.13**.

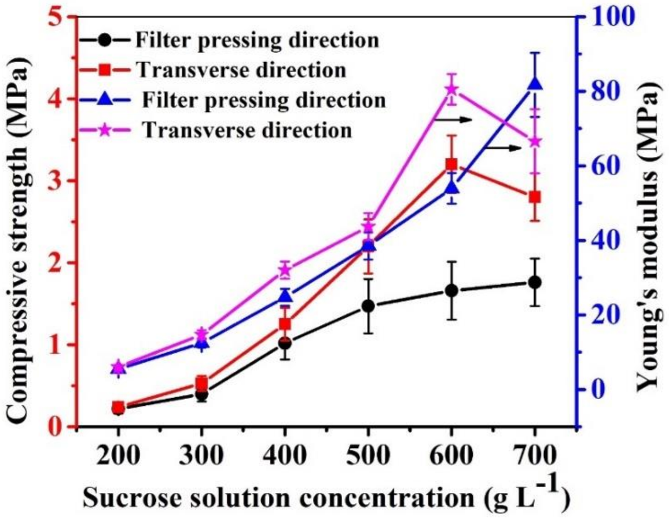

Fig. 4.13 Effect of sucrose solution concentration on the compressive strength and Young's modulus of carbon composite foams measured in the filter-pressing and transverse directions

The increase in compressive strength and Young's modulus with an increase in sucrose solution concentration is due to an increase in carbon composite foam density as well as an increase in bonding between the carbonized sawdust particles by the sucrose derived carbon. It appears that the bonding between the carbonized sawdust particles by the sucrose derived carbon reaches saturation at a sucrose solution concentration of 600 g L^{-1}. Further increase in sucrose solution concentration increases only the density of the carbon composite foam by filling the inter-particle pores. The higher compressive strength and Young's modulus observed in the transverse direction is due to the elongated nature of the sawdust particle. The elongated sawdust particles exhibit some preference to orient perpendicular to the filter pressing direction. However, the observed anisotropy in our sawdust-based carbon composite foams is much lower than that observed in the cellular carbon monolith obtained by the carbonization of mulberry wood. In the present work, the highest ratio of compressive strength in the transverse direction to the filter pressing direction is observed in carbon composite foam prepared at a sucrose solution concentration of 600 g L^{-1} and the value is 1.6. On the other hand, the ratio of compressive strength in the longitudinal to the transverse direction in mulberry wood-derived cellular carbon monolith is in the range of 13.9 to 22.3(Y. Yuan et al., 2017).

4.2.9 Thermal conductivity

Low thermal conductivity, excellent ablative property and fire resistance are the key advantages of amorphous carbon foams. The thermal conductivity of carbon composite foams prepared at various sucrose solution concentrations is presented as a function of density in **Fig. 4.14**. The carbon composite foam prepared at a sucrose solution concentration of 200 g L^{-1} shows a low thermal conductivity of 0.12 W m^{-1} K^{-1}. The thermal conductivity increases from 0.12 to 0.20 W m^{-1} K^{-1} when the sucrose solution concentration increases from 200 to 700 g L^{-1}. The low thermal conductivity of the sawdust derived carbon foam is due to the inherent pore channels and the presence of fine carbon deposits which enhance the phonon scattering. The increase in thermal conductivity with an increase in sucrose solution concentration is due to the decrease in porosity as pores are responsible for the scattering of phonons.

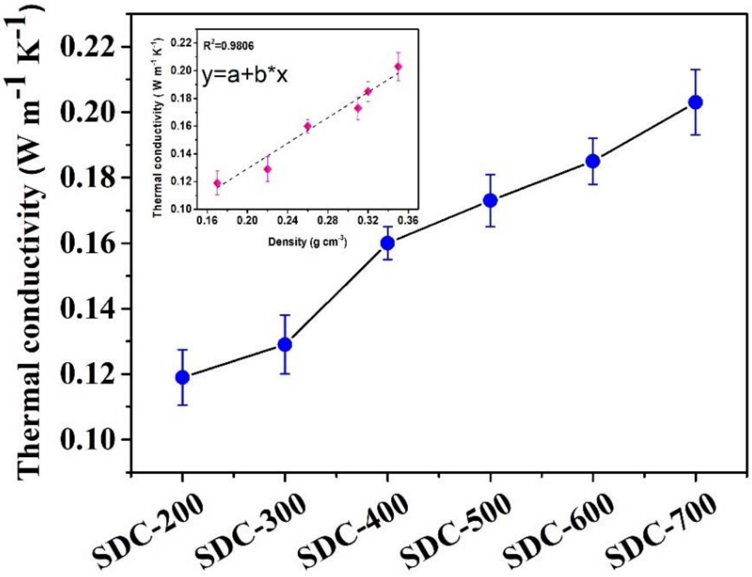

Fig. 4.14 Thermal conductivity of carbon composite foams as a function of sucrose solution concentration

4.2.10 Electrical conductivity

Electrical conductivity is one of the parameters that contribute to the EMI shielding effectiveness of materials. The electrical conductivity of carbon composite foams as a function of sucrose solution concentrations is shown in **Fig. 4.15**. The electrical conductivity of the carbon composite foams increases from 18.2 to 33.8 S cm^{-1} when the sucrose solution concentration increases from 200 to 700 g L^{-1}. The electrical conductivity of the carbon composite foam is due to the proper bonding of sawdust derived carbon with sucrose derived carbon. Another reason for electrical conductivity is the presence of graphitic domains in the matrix due to sucrose derived carbon. The increase in electrical conductivity with an increase in sucrose solution concentration is due to the decrease in porosity of the carbon foam, increase in the concentration of more conducting sucrose derived carbon and firm bonding of sawdust-based carbon by the sucrose derived carbon.

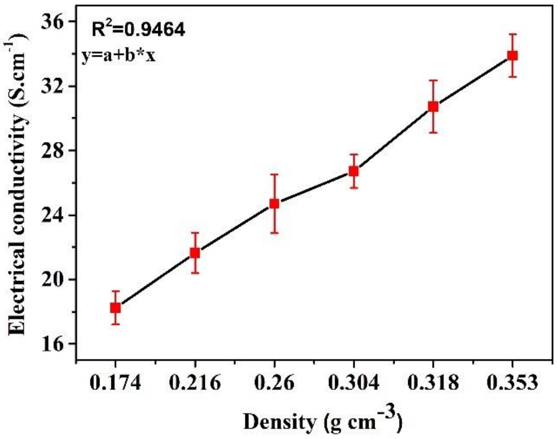

Fig. 4.15 Variation of electrical conductivity of carbon composite foams with sucrose solution concentration

4.2.11 Oxidation resistance

The oxidation behaviour of the carbon composite foams is studied by TGA analysis in air. The TGA graph of carbon foam prepared at various sucrose solution concentrations is shown in **Fig. 4.16**. The TGA graphs show weight loss due to oxidation of carbon from 400 °C onwards indicating their thermal stability in the air up to 400 °C. The complete burnout of carbon occurs at 650 °C leaving a small ash residue. The ash residue from the carbon composite foam decreases when the sucrose solution concentration increases. The carbon produced from sawdust leaves an ash residue of 4.8 wt.%. On the other hand, carbon produced from sucrose does not leave any ash. This very well explains the decreases in ash residue of carbon foam from 4.8 to 2.5 wt.% when the sucrose solution concentration increases from 0 to 700 g L^{-1}. The ash content in carbon composite foams prepared at various sucrose solution concentrations is given in **Table 4.2**.

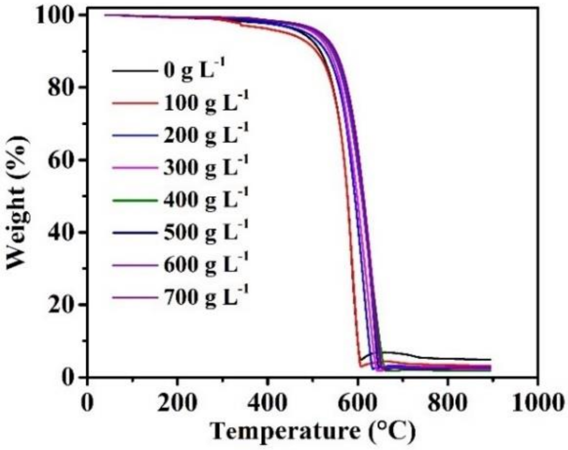

Fig. 4.16 TGA graph of carbon composite foams prepared at various sucrose solution concentrations in air atmosphere

Table 4.2 Ash content of carbon composite foams prepared at the various sucrose solution concentration

Sucrose solution concentration (g L^{-1})	**Ash content(wt.%)**
0	4.8
100	4.3
200	2.9
300	2.9
400	2.8
500	2.8
600	2.7
700	2.5

4.2.12 Fire resistance

The carbon composite foam samples do not catch fire even when exposed to the oxy-acetylene flame. However, the flame pierces through the carbon foam body due to the oxidation of carbon. The time required for the flame to pierce through the carbon foams of identical thickness increases with an increase in foam density. The time required for the flame to pierce through a 20 mm thick carbon foam body increases from 123 to 190 seconds when the foam density increases from 0.17 to 0.35 g cm^{-3}. A photograph showing the fire resistance of the carbon composite foam and the foam body after the fire resistance test containing a hole created by the flame is shown in **Fig. 4.17**.

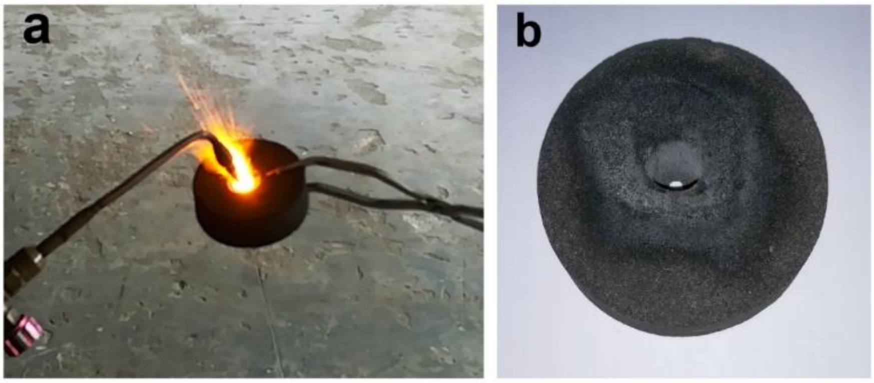

Fig. 4.17 Photograph of a carbon composite foam body exposed to oxy-acetylene flame (a) and after the flame, exposure showing fire resistance

4.2.13 EMI shielding effectiveness

Carbon foams are excellent electromagnetic interference (EMI) shielding materials due to their high electrical conductivity, low density, corrosion resistance and stability at high temperatures(Fang et al., 2007)(Chung, 2001). A typical graph showing the absorption (SE_A) and reflection (SE_R) contributions and total shielding effectiveness (SE_T) of one of the **SDC-X** as a function of frequency in the X-band region is shown in **Fig. 4.18a**. The **SDC-X** show more or less constant shielding behaviour in the entire X-band frequency. This signifies the homogeneity within the **SDC-X** as well as alludes to the fact that the polarization relaxation component of EM wave attenuation is significantly small. The shielding effectiveness of **SDC-X** is shown in **Fig. 4.18b**. The SE_T of the **SDC-X** increases from 25 to 53 dB when

X increases from 200 to 700 g L^{-1}. The linear relationship between SE_T and **X** is largely due to the increase in density of the carbon foam. Denser materials provide a much larger solid phase for ohmic and polarization losses to occur. The SE_R contribution towards the SE_T is relatively low and within a narrow range of 5.5 to 9.3 dB. The highly porous **SDC-X** permits the EM waves to penetrate the material due to impedance matching rather than reflection at the incident surface. The EM waves enter inside the **SDC-X** undergoes multiple internal reflections within the pores channels leading to enhanced absorption. In addition, the island-like carbon deposits on the pore channel surfaces provide additional interfaces for the attenuation of EM waves. The SE_A increases from 19.7 to 44 dB when **X** increases from 200 to 700 g L^{-1}. It is reasonable to infer that the **SDC-X** exhibit an absorption dominated EMI shielding. That is, the high absorption dominated SE_A of **SDC-X** is due to the superior impedance matching, relatively high electrical conductivity, multiple internal reflections of EM waves within the pore channels and polarization relaxation due to the island-like nanostructures on the pore channel surfaces.

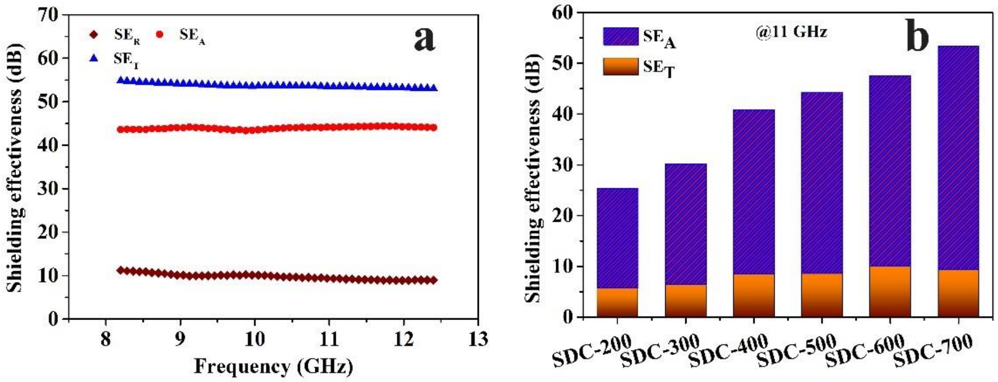

Fig. 4.18 A typical graph showing the EMI shielding effectiveness as a function of the frequency of a sawdust-based carbon composite foam (a), the effect of sucrose solution concentration on the EMI shielding effectiveness (b)

In comparison, nitrogen-doped cellular carbon monoliths decorated with silver nanowires prepared from mulberry wood is reported to exhibit an EMI shielding effectiveness of ~60 dB. The aerogel–like cellular carbon materials prepared from sugar cane by Li et al through a tedious process involving hydrothermal carbonization, freeze-drying and high-temperature heat treatment exhibited absorption dominated EMI shielding effectiveness of 51 dB at a sample thickness of 10 mm(Y.-Q. Li et al., 2015). That is, the maximum EMI shielding effectiveness obtained with sawdust-based carbon foam is comparable to that reported for cellular carbon monoliths prepared from mulberry wood and aerogel-like cellular carbon prepared from sugar cane(Y.-Q. Li et al., 2015; Y. Yuan et al., 2017). Specific shielding effectiveness (SSE), characterised as the ratio of shielding effectiveness to the density of a material is an important shielding performance parameter of porous materials. The **SDC-X** shows relatively high specific shielding effectiveness and the values obtained are in a close range of 149 to 152 dB $g^{-1}cm^{3}$.

The current method for preparation of carbon foam has remarkable advantages such as (1) the raw materials used are low cost and naturally renewable, (2) avoids processes involving liquefaction of sawdust and blowing of the resin which uses expensive and environmentally hazardous synthetic chemicals, and (3) the filter-pressing process is scalable. In addition, the sawdust based lightweight carbon foam with reasonably high mechanical strength possessing low thermal conductivity and excellent fire resistance can be a candidate for fire-resistant structural material for building compartments in the ship and high-temperature thermal protection material in aerospace application. Moreover, high EMI shielding capability coupled with low density and corrosion resistance make these carbon foams excellent candidates for building EMI enclosures for electronic equipment in aircraft.

4.3 Conclusions

Thermally insulating amorphous carbon composite foams are prepared by cementing sawdust particles with sucrose by filter-pressing followed by drying, caramelization and carbonization. The sawdust powder dispersed in sucrose solution consolidated by filter-pressing form sawdust-sucrose composites of uniform composition on freeze-drying. The density of the carbon foams is modulated in the range of 0.17 to 0.35 g cm^{-3} using the sucrose solution of concentrations in the range of 200 to 700 g L^{-1}. The compressive strength in the transverse direction (0.24 to 3.2 MPa) is higher than that in the filter-pressing direction (0.22 to 1.76 MPa) due to the preferential orientation of elongated sawdust particles transverse to the filter-pressing direction. The Young's moduli in the filter-pressing and transverse direction are in the ranges of 5.5 to 81.7 MPa and 6 to 80.5 MPa, respectively. SEM analysis reveals the random orientation of sawdust derived carbon particles in the composite foam with slight preferential orientation transverse to the filter pressing direction. It also revealed that the sucrose solution seeps into the pore channels creates island-like carbon deposits of ~50 nm thickness on the pore channel surfaces. The carbon foams exhibit excellent fire resistance and low thermal conductivity in the range of 0.12 to 0.20 W m^{-1} K^{-1}. The electrical conductivity increases from 18.2 to 33.8 S cm^{-1} when the foam density increases from 0.15 to 0.35 g cm^{-3}. The carbon foams exhibited an absorption dominated EMI shielding with a shielding effectiveness of 5 mm thick carbon foams increases from 25 to 53 dB when the sucrose solution concentration increases from 200 to 700 g L^{-1}. The increase in EMI shielding with an increase in sucrose solution concentration is due to the combined effect of an increase in foam density, increase in electrical conductivity and island-like carbon deposited on the pore-channel surfaces which creates additional interfaces for the attenuation of EM waves. The lightweight carbon foam material with moderate compressive strength, high fire resistance, low thermal conductivity and excellent EMI shielding effectiveness can be a candidate for building compartments in ships, thermal protection material in aerospace and EMI shielding materials in aircraft.

CHAPTER-5

CARBON-SILICA AND CARBON-SILICON CARBIDE COMPOSITE FOAMS FROM RICE HUSK

5.1 Introduction

Rice husk is an agro-waste produced during rice processing. Since rice is the second most consumable, rice husk is produced in huge quantities all over the world. The annual production of rice husk in India and the globe is estimated to be 24 and 120 million tonnes, respectively(Gidde & Jivani, 2007). The main constituents of rice husk are cellulose (25-35%), hemicelluloses (18-21%), lignin (26-31%) and silica (15-17%)(Singh, 2018). The rests are soluble components and moisture. A major portion of this rice husk is burnt to produce thermal energy and the resulting silica-rich ash obtained is used as a substitute for Portland cement in concrete, a source of pure silica, in brick making and to produce ceramic insulators (Bakar et al., 2016; Jittin et al., 2020; Sembiring et al., 2016; Sobrosa et al., 2017; Zareei et al., 2017). A variety of silicon-containing compounds such as silicon carbide, silicon nitride, silicon tetrachloride and pure silicon are developed from the silica obtained from rice husk(Alweendo et al., 2019; Hernández-Martínez et al., 2020; Mochizuki et al., 2020; I. A. Rahman & Riley, 1989). The biochar obtained by pyrolysis of rice husk and rice husk ash are used as adsorbents for environmental remediation (Swarnalakshmi et al., 2018). The rice husk ash and the silica produced from rice husk are used as fillers/reinforcement in polymers to produce polymer matrix composites (Fuad et al., 1995; Sethuramalingam et al., 2021; Yam & Mak, 2014). Nevertheless, no previous attempts have been reported in the literature for the processing of monolithic carbon foams from rice husk. The present chapter reports a cleaner production method for carbon-silica and carbon-silicon carbide composite foam monolith from rice husk. In this, rice husk particles are bonded by sucrose to produce a rice husk-sucrose composite. Carbon-SiO_2 (**C/SiO_2**) composite foams are produced by the carbonization of the rice husk-sucrose composites. The silica present in **C/SiO_2** composite foams is reduced carbothermal by high-temperature heat treatment to produce carbon-silicon carbide (**C/SiC**) composites foams. The **C/SiO$_2$** and **C/SiC** composite foams are evaluated for their compressive strength, thermal conductivity and EMI shielding performance and discussed as a function of sucrose solution concentration.

5.2 Results and discussion

5.2.1 Size and morphology of particles in rice husk powder

The rice husk powder obtained by grinding the rice husk in a flour mill contains particles of elongated shape. An optical micrograph of the rice husk powder showing the size and shape of the particles is shown in **Fig. 5.1**. The majority of the particles are in the size span of 1 to 2 mm in length and nearly 0.5 mm in width.

Fig. 5.1 Optical micrograph of rice husk powder

5.2.2 Processing of C/SiO$_2$ and C/SiC composite foams

The rice husk particles are readily wetted by sucrose solution and dispersed well in the solution on mechanical mixing. The filter pressing of the dispersions produces cylindrical bodies having good shape-stability for taking away from the setup and subsequent handling before freezing except at a sucrose solution concentration of 100 g L^{-1}. The filter-pressed body prepared at a sucrose solution concentration of 100 g L^{-1} fails during removal from the filter-pressing set-up due to the poor adhesion of particles. That is, the sucrose solution retained in the body functions as an adhesive to stick the rice husk particles together before freezing. The solid sucrose produced during freeze-drying binds the rice husk particle to form a rice husk-sucrose composite. The quantity of sucrose retained in the body varies with the concentration of sucrose solution. When the concentration of sucrose solution increases from 200 to 700 g L^{-1}, the retention of sucrose in the rice husk-sucrose composite increases from 31.2 to 51.2 wt.%. The annealing of the rice husk-sucrose composites at 160 °C results in the melting and caramelization of sucrose. During the caramelization, molten sucrose first decomposes to glucose and fructose anhydride and then undergoes –OH condensation to produce infusible polymeric structures called humin with molecular formula $C_{125}H_{188}O_{80}$(Darder & Ruiz-Hitzky, 2005; Wilson et al., 2018b). The composites formed at 200 to 600 g L^{-1} sucrose solution concentrations retain their shape during annealing. On the other hand, the composite prepared at 700 g L^{-1} shows a slight deformation. This indicates that at 700 g L^{-1} the samples are overloaded with sucrose such that the melt produced during annealing at 160 °C induces flow.

During inert atmosphere heat treatment at 900 °C, the organic matter (lignocellulosic part) present in the rice husk undergo carbonization to form carbon-silica composite particles. These particles are bonded together by the carbon produced from the caramel. In the case of the sample prepared at 700 g L^{-1}, a small deformation observed during annealing at 160 °C is further worsened during carbonization whereas all other samples undergo uniform shrinkage. A photograph of the **C/SiO$_2$-700** composite foam showing the deformation during carbonization is given in **Fig. 5.2**. Nevertheless, the samples prepared up to 200 g L^{-1} sucrose solution concentrations does not have sufficient strength for evaluation of properties and therefore discarded from further studies. The carbon composite foam bodies heat-treated at 900 °C and 1600 °C are designated as **C/SiO$_2$-X** and **C/SiC-X**, respectively, where **X** denotes the sucrose solution concentration.

Fig. 5.2 Photograph of **C/SiO$_2$-700** showing the deformation during carbonization

5.2.3 Carbonization shrinkage

The shrinkage of the bodies during carbonization marginally increases with an increase in the concentration of sucrose solution from 300 to 600 g L^{-1}. The shrinkage during carbonization observed in the filter-pressing and transverse directions are in the ranges of 19.4 to 22.7 % and 18.4 to 20.7%, respectively. A photograph of a rice husk-sucrose composite body and carbon-silica composite foam obtained by its carbonization showing the carbonization shrinkage is displayed in **Fig. 5.3**. However, further heat treatment at 1600 °C in an inert atmosphere did not make any significant change in the shape and size of the carbonized bodies. On the other hand, weight losses in the range of 29.5 to 22.4 wt.% are observed due to the carbothermal reduction of amorphous silica present in the carbonized rice husk particles as per the reaction shown in **Equation (5.1)**.

$$3C+SiO_2 \longrightarrow SiC+2CO \qquad \text{(Equation 5.1)}$$

Fig. 5.3 Photograph of rice husk-sucrose composite (a) and **C/SiO_2** composite foam(b)

5.2.4 XRD spectra

The carbon- silica composite foams exhibit two broad peaks in the XRD spectrum. The XRD spectra of **C/SiO_2** composite foams are shown in **Fig. 5.4a**. The broad peak that appeared at 2θ in the range from 19 to 27° is due to the amorphous silica and reflection from the (002) plane of turbostratic carbon(Sompech et al., 2016). The second broad peak that appeared at 43° is due to the reflection from the (100) plane of turbostratic carbon. Upon heat treatment at 1600 °C, sharp peaks appear in the XRD spectra corresponding to SiC. The XRD spectrum of **C/SiC** composite foams are presented in **Fig. 5.4b**. Besides the XRD peak corresponding to carbon, the five peaks observed at 2θ of 35.6°, 41.4 °, 60.6°, 71.7° and 75.5° are due to the reflections from (111), (200), (220), (311) and (222) planes of β-SiC(PDF 00-004-0757)(Peng et al., 2010). The d- spacing corresponding to each peak in the **C/SiC** composite was calculated by using Bragg's equation (**Equation 5.2**) and presented in **Table 5.1.** The calculated d-spacing values are in agreement with the reported values (Pujar & Cawley, 1995; Schulte-Fischedick et al., 2002).

Table 5.1 d-spacing of **C/SiC** composite foam

Sl.No.	Angle, 2θ (°)	d-spacing(nm)	Plane
1	25.7	0.347	(002)
2	33.8	0.265	(101)
3	35.5	0.252	(111)
4	43.3	0.209	(100)
5	60.6	0.154	(220)
6	71.9	0.131	(311)

A small peak observed at the 2θ value of 33.6° is due to the reflection from the (101) plane of α-SiC indicating the formation of a trace amount of α-SiC(Izhevskyi et al., 2000). The broad peaks corresponding to (002) and (100) reflections of turbostratic carbon in **C/SiO$_2$** composite foam became sharper after heat-treatment at 1600 °C. This indicates the formation of micro-graphite in turbostratic carbon due to the ordering of graphene layers at high temperatures.

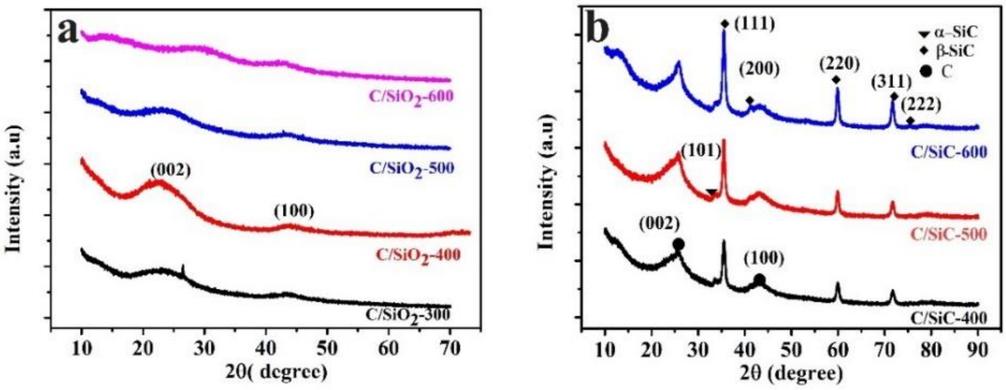

Fig. 5.4 XRD spectra of **C/SiO_2** (a) and **C/SiC**(b) composite foams

5.2.5 Raman spectra

The Raman spectra of **C/SiO_2** and **C/SiC** composite foams are shown in **Fig.5.5a** & **6b,** respectively. The peak near 1340 cm^{-1} (D-band) is related to defects and disordered carbon in the graphitic structure. The observed peak at 1580 cm^{-1} (G-band) is ascribed to the vibration of sp^2 bonded carbon in a 2D hexagonal lattice(Marton et al., 2013). Besides these peaks, a sharp peak at 785 cm^{-1} and a small hump at 956 cm^{-1} are observed in C/SiC composite foams. These peaks correspond to the transverse optic and longitudinal optic vibration modes, respectively, of β-SiC (L. Liu et al., 2010). The broad D-band and G-band observed in **C/SiO_2** composite foam become sharp in **C/SiC** composite foam. The ratio of the intensity of D-band to G-band (I_D/I_G) calculated from the Raman spectra of **C/SiO_2** composite foams decreases from 1.81 to 1.53 when the sucrose solution concentration increases from 300 to 600 g L^{-1}. This indicates that the carbon produced from sucrose is more ordered compared to that produced from rice husk. The I_D/I_G ratio of **C/SiC** composite foams decreases from 0.86 to 0.65 when the sucrose solution concentration increases from 400 to 600 g L^{-1}. That is, I_D/I_G ratio observed for **C/SiC** composite foam samples is lower than that of the corresponding **C/SiO_2** composite foams. This is due to an increase in the ordering of graphene layers during the high-temperature heat treatment. **Table 5.2** gives the comparison of the I_D/I_G values of **C/SiO_2** and **C/SiC** composite foams prepared at various sucrose solution concentrations.

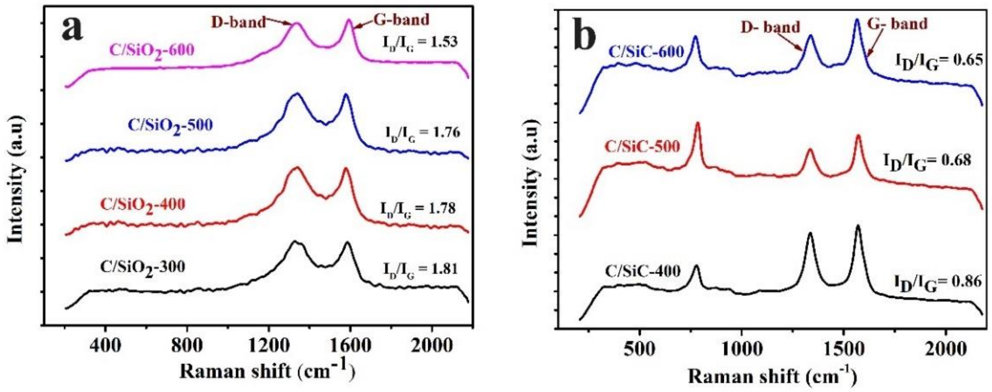

Fig. 5.5 Raman spectra of **C/SiO_2** (a) and **C/SiC**(b) composite foams

Table 5.2 I_D/I_G ratio of **C/SiO_2** and **C/SiC** composite foams

Sucrose concentration	**I_D/I_G ratio**	
	C/SiO_2 composite foam	**C/SiC composite foam**
300	1.81	-
400	1.78	0.86
500	1.76	0.68
600	1.53	0.65

5.2.6 Silica and silicon carbide content

The SiO_2 content in **C/SiO_2** and SiC content in the **C/SiC** composite foams was estimated gravimetrically by burning off carbon in a silica crucible. The **C/SiO_2** or **C/SiC** foam taken in a previously weighed silica crucible (W_1) was accurately weighed (W_2) and then heated in a muffle furnace at 800 °C for 6 hours to burn off the carbon. The crucible with residue (SiO_2 or SiC) retained (W_3) after burning off the carbon was accurately weighed after cooling the furnace to room temperature. The SiO_2 or SiC content was calculated using the formula (**Equation 5.2):**

$$SiO_2 \text{ or SiC content (wt.\%)} = \frac{W_3 - W_1}{W_2 - W_1} X100 \qquad \text{(Equation 5.2)}$$

The obtained values are given in **Table 5.3**. The silica content in **C/SiO_2** decreases from 24.7 to 16.7 wt.% when the sucrose solution concentration increases from 300 to 600 g L^{-1}. On the other hand, the SiC content in **C/SiC** composite foam decreases from 25 to 15 wt.% with an increase in sucrose solution concentration from 300 to 600 g L^{-1}.

Table 5.3 SiO_2 and SiC contents in the **C/SiO_2** and **C/SiC** composite foams, respectively

Sucrose concentration (g L^{-1})	**SiO_2 content (wt.%)**	**SiC content (wt.%)**
300	24.8	25.0
400	19.4	17.0
500	18.5	15.6
600	16.7	15.0

5.2.7 Morphology

Morphology and pore structure of the carbon composite foams were analysed on fractured surfaces using a scanning electron microscope. Typical low magnification SEM images of **C/SiO_2** and **C/SiC** composite foam are shown in **Fig. 5.6**. The random assembly of elongated carbonized rice husk particles perpendicular to the filter pressing directions is evidenced by the microstructure. These randomly assembled particles are bonded together at their junction by carbon produced from sucrose. The bonding of the carbonized rice husk particles by carbon produced from sucrose provides sufficient strength for the **C/SiO_2** composite foam bodies. The **C/SiC** composite foam shows more or less the same morphology as the **C/SiO_2** composite foam.

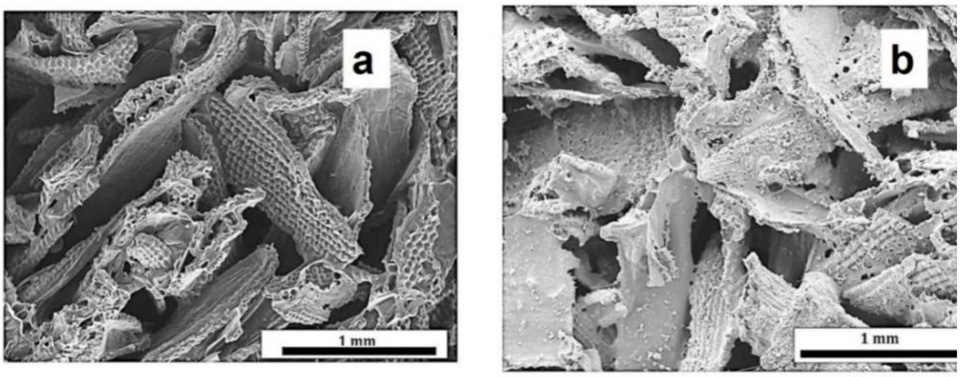

Fig. 5.6 Low magnification fractograph of **C/SiO_2-500** (a) and **C/SiC-500** (b) composite foam

The high magnification SEM images indicate that the inherited corrugated structure of the outer epidermis of rice husk and the oval-shaped pore channels remain unaltered after carbonization. The major diameter of the oval-shaped pore channels observed is in the range of 1.4 to 9.1 µm. The minor diameter is in the range of 2.8 to 4.8 µm. The high magnification SEM images showing the corrugated surface features and oval-shaped pore channels in carbonized rice husk are shown in **Fig. 5.7a** and **7b**, respectively. These microstructure features such as the corrugated surface structure and pore channels remain unaltered in **C/SiC** composite foams. The **C/SiO$_2$** and **C/SiC** composite foams mainly contain two types of pores. The primary source of porosity is the inter-particle space. That is a large volume of macropores created by the random assembly of elongated rice husk particles preferentially oriented perpendicular to the filter-pressing direction. The second source is the pore channels inherited in the rice husk particles.

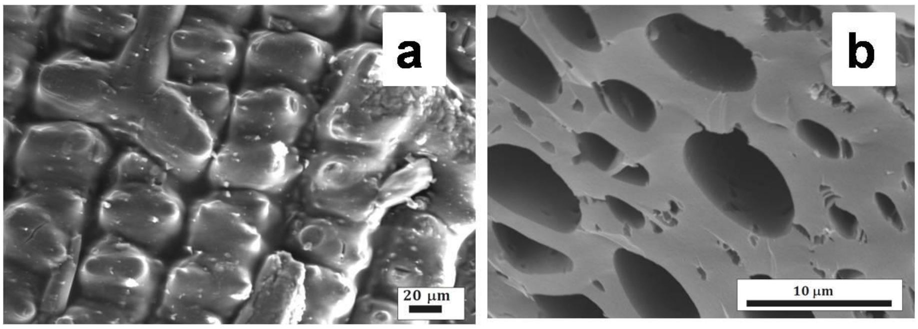

Fig. 5.7 High magnification image showing corrugated surface structure (a) and pore channel (b) of **C/SiO$_2$** composite foam

5.2.8 Microstructure

The microstructure of the carbon composite foam was studied using TEM. The presence of silica and silicon carbide particles in the carbon matrix is evidenced from the transmission electron micrographs shown in **Fig. 5.8a and 8b,** respectively. The low magnification TEM image of **C/SiO$_2$** composite foam shows uniform distribution of silica particles of size in the range of 20 to 61 nm in the carbon matrix. On the other hand, the SiC is found more diffused into the carbon matrix of **C/SiC** composite foams.

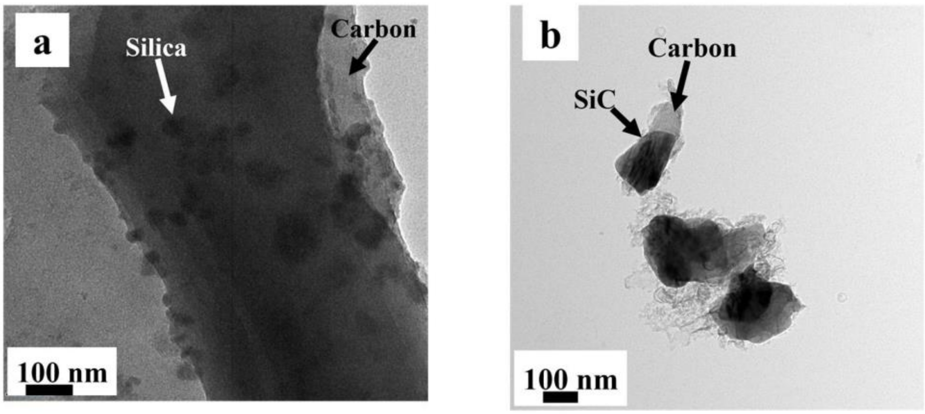

Fig. 5.8 Low magnification TEM images of **C/SiO$_2$** (a) and **C/SiC** (b) composite foams

The high magnification image of the **C/SiO$_2$** composite foam shows mostly amorphous regions. However, lattice fringes of SiC are observed in the high magnification TEM images of the **C/SiC** composite foam. The lattice spacing of 0.26 nm measured from the high magnification TEM image is in agreement with the d-spacing of the (1 1 1) plane of β-SiC. In addition, lattice fringes corresponding to graphite microcrystals in amorphous carbon matrix is observed in the high magnification TEM image of **C/SiC** composite foam. The high magnification TEM images showing the amorphous nature of **C/SiO$_2$**, lattice fringes of SiC and micro-graphite are shown in **Fig. 5.9a** to **c**.

The selected area electron diffraction pattern (SAED) of **C/SiC** shown in **Fig. 5.10** further supports the formation of the crystalline SiC phase during high-temperature heat treatment. The d-spacing calculated from the SAED pattern is 0.255 nm. This is in good agreement with the d-spacing calculated from the XRD spectra (0.256 nm)

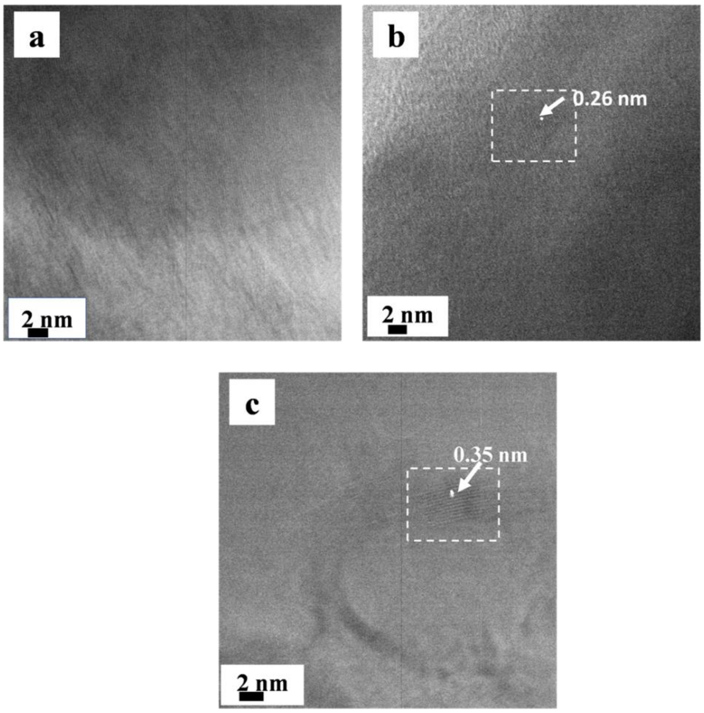

Fig. 5.9 High magnification TEM image of **C/SiO$_2$** composite foam(a) and **C/SiC** composite foam (b) showing lattice fringes of SiC and lattice fringes of microcrystalline graphite (c)

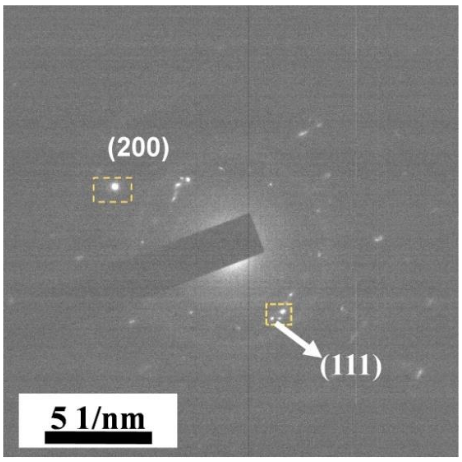

Fig. 5.10 SAED pattern of **C/SiC** composite foam

5.2.9 Foam Density

Aerospace applications demand foams of low density. The prepared **C/SiO$_2$** and **C/SiC** composite foams exhibited low density. The density of **C/SiO$_2$** and **C/SiC** composite foams with respect to the concentration of sucrose solution is presented in **Fig. 5.11**. The density of the **C/SiO$_2$** and **C/SiC** composite foams depends on the concentration of sucrose solution used for their synthesis. **C/SiO$_2$** composite foams exhibit a density from 0.26 to 0.37 g cm^{-3} when the concentration of sucrose solution varies from 300 to 600 g L^{-1}. The density of **C/SiC** composite foams exhibit the same trend but the values are lower than that of the corresponding **C/SiO$_2$** composite foams. The density of **C/SiC** composite foams observed varies from 0.18 to 0.29 g cm^{-3}. The filter-pressing of rice husk powder produces a body with a certain volume of inter-particle porosity. As the sucrose solution concentration increases, the inter-particle pores are gradually filled by sucrose. This results in the formation of more carbon at the inter-particle pores during carbonization leading to a rise in foam density. The lowering of density during heat treatment at 1600 °C is because of mass loss due to the carbothermal reduction of SiO_2 to SiC without any volume shrinkage of the body.

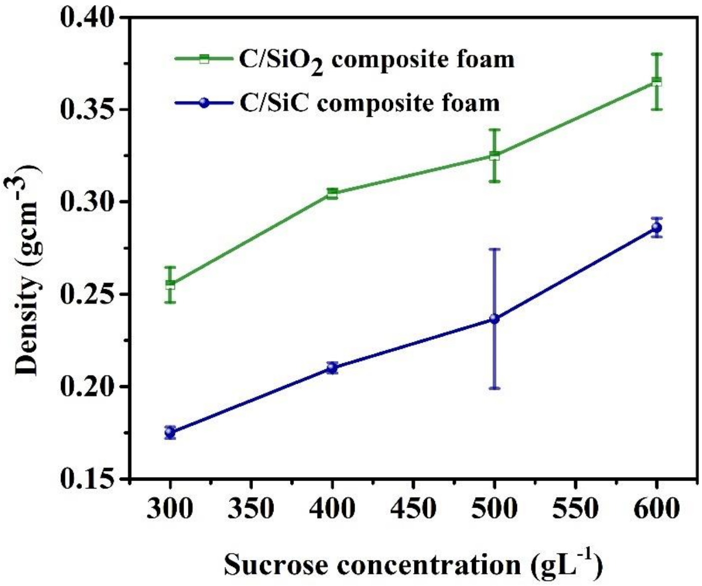

Fig. 5.11 Variation of density with respect to sucrose solution concentration

5.2.10 Compressive strength evaluation

The carbon composite foams for thermo-structural applications require structural integrity and reasonable strength. The structural integrity and strength in the **C/SiO$_2$** composite foams are achieved by the binding of carbonized rice husk particles by sucrose derived carbon. In the case of **C/SiO$_2$-200**, the carbon derived from a low concentration of sucrose in the composite body is not adequate to provide structural integrity. Hence, they crumble during the preparation of samples for compressive strength measurements and therefore are discarded from further evaluation. The stress-strain graphs of **C/SiO$_2$-300** to **C/SiO$_2$-600** are similar to that of the foam materials with brittle nature. Hence, there is an initial elastic region followed by a serrated long plateau up to ~40% strain and thereafter a densification zone. The serrated plateau region is due to the layer-by-layer brittle failure of the foam structure. The compressive stress-strain graph of **C/SiC** foams also exhibits similar behaviour. Nevertheless, the plateau is attained at low-stress levels. The compressive stress-strain graphs of **C/SiO$_2$** and **C/SiC** composite foams are shown in **Fig. 5.12a** and **Fig. 5.12b,** respectively. The stress at 20% strain is taken as the compressive strength and the slope of the initial linear region is considered as Young's modulus.

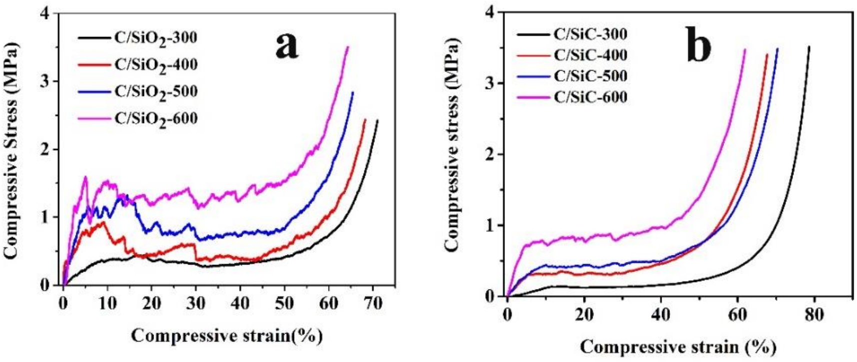

Fig. 5.12 Compressive stress-strain graph of **C/SiO$_2$** (a) and **C/SiC** composite foams prepared at various sucrose solution concentrations(b)

The compressive strength and Young's modulus of **C/SiO$_2$** and **C/SiC** composite foams are presented as a function of their density in **Fig. 5.13**. The compressive strength of **C/SiO$_2$** composite foams increases from 0.32 to 1.67 MPa when the foam density increases from 0.255 to 0.365 g cm^{-3}. The corresponding increase in Young's modulus is from 1.9 to 41.1 MPa. Regarding **C/SiC** foams, compressive strength and Young's modulus rises from 0.19 to 1.19 and 1.43 to 36.8 MPa, respectively, when foam density increases from 0.175 to 0.286 g cm^{-3}. It is an interesting observation that the specific strength of **C/SiO$_2$** and **C/SiC** composite foams observed are more or less in the same range. The specific strength of **C/SiO$_2$**

and **C/SiC** composite foams are in the ranges of 1.42 to 4.57 MPa $g^{-1}cm^3$ and 1.08 to 4.16 MPa $g^{-1}cm^3$, respectively.

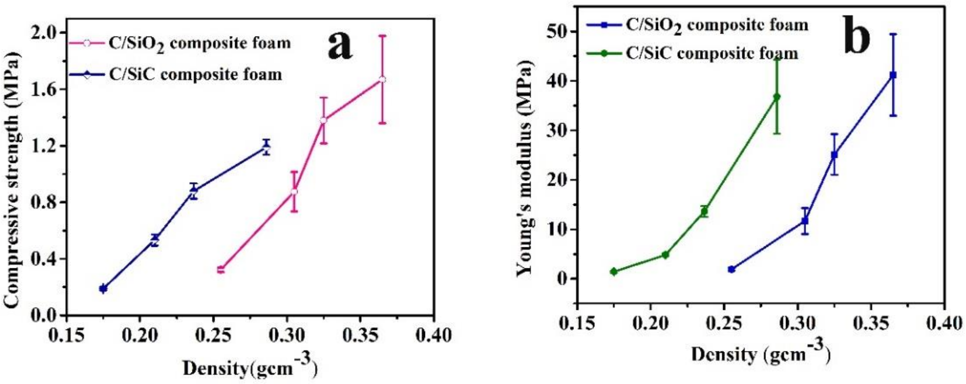

Fig. 5.13 Effect of density on the compressive strength (a)and Young's modulus (b) of **C/SiO2** and **C/SiC** composite foams

5.2.11 Thermal conductivity

The low density, thermal conductivity and high strength are the essential requirements for the foams to be used for thermo-structural applications in the aerospace industry. **Fig. 5.14** shows the thermal conductivity of **C/SiO2** and **C/SiC** composite foams as a function of density**.** The thermal conductivity of **C/SiO2** foams increases from 0.150 to 0.205 W $m^{-1}K^{-1}$ with an increase in density from 0.255 to 0.365 g cm^{-3}. The low thermal conductivity is mainly attributed to the strong scattering of phonon due to the high porosity and the amorphous SiO_2 in the carbonized rice husk particles. However, the **C/SiC** composite foams exhibit higher thermal conductivity values even though their densities are lower. The thermal conductivities of **C/SiC** composite foams increase from 0.165 to 0.431 W $m^{-1}K^{-1}$ when the density increases from 0.175 to 0.286 g cm^{-3}. The higher thermal conductivity of **C/SiC** composite foam is due to the presence of SiC and microcrystalline graphite having higher thermal conductivity in place of amorphous silica and carbon in **C/SiO2** composite foam.

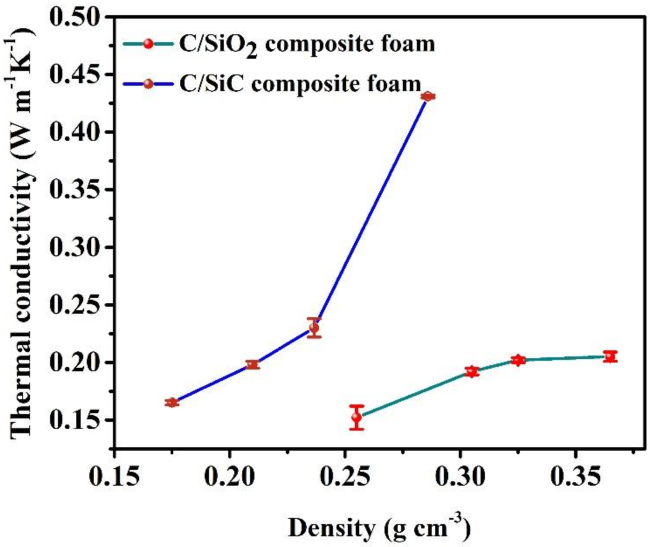

Fig. 5.14 Effect of density on the thermal conductivity of **C/SiO$_2$** and **C/SiC** composite foams

5.2.12 Oxidation and fire resistance

The oxidation resistance of the carbon composite foam was studied by thermogravimetric analysis. The TGA graph of **C/SiO$_2$** and **C/SiC** composite foams in an air atmosphere are shown in **Fig. 5.15**. The **C/SiO$_2$** composite foam is stable up to 490 °C. The major weight loss occurs from 490 °C onwards. The complete burnout of carbon from the **C/SiO$_2$** composite foam takes place at 670 °C. On the other hand, **C/SiC** composite foam is stable up to 520 ^{0}C. A major weight loss due to burnout of carbon takes place at a temperature in the range of 520 to 720 ^{o}C. The higher oxidation resistance of carbon in **C/SiC** is due to more ordering of graphene layers during heat-treatment at 1600 °C. The **C/SiO$_2$** and **C/SiC** composite foams have excellent fire resistance. They do not catch fire even when exposed to oxyacetylene flame. However, the flame pierces through the foam body on prolonged exposure due to oxidation of carbon and melting of silica or SiC. **Fig. 5.16** shows exposure of **C/SiO$_2$** composite foam to the oxyacetylene flame and the foam body after flame exposure showing the hole created by the piercing of the flame.

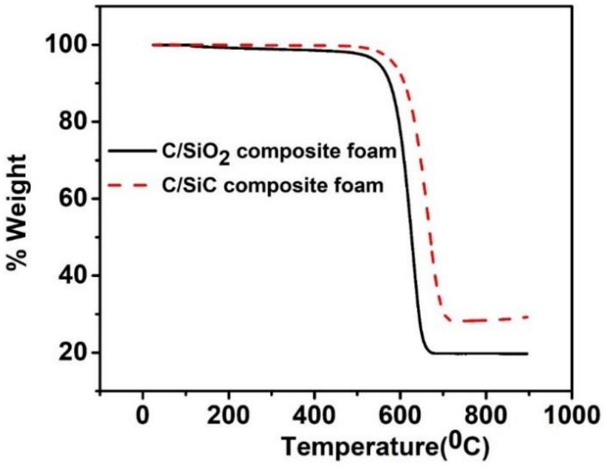

Fig. 5.15 TGA graph of C/SiO_2 and C/SiC composite foam

Fig. 5.16 Photograph showing **C/SiO_2** composite foam during (a) and after (b)exposure to oxyacetylene flame

5.2.13 Electrical conductivity

The electrical conductivity of **C/SiO_2** and **C/SiC** composite foams is plotted as a function of sucrose solution concentration in **Fig. 5.18**. The electrical conductivity of **C/SiO_2** composite foams increases from 19 to 94 S cm^{-1} when the sucrose solution concentration increase from 300 to 600 g L^{-1}. The observed enhancement in electrical conductivity is due to an increase in foam density and reduction in silica content with an increase in the concentration of sucrose solution. **C/SiC** composite foams show higher electrical conductivity compared to the corresponding **C/SiO_2** composite foam samples. The electrical conductivity of the **C/SiC** composite foams is in the range of 102 to 371 S cm^{-1}. The greater electrical conductivity of **C/SiC** composite foam samples is due to the formation of graphite micro-crystals during heat-treatment at 1600 ˚C for carbothermal reduction.

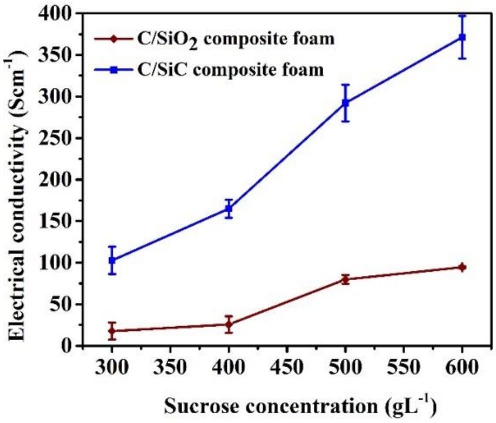

Fig. 5.17 Variation of electrical conductivity of **C/SiO$_2$** and **C/SiC** composite foams with the concentration of sucrose solution

5.2.14 EMI shielding effectiveness

The composition, microstructural features and electrical conductivity of **C/SiO$_2$** and **C/SiC** composite foams are suitable for EMI shielding application. That is, the carbon in the composite materials contributes to EMI shielding by conduction losses whereas the silica and SiC being dielectric materials contribute by dipolar relaxation. The pore channels and corrugated surface structure in the carbonized and carbothermal reduced rice husk particles create a large area of interfaces for the attenuation of EM waves. Besides, the inter-particle pores facilitate multiple internal reflections leading to improved absorption of EM waves.

A representative graph showing EMI shielding effectiveness of **C/SiO$_2$** composite foam as a function of frequency in the 8-12 GHz range (X-band) is shown in **Fig. 5.18 a**. The **C/SiO$_2$** composite foams show more or less uniform values of shielding effectiveness throughout the entire X-band region indicating the homogeneity of the composition and pore structure of the foam material. The EMI shielding of the **C/SiO$_2$** composite foams is dominated by the absorption contribution. The **C/SiO$_2$** composite foams at various sucrose solution concentrations exhibit more or less the same reflection component (~ 8dB) to the total EMI shielding effectiveness. However, the absorption component of the total EMI shielding effectiveness of these **C/SiO$_2$** composite foams increases from 11 to 30.5 dB when the sucrose solution concentration increases from 300 to 600 g L^{-1}. The total shielding effectiveness observed is in the range of 18 to 38.5 dB. The increase in shielding effectiveness is due to an increase in foam density. The EMI shielding effectiveness at 11 GHz as a function of sucrose solution concentration is exhibited in **Fig. 5.18b**. The specific shielding effectiveness obtained by dividing shielding effectiveness with foam density is in the range of 76.2 to 106.9 dB $g^{-1}cm^{3}$.

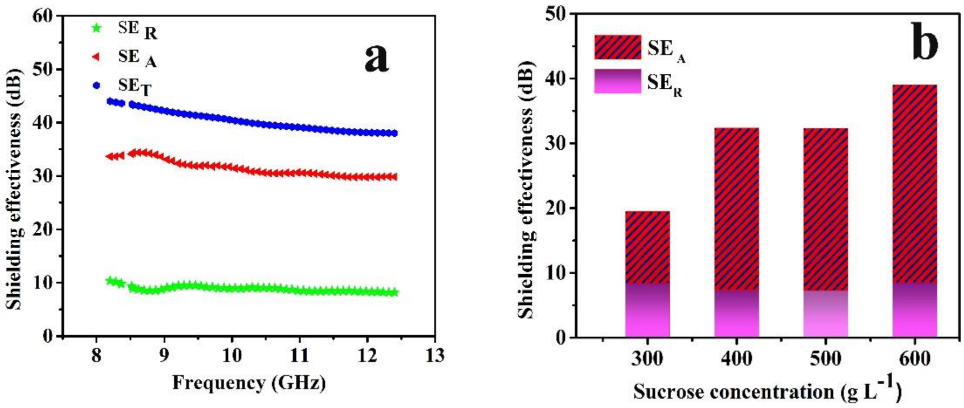

Fig. 5.18 Typical EMI shielding effectiveness as a function of frequency (a)and EMI shielding effectiveness as a function of sucrose solution concentration of **C/SiO_2** composite foams(b)

The low strength of **C/SiC-300** does not allow the preparation of thin samples for EMI shielding measurements. All the remaining **C/SiC** composite foam samples show low and more or less the same (9 to 9.4 dB) reflection contribution to the total shielding effectiveness. The total EMI shielding effectiveness of **C/SiC** composite foams increase from 20 to 43.7 dB when the concentration of sucrose solution varies from 400 to 600 g L^{-1}. That is, the total EMI shielding effectiveness of **C/SiC** composite foams is dominated by the absorption contribution (11 to 34.3 dB). The typical graph of shielding effectiveness with the frequency in the X-band and the shielding effectiveness at 11 GHz vs concentration of sucrose solution is presented in **Fig. 5.19**. The specific shielding effectiveness of C/**SiC** composite foams is in the range of 100 to 152.8 dB $g^{-1}cm^{3}$. The specific shielding effectiveness is higher than that observed for the corresponding **C/SiO_2** composite foams. The increase in specific shielding effectiveness is due to an increase in electrical conductivity of the samples as a result of the formation of the graphite micro-crystals during heat treatment at 1600 °C.

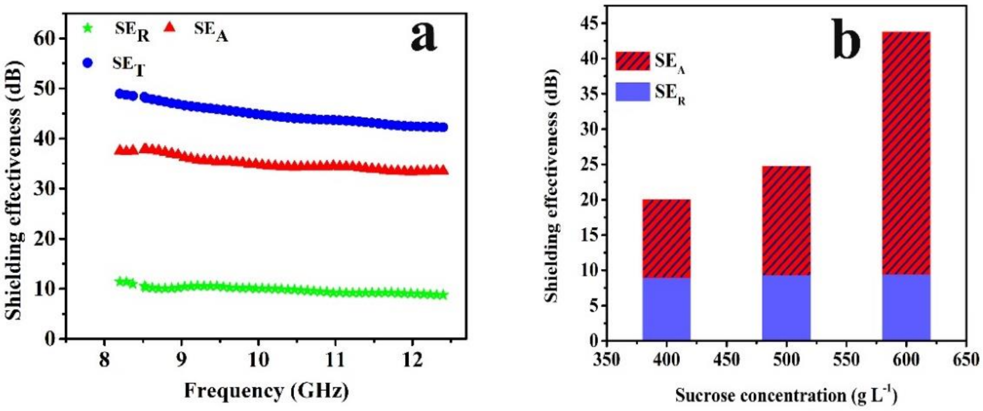

Fig. 5.19 The EMI shielding effectiveness as a function of the frequency of **C/SiC-600** (a) and (b) the EMI shielding effectiveness as a function of sucrose solution concentration of **C/SiC** composite foams

5.3 Conclusions

Robust **C/SiO$_2$** and **C/SiC** composite foam monoliths are prepared from rice husk powder through an eco-friendly processing route. The **C/SiO$_2$** and **C/SiC** composite foams are obtained by the carbonization and subsequent carbothermal reduction, respectively, of rice husk-sucrose composites prepared by filter-pressing rice husk powder dispersion in sucrose solutions. The uniform distribution of sucrose in the rice husk-sucrose composite is ensured by freeze-drying. The XRD analysis indicates the amorphous nature of silica in **C/SiO$_2$** composite foam and β-SiC and microcrystalline graphite in **C/SiC** composite foams. The formation of β-SiC and graphite microcrystals is further confirmed by HR-TEM analysis and Raman spectra. The uniform distribution of SiO$_2$ and SiC particles in the carbon matrix is evidenced from the TEM analysis. The lattice fringes of SiC and the microcrystalline graphite are observed in the TEM images of **C/SiC** composite foams. The density of **C/SiO$_2$**(0.26 to 0.37 g cm^{-3}) and **C/SiC** (0.18 to 0.29 g cm^{-3}) composite foams increases with an increase in the concentration of sucrose solution (300 to 600 g L^{-1}). The electrical conductivity of **C/SiO$_2$** increases from 19 to 94 S cm^{-1} when the sucrose solution concentration increase from 300 to 600 g L^{-1}. The **C/SiC** composite foams show higher electrical conductivity in the range of 102 to 371 S cm^{-1} due to the formation of graphite micro-crystals during heat-treatment at

1600 ^{o}C for carbothermal reduction. The compressive strength, thermal conductivity and EMI shielding effectiveness of the carbon composite foams increase with an increase in density. The compressive strength, thermal conductivity and EMI shielding effectiveness of the **C/SiO$_2$** composite foams are in the ranges of 0.32 to 1.67 MPa, 0.150 to 0.205 Wm^{-1}K^{-1} and 18 to 38.5 dB, respectively. The compressive strength decreases to the range of 0.19 to 1.19 MPa and thermal conductivity and EMI shielding effectiveness increase to the ranges of 0.165-0.431 Wm^{-1}K^{-1} and 20 to 43.7 dB, respectively, by carbothermal reduction of silica in the **C/SiO$_2$** composite foam to SiC. The inherited pore channels and corrugated surface features of rice husk and the inter-particle porosity contribute to EM absorption by promoting multiple internal reflections and providing additional interfaces for attenuation. The dielectric SiO$_2$ and SiC contribute by dipolar relaxation and carbon contributes by conductive loss to the total EMI shielding effectiveness. The lightweight, low thermal conductivity, high-temperature stability and absorption dominated EMI shielding effectiveness make the carbon composite foams attractive for high-temperature thermal insulation and EMI shielding in aerospace and defence.

CHAPTER-6

CARBON- GEHLENITE COMPOSITE FOAMS FROM NEWSPAPER

6.1 Introduction

Paper waste is creating major concerns for most of the municipalities all over the world. The newspaper contains cellulose and inorganic filler materials(Sahin & Arslan, 2008). Cellulose is a well-known carbon precursor. Preparation of carbon-based products utilizing newspaper waste not only generate wealth but also helps the management of solid waste. In addition, this avoids the generation of carbon dioxide during the biodegradation of paper waste dumped in the land(Katinas et al., 2019). Preparation of cellulose aerogels from paper waste is well reported in the literature(Y. Chen et al., 2020; Zhanying Li et al., 2018; Nguyen et al., 2013; K. Shi et al., 2019). In the majority of the reported methods, waste paper dispersed in NaOH/urea solution is refrigerated for 24 hours followed by thawing and coagulation in ethanol to form a gel. This gel is subsequently solvent exchanged with de-ionized water and freeze-dried to produce the cellulose aerogels(L. Li et al., 2017; Nguyen et al., 2013). Feng et al produced cellulose aerogels by cross-linking the waste paper dispersed in water with Kymene followed by freeze-drying(Feng et al., 2015). Jin et al used an ionic liquid-based process for the preparation of cellulose aerogel from the waste newspaper. These aerogels are used as recyclable oil absorbers after modifying their surfaces to hydrophobic with molecules such as trimethylchlorosilane and methyl trimethoxy silane(Jin et al., 2015). The cellulose-based aerogels are also used as low-temperature thermal insulation materials(Fischer et al., 2006; Gupta et al., 2018; Seantier et al., 2016). In an alternative approach, the cellulose aerogels produced from paper waste are converted into flexible carbon aerogels by pyrolysis and then used as recyclable oil-absorbing materials(Han et al., 2016). However, the carbon aerogels reported from the paper waste are having a very low density (6 to 24 mg cm^{-3})(Bi et al., 2014; L. Li et al., 2017). Therefore, they do not possess adequate mechanical strength to use in any thermo-structural applications. In the present chapter, the preparation of mechanically robust carbon composite foams from the waste newspaper is presented. In this, filter-pressing of newspaper pulp prepared in sucrose solution followed by drying and carbonization is used for the preparation of robust carbon composite foams. The density, compressive strength, thermal conductivity and EMI shielding effectiveness of the carbon composite foams are evaluated as a function of sucrose solution concentration and discussed.

6.2 Results and discussion

6.2.1 Characterization of newspaper ash

The TGA graph of the newspaper is shown in **Fig. 6.1**. The newspaper is thermally stable up to 200 ^{o}C in air. A rapid weight loss of ~60% is observed in the temperature range of 200 to 310 °C due to oxidation of cellulosic component. Further increase of temperature results in a slow weight loss of ~28% up to 600 ^{o}C. The ash content of ~12 wt.% is remained at 900 ^{o}C.

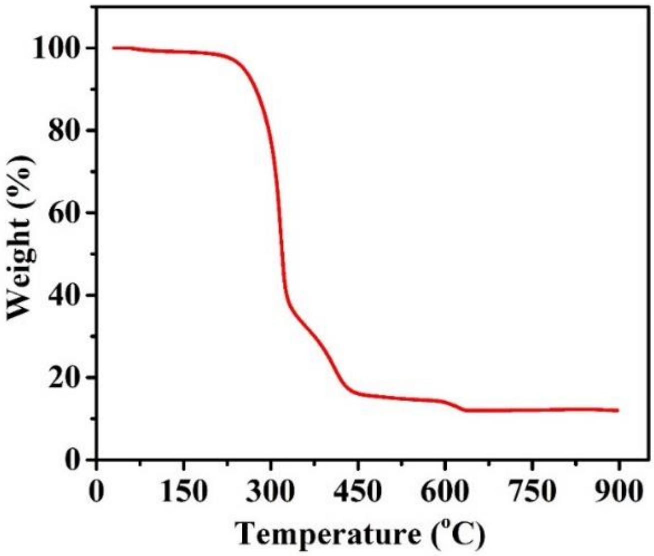

Fig. 6.1 TG curve of newspaper

The XRD spectrum of the ash obtained by burning off the organic matter present in the newspaper at 900 ^{o}C indicates the presence of gehlenite as a major phase. Besides this, calcium aluminium silicate (PDF 00-062-0853) and silica (PDF 01-

073-3466) are also present. The kaolinite and calcium carbonate generally used as additives in newspapers undergo thermal decomposition on heating at 900 °C to form metakalonite($Al_2O_3.2SiO_2$) and lime. These two further react to form gehlenite. (Ptáček et al., 2013). The XRD pattern of the newspaper ash is shown in **Fig. 6.2**. The standard XRD spectra of gehlenite, calcium aluminium silicate and silica overlaid and provided as an inset in **Fig.6.2**.

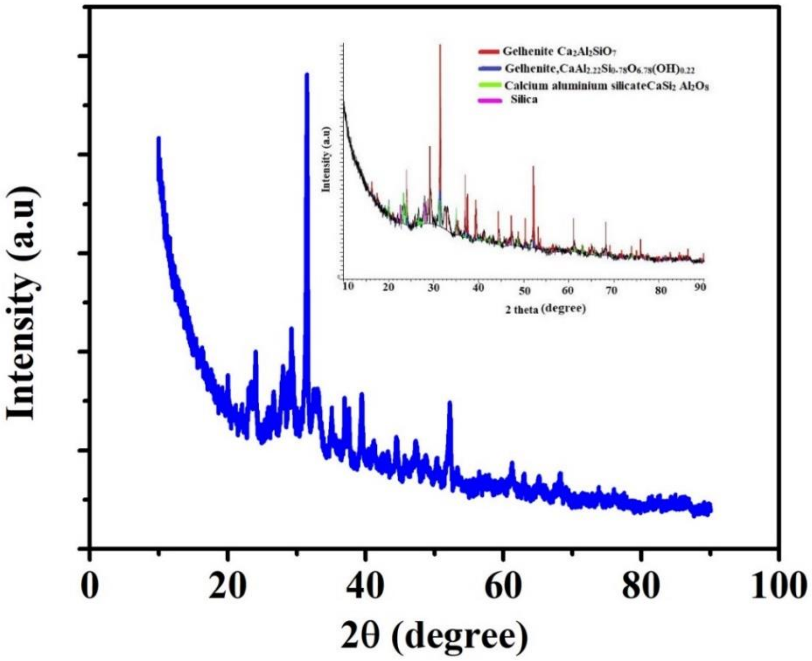

Fig. 6.2 XRD pattern of newspaper ash

The SEM image shows that the newspaper ash contains a mixture of spherical and irregular particles. The SEM micrograph of newspaper ash is shown in **Fig. 6.3**.

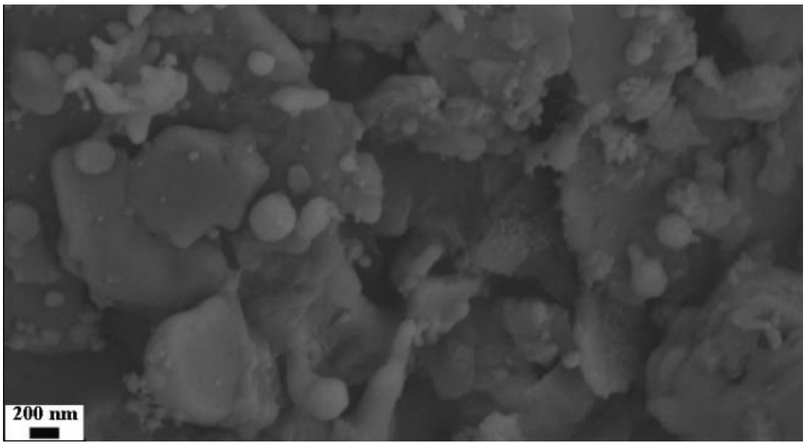

Fig. 6.3 SEM micrograph of newspaper ash

The EDAX analysis of the ash shows the presence of calcium, aluminium, silicon and oxygen with atomic percentages of 22.25, 10.9, 19.19, and 47.99, respectively. The EDAX graph of the ash is shown in **Fig. 6.4.**

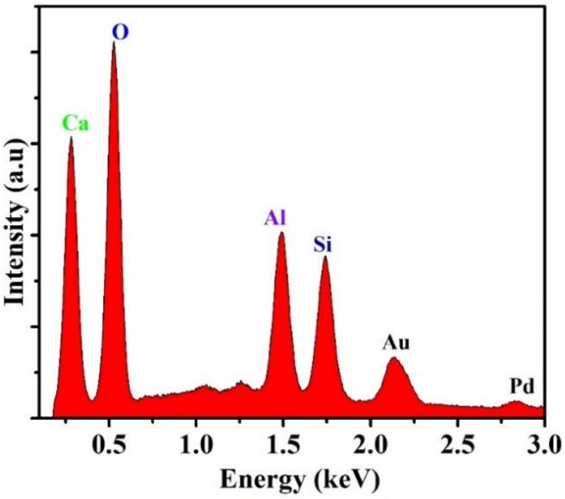

Fig. 6.4 EDAX spectrum of newspaper ash

The particle size of the newspaper ash was measured using the laser scattering method. The particle size distribution of the newspaper ash is displayed in **Fig. 6.5**. The newspaper ash contains particles in the size range of 0.4 to 22.5 µm. The average particle size observed is 5.2 µm.

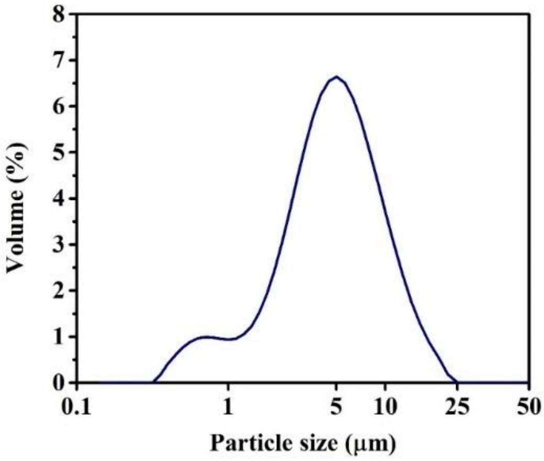

Fig. 6.5 Particle size distribution of the newspaper ash

6.3.2 Preparation and characterization of newspaper pulp

The newspaper soaked in sucrose solution for 1 hour turned into a pulp up on thorough mixing using a kitchen mixture for 5 minutes. The SEM analysis of samples prepared by drop-casting the newspaper pulp indicated the presence of micro-ribbons. For the preparation of the sample for SEM, the water present in the newspaper pulp prepared at zero sucrose solution concentration was exchanged with acetone before drop-casting. The exchange of water with acetone was carried out by repeated dispersion and centrifugation of the newspaper pulp in acetone. The SEM photomicrograph of the newspaper pulp is shown in **Fig. 6.6**. The width of micro ribbons measured from the SEM image is ~ 15 μm. In addition to the micro-ribbons, some smaller fibres and particles formed from the newspaper is also seen in the SEM micrograph. That is, during the mixing with sucrose solution, the wet newspaper splits mainly into micro-ribbons of ~ 15 μm width.

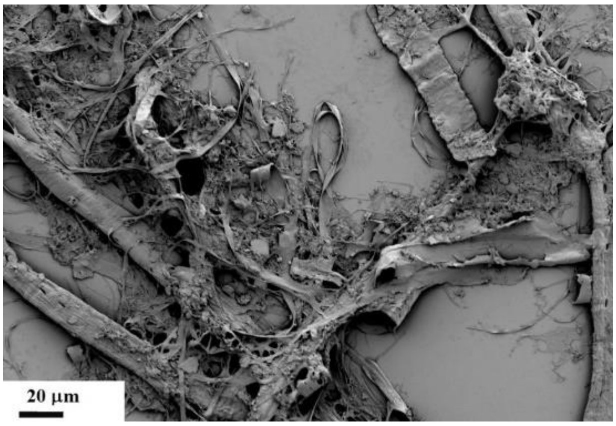

Fig. 6.6 SEM image of newspaper pulp

The newspaper pulp prepared in sucrose solution shows sufficiently low viscosity to pour into the PVC pipe of the filter-pressing setup. The pulps show highly shear-thinning flow behaviour with high viscosities in the range of 2.2 to 4.5 Pa.s at a low shear rate of 4.65 s^{-1} and low viscosities in the range of 0.31 to 0.45 Pa.s at a high shear rate of 93 s^{-1}. The rapid decrease in viscosity with an increase in shear rate is due to the disentanglement of the newspaper micro-ribbons at higher shear rates. **Fig. 6.7** shows the viscosity versus shear rate plots of newspaper pulp prepared at various sucrose solution concentrations. The viscosity of the newspaper pulp initially shows a decrease with an increase of sucrose solution concentration up to 200 g L^{-1}. Further increase in sucrose solution concentration increases the viscosity of the pulp. The initial decrease in viscosity observed is attributed to the improvement in the dispersion of newspaper micro-ribbons due to the hydrophilic sucrose molecules. However, the increase in viscosity of the dispersion medium at sucrose solution concentrations higher than 200 g L^{-1} overshadows the observed decrease in viscosity due to the improvement of dispersion at lower sucrose concentrations.

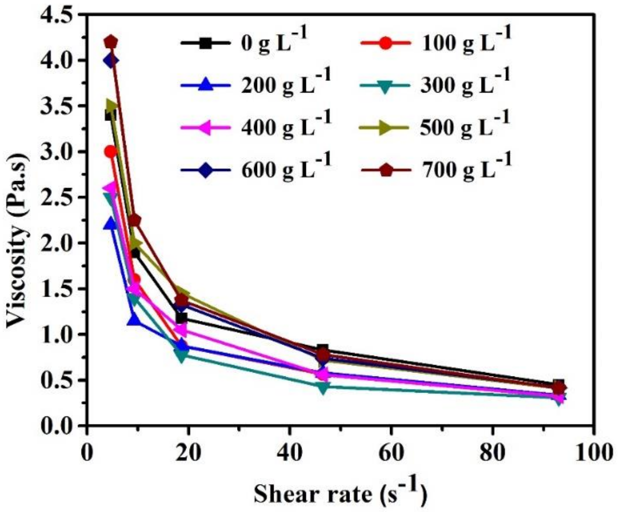

Fig. 6.7 Variation of sucrose solution concentration on the viscosity at various shear rates of newspaper pulp

6.3.3 Consolidation of newspaper pulp and compressive strength of consolidated wet-bodies

The vacuum filtration of the newspaper pulp using the filter-pressing setup consolidates the micro-ribbons into a cylindrical wet body. A slight pressing by the piston over the pulp towards the end of consolidation prevents the lateral shrinkage, resulting in a wet body with a uniform cylindrical shape. The filter pressed wet bodies are likely to have a network of newspaper micro-ribbons and the space in between them is filled with the sucrose solution. The filter-pressed bodies are sufficiently stable for easy removal from the PVC pipe and further handling without any deformation. This is further evidenced by their compressive stress-strain measurements. The filter-pressed wet bodies prepared at sucrose solution concentrations in the range of 0 to 700 g L^{-1} show compressive stress of nearly 1kPa at 10 % strain. The compressive stress-strain graphs of filter-pressed wet bodies prepared at 0 and 700 g L^{-1} are shown in **Fig. 6.8**.

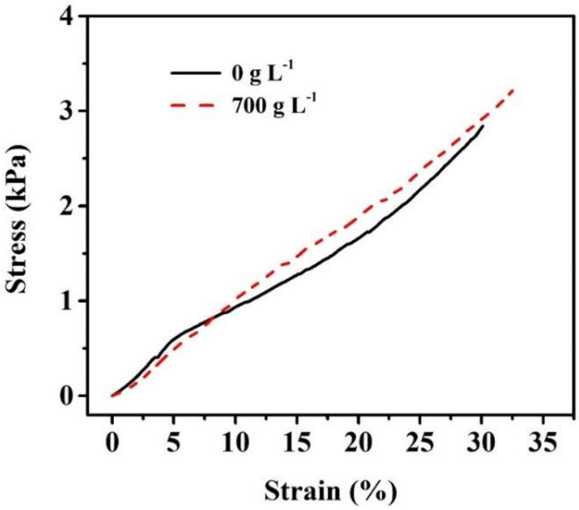

Fig. 6.8 Compressive stress-strain graph of filter-pressed wet bodies

6.3.4 Newspaper-sucrose composite

Newspaper-sucrose composite was formed as a result of drying of the filter-pressed wet bodies at 70°C. During drying of the filter pressed wet bodies, the sucrose binds the newspaper micro-ribbons to form newspaper-sucrose composites. A photograph of the wet filter-pressed body and newspaper-sucrose composite is shown in **Fig. 6.9**.

Fig. 6.9 Photograph showing wet filter-pressed body (a) and newspaper-sucrose composite(b)

As the weight of the newspaper is constant, the amount of sucrose retained in the body depends on the sucrose solution concentration. An estimate of sucrose concentration in the composite is obtained from the final weight of the newspaper-sucrose composite and the initial weight of the newspaper taken. The weight percentage of sucrose in the composites increases from 0 to 66 % when the sucrose solution concentration increases from 0 to 700 g L^{-1}. **Fig. 6.10** depicts a variation of sucrose retained in the body as a function of sucrose solution concentration.

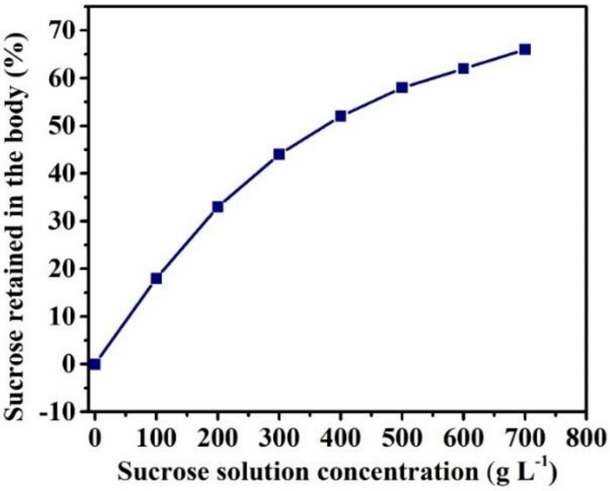

Fig. 6.10 Variation of sucrose retained in the body as a function of sucrose solution concentration

A considerable shrinkage of the wet-filter pressed body was observed during the drying process. The drying shrinkage of the filter-pressed wet bodies as a function of sucrose solution concentration is shown in **Fig. 6.11**. The wet filter-pressed bodies show a major linear (filter pressing direction) shrinkage and a marginal diametrical shrinkage during drying. The linear shrinkage decreases rapidly from 45.8 to 32.0% when the sucrose solution concentration increases from 0 to 100 g L^{-1}. Further increase in sucrose solution concentration to 700 g L^{-1} slowly decreases the linear shrinkage to 15.2%. The filter pressed wet bodies prepared at zero sucrose solution concentration shows a diametrical drying shrinkage of 1.6 wt.%. The diametrical drying shrinkage decreases marginally from 1.6 to 0.43% when the sucrose solution concentration increases from 0 to 700 g L^{-1}. The low diametrical drying shrinkage indicates that the majority of newspaper micro-ribbons orient themselves in the X-Y plane (perpendicular to the filter pressing direction) during the filter pressing. The decrease in drying shrinkage with an increase in sucrose solution concentration shows that the sucrose precipitated in between the newspaper micro-ribbons during drying prevents the shrinkage.

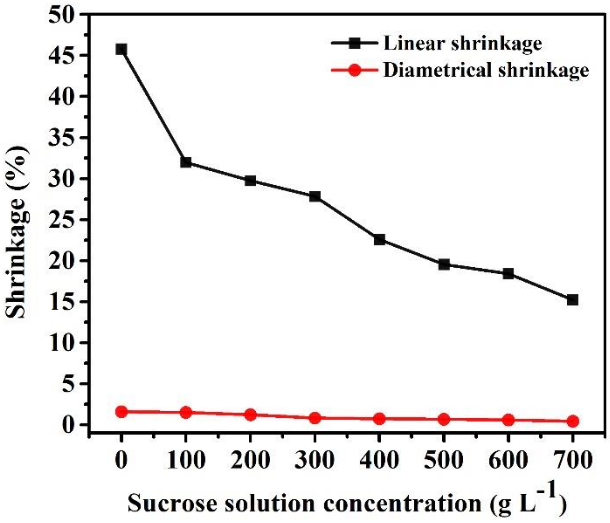

Fig. 6.11 Effect of sucrose solution concentration on the drying shrinkage of wet bodies obtained by filter-pressing of newspaper pulp

This study evidences that the shrinkage in the filter pressing direction is governed by the sucrose solution concentration whereas the diametrical shrinkage is controlled by the orientation of newspaper micro-ribbons perpendicular to the filter pressing direction. The microstructure of the dried filter-pressed body prepared at zero sucrose solution concentration clearly shows the orientation of the newspaper micro-ribbons perpendicular to the filter pressing direction. The large volume of pores in between the micro-ribbons is visible in the microstructure. These pores are progressively filled by sucrose with an increase in sucrose solution concentration. At a sucrose solution concentration of 700 g L^{-1}, the pores created by the newspaper micro ribbons are almost filled by the sucrose. The SEM microstructure of newspaper-sucrose composites prepared at sucrose solution concentrations of 0 and 700 g L^{-1} are shown in **Fig. 6.12**.

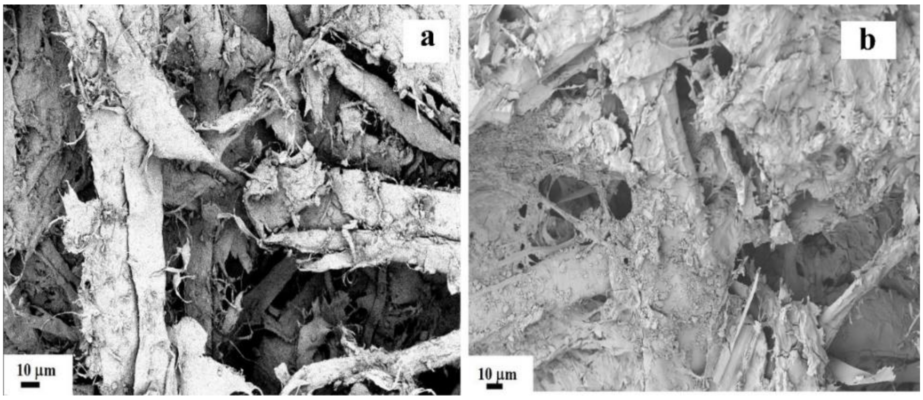

Fig. 6.12 SEM micrograph of newspaper-sucrose composites prepared at sucrose solution concentrations of 0 g L^{-1} (a) and 700 g L^{-1}(b)

The density of the newspaper-sucrose composite depends on the amount of sucrose retained in the body during filter-pressing as well as the shrinkage during drying. The density of the newspaper-sucrose composites increases from 0.27 to 0.59 g cm^{-3} when the sucrose solution concentration increases from 0 to 700 g L^{-1}. The increase in density is due to the progressive filling of the pores created by the assembly of newspaper micro-ribbons by sucrose with an increase in sucrose solution concentration. The density of the newspaper-sucrose composite as a function of sucrose solution concentration is shown in **Fig. 6.13**.

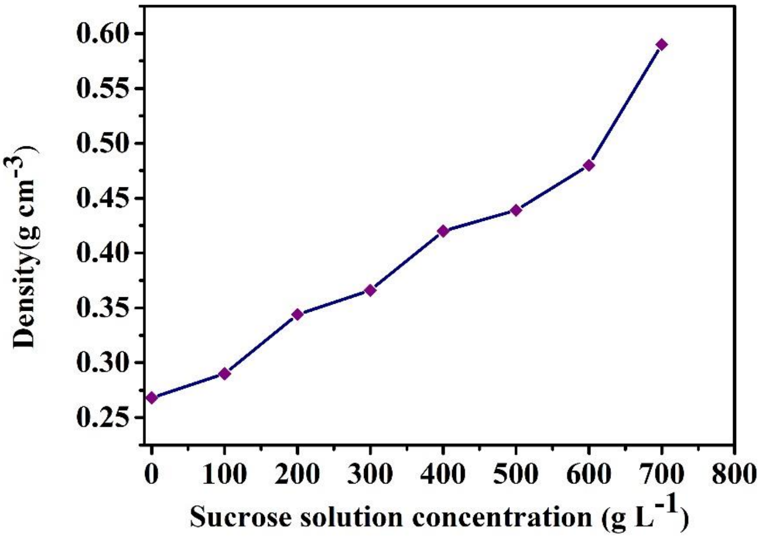

Fig. 6.13 Variation of density as a function of sucrose concentration

The compressive stress-strain curves of the newspaper-sucrose composites are displayed in **Fig. 6.14**. The newspaper-sucrose composite prepared at sucrose solution concentrations in the range from 0 to 300 g L^{-1} shows a slow and linear increase of stress with strain up to the point of strain hardening. The bending of the newspaper microribbons is responsible for the linear region at low-stress values. On the other hand, newspaper-sucrose composites prepared at sucrose solution concentrations in the range of 400 to 700 g L^{-1} show a rapid increase in stress with strain in the beginning up to a yield point followed by strain hardening. The strain hardening is due to the densification of the composite. The slope of the initial linear region is taken as Young's modulus and the stress at 10% strain is taken as the compressive strength.

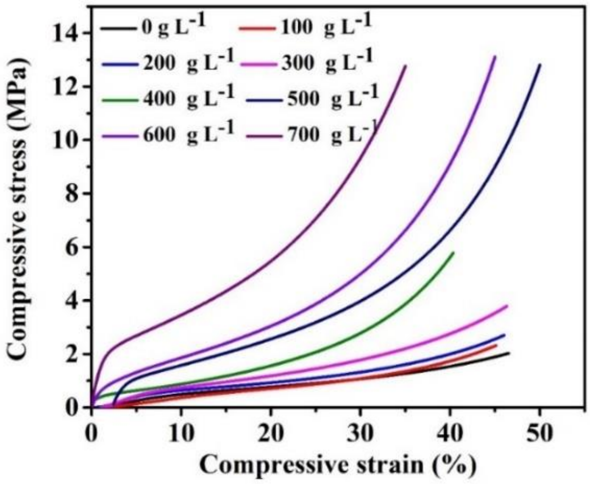

Fig. 6.14 Stress-strain curve of the newspaper-sucrose composite

The compressive strength of the newspaper-sucrose composites increases slowly from 0.4 to 0.9 MPa when the sucrose solution concentration increases from 0 to 500 g L^{-1}. Further increase in sucrose solution concentration to 700 g L^{-1} rapidly increases the compressive strength to 3.43 MPa. Young's modulus also shows a similar trend as that of compressive strength data. That is, Young's modulus slowly increases from 5.2 to 23 MPa when the sucrose solution concentration increases from 0 to 500 g L^{-1}. Further increase in sucrose solution concentration to 700 g L^{-1} rapidly increases Young's modulus value to 95.3 MPa. The compressive strength and Young’s modulus of the newspaper-sucrose composites prepared at various sucrose solution concentrations are shown in **Fig.6.15**.

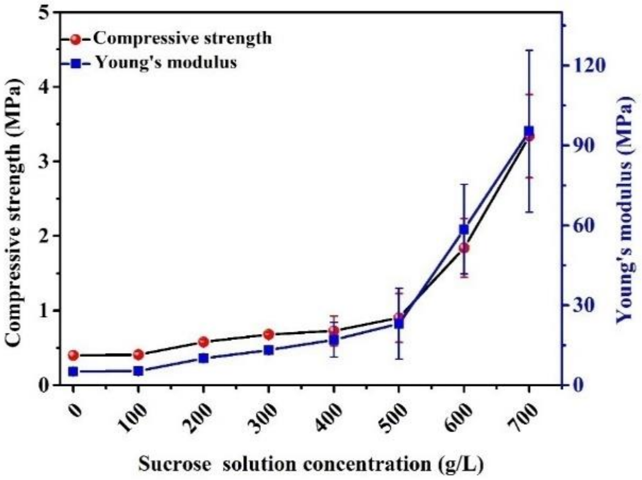

Fig. 6.15 The compressive strength and Young’s modulus of newspaper-sucrose composites as a function of sucrose solution concentration

6.2.5 Newspaper-caramelin composite

On annealing at 160 °C, sucrose in the newspaper-sucrose composites melts before caramelization. The caramelization involves the decomposition of sucrose to glucose and fructose anhydride and their subsequent condensation to form compounds such as caramelan and caramelen with the molecular formula $C_{24}H_{36}O_{18}$ and $C_{36}H_{50}O_{25}$, respectively. These compounds undergo further condensation with their precursors to produce infusible polymeric compounds such as humin or carameline with an average molecular formula of $C_{125}H_{188}O_{80}$(DeMan, 1999; R Narasimman & Prabhakaran, 2012). The colour of the newspaper-sucrose composites turned dark brown during the annealing due to oxidation. No deformation or bloating of the composites is observed during the caramelization. In addition, no molten sucrose oozes out as the newspaper micro-ribbon assembly acts like a sponge to contain the molten sucrose.

The SEM microstructure of the newspaper-caramel composites prepared at sucrose solution concentrations of 300 g L^{-1} and 700 g L^{-1} are shown in **Fig. 6.16**. From the microstructure, it is evident that the newspaper micro-ribbons in the composites are properly welded together by the melting and caramelization of the sucrose. As the sucrose content increases, the bonding between the newspaper microribbon and caramel enhances and the inter-newspaper micro ribbon spaces are progressively filled with caramelin.

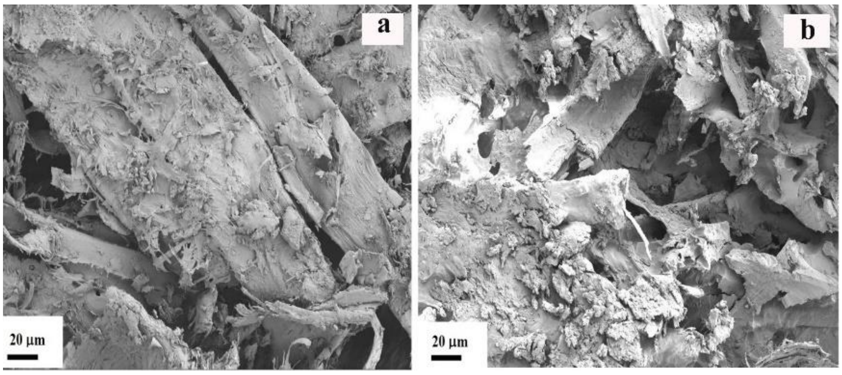

Fig. 6.16 SEM micrograph of the newspaper-caramel composite prepared at sucrose solution concentrations of 300 g L^{-1}(a) and 700 g L^{-1}(b)

6.2.6 Carbon- gehlenite composite foams

6.2.6.1 Carbonization shrinkage

The caramelized sucrose and newspaper micro-ribbons in the newspaper-caramel composites undergo carbonization during heating in an inert atmosphere to form composite foams consisting of carbon and gehlenite (inorganic matter present in the newspaper). The carbon composite foam yield (percentage weight retention after carbonization) observed is in the range of 26.15 to 28.45% of the newspaper-sucrose composite. The newspaper-caramel composites do not show any deformation during the carbonization. However, there is a uniform shrinkage during the carbonization. The newspaper composite prepared at zero sucrose solution concentration shows the lowest linear shrinkage of 36.6% during carbonization. The linear shrinkage increases to 44.6% when the sucrose solution concentration increases to 100 g L^{-1}. Further increase in sucrose solution concentration to 700 g L^{-1} gradually decreases the linear shrinkage to 36.8%. Unlike the marginal diametrical shrinkage observed during drying, the newspaper-sucrose composites undergo considerable diametrical shrinkage during carbonization. The diametrical carbonization shrinkage decreases from 23.8 to 21.8 % when the sucrose solution concentration increases from 0 to 700 g L^{-1}. That is, the variation of diametrical shrinkage with sucrose solution concentration is again marginal. This indicates that the diametrical shrinkage during carbonization is also controlled by the newspaper micro-ribbons oriented perpendicular to the filter-pressing direction. The effect of sucrose solution concentration on linear and diametrical shrinkage during carbonization are shown in **Fig. 6.17.** The newspaper micro-ribbons in the newspaper composite prepared at zero sucrose solution concentration form a very compact structure during drying as evidenced from the observed highest drying shrinkage. The observed lower linear carbonization shrinkage at zero sucrose solution concentration is due to the compact structure of the newspaper micro-ribbons before the carbonization. On the other hand, at a sucrose solution concentration of 100 g L^{-1}, the sucrose precipitated in between the micro-ribbons during drying prevents their close packing. The increase in linear shrinkage during carbonization when the sucrose concentration increases from 0 to 100 g L^{-1} is due to the poor packing of the micro ribbons in the newspaper-sucrose composites. Further increase in sucrose solution concentration progressively fills the voids between micro-ribbons with sucrose resulting in a gradual decrease of linear carbonization shrinkage

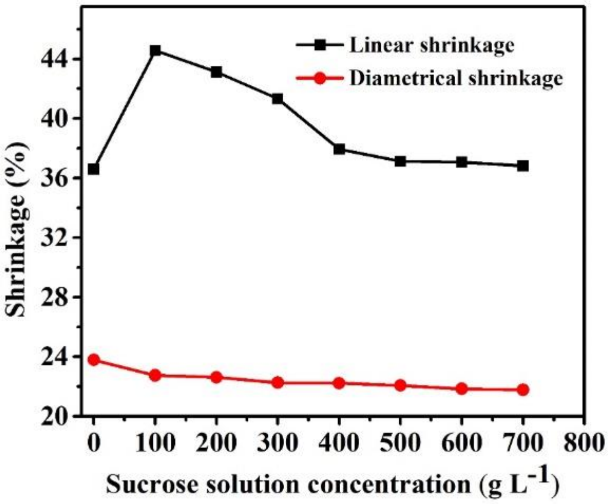

Fig. 6.17 Effect of sucrose solution concentration on carbonization shrinkage of newspaper-sucrose composite

6.2.6.2 XRD and Raman spectra

Like other carbon foam materials, carbon composite foams exhibited two broad peaks at 2θ values of ~ 23.5° and 44° in XRD spectrum corresponding to (002) and (100) plane, respectively, of turbostratic carbon(Barnakov et al., 2015a). In addition to these, some peaks are also visible in the XRD spectrum corresponding to the gehlenite present in the carbon composite foam. **Fig. 6.18** depicts the XRD spectrum of a typical carbon- gehlenite composite foam. The d- spacing values calculated from (002) reflection of the carbon composite foams prepared at sucrose solution concentrations of 0, 300 and 700 g L^{-1} are 0.367, 0.378 and 0.376 nm, respectively. The obtained values confirm poor stacking of graphene layers in the turbostratic carbon.

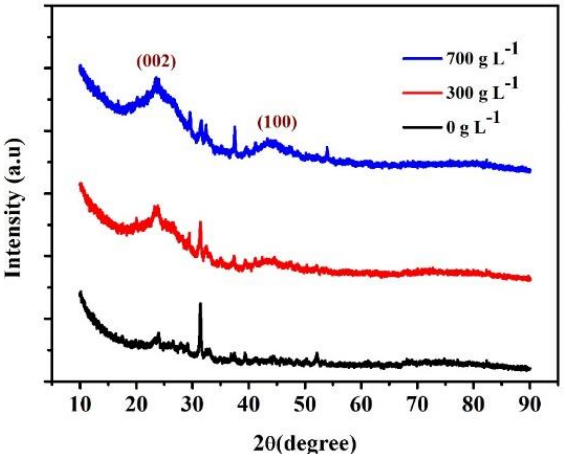

Fig. 6.18 XRD spectra of the carbon composite foams

The crystalline nature of the carbon composite foam is further confirmed by Raman spectra. Similar to other carbon foam materials, the newspaper derived composite foams show two broad peaks at 1345 cm^{-1} (D band) and 1590 cm^{-1} (G band) corresponding to disordered (sp^3) and the graphitic (sp^2) carbon, respectively(Konstantin et al., 2008). **Fig. 6.19** shows Raman spectra of the representative carbon composite foams. I_D/I_G ratio of the carbon composite foams are in the narrow range of 2.20 to 2.18. This indicates that the carbon in carbon-gehlenite composite foams prepared at all sucrose solution concentrations are more or less equally disordered.

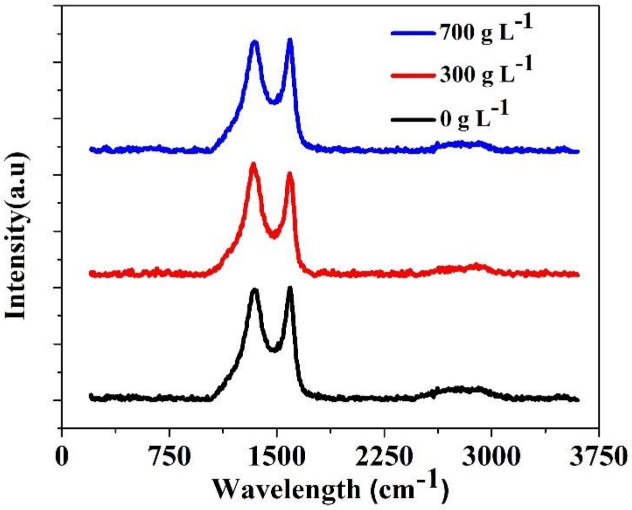

Fig. 6.19 Raman spectra of the carbon composite foams

6.2.6.3 Microstructure

During the carbonization, newspaper micro-ribbons form carbon-gehlenite composite micro-ribbons. That is, the carbon composite foam prepared at zero sucrose solution concentration contains an assembly of carbon-gehlenite composite micro-ribbons. The pores created in between the micro-ribbons are progressively filled by carbon produced by the pyrolysis of sucrose. This is evidenced by the SEM micrograph of the carbon- gehlenite composite foams as shown in **Fig. 6.20**. The macropores produced in between the carbonized newspaper micro-ribbons are visible in the SEM micrograph of carbon composite foam prepared without sucrose. These macropores are progressively filled by the carbon produced from the sucrose in samples prepared at higher sucrose solution concentrations. In carbon composite foam prepared at the sucrose solution concentration of 700 g L^{-1}, the carbon produced from sucrose dominates and cover the carbonized newspaper micro-ribbons. However, the quantification of macropore pore size from the SEM images is not possible due to their irregular shape. In addition to the macropore formed by the assembly of carbon composite micro-ribbons, the high magnification SEM micrographs show the presence of mesopores. The size of mesopores measured from the SEM image using ImageJ software is in the range of 5 to 27 nm. These mesopores are formed due to the smaller bubbles formed in sucrose by the water vapour produced due to –OH condensation during the caramelization. It is reported that the preparation of carbon foams by thermo-foaming demonstrate the formation of bubbles of large size (>100 nm) in molten sucrose due to water vapour generated by –OH condensation. In the present work, the sucrose was deposited in between the newspaper microribbons. It appears that the newspaper micro-ribbons restrict the bubble growth in molten sucrose during the caramelization resulting in bubbles of less than 50 nm size. A typical high magnification SEM micrograph of carbon composite foam is shown in **Fig. 6.21**.

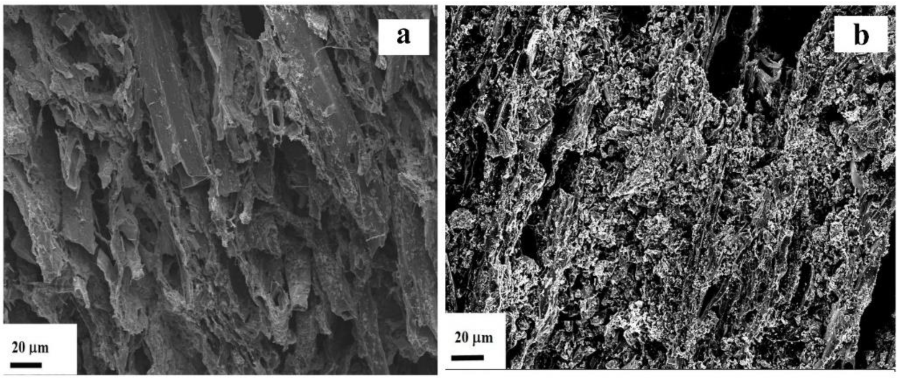

Fig. 6.20 Low magnification SEM micrograph of carbon-gehlenite composite foams prepared at sucrose solution concentrations of (a) 0 g L^{-1} and (b) 700 g L^{-1}

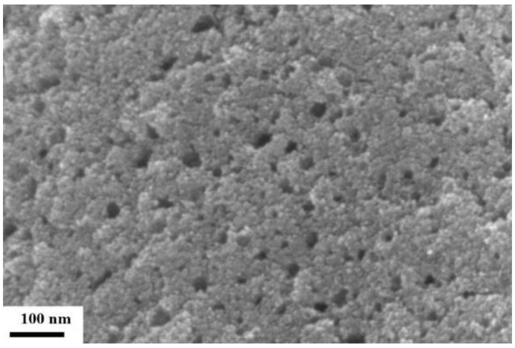

Fig. 6.21 A typical high magnification image showing porous nature of carbon-gehlenite composite foam

6.2.6.4 Textural properties

The porous structure of the carbon composite-gehlenite foams is also demonstrated from the N_2 adsorption-desorption isotherms evaluated at 77 K. The carbon-gehlenite composite foams show a combination of type I and type IV adsorption isotherms typical for samples with a combination of micro and mesopores. The microporous nature is evidenced from adsorption-desorption isotherms, showing a rapid uptake of N_2 gas at lower relative pressures and hysteresis at higher relative pressures. The shape of the hysteresis loop indicates the presence of narrow slit-like pores made by the stacking of the newspaper microribbons. It also reveals the presence of internal voids with broad pore size distribution (Cychosz et al., 2017; Thommes & Cychosz, 2014). The adsorption-desorption isotherm of the carbon-gehlenite composite foams prepared at various sucrose solution concentrations is shown in **Fig. 6.22** and the textural properties are given in **Table 6.1**. The carbon-gehlenite composite foam prepared without sucrose shows a specific surface area of 251 m^2 g^{-1}. The specific surface area of the carbon-gehlenite composite foams increases from 251 to 400 m^2g^{-1} when the sucrose solution concentration increases from 0 to 700 g L^{-1}. The ash (gehlenite) obtained by burning off the carbon shows a surface area of 3.9 m^2g^{-1}. That is, 42.8 wt.% gehlenite and 57.8 wt.% carbon present contribute 1.66 m^2 and 249.34 m^2 towards the specific surface area of the carbon-gehlenite composite foam prepared without sucrose. This indicates that the carbon obtained from the newspaper has a specific surface area of 435.9 m^2g^{-1}. On the other hand, the carbon obtained by the carbonization of sucrose at 900 °C shows a specific surface area of 367 m^2g^{-1}. Therefore, the observed increase in surface area of the carbon-gehlenite composite foams with an increase in sucrose solution concentration is due to the decrease in the concentration of gehlenite having low surface area. The total pore volume of carbon-gehlenite composite foams obtained from the N_2 adsorption-desorption studies are not strictly following any specific trend, However, the values of total pore volume observed are in a close range of 0.159 to 0.239 cm^3g^{-1}. The carbon-gehlenite composite foam prepared at zero sucrose solution concentration shows a micropore volume of 0.078 cm^3 g^{-1}. The micropore volume increases from 0.078 to 0.15 cm^3g^{-1} when the sucrose solution concentration increases from 0 to 700 g L^{-1}. The micropores are formed by an *in* *situ* activation. That is, the oxygen retained in the form of C-O-C linkages as a result of –OH condensation reacts with the carbon at higher temperatures to form CO, which results in the formation of micropores(R Narasimman et al., 2014a). The micropore volume of the carbon produced from the newspaper was calculated by excluding the 42.8 wt.% of gehlenite present in carbon composite foam prepared at zero sucrose solution concentration is 0.135 cm^3 g^{-1}. On the other hand, the carbon produced by the carbonization of sucrose at 900 °C exhibited a micropore volume of 0.18 cm^3 g^{-1}. The observed increase in micropore volume of the carbon-gehlenite composite foams with an increase in sucrose solution concentration is due to a decrease in the concentration of gehlenite and an increase in the concentration of carbon produced from sucrose. The DFT pore size distribution of the carbon-gehlenite composite foams is shown in **Fig. 6.23**. The DFT plots do not show prominent peaks in the microporous region (< 2nm). However, there is a prominent peak in the pore size range of 2.5 to 2.8 nm. In addition, broad peaks are observed at pore sizes in the range of 4 to 110 nm. The steep uptake of N_2 gas at lower relative pressures observed in N_2 adsorption-desorption isotherm is not reflected in the DFT pore size distribution. It appears that the micropores in the carbon composite foams are in the ultramicropore range (<1 nm).

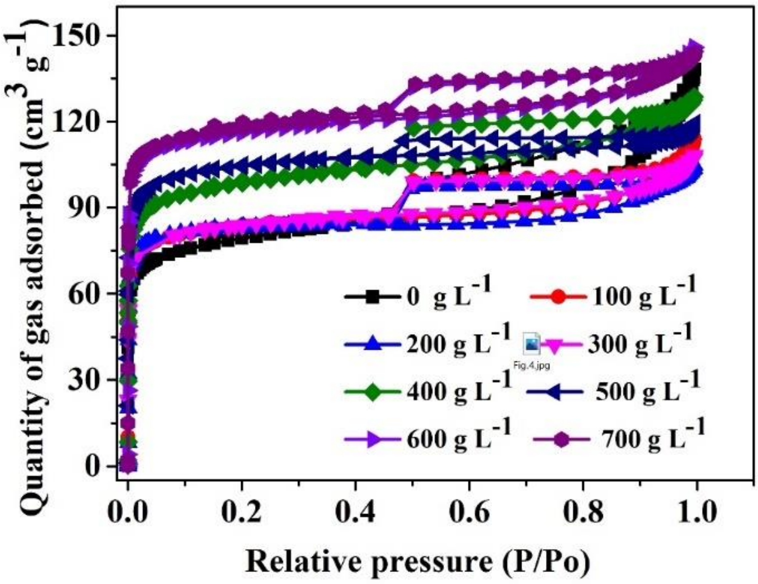

Fig. 6.22 N_2 adsorption-desorption isotherms of carbon composite foams

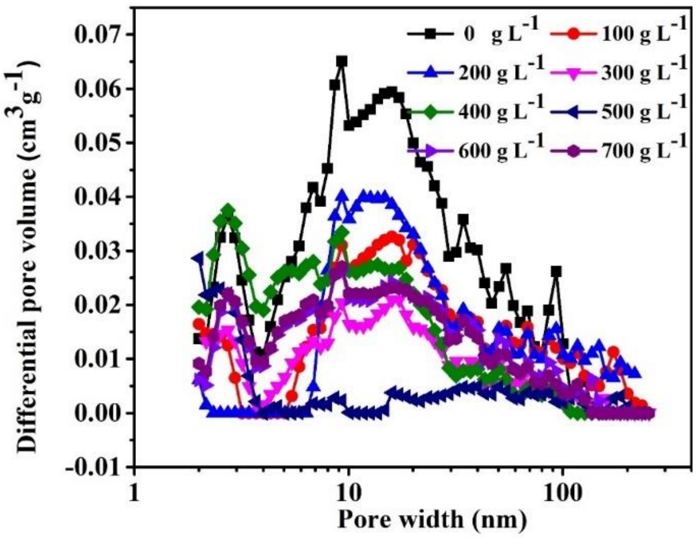

Fig. 6.23 DFT pore size distribution curve of carbon-gehlenite composite foams

Table 6.1 Textural properties of carbon-gehlenite composite foams

Concentration of sucrose (g L^{-1})	**BET Surface area (m^2 g^{-1})**	**Micropore area (m^2 g^{-1})**	**Total pore volume (cm^3 g^{-1})**	**Micropore volume (cm^3 g^{-1})**
0	251	172	0.205	0.078
100	256	196	0.171	0.096
200	252	200	0.159	0.10
300	274	212	0.167	0.09
400	306	227	0.196	0.11
500	315	245	0.181	0.12
600	369	298	0.222	0.14
700	400	329	0.239	0.15

6.2.6.5 Density

The carbon-gehlenite composite foam prepared at zero sucrose solution concentration shows a bulk density of 0.18 g cm^{-3}. The carbon-gehlenite composite foam density increases slowly from 0.18 to 0.22 g cm^{-3} when the sucrose solution concentration increases from 0 to 300 g L^{-1}. Further increase in sucrose solution concentration to 700 g L^{-1} rapidly increases the carbon-gehlenite composite foam density to 0.39 g cm^{-3}. **Fig. 6.24** depicts the effect of sucrose solution concentration on the density of the carbon - gehlenite composite foams.

The skeletal density of the carbon-gehlenite composite foam samples decreases from 2.52 to 2.26 g cm^{-3} when the sucrose solution concentration increases from 0 to 700 g L^{-1}. The observed skeletal density is more than the density of graphite. This is due to the presence of gehlenite with a higher theoretical density of 2.98 g cm^{-3}. The porosity of the carbon composite foams, calculated from their bulk and skeletal densities, decreases from 92.3 to 84.6% when the sucrose solution concentration increases from 0 to 700 g L^{-1}. **Table 6.2** summarizes the density, skeletal density and porosity of the carbon-gehlenite composite foams prepared at various sucrose solution concentrations.

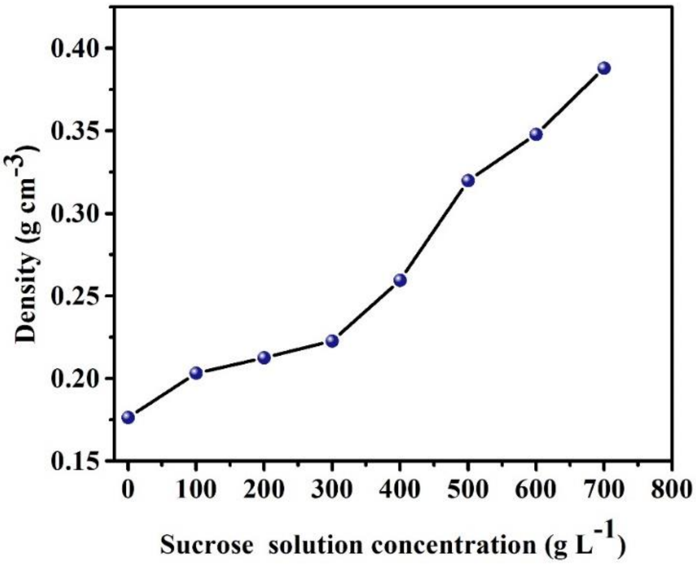

Fig. 6.24 Effect of sucrose solution concentration on bulk density of carbon-gehlenite composite foams

Table 6.2 Density and porosity of carbon-gehlenite composite foams

Sucrose solution concentration ($g\ L^{-1}$)	**Bulk density ($g\ cm^{-3}$)**	**Skeletal density ($g\ cm^{-3}$)**	**Porosity (%)**
0	0.18	2.28	92.3
100	0.20	2.26	91.0
200	0.21	2.28	90.7
300	0.22	2.31	90.4
400	0.26	2.33	88.9
500	0.32	2.36	86.4
600	0.35	2.28	84.7
700	0.39	2.52	84.6

6.2.6.6 Compressive strength

Mechanically robust materials are required for thermo-structural application. The compressive stress-strain graph of the carbon-gehlenite composite foams is shown in **Fig. 6.25**. The compressive stress-strain graph of carbon- gehlenite composite foam is different from that of brittle carbon foams. Instead of the serrated plateau region due to the brittle failure, smooth curves with a positive slope over the whole deformation range is observed. During the compression of the carbon-gehlenite composite foams, densification occurs due to the bending and deformation of the carbon-gehlenite microribbons rather than the pore collapse by the failure of the brittle pore walls in conventional carbon foams. The carbon-gehlenite composite foams prepared at sucrose solution concentrations in the range of 0 to 300 g L^{-1} shows a slow and linear increase of stress with strain up to the point of strain hardening. On the other hand, the foams prepared at sucrose solution concentrations in the range of 400 to 700 g L^{-1} show a rapid increase in stress with strain in the beginning up to a yield point. Thereafter, the stress slowly increases with strain up to the point of strain hardening. The slope of the initial linear region is taken as Young’s modulus and the stress at 10% strain is taken as the compressive strength. The compressive strength and Young’s modulus of carbon-gehlenite composite foams as a function of sucrose solution concentration are shown in **Fig. 6.26**. The compressive strength and Young's modulus increases slowly with an increase in sucrose solution concentration up to 300 g L^{-1} and thereafter rapidly up to 700 g L^{-1}. The carbon-gehlenite composite foam prepared without sucrose shows a compressive strength and Young’s modulus of 0.2 and 3.44 MPa, respectively. The compressive strength and Young’s modulus slowly increase to 0.32 and 8 MPa, respectively, when the sucrose solution concentration increases to 300 g L^{-1}. Further increase in sucrose solution concentration to 700 g L^{-1} results in a rapid increase of compressive strength and Young’s modulus to 1.7 and 69.9 MPa, respectively. The carbon aerogels prepared from waste paper reported in the literature shows compressive stress of less than 1 kPa at 10 % strain. Nevertheless, our carbon-gehlenite composite foams are not exhibiting reversible compressibility unlike the carbon aerogels reported from waste paper. Hence, the prepared carbon-gehlenite composite foam is mechanically robust for thermo-structural applications.

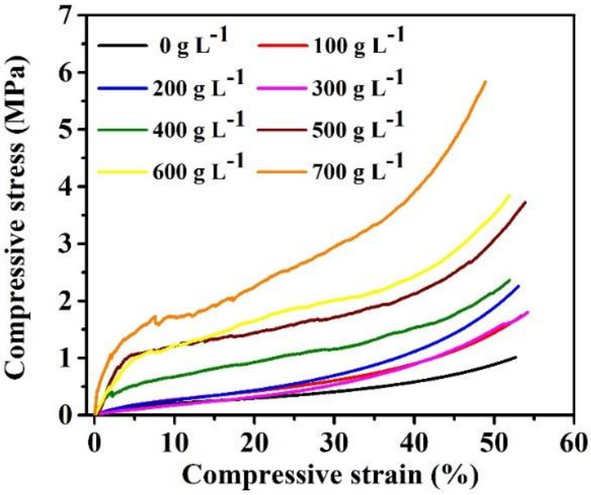

Fig. 6.25 Compressive stress-strain curve of carbon-gehlenite composite foams

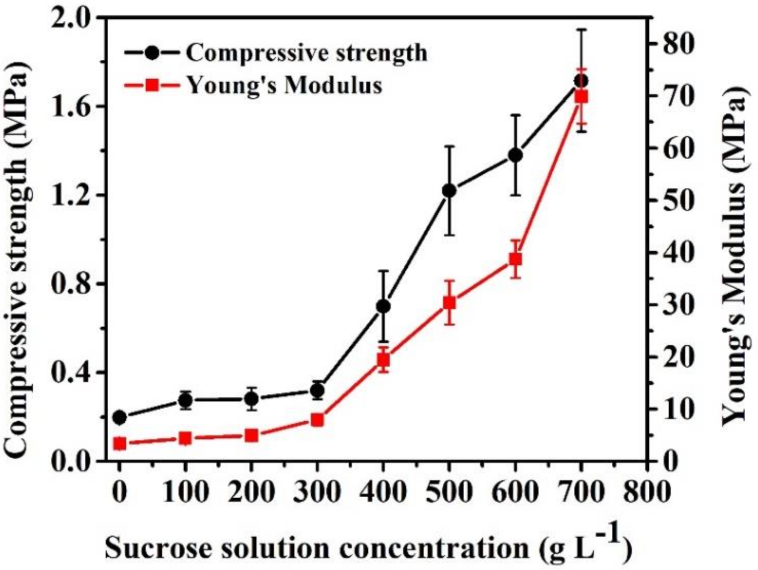

Fig. 6.26 Effect of sucrose solution concentration on compressive strength and Young's modulus of carbon-gehlenite composite foams

6.2.6.7 Machinability

The ability to produce in required contour is one of the important criteria for a material to be used in practical applications. The carbon-gehlenite composite foams are amenable to minor machining operations such as cutting with a blade, shaping using abrasive paper etc. However, they damage when attempted to hold them in a lath, a milling machine or a drilling machine due to the relatively low compressive strength. On the other hand, the compressive strength and Young's modulus of newspaper-sucrose composites are sufficient for holding them in the lathe, milling machine and drilling machine without any damage. The newspaper-sucrose composites prepared at sucrose solution concentrations in the range of 400 to 700 g L^{-1} are amenable for machining. The recessed steps, a cylindrical hole and rectangular slots are made on the newspaper-sucrose composites by lathing, drilling and milling, respectively, using conventional machines and tools. The machined newspaper-sucrose composite bodies undergo uniform shrinkage retaining their shape during subsequent carbonization. **Fig. 6.26** is a photograph showing recessed steps, a cylindrical hole and rectangular slots made on newspaper-sucrose composites and the carbon-gehlenite composite foams produced by carbonizing the machined bodies. Therefore, machining the newspaper-sucrose composite followed by carbonization is the right strategy to fabricate carbon composite foams with contoured surfaces.

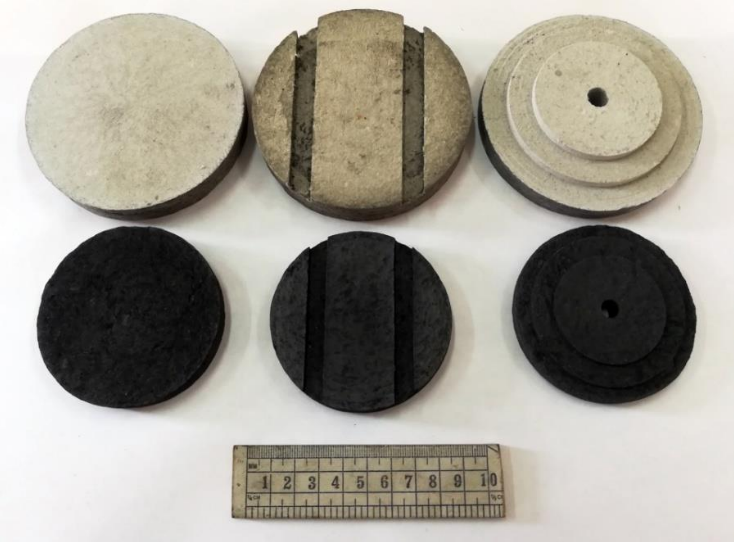

Fig. 6.27 Photograph showing machinability of newspaper-sucrose composites and the carbon-gehlenite composite foams produced by carbonizing the machined composite

6.2.6.8 Thermal conductivity

The amorphous carbon foams are candidate materials for high-temperature thermal insulation and fire-resistant lightweight structural applications due to their low thermal conductivity. The thermal conductivity of carbon-gehlenite composite foams is presented as a function of their density in **Fig. 6.27**. The thermal conductivity shows an increasing trend with an increase in density. The carbon-gehlenite composite foam prepared at zero sucrose solution concentration shows a thermal conductivity of 0.096 W $m^{-1}K^{-1}$. The thermal conductivity of the carbon-gehlenite composite foams increases with an increase in foam density due to an increase in sucrose solution concentration. The thermal conductivity increases to 0.2 W $m^{-1}K^{-1}$ when the foam density increases to 0.39 g cm^{-3} as a result of an increase in the sucrose solution concentration to 700 g L^{-1}. The thermal conductivity values observed are lower than that of some of the amorphous carbon foams of similar densities reported in the literature(R Narasimman & Prabhakaran, 2012, 2013; Tondi et al., 2009; Wilson et al., 2017). The lower thermal conductivity values are due to the micro and mesoporous structure in the carbon composite foams which may restrict the heat transfer by convection**.**

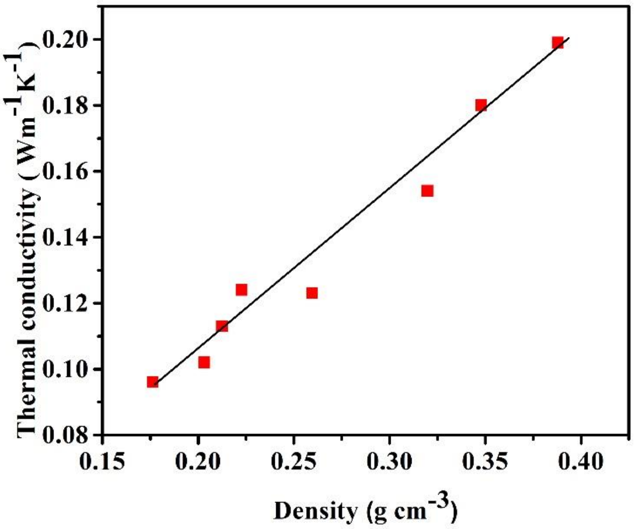

Fig. 6.28 Effect of density on thermal conductivity of carbon-gehlenite composite foams

6.2.6.9 Oxidation resistance

The oxidation resistance of the carbon composite was evaluated by TG analysis in the air atmosphere. The carbon-gehlenite composite foam exhibit slow and a small weight loss **(** ~2.4%) due to the elimination of moisture and slight oxidation of carbon up to 450°C. It means that the composite foam has thermal stability up to 450°C in an air atmosphere. Further, an increase in temperature results in rapid weight loss due to the oxidation of carbon. The weight loss completes at a temperature of 650 ^{o}C. The TGA graph of carbon-gehlenite composite foams prepared at various sucrose solution concentrations is shown in **Fig. 6.28**. The residue that remains after 650 ^{o}C is due to the gehlenite present in the newspaper. The gehlenite content in carbon-gehlenite composite foams estimated from TGA is given in **Table 6.3**. The carbon-gehlenite composite foam prepared at zero sucrose solution concentration shows a gehlenite content of 41.8 wt.%. The gehlenite content decreases rapidly from 41.8 to 24.10 wt.% when the sucrose solution concentration increases from 0 to 200 g L^{-1}. Further increase in sucrose solution concentration to 700 g L^{-1} slowly decreases the gehlenite content to 13.6 wt.%. The decrease in gehlenite content is due to the increase in the concentration of carbon produced from sucrose which does not leave any ash during oxidation.

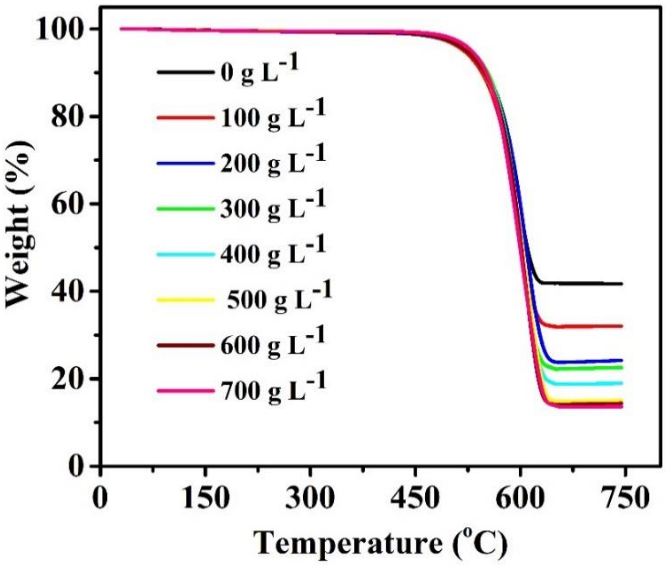

Fig. 6.29 TGA graph of carbon composite foams prepared at various sucrose solution concentrations

Table 6.3 Gehlenite content in carbon-gehlenite composite foams prepared at various sucrose solution concentrations

Sucrose concentration (g L^{-1})	**Gehlenite Content (wt.%)**
0	41.8
100	32.7
200	24.1
300	22.7
400	18.8
500	15.0
600	14.1
700	13.6

6.2.6.10 Fire resistance

The fire resistance was tested by exposing the carbon-gehlenite composite foam to oxyacetylene flame. The carbon foams do not catch fire when exposed to oxyacetylene flame. The splashing of oxyacetylene flame oxidizes a thin layer of carbon from the surface leaving white patches of gehlenite. However, the flame pierces through the carbon-gehlenite composite foam due to oxidation of carbon and melting & evaporation of gehlenite. The oxyacetylene flame takes nearly 65 s to pierce through a carbon-gehlenite composite foam body of 12 mm thickness prepared at a sucrose solution concentration of 300 g L^{-1}. Photographs showing the fire resistance of the carbon composite foam and a hole produced due to the piercing of the oxyacetylene flame is shown in **Fig. 6.30**.

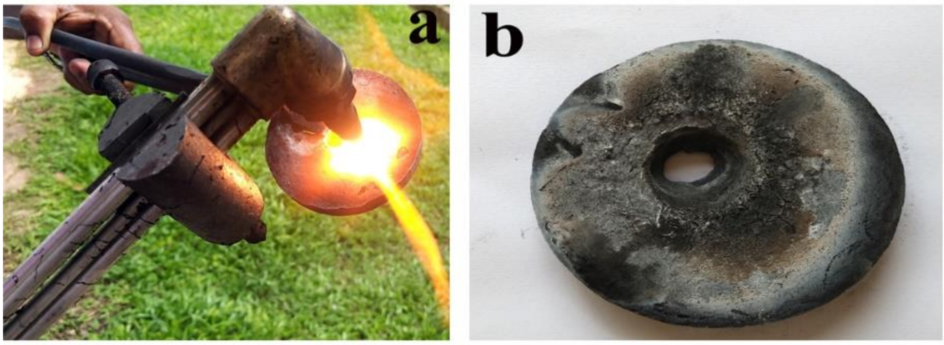

Fig. 6.30 Photographs showing fire resistance of carbon composite foam(a) and a hole formed due to the piercing of oxyacetylene flame(b)

6.2.6.11 EMI shielding effectiveness

The EMI shielding effectiveness of the carbon-gehlenite composite foams was analysed over the entire X- band region. **Fig. 6.31** is a typical graph showing the variation of SE_R, SE_A and SE_T as a function of frequency in the X- band region. EMI shielding effectiveness, SE_R, SE_A, SE_T of carbon-gehlenite composite foam is more or less constant over the entire X- band region. The steady EMI shielding effectiveness of the carbon-gehlenite composite is attributed to its homogeneous structure. **Fig. 6.32** shows the effect of sucrose solution concentration on the EMI shielding effectiveness of carbon-gehlenite composite foam at 11 GHz. The carbon-gehlenite composite foams at various sucrose solution concentrations exhibit more or less the same reflection contribution. The reflection contribution to the total EMI shielding effectiveness observed is in the narrow range of 3.5 to 5.7 dB. The total EMI shielding effectiveness of carbon-gehlenite composite foams increases from 15.9 to 44.9 dB when sucrose solution concentration increases from 0 to 700 g L^{-1}. The absorption contribution to the total EMI shielding effectiveness increases from 12.6 to 41.9 dB when the sucrose solution concentration increases from 0 to 700 g L^{-1}. That is, the carbon-gehlenite composite foams exhibited absorption dominated EMI shielding effectiveness over the entire X- band region.

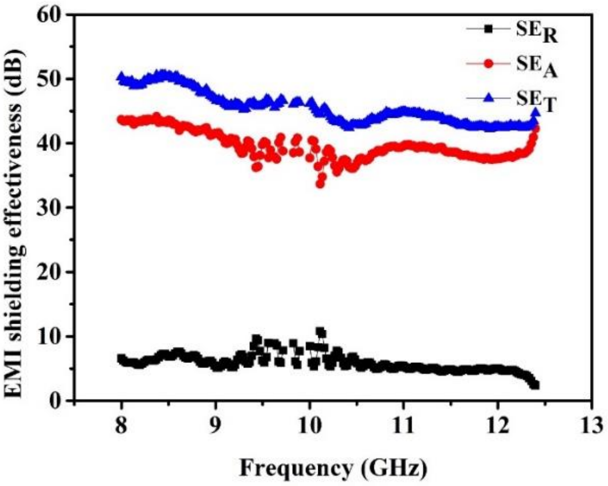

Fig. 6.31 A Typical graph of variation of SE_R, SE_A and SE_T as a function of frequency in the X- band region

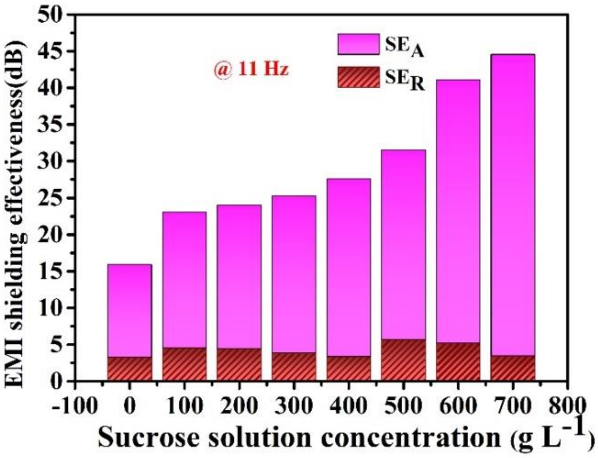

Fig. 6.32 Effect of sucrose solution concentration on SE_R, SE_R and SE_T carbon-gehlenite composite foams at 11 GHz

When EM waves strike the surface of carbon-gehlenite composite foam, a major portion of the waves penetrate because of the better impedance matching due to the highly porous nature and the remaining is reflected from the surface. The EM waves penetrated the carbon-gehlenite composite will be attenuated by conductive losses due to carbon, dielectric loss due to the gehlenite and polarization losses at a large area of interfaces present between carbon and gehlenite. The large surface area, defects and oxygen-containing functional groups also contribute to EM absorption by polarization. The EM waves enter the pores undergo multiple internal reflections leading to absorption of its major portion rather than transmitting. The increase in total EMI shielding effectiveness with an increase in sucrose solution concentration is due to an increase in foam density and an increase in the concentration of conductive carbon (decrease in the concentration of gehlenite). The specific EMI shielding effectiveness obtained by dividing total shielding effectiveness with a density of the foam is in the range of 88.9 to 115.1 dB $g^{-1}cm^3$. The observed EMI shielding effectiveness and specific shielding effectiveness are comparable to that of carbon foams of a similar density range reported in the literature(Q. Li et al., 2016a; R Narasimman et al., 2015, 2016).

The low density, high thermal stability, low thermal conductivity, excellent fire resistance, high EMI shielding effectiveness and reasonably high compressive strength of carbon-carbon-gehlenite composite foam make it a candidate material for thermo-structural and EMI shielding applications in aerospace.

6.3 Conclusions

The waste newspaper has been successfully used for the preparation of mechanically robust carbon-gehlenite composite foams by filter-pressing and subsequent carbonization. The pulp obtained by mixing shredded newspaper and sucrose solution contains newspaper micro-ribbons of width ~15 µm. The filter-pressing of the pulp prepared at sucrose solution concentrations in the range of 0 to 700 g L^{-1} produces wet bodies with adequate strength (~ 1 kPa) for withstanding stresses during removal from the filter-pressing setup and further handling during dying. The newspaper micro-ribbons preferentially orient perpendicular to the filter-pressing direction. The carbonization of the newspaper-sucrose composite at

900 ^{o}C produces carbon-gehlenite composite foam with a density in the range of 0.18 to 0.39 g cm^{-3}. The shrinkages in the filter-pressing direction during drying and carbonization are governed by sucrose solution concentration whereas the diametrical shrinkage is controlled by the newspaper micro-ribbons oriented perpendicular to the filter-pressing direction. The carbon-gehlenite composite foams show compressive strength and Young's modulus in the ranges of 0.2 to 1.7 MPa and 3.4 to 69.9 MPa, respectively. The newspaper-sucrose composites obtained by drying the filter-pressed bodies prepared at sucrose solution concentrations in the range of 400 to 700 g L^{-1} are amenable for machining using conventional tools and equipment. The machined materials perfectly retained their shape after the carbonization. The carbon-gehlenite composite foams show a room temperature thermal conductivity in the range of 0.1 to 0.2 W m^{-1}K^{-1} and excellent fire resistance, suitable for lightweight fire-resistant structural and thermal protection applications. The carbon-gehlenite composite foam exhibited absorption dominated EMI shielding. The total EMI shielding effectiveness increases from 15.9 to 44.9 dB when sucrose solution concentration increases from 0 to 700 g L^{-1}.

CHAPTER -7

CONCLUSIONS AND FUTURE SCOPE

7.1 Conclusions

Carbon foams are three-dimensional rigid macroporous materials. These are getting renewed interest due to their unique properties such as lightweight, chemical inertness, high-temperature tolerance, tuneable electrical and thermal conductivities, fire resistance, low thermal expansion coefficient, high electromagnetic interference shielding effectiveness and acoustic absorption. Hence, they find applications in various fields such as thermal protection and ablative systems in aircraft, fire-resistant structures, EMI shielding materials in the electronic industry, acoustic protection, heat sink, radiators and host for phase change materials. The carbon foams are also used as an adsorbent material for the removal of trace contaminants from water, catalytic support and electrodes in energy storage devices. Generally, carbon foams are prepared either from synthetic polymers such as polyimide, polybenzoxazine, phenol-formaldehyde resin or pitches. Synthetic polymers yield amorphous carbon foams whereas pitches produce graphitic carbon foams. Fossil fuels which are the sources of synthetic organic polymers and pitches are depleting as a consequence of rapid industrialization. Researchers are focusing on alternative precursors of carbon foams for sustainable development. Biomasses are good candidate precursors for valuable carbon products because they are available in large quantities at low cost, renewable and environmentally friendly. Biomasses such as tannin, lignin, cellulose and sucrose are widely studied for the preparation of carbon foams. The general strategy for the preparation of carbon foams involves foaming and setting of the precursor resins followed by pyrolysis and graphitization. Polymer foam replication using polyurethane foams as a template is used for the preparation of reticulated carbon foams. In this, the carbon precursor resin coated on the webs of polyurethane foam template by impregnation followed by squeezing by rolling and curing is pyrolyzed to produce carbon foam which is a replica of the polyurethane foam. Additives such as graphite particles, graphene, clay, CNTs, and iron-containing compounds are incorporated in carbon foams to modulate their structural and functional properties

The agricultural residues such as rice husk, cotton, sawdust and newspaper are either unutilized or underutilized. The effective utilization of these materials helps waste management as well as generate wealth. This thesis investigates the eco-friendly processing of carbon composite foams by using agricultural residues such as newspaper, cotton, sawdust and rice husk. Sucrose, an agricultural product with 42 wt% carbon content is used as a binder for the preparation of carbon composite foams. The produced composite carbon foams are well characterized and evaluated for thermal insulation and EMI shielding applications.

Chapter 1 gives a brief review of porous carbon materials with a focus on carbon foams, their precursors and processing methods. The chapter briefly introduces the properties and applications of carbon foams. A review of carbon foams produced from biomasses is also presented in **Chapter 1**.

The materials, processing methods and characterization details are described in **Chapter 2**.

Processing and characterization of carbon composite foams from natural cotton and sucrose by filter-pressing are discussed in **Chapter 3**. The filter-pressing of natural cotton fibre dispersed in sucrose solution of concentrations in the range of 100 to 700 g L^{-1} followed by freeze-drying produces cotton-sucrose composites. The cotton fibres in the cotton-sucrose composites are preferentially oriented transverse to the filter pressing direction. The caramelization of sucrose in the cotton-sucrose composite followed by carbonization produce carbon composite foams. The carbon yield from the cotton-sucrose composites increases from 15.2 to 21.4 wt. % when the sucrose solution concentration increase from 100 to 700 g L^{-1}. The tubular carbon fibres formed from cotton are welded at their contact points by the amorphous carbon produced from sucrose. This leads to partially reversible compressibility at low sucrose solution concentrations. Advancement of fibre- to-fibre bonding area results in rigid carbon composite foams at sucrose concentration above 200 g L^{-1}. The density of carbon composite foam increases from 0.06 to 0.31 g cm^{-3} when sucrose solution concentration increases from 100 to 700 g L^{-1}. The carbon composite foams processed at sucrose solution concentrations in the range of 100 to 700 g L^{-1} exhibits a reasonably high compressive strength in the range of 5 kPa to 2.2 MPa. The N_2 adsorption-desorption of carbonized cotton and carbon composite foams shows a combination of type I and type IV isotherms with a sharp increase in the extent of adsorption at lower relative pressure and a prominent hysteresis loop at relative pressures in the range of 0.4-0.9. This indicates the presence of micro, meso and macropores in the carbon composite foams. The DFT pore size distribution curves exhibit multiple peaks, with three major peaks at 1.23, 1.55 and 1.82 nm. The carbon composite foams prepared at a sucrose solution concentration of 500 g $L^{-1}$and above are amenable to machining using conventional machines and tools. The carbon composite foams processed at sucrose solution concentrations in the range of 100 to 700 g L^{-1} exhibits excellent fire resistance and low thermal conductivity in the range 0.069 to 0.185 W $m^{-1}K^{-1.}$ The porosity in the inter-fibre space and lumen of the carbonized cotton fibre contributes to the low thermal conductivity. The electrical conductivity increases from 3.4 to 54.2 S cm^{-1} when sucrose solution concentration increases from 0.16 to 0.31 g cm^{-3}. As the density increases, inter-fibre bonding also increases which facilitate the improved electron movement. The rigid carbon foams show absorption dominated EMI shielding effectiveness and specific shielding effectiveness in the ranges of 21.5 to 38.9 dB and 108-138 dB cm^3g^{-1}, respectively.

Chapter 4 describes the processing and characterization of carbon composite foams from sawdust and sucrose by filter-pressing. Composites are prepared by cementing sawdust particles with sucrose by filter-pressing sawdust powder dispersions in sucrose solution followed by freeze-drying. The caramelization of sucrose in the sawdust-sucrose composites followed by carbonization produces carbon composite foams. The carbon composite foams produced at sucrose solution concentrations less than 200 g L^{-1} are not robust. The density of the carbon composite foams is modulated in the range of 0.17 to 0.35 g cm^{-3} by using a sucrose solution of concentrations in the range of 200 to 700 g L^{-1}. The sucrose solution seeps into the pore channels and produces ~50 nm thick deposits of carbon on the pore channel surfaces. The compressive strength in the transverse direction (0.24 to 3.2 MPa) is higher than that in the filter-pressing direction (0.22 to 1.76 MPa) due to the preferential orientation of elongated sawdust particles transverse to the filter-pressing direction. The Young's moduli in the filter-pressing and transverse direction are in the ranges of 5.5 to 81.7 MPa and 6 to 80.5 MPa, respectively. The carbon foams exhibited excellent fire resistance and low thermal conductivity in the range of 0.12 to 0.20 W m^{-1} K^{-1} at sucrose solution concentration in the range of 200 to 700 g L^{-1}. The electrical conductivity of the carbon composite foam increases from 18.2 to 33.8 S cm^{-1} when sucrose solution concentration increases from 200 to 700 g L^{-1}. The carbon composite foams showed absorption dominated EMI shielding. The EMI shielding effectiveness increases from 25 to 53 dB when sucrose solution concentration increases from 200 to 700 g L^{-1}. The increase in EMI shielding effectiveness with an increase in sucrose solution concentration is due to the combined effect of an increase in foam density, increase in electrical conductivity and island-like carbon deposited on the pore-channel surfaces which creates additional interfaces for the attenuation of EM waves.

Processing and characterization of carbon-silica (**C/SiO$_2$**) and carbon-silicon carbide (**C/SiC**) composite foam from rice husk and sucrose are discussed in **Chapter 5**. The rice husk-sucrose composites are obtained consolidating rice husk powder dispersed in sucrose solution by filter-pressing followed by freeze-drying. The **C/SiO$_2$** and **C/SiC** composites are obtained by caramelization of the sucrose followed by carbonization and carbothermal reduction, respectively. The **C/SiO$_2$** composites prepared at sucrose solution concentrations of 100 and 200 g L^{-1} lacks mechanical robustness. On the other hand, severe deformation was observed during the carbonization of rice husk sucrose composite prepared at a sucrose solution concentration of 700 g L^{-1}. The elongated rice husk derived carbon-SiO_2 composite particles are welded at their contact points by sucrose derived carbon. The shrinkage of the bodies during carbonization marginally increases with an increase in the concentration of sucrose solution from 300 to 600 g L^{-1}. The shrinkage during carbonization observed in the filter-pressing and transverse directions are in the ranges of 19.4 to 22.7 % and 18.4 to 20.7%, respectively. However, further heat treatment at 1600 °C in an inert atmosphere did not make any significant change in the shape and size of the carbonized bodies. On the other hand, weight losses in the range of 29.5 to 22.4 wt.% are observed due to the carbothermal reduction of amorphous silica present in the carbonized rice husk particles. The silica content in

C/SiO$_2$ and SiC content in **C/SiC** composite foams decreases from 24.7 to 16.7 and from 25 to 15 wt.%, respectively, with an increase of sucrose solution concentration from 300 to 600 g L^{-1}. The amorphous nature of silica in **C/SiO$_2$** and the presence of β-SiC in **C/SiC** are evidenced from XRD, Raman spectral and TEM analysis. The compressive strength and thermal conductivity are depending on the foam density which is tailored by sucrose solution concentration. The compressive strength in the ranges of 0.32 to 1.67 and 0.19 to 1.19 MPa are observed for **C/SiO$_2$** and **C/SiC** composite foams, respectively, with density in the ranges of 0.26 to 0.37 and 0.18 to 0.29 g cm^{-3}. The **C/SiO$_2$** and **C/SiC** composite foams exhibited thermal conductivity in the ranges of 0.150 to 0.205 and 0.165-0.431 $Wm^{-1}K^{-1}$, respectively. The electrical conductivity of **C/SiO$_2$** composite foams increases from 19 to 94 S cm^{-1} when the sucrose solution concentration increase from 300 to 600 g L^{-1}.The observed enhancement in electrical conductivity is due to an increase in foam density and the reduction in silica content with an increase in the concentration of sucrose solution. **C/SiC** composite foams show higher electrical conductivity (102 to 371 S cm^{-1}) compared to the corresponding **C/SiO$_2$** composite foam samples due to the formation of graphite micro-crystals during heat-treatment at 1600 ^{o}C. The **C/SiO$_2$** and **C/SiC** composite foams show absorption dominated EMI shielding effectiveness in the ranges of 18 to 38.5 and 20 to 43.7 dB, respectively. The inherent pore channels and corrugated surface structure in rice husk, electrically conducting carbon and dielectric SiO_2 and SiC contribute to the total EMI shielding effectiveness.

Processing and characterization of carbon–gehlenite composite foams from newspaper waste and sucrose are described in **Chapter-6.** The newspaper contains ~12 wt.% of gehlenite. The pulp prepared by mixing newspaper waste with sucrose solution contains newspaper micro ribbons of ~15 μm width. The consolidation by vacuum filtration followed by filter-pressing and drying results in the newspaper – sucrose composites. The caramelization of sucrose in the newspaper-sucrose composites followed by carbonization produces carbon-gehlenite composite foams. The gehlenite content in the carbon composite foams decreases from 41.8 to 13.6 wt.% when the sucrose solution concentration increases from 0 to 700 g L^{-1}. The drying and carbonization shrinkage in the filter-pressing direction depends on the sucrose solution concentration. However, the diametrical shrinkage during drying (marginal) and carbonization was controlled by the newspaper micro-ribbons in the pulp oriented perpendicular to the filter-pressing direction. The newspaper-sucrose composites prepared at sucrose solution concentrations in the range of 400 to 700 g L^{-1} were amenable to machining using conventional machines and tools. The density, compressive strength and Young's modulus of the carbon composite foams increase with an increase in sucrose solution concentration and the values observed were in the ranges of 0.18 to 0.39 g cm^{-3}, 0.2 to 1.7 MPa and 3.4 to 69.9 MPa, respectively. The carbon composite foams had a hierarchical micro, meso and macropore structure as evidenced from SEM analysis and N_2 adsorption-desorption isotherms. The carbon- gehlenite composite foams show excellent fire resistance and low thermal conductivity values in the range of 0.1 to 0.2 W $m^{-1}K^{-1}$. The carbon-gehlenite composite foam exhibited absorption dominated EMI shielding. The total EMI shielding effectiveness increases from 15.9 to 44.9 dB when sucrose solution concentration increases from 0 to 700 g L^{-1}.

The thermal conductivity and EMI shielding effectiveness of carbon composite foams prepared from natural cotton, sawdust. rice husk and waste newspaper as a function of density is presented in **Fig. 7.1a-b** for comparison. The carbon-gehlenite composite foam prepared from newspaper waste shows the lowest thermal conductivity at a particular foam density. The carbon composite foams prepared from natural cotton, sawdust and C/SiO_2 composites of similar density range exhibited thermal conductivity in the more or less same range. On the other hand, the C/SiC composite foam produced by carbothermal reduction of C/SiO_2 composite foams exhibited higher thermal conductivity than all others of similar density. In the case of EMI shielding effectiveness, the carbon composite foams derived from sawdust exhibited the highest value compared to others of similar density. The carbon composite foams produced from natural cotton and newspaper waste show more or less the same EMI shielding effectiveness at density in the range of 0.20 to 0.25 g cm^{-3}. At density higher than 0.25 g cm^{-3}, the carbon composite foams produced from natural cotton demonstrates higher EMI shielding effectiveness than the newspaper derived carbon foam. The C/SiO_2 and C/SiC composite foams show lower values of EMI shielding effectiveness than that of others at a lower density range. However, the values overtake that of cotton derived and newspaper derived carbon composite foams at higher density ranges.

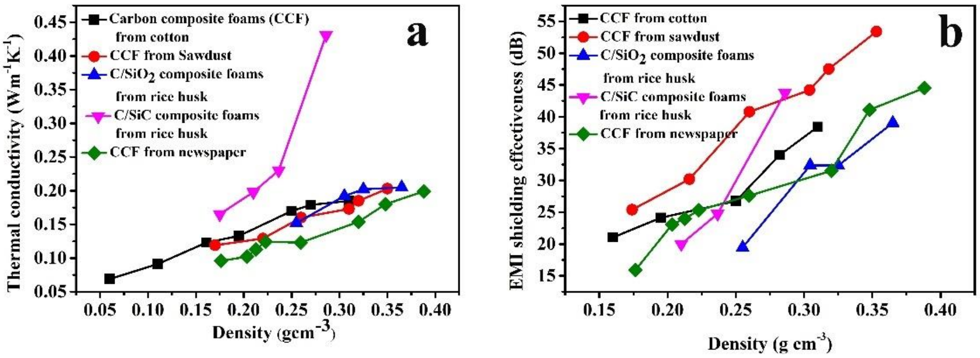

Fig 7.1 Variation of thermal conductivity(a) and EMI shielding effectiveness of carbon composite foams as a function of density

The thermal conductivity and EMI shielding effectiveness of carbon foams prepared from various precursors reported in the literature are presented in **Table 7.1** in comparison with that of the carbon composite foams prepared in the present work. The carbon composite foams prepared in the present work shows thermal conductivity lower than that of most of the carbon foams of similar density ranges reported in the literature. The EMI shielding values obtained are also comparable with that of the majority of carbon foams reported in the literature.

Table 7.1 Density, EMI shielding effectiveness and thermal conductivity of carbon foams from various precursors reported in the literature

Sl. No.	Precursors	Thermal conductivity ($Wm^{-1}K^{-1}$)	EMI shielding effectiveness (dB)	Density (gcm^{-3})	Ref
1.	Tannin	0.35	-	0.07	(Tondi et al., 2009)

2.	Fe graphitized wood derived	0.7	-	0.59	(Ramirez-Rico et al., 2016)
3	phenolic resin and cenospheres into polyurethane (PU) foam substrate	0.02	-	0.30	
4	Cotton with graphene oxide	-	36	0.05	(Gu et al., 2020)
5	$Ti_3C_2T_x$ MXene/starch	-	75	0.32	(Qi et al., 2021)
6	$Ti_3C_2T_x$ Mxene/ compressed wood	-	25-44.4	0.15	(Jia et al., 2021)
7	Lignin -GO	-	28.5-70.5		(Z. Zeng et al., 2018)
8	Bread	-	16.3-17.2	0.08-0.27	(Y. Yuan et al., 2016b)
9	Adenine building block with polyimide	-	41.1	0.018	(C. Li et al., 2019)

10	Polyimide and GO	0.08-0.17	54	0.07-0.09	(Y. Li et al., 2016)
11	Platanus Orientalis fruits	-	14.0-16.0	0.54-0.58	(Farhan et al., 2018)
12	Sucrose by NaCl particle templating	-	24.7 to 41.7	0.1-0.21	(Wilson et al., 2018b)
13	Sucrose with MWCNT	0.22-0.67	20-38	0.23-0.26	(R. Narasimman et al., 2016)
14	Sucrose with graphene	0.09-0.23	25-38.6	0.13-0.25	(R Narasimman et al., 2015)
15	wood	-	-	0.12-0.17	(Zimmermann et al., 2020)
16	Phenolic resin with red mud	-	20.8-49.0	0.30-0.46	(Kumar et al., 2020)
17	Natural cotton	0.069-0.185	21.5 to 38.9	0.06-0.31	Present work
18	Sawdust	0.12-0.20	25-53	0.15-0.35	

19	Rice husk	0.150-0.205	18-38.5	0.255-0.365 (C/SiO_2)	Present work
		0.165-0.431	20-43.7	0.18-0.29 (C/SiC)	Present work
21	Newspaper waste	0.096-0.2	15.9-44.9	0.18-0.39	Present work

7.2 Future scope of work

The carbon composite foams prepared from the agricultural residues exhibit excellent fire resistance, reasonably high compressive strength and low thermal conductivity. The present study prepares cylindrical composite foam bodies of smaller sizes. However, real thermal protection applications demand carbon-composite foams of large sizes in diverse shapes. Extension of the filter-pressing process for the production of large bodies in various simple shapes is proposed as one of the future studies. The evaluation of the thermal protection capability of carbon composite foams in the actual system would be another future scope of the study. Sandwich composites using the prepared lightweight carbon composite foams as the core would be a good thermo-structural material. It proposed to fabricate sandwich composites using carbon composite foams and evaluate their performance as thermo-structural material. The carbon composite foams of high surface area and good textural properties can be candidates for electrodes in energy storage systems. It is also proposed to evaluate the electrochemical performance of the carbon composite foams for their possible applications in energy storage systems.

REFERENCES

1. Abdul, W., Darain, F., Karim, A., & Beltramini, J. (2015). Nano-confined Synthesis of Highly Ordered Mesoporous Carbon and its Performance as Electrode Material for Electrochemical Behavior of Riboflavin (Vitamin B2) and Dopamine. *International Journal of Electrochemical Science*, *10*, 7732–7742.
2. Agrawal, P. R., Kumar, R., Teotia, S., Kumari, S., Mondal, D. P., & Dhakate, S. R. (2019). Lightweight, high electrical and thermal conducting carbon-rGO composites foam for superior electromagnetic interference shielding. *Composites Part B: Engineering*, *160,* 131–139. https://doi.org/10.1016/j.compositesb.2018.10.033
3. Albert, B., P, C. A., & J, M. A.-M. E. (1981). *Process for preparing pitch foams and products so produced*. BRITISH PETROLEUM CO OP - FR 7737747 A OP - FR 7737748 A.
4. Alweendo, S. T., Johnson, O. T., Shongwe, M. B., Kavishe, F. P. L., & Borode, J. O. (2019). Synthesis, Optimization and Characterization of Silicon Carbide (SiC) from Rice Husk. *Procedia Manufacturing*, *35*, 962–967. https://doi.org/10.1016/j.promfg.2019.06.042
5. Amaral-Labat, G., Gourdon, E., Fierro, V., Pizzi, A., & Celzard, A. (2013). Acoustic properties of cellular vitreous carbon foams. *Carbon*, *58*, 76–86. https://doi.org/10.1016/j.carbon.2013.02.033
6. Amini, N., Aguey-Zinsou, K.-F., & Guo, Z.-X. (2011). Processing of strong and highly conductive carbon foams as electrode. *Carbon*, *49*(12), 3857–3864. https://doi.org/10.1016/j.carbon.2011.05.022
7. Bakar, R. A., Yahya, R., & Gan, S. N. (2016). Production of High Purity Amorphous Silica from Rice Husk. *Procedia Chemistry*, *19*, 189–195. https://doi.org/10.1016/j.proche.2016.03.092
8. Baran, D., Yardim, M. F., Atakül, H., & Ekinci, E. (2013). Synthesis of carbon foam with high compressive strength from an asphaltene pitch. *New Carbon Materials*, *28*(2), 127–132. https://doi.org/10.1016/S1872-5805(13)60071-2
9. Barnakov, C. N., Khokhlova, G. P., Popova, A. N., Sozinov, S. A., &

Ismagilov, Z. R. (2015). XRD characterization of the structure of graphites and carbon materials obtained by the low-temperature graphitization of coal tar pitch. *Eurasian Chemico-Technological Journal*, *17*(2), 87–93. https://doi.org/10.18321/ectj198

10. Baumann, T. F., & Satcher, J. H. (2003). Homogeneous Incorporation of Metal Nanoparticles into Ordered Macroporous Carbons. *Chemistry of Materials*, *15*(20), 3745–3747. https://doi.org/10.1021/cm0343960

11. Bi, H., Huang, X., Wu, X., Cao, X., Tan, C., Yin, Z., Lu, X., Sun, L., & Zhang, H. (2014). Carbon Microbelt Aerogel Prepared by Waste Paper: An Efficient and Recyclable Sorbent for Oils and Organic Solvents. *Small (Weinheim an Der Bergstrasse, Germany)*, *10*. https://doi.org/10.1002/smll.201303413

12. Bi, H., Yin, Z., Cao, X., Xie, X., Tan, C., Huang, X., Chen, B., Chen, F., Yang, Q., Bu, X., Lu, X., Sun, L., & Zhang, H. (2013). Carbon Fiber Aerogel Made from Raw Cotton: A Novel, Efficient and Recyclable Sorbent for Oils and Organic Solvents. *Advanced Materials (Deerfield Beach, Fla.)*, *25*. https://doi.org/10.1002/adma.201302435

13. Burchell, T. D. (1999). *Carbon Materials for Advanced Technologies*. Elsevier Science. https://books.google.co.in/books?id=CEeVS3LcuuoC

14. Byrne, C. E., & Nagle, D. C. (1997). Carbonization of wood for advanced materials applications. *Carbon*, *35*(2), 259–266. https://doi.org/10.1016/S0008-6223(96)00136-4

15. Cao, J., & Ma, Y. (2020). Direct preparation of activated carbon fiber aerogel via pyrolysis of cotton under CO_2 atmosphere and its adsorption of methylene blue. *Energy Sources, Part A: Recovery, Utilization, and Environmental Effects*, *42*(9), 1108–1117. https://doi.org/10.1080/15567036.2019.1602221

16. *carbon aerogel - Bing images*. (n.d.). https://www.bing.com

17. Celzard, A, & Cedex, E. (2013). Acoustic properties of cellular vitreous carbon foams. *Carbon*, *58*, 76–86. https://doi.org/10.1016/j.carbon.2013.02.033

18. Celzard, A, Fierro, V., Amaral-Labat, G., Pizzi, A., & Torero, J. (2011).

Flammability assessment of tannin-based cellular materials. *Polymer Degradation and Stability*, *96*(4), 477–482. https://doi.org/https://doi.org/10.1016/j.polymdegradstab.2011.01.014

19. Celzard, A, Tondi, G., Lacroix, D., Jeandel, G., Monod, B., Fierro, V., & Pizzi, A. (2012). Radiative properties of tannin-based, glasslike, carbon foams. *Carbon*, *50*(11), 4102–4113. https://doi.org/https://doi.org/10.1016/j.carbon.2012.04.058

20. Celzard, A, Zhao, W., Pizzi, A., & Fierro, V. (2010). Mechanical properties of tannin-based rigid foams undergoing compression. *Materials Science and Engineering: A*, *527*(16), 4438–4446. https://doi.org/10.1016/j.msea.2010.03.091

21. Celzard, Alain, Szczurek, A., Jana, P., Fierro, V., Basso, M.-C., Bourbigot, S., Stauber, M., & Pizzi, A. (2015). Latest progresses in the preparation of tannin-based cellular solids. *Journal of Cellular Plastics*, *51*(1), 89–102.

22. Chai, G. S., Yoon, S. B., Yu, J.-S., Choi, J.-H., & Sung, Y.-E. (2004). Ordered Porous Carbons with Tunable Pore Sizes as Catalyst Supports in Direct Methanol Fuel Cell. *The Journal of Physical Chemistry B*, *108*(22), 7074–7079. https://doi.org/10.1021/jp0370472

23. Chen, Changle, & Chen, Q. (2008). Recent Development in Diamond Synthesis. *International Journal of Modern Physics B - IJMPB*, *22*, 309–326. https://doi.org/10.1142/S0217979208038685

24. Chen, Chong, Kennel, E. B., Stiller, A. H., Stansberry, P. G., & Zondlo, J. W. (2006). Carbon foam derived from various precursors. *Carbon*, *44*(8), 1535–1543. https://doi.org/https://doi.org/10.1016/j.carbon.2005.12.021

25. Chen, Chong, Kennel, E., Stiller, A., Stansberry, P., & Zondlo, J. (2004). *Development of carbon foam using coal-derived precursors*.

26. Chen, H., Wang, X., Li, J., & Wang, X. (2015). Cotton derived carbonaceous aerogels for the efficient removal of organic pollutants and heavy metal ions. *Journal of Materials Chemistry A*, *3*(11), 6073–6081. https://doi.org/10.1039/C5TA00299K

27. Chen, Li, Song, N., Shi, L., & Ding, P. (2018). Anisotropic thermally conductive composite with wood-derived carbon scaffolds. *Composites*

Part A: Applied Science and Manufacturing, *112*, 18–24. https://doi.org/https://doi.org/10.1016/j.compositesa.2018.05.023

28. Chen, Long, Ji, T., Mu, L., & Zhu, J. (2017). Cotton fabric derived hierarchically porous carbon and nitrogen doping for sustainable capacitor electrode. *Carbon*, *111*, 839–848. https://doi.org/https://doi.org/10.1016/j.carbon.2016.10.054

29. Chen, S., He, G., Hu, H., Jin, S., Zhou, Y., He, Y., He, S., Zhao, F., & Hou, H. (2013). Elastic carbon foam via direct carbonization of polymer foam for flexible electrodes and organic chemical absorption. *Energy & Environmental Science*, *6*(8), 2435–2439. https://doi.org/10.1039/C3EE41436A

30. Chen, T., Lin, Q., Xiong, L., Lü, Q., & Fang, C. (2015). Preparation and characterization of carbon foams from cyanate ester mixtures. *Journal of Analytical and Applied Pyrolysis*, *113*, 539–544. https://doi.org/https://doi.org/10.1016/j.jaap.2015.03.014

31. Chen, Y., Liu, Y., Li, Y., Zhao, L., Chen, Y., Li, H., Liu, Y., Li, L., Xu, F., & Li, M. (2020). Functional wastepaper-montmorillonite composite aerogel for Cd2+ adsorption. *Environmental Science and Pollution Research*, *27*(31), 38644–38653. https://doi.org/10.1007/s11356-020-09907-6

32. Chung, D. D. . (2001). Electromagnetic interference shieldingeffectiveness of carbon materials. *Carbon*, *39*(2), 279–285. https://doi.org/10.1016/S0008-6223(00)00184-6

33. Cychosz, K. A., Guillet-Nicolas, R., García-Martínez, J., & Thommes, M. (2017). Recent advances in the textural characterization of hierarchically structured nanoporous materials. *Chemical Society Reviews*, *46*(2), 389–414. https://doi.org/10.1039/C6CS00391E

34. da Silva, R. S. R., Oishi, S. S., Botelho, E. C., & Ferreira, N. G. (2020). Carbon foam composites based on expanded graphite for electrochemical application. *Diamond and Related Materials*, *103,* 107730. https://doi.org/https://doi.org/10.1016/j.diamond.2020.107730

35. Darder, M., & Ruiz-Hitzky, E. (2005). Caramel–clay nanocomposites. *Journal of Materials Chemistry*, *15*(35–36), 3913–3918.

https://doi.org/10.1039/B505958E

36. De, S., Balu, A. M., van der Waal, J. C., & Luque, R. (2015). Biomass-Derived Porous Carbon Materials: Synthesis and Catalytic Applications. *ChemCatChem*, *7*(11), 1608–1629. https://doi.org/https://doi.org/10.1002/cctc.201500081

37. DeMan, J. M. (1999). *Principles of food chemistry*. Aspen Publishers.

38. Deng, H., Li, G., Yang, H., Tang, J., & Tang, J. (2010). Preparation of activated carbons from cotton stalk by microwave assisted KOH and K_2CO_3 activation. *Chemical Engineering Journal*, *163*(3), 373–381. https://doi.org/10.1016/j.cej.2010.08.019

39. Dochia, M., Sirghie, C., Kozłowski, R. M., & Roskwitalski, Z. (2012). 2 - Cotton fibres. In R. M. B. T.-H. of N. F. Kozłowski (Ed.), *Woodhead Publishing Series in Textiles* (Vol. 1, pp. 11–23). Woodhead Publishing. https://doi.org/10.1533/9780857095503.1.9

40. Du, J., Liu, L., Hu, Z., Yu, Y., Zhang, Y., Hou, S., & Chen, A. (2018). Raw-Cotton-Derived N-Doped Carbon Fiber Aerogel as an Efficient Electrode for Electrochemical Capacitors. *ACS Sustainable Chemistry and Engineering*, *6*(3), 4008–4015. https://doi.org/10.1021/acssuschemeng.7b04396

41. Dychalska, A., Popielarski, P., Franków, W., Fabisiak, K., Paprocki, K., & Szybowicz, M. (2015). Study of CVD diamond layers with amorphous carbon admixture by Raman scattering spectroscopy. *MATERIALS SCIENCE-POLAND*, *33*. https://doi.org/10.1515/msp-2015-0067

42. El-Sayed, G. O., Yehia, M. M., & Asaad, A. A. (2014). Assessment of activated carbon prepared from corncob by chemical activation with phosphoric acid. *Water Resources and Industry*, *7–8*, 66–75. https://doi.org/10.1016/j.wri.2014.10.001

43. El Nemr, A., Abdelwahab, O., El-Sikaily, A., & Khaled, A. (2009). Removal of direct blue-86 from aqueous solution by new activated carbon developed from orange peel. *Journal of Hazardous Materials*, *161*(1), 102–110.

44. *EMI Shielding - CFOAM® Carbon Foam*. (n.d.).

https://www.cfoam.com/emishielding/

45. Estevez, L., Barpaga, D., Zheng, J., Sabale, S., Patel, R. L., Zhang, J.-G., McGrail, B. P., & Motkuri, R. K. (2018). Hierarchically Porous Carbon Materials for CO_2 Capture: The Role of Pore Structure. *Industrial & Engineering Chemistry Research*, *57*(4), 1262–1268.

46. Farhan, S., Wang, R., Jiang, H., & Li, K. (2016). Use of waste rigid polyurethane for making carbon foam with fireproofing and anti-ablation properties. *Materials & Design*, *101*, 332–339. https://doi.org/https://doi.org/10.1016/j.matdes.2016.04.008

47. Farhan, S., Wang, R., & Li, K. (2018). Physical and electromagnetic shielding properties of green carbon foam prepared from biomaterials. *Transactions of Nonferrous Metals Society of China*, *28*(1), 103–113. https://doi.org/10.1016/S1003-6326(18)64643-6

48. Farhan, S., Wang, R. M., Jiang, H., & Ul-Haq, N. (2014). Preparation and characterization of carbon foam derived from pitch and phenolic resin using a soft templating method. *Journal of Analytical and Applied Pyrolysis*, *110*(1), 229–234. https://doi.org/10.1016/j.jaap.2014.09.003

49. Feng, J., Nguyen, S. T., Fan, Z., & Duong, H. M. (2015). Advanced fabrication and oil absorption properties of super-hydrophobic recycled cellulose aerogels. *Chemical Engineering Journal*, *270*, 168–175. https://doi.org/https://doi.org/10.1016/j.cej.2015.02.034

50. Fischer, F., Rigacci, A., Pirard, R., Berthon-Fabry, S., & Achard, P. (2006). Cellulose-based aerogels. *Polymer*, *47*(22), 7636–7645. https://doi.org/https://doi.org/10.1016/j.polymer.2006.09.004

51. Fuad, M. Y. A., Ismail, Z., Mansor, M. S., Ishak, Z. A. M., & Omar, A. K. M. (1995). Mechanical properties of rice husk ash/polypropylene composites. *Polymer Journal*, *27*(10), 1002–1015.

52. Gallego, N. C., & Klett, J. W. (2003). Carbon foams for thermal management. *Carbon*, *41*(7), 1461–1466. https://doi.org/https://doi.org/10.1016/S0008-6223(03)00091-5

53. Gao, N., Cheng, B., Hou, H., & Zhang, R. (2018). Mesophase pitch based carbon foams as sound absorbers. *Materials Letters*, *212*, 243–246.

https://doi.org/https://doi.org/10.1016/j.matlet.2017.10.074

54. Gao, P.-C., Tsai, W.-Y., Daffos, B., Taberna, P.-L., Pérez, C. R., Gogotsi, Y., Simon, P., & Favier, F. (2015). Graphene-like carbide derived carbon for high-power supercapacitors. *Nano Energy*, *12*, 197–206. https://doi.org/https://doi.org/10.1016/j.nanoen.2014.12.017

55. Gao, S., Tang, Y., Wang, L., Liu, L., Sun, Z., Wang, S., Zhao, H., Kong, L., & Jia, D. (2018). Coal-Based Hierarchical Porous Carbon Synthesized with a Soluble Salt Self-Assembly-Assisted Method for High Performance Supercapacitors and Li-Ion Batteries. *ACS Sustainable Chemistry & Engineering*, *6*(3), 3255–3263. https://doi.org/10.1021/acssuschemeng.7b03421

56. Gao, X., Xing, Z., Li, Z., Dong, X., Ju, Z., & Guo, C. (2020). A review on recent advances in carbon aerogels: their preparation and use in alkali-metal ion batteries. *New Carbon Materials*, *35*(5), 486–507. https://doi.org/https://doi.org/10.1016/S1872-5805(20)60504-2

57. Geetha, S., Kumar, K. K. S., Rao, C. R. K., Vijayan, M., & Trivedi, D. C. (2009). *EMI Shielding : Methods and Materials — A Review*. *112*(1), 2073–2086. https://doi.org/10.1002/app

58. Geng, S., Wei, J., Jonasson, S., Hedlund, J., & Oksman, K. (2020). Multifunctional Carbon Aerogels with Hierarchical Anisotropic Structure Derived from Lignin and Cellulose Nanofibers for CO2 Capture and Energy Storage. *ACS Applied Materials & Interfaces*, *12*(6), 7432–7441. https://doi.org/10.1021/acsami.9b19955

59. Gibson, L. J., & Ashby, M. F. (1997). Cellular Solids: Structure and Properties. In *Cambridge Solid State Science Series* (2nd ed.). Cambridge University Press. https://doi.org/DOI: 10.1017/CBO9781139878326

60. Gidde, M., & Jivani, A. (2007). Waste to Wealth -Potential of Rice Husk in India a Literature Review. *Proceeding of International Conference on Cleaner Technologies and Environmental Management*.

61. Girgis, B. S., & El-Hendawy, A.-N. A. (2002). Porosity development in activated carbons obtained from date pits under chemical activation with phosphoric acid. *Microporous and Mesoporous Materials*, *52*(2), 105–117.

https://doi.org/https://doi.org/10.1016/S1387-1811(01)00481-4

62. Gowariker, V. R., Viswanathan, N. V, & Sreedhar, J. (1986). *Polymer Science*. Wiley. https://books.google.co.in/books?id=mvCzE_AflUIC

63. Graebner, J. E. (1995). *Thermal Conductivity of Diamond BT - Diamond: Electronic Properties and Applications* (L. S. Pan & D. R. Kania (Eds.); pp. 285–318). Springer US. https://doi.org/10.1007/978-1-4615-2257-7_7

64. Gu, H., Xu, Y., Shen, Y., Zhu, P., Zhao, T., Hu, Y., Sun, R., & Wong, C.-P. (2020). Versatile Biomass Carbon Foams for Fast Oil–Water Separation, Flexible Pressure-Strain Sensors, and Electromagnetic Interference Shielding. *Industrial & Engineering Chemistry Research*, *59*(47), 20740–20748. https://doi.org/10.1021/acs.iecr.0c04316

65. Gudavalli, G. S., & Dhakal, T. P. (2018). *Chapter 8 - Simple Parallel-Plate Capacitors to High–Energy Density Future Supercapacitors: A Materials Review* (K. Y. Cheong, G. Impellizzeri, & M. A. B. T.-E. M. for E. C. and S. Fraga (Eds.); pp. 247–301). Elsevier. https://doi.org/https://doi.org/10.1016/B978-0-12-813794-9.00008-9

66. Gupta, P., Singh, B., Agrawal, A. K., & Maji, P. K. (2018). Low density and high strength nanofibrillated cellulose aerogel for thermal insulation application. *Materials & Design*, *158*, 224–236.

67. Han, S., Sun, Q., Zheng, H., Li, J., & Jin, C. (2016). Green and facile fabrication of carbon aerogels from cellulose-based waste newspaper for solving organic pollution. *Carbohydrate Polymers*, *136*, 95–100. https://doi.org/10.1016/j.carbpol.2015.09.024

68. Hayashi, J., Horikawa, T., Muroyama, K., & Gomes, V. G. (2002). Activated carbon from chickpea husk by chemical activation with K2CO3: preparation and characterization. *Microporous and Mesoporous Materials*, *55*(1),63–68. https://doi.org/https://doi.org/10.1016/S1387-1811(02)00406-7

69. He, X., Tang, Z., Zhu, Y., & Yang, J. (2013). Fabrication of carbon foams with low thermal conductivity using the protein foaming method. *Materials Letters*, *94*, 55–57. https://doi.org/10.1016/j.matlet.2012.12.023

70. Hernández-Martínez, D., Leyva-Verduzco, A. A., Rodríguez-Félix, F., Acosta-Elías, M., & Wong-Corral, F. J. (2020). Obtaining and characterization of silicon(Si) from wheat husk ash for its possible application in solar cells. *Journal of Cleaner Production*, *271*, 122698. https://doi.org/https://doi.org/10.1016/j.jclepro.2020.122698

71. Hu, H., Li, Y., Gao, T., Yan, S., Wu, S., Bandaru, S., Zheng, Y., Qin, G., & Zhang, X. (2021). Sulfur-doped wood-derived porous carbon for optimizing electromagnetic response performance. *Nanoscale*, *13*(38), 16084–16093. https://doi.org/10.1039/D1NR04232G

72. Inagaki, M. (2013). *Handbook of Advanced Ceramics: Chapter 2.1. Advanced Carbon Materials*. Elsevier Inc. Chapters.

73. Inagaki, M., Morishita, T., Kuno, A., Kito, T., Hirano, M., Suwa, T., & Kusakawa, K. (2004). Carbon foams prepared from polyimide using urethane foam template. *Carbon*, *42*(3), 497–502.

74. Inagaki, M., Qiu, J., & Guo, Q. (2015). Carbon foam: Preparation and application. *Carbon*, *87*, 128–152. https://doi.org/https://doi.org/10.1016/j.carbon.2015.02.021

75. Inagaki, M., Toyoda, M., Soneda, Y., Tsujimura, S., & Morishita, T. (2016). Templated mesoporous carbons: Synthesis and applications. *Carbon*, *107*, 448–473. https://doi.org/https://doi.org/10.1016/j.carbon.2016.06.003

76. Izhevskyi, V. A., Genova, L., Bressiani, A., & Bressiani, J. (2000). Liquid-Phase Sintered SiC Processing and Transformation Controlled Microstructure Tailoring. *Materials Research*, *3*. https://doi.org/10.1590/S1516-14392000000400007

77. Jana, P., Fierro, V., & Celzard, A. (2013). Ultralow cost reticulated carbon foams from household cleaning pad wastes. *Carbon*, *62*, 517–520.

78. Jana, P., Fierro, V., & Celzard, A. (2016). Sucrose-based carbon foams with enhanced thermal conductivity. *Industrial Crops and Products*, *89*, 498–506. https://doi.org/10.1016/j.indcrop.2016.06.001

79. Jana, P., Fierro, V., Pizzi, A., & Celzard, A. (2014). Biomass-derived, thermally conducting, carbon foams for seasonal thermal storage. *Biomass and Bioenergy*, *67*, 312–318. https://doi.org/https://doi.org/10.1016/j.biombioe.2014.04.031

80. Jaroszewski, M., Thomas, S., & Rane, A. V. (2018). *Advanced Materials for Electromagnetic Shielding: Fundamentals, Properties, and Applications*. Wiley.

81. Ji, H., Huang, Z., Wu, X., Huang, J., Chen, K., Fang, M., & Liu, Y. (2014). Preparation, microstructure, and compressive strength of carbon foams derived from sucrose and kaolinite. *Journal of Materials Research*, *29*(8), 1018–1025. https://doi.org/DOI: 10.1557/jmr.2014.45

82. Jia, X., Shen, B., Zhang, L., & Zheng, W.-G. (2020). Construction of Shape-Memory Carbon Foam Composites for Adjustable EMI Shielding under Self-Fixable Mechanical Deformation. *Chemical Engineering Journal*, *405*. https://doi.org/10.1016/j.cej.2020.126927

83. Jin, C., Han, S., Li, J., & Sun, Q. (2015). Fabrication of cellulose-based aerogels from waste newspaper without any pretreatment and their use for absorbents. *Carbohydrate Polymers*, *123*, 150–156. https://doi.org/https://doi.org/10.1016/j.carbpol.2015.01.056

84. Jittin, V., Bahurudeen, A., & Ajinkya, S. D. (2020). Utilisation of rice husk ash for cleaner production of different construction products. *Journal of Cleaner Production, 263*, 121578. https://doi.org/https://doi.org/10.1016/j.jclepro.2020.121578

85. Jüntgen, H., Knoblauch, K., & Harder, K. (1981). Carbon molecular sieves: production from coal and application in gas separation. *Fuel*, *60*(9), 817–822. https://doi.org/https://doi.org/10.1016/0016-2361(81)90144-7

86. Kang, S., Yu, J.-S., Kruk, M., & Jaroniec, M. (2002). Synthesis of an ordered macroporous carbon with 62 nm spherical pores that exhibit unique gas adsorption properties. *Chemical Communications*, *16*, 1670–1671. https://doi.org/10.1039/B204756J

87. Katinas, V., Marčiukaitis, M., Perednis, E., & Dzenajavičienė, E. F. (2019). Analysis of biodegradable waste use for energy generation in Lithuania. *Renewable and Sustainable Energy Reviews*, *101*, 559–567. https://doi.org/https://doi.org/10.1016/j.rser.2018.11.022

88. Kaur, P., Verma, G., & Sekhon, S. S. (2019). Biomass derived hierarchical porous carbon materials as oxygen reduction reaction electrocatalysts in fuel cells. *Progress in Materials Science*, *102*, 1–71. https://doi.org/https://doi.org/10.1016/j.pmatsci.2018.12.002

89. Kernas Kristen, M. (1999). *Process for preparing pitch foams*. US AIR FORCE OP - US 97971097 A. https://lens.org/047-079-528-934-590

90. Kershaw, J. R., & Black, K. J. T. (1993). Structural characterization of coal-tar and petroleum pitches. *Energy & Fuels*, *7*(3), 420–425. https://doi.org/10.1021/ef00039a014

91. Khan, A., Jawaid, M., & Asiri, A. M. A. M. (2018). *Nanocarbon and Its Composites: Preparation, Properties and Applications*. Elsevier Science.

92. Kharisov, B. I., & Kharissova, O. V. (2019). *Carbon Allotropes: Metal-Complex Chemistry, Properties and Applications*. Springer International Publishing.

93. Kim, J.-E., Oh, J.-H., Kotal, M., Koratkar, N., &Oh, I.-K. (2017). Self-assembly and morphological control of three-dimensional macroporous architectures built of two-dimensional materials. *Nano Today*, *14*, 100–123. https://doi.org/https://doi.org/10.1016/j.nantod.2017.04.008

94. Klett, J. (2005). Carbon Foams. In *Cellular Ceramics* (pp. 137–157). https://doi.org/https://doi.org/10.1002/3527606696.ch2f

95. Klett, J., & Conway, B. (2000). Thermal management solutions utilizing high thermal conductivity graphite foams. *International SAMPE Symposium and Exhibition (Proceedings)*, *45*(1), 1–11.

96. Klett, J., Hardy, R., Romine, E., Walls, C., & Burchell, T. (2000). High-thermal-conductivity, mesophase-pitch-derived carbon foams: Effect of precursor on structure and properties. *Carbon*, *38*(7), 953–973. https://doi.org/10.1016/S0008-6223(99)00190-6

97. Klett, J W, McMillan, A. D., Gallego, N. C., & Walls, C. A. (2004). The role of structure on the thermal properties of graphitic foams. *Journal of Materials Science*, *39*(11), 3659–3676. https://doi.org/10.1023/B:JMSC.0000030719.80262.f8

98. Klett, James W. (2000). *Process for making carbon foam*. LOCKHEED MARTIN ENGERY RESEARC OP - US 92187597 A. https://lens.org/164-590-383-070-591

99. Konstantin, N. K., Ozbas, B., Hannes, C. S., Robert, P., Aksayand, I. A., & Roberto, C. (2008). Raman Spectra of Graphite Oxide and Functionalized Graphene Sheets. *Nano Letters*, *8*(1), 36–41. https://doi.org/10.1021/NL071822Y

100. Kouchi, A. (2011). *Amorphous Carbon BT - Encyclopedia of Astrobiology* (M. Gargaud, R. Amils, J. C. Quintanilla, H. J. (Jim) Cleaves, W. M. Irvine, D. L. Pinti, & M. Viso (Eds.); pp. 41–42). Springer Berlin Heidelberg. https://doi.org/10.1007/978-3-642-11274-4_70

101. Kumar, R., Dhakate, S. R., Gupta, T., Saini, P., Singh, B. P., & Mathur, R. B. (2013). Effective improvement of the properties of light weight carbon foam by decoration with multi-wall carbon nanotubes. *Journal of Materials Chemistry A, 1*(18), 5727–5735. https://doi.org/10.1039/C3TA10604G

102. Kumar, R., Dhakate, S. R., & Mathur, R. B. (2013). The role of ferrocene on the enhancement of the mechanical and electrochemical properties of coal tar pitch-based carbon foams. *Journal of Materials Science, 48*(20), 7071–7080. https://doi.org/10.1007/s10853-013-7518-z

103. Kumar, R., Jain, H., Chaudhary, A., Kumari, S., Mondal, D. P., & Srivastava, A. K. (2019). Thermal conductivity and fire-retardant response in graphite foam made from coal tar pitch derived semi coke. *Composites Part B: Engineering*, *172*, 121–130. https://doi.org/https://doi.org/10.1016/j.compositesb.2019.05.036

104. Kumar, R., Mondal, D. P., Chaudhary, A., Shafeeq, M., & Kumari, S. (2018). Excellent EMI shielding performance and thermal insulating properties in lightweight, multifunctional carbon-cenosphere composite foams. In *Composites Part A: Applied Science and Manufacturing* (Vol. 112, pp. 475–484). https://doi.org/10.1016/j.compositesa.2018.07.003

105. Kumar, R., Sharma, A., Pandey, A., Chaudhary, A., Dwivedi, N., Shafeeq M, M., Mondal, D. P., & Srivastava, A. K. (2020). Lightweight carbon-red mud hybrid foam toward fire-resistant and efficient shield against electromagnetic interference. *Scientific Reports*, *10*(1), 9913. https://doi.org/10.1038/s41598-020-66929-3

106. Kuruvilla, J., Wilson, R., & Gejo, G. (2019). *Materials for Potential EMI*

Shielding Applications: Processing, Properties and Current Trends. Elsevier Science.

107. Kuznetsov, P. N., Kuznetsova, L. I., Buryukin, F. A., Marakushina, E. N., & Frizorger, V. K. (2015). Methods for the preparation of coal-tar pitch. *Solid Fuel Chemistry*, *49*(4), 213–225. https://doi.org/10.3103/S0361521915040059

108. Kyotani, T. (2003). *Chapter 7 - Porous Carbon* (E. YASUDA, M. INAGAKI, K. KANEKO, M. ENDO, A. OYA, & Y. B. T.-C. A. TANABE (Eds.); pp. 109–127). Elsevier Science.

109. Lee, B. J., Kim, J., & Hyeon, T. (2006). *Recent Progress in the Synthesis of Porous Carbon Materials*. 2073–2094.

110. Lee, C.-G., Jeon, J.-W., Hwang, M.-J., Ahn, K.-H., Park, C., Choi, J.-W., & Lee, S.-H. (2015). Lead and copper removal from aqueous solutions using carbon foam derived from phenol resin. *Chemosphere*, *130*, 59–65. https://doi.org/https://doi.org/10.1016/j.chemosphere.2015.02.055

111. Lei, S., Guo, Q., Shi, J., & Liu, L. (2010). Preparation of phenolic-based carbon foam with controllable pore structure and high compressive strength. In *Carbon* (Vol. 48, Issue 9, pp. 2644–2646). Elsevier Ltd. https://doi.org/10.1016/j.carbon.2010.03.017

112. Letellier, M., Ghaffari Mosanenzadeh, S., Naguib, H., Fierro, V., & Celzard, A. (2017). Acoustic properties of model cellular vitreous carbon foams. *Carbon*, *119*, 241–250.

113. Letellier, M., Macutkevic, J., Paddubskaya, A., Klochkov, A., Kuzhir, P., Banys, J., Fierro, V., & Celzard, A. (2015). Microwave Dielectric Properties of Tannin-Based Carbon Foams. *Ferroelectrics*, *479*(1), 119–126. https://doi.org/10.1080/00150193.2015.1012036

114. Letellier, M., Macutkevic, J., Paddubskaya, A., Plyushch, A., Kuzhir, P., Ivanov, M., Banys, J., Pizzi, A., Fierro, V., & Celzard, A. (2015). Tannin-Based Carbon Foams for Electromagnetic Applications. *IEEE Transactions on Electromagnetic Compatibility*, *57*(5), 989–995.

115. Li, C., Zhou, C., Lv, J., Liang, B., Li, R., Liu, Y., Hu, J., Zeng, K., & Yang, G. (2019). Bio-molecule adenine building block effectively enhances electromagnetic interference shielding performance of polyimide-derived carbon foam. *Carbon*, *149*, 190–202.

116. Li, F., Xie, L., Sun, G., Kong, Q., Su, F., Cao, Y., Wei, J., Ahmad, A., Guo, X., & Chen, C.-M. (2019). Resorcinol-formaldehyde based carbon aerogel: Preparation, structure and applications in energy storage devices. *Microporous and Mesoporous Materials*, *279*, 293–315.

117. Li, K., Zheng, Z., & Li, Y. (2010). Characterization and lead adsorption properties of activated carbons prepared from cotton stalk by one-step H3PO4 activation. *Journal of Hazardous Materials*, *181*(1), 440–447. https://doi.org/https://doi.org/10.1016/j.jhazmat.2010.05.030

118. Li, L., Li, B., Sun, H., & Zhang, J. (2017). Compressible and conductive carbon aerogels from waste paper with exceptional performance for oil/water separation. *Journal of Materials Chemistry A*, *5*(28), 14858–14864. https://doi.org/10.1039/C7TA03511J

119. Li, Q., Chen, L., Ding, J., Zhang, J., Li, X., Zheng, K., Zhang, X., & Tian, X. (2016). Open-cell phenolic carbon foam and electromagnetic interference shielding properties. *Carbon*, *104,* 90–105. https://doi.org/https://doi.org/10.1016/j.carbon.2016.03.055

120. Li, Shijie, Han, K., Li, J., Li, M., & Lu, C. (2017). Preparation and characterization of super activated carbon produced from gulfweed by KOH activation. *Microporous and Mesoporous Materials*, *243,* 291–300. https://doi.org/10.1016/j.micromeso.2017.02.052

121. Li, Sizhong, Song, Y., Song, Y., Shi, J., Liu, L., Wei, X., & Guo, Q. (2007). *Carbon foams with high compressive strength derived from mixtures of mesocarbon microbeads and mesophase pitch*. *45,* 2092–2097. https://doi.org/10.1016/j.carbon.2007.05.014

122. Li, Sizhong, Tian, Y., Zhong, Y., Yan, X., Song, Y., Guo, Q., Shi, J., & Liu, L. (2011). Formation mechanism of carbon foams derived from mesophase pitch. *Carbon*, *49*(2), 618–624.

123. Li, W., Huang, Z., Wu, Y., Zhao, X., & Liu, S. (2015). Honeycomb carbon foams with tunable pore structures prepared from liquefied larch sawdust by self-foaming. *Industrial Crops and Products*, *64,* 215–223.

https://doi.org/https://doi.org/10.1016/j.indcrop.2014.09.043

124. Li, Y.-Q., Samad, Y. A., Polychronopoulou, K., & Liao, K. (2015). Lightweight and Highly Conductive Aerogel-like Carbon from Sugarcane with Superior Mechanical and EMI Shielding Properties. *ACS Sustainable Chemistry & Engineering*, *3*(7), 1419–1427.

125. Li, Y., Shen, B., Pei, X., Zhang, Y., Yi, D., Zhai, W., Zhang, L., Wei, X., & Zheng, W. (2016). Ultrathin carbon foams for effective electromagnetic interference shielding. *Carbon*, *100*, 375–385.

126. Li, Zhanying, Shao, L., Ruan, Z., Hu, W., Lu, L., & Chen, Y. (2018). Converting untreated waste office paper and chitosan into aerogel adsorbent for the removal of heavy metal ions. *Carbohydrate Polymers*, *193*, 221–227.

127. Li, Ziyu, Jia, Z., Ni, T., & Li, S. (2017). Adsorption of methylene blue on natural cotton based flexible carbon fiber aerogels activated by novel air-limited carbonization method. *Journal of Molecular Liquids*, *242*, 747–756.

128. Liang, C., Li, Z., & Dai, S. (2008). Mesoporous Carbon Materials: Synthesis and Modification. *Angewandte Chemie International Edition*, *47*(20), 3696–3717.

129. Libbrecht, W., Verberckmoes, A., Thybaut, J. W., Van Der Voort, P., & De Clercq, J. (2017). Soft templated mesoporous carbons: Tuning the porosity for the adsorption of large organic pollutants. *Carbon*, *116*, 528–546. h

130. Libin, W., & Hu, X. (2018). Recent Advances in Porous Carbon Materials for Electrochemical Energy Storage. *Chemistry - An Asian Journal*, *13*, 1518 –1529. https://doi.org/10.1002/asia.201800553

131. https://www.acs.org/content/acs/en/molecule-of-the week/archive/l/lignin.html

132. Liu, H., Wu, J., Zhuang, Q., Dang, A., Li, T., & Zhao, T. (2016). Preparation and the electromagnetic interference shielding in the X-band of carbon foams with Ni-Zn ferrite additive. *Journal of the European Ceramic Society*, *36*. https://doi.org/10.1016/j.jeurceramsoc.2016.06.017

133. Liu, H., Wu, S., Tian, N., Yan, F., You, C., & Yang, Y. (2020). Carbon foams: 3D porous carbon materials holding immense potential. *Journal of*

Materials Chemistry A, *8*(45), 23699–23723.

134. Liu, H., Xu, Y., Tang, C., Li, Y., & Chopra, N. (2019). SiO_2 aerogel-embedded carbon foam composite with Co-Enhanced thermal insulation and mechanical properties. *Ceramics International*, *45*(17), 23393–23398. https://doi.org/10.1016/j.ceramint.2019.08.041

135. Liu, L., Wang, J., Wu, X., li, T., & Chu, P. (2010). Longitudinal optical phonon–plasmon coupling in luminescent 3C–SiC nanocrystal films. *Optics Letters*, *35*, 4024–4026. https://doi.org/10.1364/OL.35.004024

136. Liu, M., Gan, L., Zhao, F., Fan, X., Xu, H., Wu, F., Xu, Z., Hao, Z., & Chen, L. (2007). Carbon foams with high compressive strength derived from polyarylacetylene resin. *Carbon*, *45*(15), 3055–3057. https://doi.org/https://doi.org/10.1016/j.carbon.2007.10.003

137. Lorjai, P., Wongkasemjit, S., & Chaisuwan, T. (2009). Preparation of polybenzoxazine foam and its transformation to carbon foam. *Materials Science and Engineering: A*, *527*(1), 77–84.

138. Luo, R., Ni, Y., Li, J., Yang, C., & Wang, S. (2011). The mechanical and thermal insulating properties of resin-derived carbon foams reinforced by K2Ti6O13 whiskers. *Materials Science and Engineering A*, *528*(4–5), 2023–2027. https://doi.org/10.1016/j.msea.2010.10.106

139. Ma, Z., Kyotani, T., & Tomita, A. (2000). Preparation of a high surface area microporous carbon having the structural regularity of Y zeolite. *Chemical Communications*, *23*, 2365–2366.

140. Maleki, M., Imani, A., Ahmadi, R., Banna Motejadded Emrooz, H., & Beitollahi, A. (2020). Low-cost carbon foam as a practical support for organic phase change materials in thermal management. *Applied Energy*, *258*, 114108.

141. Maneechakr, P., & Karnjanakom, S. (2017). Adsorption behaviour of Fe(II) and Cr(VI) on activated carbon: Surface chemistry, isotherm, kinetic and thermodynamic studies. *The Journal of Chemical Thermodynamics*, *106*, 104–112. https://doi.org/10.1016/j.jct.2016.11.021

142. Marsh, H., & Reinoso, F. R. (2006). *Activated Carbon*. Elsevier Science.

143. Marton, M., Vojs, M., Zdravecká, E., Himmerlich, M., Haensel, T., Krischok, S., Kotlár, M., Michniak, P., Veselý, M., & Redhammer, R. (2013). Raman Spectroscopy of Amorphous Carbon Prepared by Pulsed Arc Discharge in Various Gas Mixtures. *Journal of Spectroscopy*, *2013*, 467079. https://doi.org/10.1155/2013/467079

144. Men, Y., Siebenbürger, M., Qiu, X., Antonietti, M., & Yuan, J. (2013). Low fractions of ionic liquid or poly(ionic liquid) can activate polysaccharide biomass into shaped, flexible and fire-retardant porous carbons. *Journal of Materials Chemistry A*, *1*(38), 11887–11893. https://doi.org/10.1039/C3TA12302B

145. Mochizuki, Y., Bud, J., Liu, J., & Tsubouchi, N. (2020). Production of Silicone Tetrachloride from Rice Husk by Chlorination and Performance of Mercury Adsorption from Aqueous Solution of the Chlorinated Residue. *ACS Omega*, *5*(45), 29110–29120.

146. Mohamed, A. R., Mohammadi, M., & Darzi, G. N. (2010). Preparation of carbon molecular sieve from lignocellulosic biomass: A review. *Renewable Sustainable Energy Rev.*, *14*, 1591.

147. Mohammad, S. G., Ahmed, S. M., Badawi, A. F. M., & El-Desouki, D. S. (2015). Activated carbon derived from egyptian banana peels for removal of cadmium from water. *Journal of Applied Life Sciences International*, 77–88.

148. Mohanty, K., Jha, M., Meikap, B. C., & Biswas, M. N. (2005). Removal of chromium (VI) from dilute aqueous solutions by activated carbon developed from Terminalia arjuna nuts activated with zinc chloride. *Chemical Engineering Science*, *60*(11), 3049–3059.

149. Mondal, A. K., Kretschmer, K., Zhao, Y., Liu, H., Fan, H., & Wang, G. (2017). Naturally nitrogen doped porous carbon derived from waste shrimp shells for high-performance lithium ion batteries and supercapacitors. *Microporous and Mesoporous Materials*, *246*, 72–80.

150. Nagel, B., Pusz, S., & Trzebicka, B. (2014). Review: tailoring the properties of macroporous carbon foams. *Journal of Materials Science*, *49*(1), 1–17. https://doi.org/10.1007/s10853-013-7678-x

151. Nakagawa, H., Watanabe, K., Harada, Y., & Miura, K. (1999). Control of micropore formation in the carbonized ion exchange resin by utilizing pillar effect. *Carbon*, *37*, 1455–1461.

152. Narasimman, R., Vijayan, S., Dijith, K. S., Surendran, K. P., & Prabhakaran, K. (2016). Carbon composite foams with improved strength and electromagnetic absorption from sucrose and multi-walled carbon nanotube. *Materials Chemistry and Physics*, *181*, 538–548.

153. Narasimman, R., Vijayan, S., & Prabhakaran, K. (2014). Carbon foam with microporous cell wall and strut for CO_2 capture. *RSC Advances*, *4*(2), 578–582. https://doi.org/10.1039/c3ra46240d

154. Narasimman, R, & Prabhakaran, K. (2012). Preparation of low density carbon foams by foaming molten sucrose using an aluminium nitrate blowing agent. *Carbon*, *50*(5), 1999–2009.

155. Narasimman, R, & Prabhakaran, K. (2013). Preparation of carbon foams with enhanced oxidation resistance by foaming molten sucrose using a boric acid blowing agent. *Carbon*, *55*, 305–312.

156. Narasimman, R, Vijayan, S., Dijith, K. S., Surendran, K. P., & Prabhakaran, K. (2016). Carbon composite foams with improved strength and electromagnetic absorption from sucrose and multi-walled carbon nanotube. *Materials Chemistry and Physics*, *181*, 538–548.

157. Narasimman, R, Vijayan, S., & Prabhakaran, K. (2014). Carbon foam with microporous cell wall and strut for CO_2 capture. *RSC Advances*, *4*(2), 578–582. https://doi.org/10.1039/C3RA46240D

158. Narasimman, R, Vijayan, S., & Prabhakaran, K. (2015). Graphene-reinforced carbon composite foams with improved strength and EMI shielding from sucrose and graphene oxide. *Journal of Materials Science*, *50*(24), 8018–8028. https://doi.org/10.1007/s10853-015-9368-3

159. Narasimman, Rajaram, Vijayan, S., & Prabhakaran, K. (2015). Effect of activated carbon particle size on the thermo-foaming of aqueous sucrose resin and properties of the carbon foams. *Journal of Materials Research*, *30*(1), 46–54. https://doi.org/10.1557/jmr.2014.294

160. Nguyen, S. T., Feng, J., Le, N. T., Le, A. T. T., Hoang, N., Tan, V. B. C., & Duong, H. M. (2013). Cellulose Aerogel from Paper Waste for Crude Oil

Spill Cleaning. *Industrial & Engineering Chemistry Research*, *52*(51), 18386–18391. https://doi.org/10.1021/ie4032567

161. Ogale, A., Lin, C., Anderson, D. P., & Kearns, K. M. (2002). Orientation and dimensional changes in mesophase pitch-based carbon fibers. *Carbon*, *40*, 1309–1319. https://doi.org/10.1016/S0008-6223(01)00300-1

162. Okabe, T., Saito, K., & Hokkirigawa, K. (1996). *New Porous Carbon Materials , Woodeeramics : Development and Fundamental Properties IL-. 213*, 207–213.

163. Otowa, T., Nojima, Y., & Miyazaki, T. (1997). Development of KOH activated high surface area carbon and its application to drinking water purification. *Carbon*, *35*(9), 1315–1319.

164. Ozbay, N., & Yargic, A. S. (2019). Carbon foam production from bio-based polyols of liquefied spruce tree sawdust: Effects of biomass/solvent mass ratio and pyrolytic oil addition. *Journal of Applied Polymer Science*, *136*(11), 47185. https://doi.org/10.1002/app.47185

165. Ozdemir, I., Şahin, M., Orhan, R., & Erdem, M. (2014). Preparation and characterization of activated carbon from grape stalk by zinc chloride activation. *Fuel Processing Technology, 125,* 200–206.

166. Park, H., Seo, J., Kim, M., Baeck, S.-H., & Shim, S. E. (2015). Development of a carbon foam supercapacitor electrode from resorcinol–formaldehyde using a double templating method. *Synthetic Metals*, *199*, 121–127. https://doi.org/https://doi.org/10.1016/j.synthmet.2014.11.008

167. Patle, V. K., Kumar, R., Sharma, A., Dwivedi, N., Muchhala, D., Chaudhary, A., Mehta, Y., Mondal, D. P., & Srivastava, A. K. (2020). Three dimension phenolic resin derived carbon-CNTs hybrid foam for fire retardant and effective electromagnetic interference shielding. *Composites Part C: Open Access*, *2*, 100020.

168. Peng, X., li, Z., Zi-Bing, Z., & Xiang, X. (2010). The morphology and mechanism of formation of SiC in C/C-SiC composites fabricated by liquid silicon infiltration. *Journal of Ceramic Processing Research*, *11*.

169. Pham, T. H., Jung, S. H., Kim, Y. J., & Kim, T. (2021). Adsorptive removal and recovery of organic pollutants from wastewater using waste paper-derived carbon-based aerogel. *Chemosphere*, *268*, 129319. https://doi.org/https://doi.org/10.1016/j.chemosphere.2020.129319

170. Pierson, H. O. (1993). *Handbook of Carbon, Graphite, Diamond, and Fullerenes: Properties, Processing, and Applications*. Noyes Publications.

171. Pierson, H. O. (2012). *Handbook of Carbon, Graphite, Diamonds and Fullerenes: Processing, Properties and Applications*. Elsevier Science.

172. Prabhakaran, K., Singh, P. K., Gokhale, N. M., & Sharma, S. C. (2007). Processing of sucrose to low density carbon foams. *Journal of Materials Science*, *42*(11), 3894–3900. https://doi.org/10.1007/s10853-006-0481-1

173. Prasetyo, I., Rochmadi, R., Wahyono, E., & Ariyanto, T. (2017). Controlling Synthesis of Polymer-Derived Carbon Molecular Sieve and Its Performance for CO_2/CH_4 Separation. *Engineering Journal*, *21*, 83–94.

174. Ptáček, P., Opravil, T., Šoukal, F., Havlica, J., & Holešinský, R. (2013). Kinetics and mechanism of formation of gehlenite, Al–Si spinel and anorthite from the mixture of kaolinite and calcite. *Solid State Sciences*, *26*, 53–58.

https://doi.org/https://doi.org/10.1016/j.solidstatesciences.2013.09.014

175. Pujar, V. V, & Cawley, J. D. (1995). Effect of Stacking Faults on the X-ray Diffraction Profiles of β-SiC Powders. *Journal of the American Ceramic Society*, *78*(3), 774–782. https://doi.org/https://doi.org/10.1111/j.1151-2916.1995.tb08246.x

176. Qi, F., Wang, L., Zhang, Y., Ma, Z., Qiu, H., & Gu, J. (2021). Robust $Ti_3C_2T_x$ MXene/starch derived carbon foam composites for superior EMI shielding and thermal insulation. *Materials Today Physics*, *21*, 100512. https://doi.org/https://doi.org/10.1016/j.mtphys.2021.100512

177. Qiu, R., Fei, R., Zhang, T., Liu, X., Jin, J., Fan, H., Wang, R., He, B., Gong, Y., & Wang, H. (2020). Biomass-derived, 3D interconnected N-doped carbon foam as a host matrix for Li/Na/K-selenium batteries. *Electrochimica Acta*, *356*, 136832.

178. Qu, J., Han, Q., Gao, F., & Qiu, J. (2017). Carbon foams produced from lignin-phenol-formaldehyde resin for oil / water separation. *New Carbon Materials*, *32*(1), 86–91. https://doi.org/10.1016/S1872-5805(17)60109-4

179. Rahman, I. A., & Riley, F. L. (1989). The control of morphology in silicon nitride powder prepared from rice husk. *Journal of the European Ceramic Society*, *5*(1), 11–22. https://doi.org/https://doi.org/10.1016/0955-2219(89)90004-6

180. Rahman, M. M., Adil, M., Yusof, A. M., Kamaruzzaman, Y. B., & Ansary, R. H. (2014). *Removal of Heavy Metal Ions with Acid Activated Carbons Derived from Oil Palm and Coconut Shells*. *Ii*, 3634–3650. https://doi.org/10.3390/ma7053634

181. Rajaram, N., Vijayan, S., & Prabhakaran, K. (2015). Carbon-carbon composite foams with high specific strength from sucrose and milled carbon fiber. *Materials Letters*, *144*. https://doi.org/10.1016/j.matlet.2015.01.016

182. Ramirez-Rico, J., Gutierrez-Pardo, A., Martinez-Fernandez, J., Popov, V. V, & Orlova, T. S. (2016). Thermal conductivity of Fe graphitized wood derived carbon. *Materials & Design*, *99*, 528–534. https://doi.org/https://doi.org/10.1016/j.matdes.2016.03.070

183. Rao, G.-S., Nabipour, H., Zhang, P., Wang, X., Xing, W., Song, L., & Hu, Y. (2020). Lightweight, hydrophobic and recyclable carbon foam derived from lignin–resorcinol–glyoxal resin for oil and solvent spill capture. *Journal of Materials Research and Technology*, *9*(3), 4655–4664. https://doi.org/https://doi.org/10.1016/j.jmrt.2020.02.092

184. Ren, G., Li, S., Fan, Z. X., Warzywoda, J., & Fan, Z. (2016). Soybean-derived hierarchical porous carbon with large sulfur loading and sulfur content for high-performance lithium-sulfur batteries. *Journal of Materials Chemistry A*, *4*(42), 16507–16515. https://doi.org/10.1039/c6ta07446d

185. *retculated carbon foam* -https://www.bing.com/images

186. Rios, R. V. R. A., Martínez-Escandell, M., Molina-Sabio, M., & Rodríguez-Reinoso, F. (2006). Carbon foam prepared by pyrolysis of olive stones under steam. *Carbon*, *44*(8), 1448–1454.

187. Rodríguez-García, J., Cameán, I., Ramos, A., Rodríguez, E., & García, A. B. (2018). Graphitic carbon foams as anodes for sodium-ion batteries in glyme-based electrolytes. *Electrochimica Acta*, *270*, 236–244. https://doi.org/https://doi.org/10.1016/j.electacta.2018.03.084

188. Sadighi, M., & Salami, S. (2012). An investigation on low-velocity impact response of elastomeric & crushable foams. *Central European Journal of Engineering*, *2*. https://doi.org/10.2478/s13531-012-0026-0

189. Sahin, H. T., & Arslan, M. B. (2008). A study on physical and chemical properties of cellulose paper immersed in various solvent mixtures. *International Journal of Molecular Sciences*, *9*(1), 78–88. https://doi.org/10.3390/ijms9010078

190. Sankaran, S., Deshmukh, K., Ahamed, M. B., & Khadheer Pasha, S. K. (2018). Recent advances in electromagnetic interference shielding properties of metal and carbon filler reinforced flexible polymer composites: A review. *Composites Part A: Applied Science and Manufacturing*, *114*, 49–71.

191. Sarathchandran, C., & Ilangovan, S. A. (2021). Chapter 18 - Carbon aerogels: Synthesis, properties, and applications. In S. Thomas, C. Sarathchandran, S. A. Ilangovan, & J. C. B. T.-H. of C.-B. N. Moreno-Piraján (Eds.), *Micro and Nano Technologies* (pp. 739–781). Elsevier. https://doi.org/https://doi.org/10.1016/B978-0-12-821996-6.00002-6

192. Sartova, K., Omurzak, E., Kambarova, G., Dzhumaev, I., Borkoev, B., & Abdullaeva, Z. (2019). Activated carbon obtained from the cotton processing wastes. *Diamond and Related Materials*, *91*(October 2018), 90–97. https://doi.org/10.1016/j.diamond.2018.11.011

193. Scheffler, M., & Colombo, P. (2006). *Cellular Ceramics: Structure, Manufacturing, Properties and Applications*. Wiley.

194. Schulte-Fischedick, J., Zern, A., Mayer, J., Rühle, M., Frieß, M., Krenkel, W., & Kochendörfer, R. (2002). The morphology of silicon carbide in C/C–SiC composites. *Materials Science and Engineering: A*, *332*(1), 146–152. https://doi.org/https://doi.org/10.1016/S0921-5093(01)01719-1

195. Seantier, B., Bendahou, D., Bendahou, A., Grohens, Y., & Kaddami, H. (2016). Multi-scale cellulose based new bio-aerogel composites with thermal super-insulating and tunable mechanical properties. *Carbohydrate Polymers*, *138*, 335–348.

196. Sembiring, S., Simanjuntak, W., Situmeang, R., Riyanto, A., & Sebayang,

K. (2016). Preparation of refractory cordierite using amorphous rice husk silica for thermal insulation purposes. *Ceramics International*, *42*(7), 8431–8437. https://doi.org/https://doi.org/10.1016/j.ceramint.2016.02.062

197. Seo, J., Park, H., Shin, K., Baeck, S. H., Rhym, Y., & Shim, S. E. (2014a). Lignin-derived macroporous carbon foams prepared by using poly(methyl methacrylate) particles as the template. *Carbon*, *76*, 357–367. https://doi.org/https://doi.org/10.1016/j.carbon.2014.04.087

198. Seo, J., Park, H., Shin, K., Baeck, S. H., Rhym, Y., & Shim, S. E. (2014b). Lignin-derived macroporous carbon foams prepared by using poly(methyl methacrylate) particles as the template. *Carbon*, *76*, 357–367. https://doi.org/https://doi.org/10.1016/j.carbon.2014.04.087

199. Seo, J., Park, H., Shin, K., Hyeon, S., Rhym, Y., & Eun, S. (2014). *Lignin derived macroporous carbon foams prepared by using poly (methyl methacrylate) particles as the template* (Vol. 6).

200. Serp, P. (2013). *7.13 - Carbon* (J. Reedijk & K. B. T.-C. I. C. I. I. (Second E. Poeppelmeier (Eds.); pp. 323–369). Elsevier.

201. Sethuramalingam, V. C., Prabagaran, S., & Ganesan, K. (2021). Studies on influence of silica filler and rice husk ash on the mechanical properties of vulcanized hybrid rubber composite. *Materials Today: Proceedings*, *37*, 2207–2213.

202. Sevilla, M., & Fuertes, A. B. (2011). Sustainable porous carbons with a superior performance for CO2 capture. *Energy Environ. Sci.*, *4*, 1765.

203. Sharma, A., Kumar, R., Patle, V. K., Dhawan, R., Abhash, A., Dwivedi, N., Mondal, D. P., & Srivastava, A. K. (2020). Phenol formaldehyde resin derived carbon-MCMB composite foams for electromagnetic interference shielding and thermal management applications. *Composites Communications*, *22*, 100433.

204. Shen, F., Luo, W., Dai, J., Yao, Y., Zhu, M., Hitz, E., Tang, Y., Chen, Y., Sprenkle, V. L., Li, X., & Hu, L. (2016). Ultra-Thick, Low-Tortuosity, and Mesoporous Wood Carbon Anode for High-Performance Sodium-Ion Batteries. *Advanced Energy Materials*, *6*(14), 1600377.

205. Shen, Z., Kwon, S., Lee, H. L., Toivakka, M., & Oh, K. (2021). Cellulose nanofibril/carbon nanotube composite foam-stabilized paraffin phase change material for thermal energy storage and conversion. *Carbohydrate Polymers*, *273*, 118585.

206. Sheng, N., Nomura, T., Zhu, C., Habazaki, H., & Akiyama, T. (2019). Cotton-derived carbon sponge as support for form-stabilized composite phase change materials with enhanced thermal conductivity. *Solar Energy Materials and Solar Cells*, *192*, 8–15.

207. Shi, H.-G., Wang, T., Cheng, J.-B., Zhao, H.-B., Li, S.-L., & Wang, Y.-Z. (2021). Ultralow-density carbon foam composites with bean-like Co-embedded carbon nanotube whiskers towards high-performance microwave absorption. *Journal of Alloys and Compounds*, *863*, 158090.

208. Shi, K., Huang, X., Sun, B., Wu, Z., He, J., & Jiang, P. (2019). Cellulose/BaTiO3 aerogel paper based flexible piezoelectric nanogenerators and the electric coupling with triboelectricity. *Nano Energy*, *57*, 450–458.

209. Singh, B. (2018). 13 - Rice husk ash. In R. Siddique & P. B. T.-W. and S. C. M. in C. Cachim (Eds.), *Woodhead Publishing Series in Civil and Structural Engineering* (pp. 417–460). Woodhead Publishing. https://doi.org/https://doi.org/10.1016/B978-0-08-102156-9.00013-4

210. Sivadas, D. L., Narasimman, R., Rajeev, R., Prabhakaran, K., & Ninan, K. N. (2015). Solvothermal synthesis of microporous superhydrophobic carbon with tunable morphology from natural cotton for carbon dioxide and organic solvent removal applications. *Journal of Materials Chemistry A*, *3*(31), 16213–16221. https://doi.org/10.1039/c5ta01874a

211. Sobrosa, F. Z., Stochero, N. P., Marangon, E., & Tier, M. D. (2017). Development of refractory ceramics from residual silica derived from rice husk ash. *Ceramics International*, *43*(9), 7142–7146.

212. Sompech, S., Dasri, T., & Thaomola, S. (2016). Preparation and characterization of amorphous silica and calcium oxide from agricultural wastes. *Orient J Chem*, *32*(4), 1923–1928.

213. Stiller, A. H., Plucinski, J., & Yocum, A. (2005). *Method of making a carbon foam material and resultant product*. UNIV WEST VIRGINIA OP

- US 64886000 A. https://lens.org/058-390-220-065-465

214. Su, F., Zeng, J., Yu, Y., Lv, L., Lee, J. Y., & Zhao, X. S. (2005). Template synthesis of microporous carbon for direct methanol fuel cell application. *Carbon*, *43*(11), 2366–2373.

215. Sundqvist, B. (2021). Carbon under pressure. *Physics Reports*. https://doi.org/10.1016/j.physrep.2020.12.007

216. Swarnalakshmi, K. S., Chinnaiyan, P., Nivetha, S., & Nair, A. S. (2018). Use of rice husk ash as an adsorbent to remove contaminants in water and comparison with advanced oxidation process – a study. *Materials Today: Proceedings*, *5*(11, Part 3), 24248–24257.

217. Szczurek, A., Fierro, V., Pizzi, A., Celzard, A., Lorraine, D., & Se, P. (2014). Emulsion-templated porous carbon monoliths derived from tannins. *Carbon*, *74*, 352–362. https://doi.org/10.1016/j.carbon.2014.03.047

218. Szczurek, A., Martinez de Yuso, A., Fierro, V., Pizzi, A., & Celzard, A. (2015). Tannin-based monoliths from emulsion-templating. *Materials & Design*, *79*, 115–126.

219. Tang, Y., Li, D., Ao, D., Li, S., & Zu, X. (2018). Ultralight, highly flexible and conductive carbon foams for high performance electromagnetic shielding application. *Journal of Materials Science: Materials in Electronics*, *29*(16), 13643–13652. https://doi.org/10.1007/s10854-018-9493-2

220. Teboho, M., Mochane, M., Sefadi, J., & Motloung, S. (2018). *"Thermal conductivity of graphite-based polymer composites* (pp. 181–197).

221. Thommes, M., & Cychosz, K. A. (2014). Physical adsorption characterization of nanoporous materials: progress and challenges. *Adsorption*, *20*(2), 233–250. https://doi.org/10.1007/s10450-014-9606-z

222. Tian, D., Xu, Z., Zhang, D., Chen, W., Cai, J., Deng, H., Sun, Z., & Zhou, Y. (2019). Micro–mesoporous carbon from cotton waste activated by FeCl3/ZnCl2: Preparation, optimization, characterization and adsorption of methylene blue and eriochrome black T. *Journal of Solid State Chemistry*, *269*(August 2018), 580–587. https://doi.org/10.1016/j.jssc.2018.10.035

223. Tjandra, R., Liu, W., Lim, L., & Yu, A. (2018). Melamine based, n-doped carbon/reduced graphene oxide composite foam for Li-ion Hybrid Supercapacitors. *Carbon*, *129*, 152–158.

224. Tondi, G., Fierro, V., Pizzi, A., & Celzard, A. (2009). Tannin-based carbon foams. *Carbon*, *47*(6), 1480–1492.

225. Tursi, A. (2019). A review on biomass: importance, chemistry, classification, and conversion. *Biofuel Research Journal*, *6*(2), 962–979. https://doi.org/10.18331/BRJ2019.6.2.3

226. Vazhayal, L., Wilson, P., & Prabhakaran, K. (2019). Waste to Wealth: Lightweight, Mechanically Strong and Conductive Carbon Aerogels from Waste Tissue Paper for Electromagnetic Shielding and CO2 Adsorption. *Chemical Engineering Journal*, *381*, 122628.

227. Vazquez-Samperio, J., Acevedo-Peña, P., Guzmán-Vargas, A., Reguera, E., & Córdoba-Tuta, E. (2020). Sucrose-based reticulated vitreous carbon foams and their modification with nickel hexacyanoferrate for energy storage applications. *Diamond and Related Materials*, *109*, 108084. https://doi.org/10.1016/j.diamond.2020.108084

228. Vyas, S. N., patwardhan, S. R., & gangadhar, B. (1992). Carbon molecular sieves from bituminous coal by controlled coke deposition. *Carbon*, *30*(4), 605–612. https://doi.org/10.1016/0008-6223(92)90179-Z

229. Wang, B., R, K., Lu, X.-Y., Xuan, J., & Leung, M. K. H. (2013). Hollow Carbon Fibers Derived from Natural Cotton as Effective Sorbents for Oil Spill Cleanup. *Industrial & Engineering Chemistry Research*, *52*, 18251–18261. https://doi.org/10.1021/ie402371n

230. Wang, C., Li, Y., He, X., Ding, Y., Peng, Q., Zhao, W., Shi, E., Wu, S., & Cao, A. (2015). Cotton-derived bulk and fiber aerogels grafted with nitrogen-doped graphene. *Nanoscale*, *7*(17), 7550–7558.

231. Wang, H., Shao, Y., Mei, S., Lu, Y., Zhang, M., Sun, J., Matyjaszewski, K., Antonietti, M., & Yuan, J. (2020). Polymer-Derived Heteroatom-Doped Porous Carbon Materials. *Chemical Reviews*, *120*(17), 9363–9419.

232. Wang, K., Xu, M., Wang, X., Gu, Z., Fan, Q. H., Gibbons, W., & Croat, J. (2017). Porous carbon derived from aniline-modified fungus for symmetrical supercapacitor electrodes. *RSC Adv.*, *7*(14), 8236–8240.

https://doi.org/10.1039/C6RA27600H

233. Wang, L., Shi, X., Zhang, J., Zhang, Y., & Gu, J. (2020). Lightweight and robust rGO/sugarcane derived hybrid carbon foams with outstanding EMI shielding performance. *Journal of Materials Science and Technology*, *52*. https://doi.org/10.1016/j.jmst.2020.03.029

234. Wang, R., Li, W., & Liu, S. (2012). A porous carbon foam prepared from liquefied birch sawdust. *Journal of Materials Science*, *47*(4), 1977–1984. https://doi.org/10.1007/s10853-011-5993-7

235. Wang, T., Tan, S., & Liang, C. (2009). Preparation and characterization of activated carbon from wood via microwave-induced $ZnCl_2$ activation. *Carbon*, *47*(7), 1880–1883.

236. Wang, X., Zhong, J., Wang, Y., & Yu, M. (2006). A study of the properties of carbon foam reinforced by clay. *Carbon*, *44*(8), 1560–1564. https://doi.org/10.1016/j.carbon.2005.12.025

237. Wang, Y., Liu, Y., Lin, Q., Dong, S., & Xiong, L. (2017). Preparation and properties of montmorillonite/carbon foam nanocomposites. *Applied Clay Science*, *140*, 31–37.

238. Wei, Q., Qin, F., Ma, Q., & Shen, W. (2019). Coal tar- and residual oil-derived porous carbon as metal-free catalyst for nitroarene reduction to aminoarene. *Carbon*, *141*, 542–552.

239. Wei, Y., Liu, H., Liu, S., Zhang, M., Shi, Y., Zhang, J., Zhang, L., & Gong, C. (2018). Waste cotton-derived magnetic porous carbon for high-efficiency microwave absorption. *Composites Communications*, *9*, 70–75. https://doi.org/https://doi.org/10.1016/j.coco.2018.06.007

240. White, R. J., Antonietti, M., & Titirici, M.-M. (2009). Naturally inspired nitrogen doped porous carbon. *Journal of Materials Chemistry*, *19*(45), 8645–8650. https://doi.org/10.1039/B911528E

241. White, R. J., Budarin, V., Luque, R., Clark, J. H., & Macquarrie, D. J. (2009). Tuneable porous carbonaceous materials from renewable resources. *Chemical Society Reviews*, *38*(12), 3401–3418.

242. Wiener, M., Reichenauer, G., Braxmeier, S., Hemberger, F., & Ebert, H.-P. (2009). Carbon Aerogel-Based High-Temperature Thermal Insulation.

International Journal of Thermophysics, *30*, 1372–1385.

243. Wilson, P., Vijayan, S., & Prabhakaran, K. (2017). Carbon foams with a triplex pore structure by compression molding of molten sucrose–NaCl powder pastes. *Carbon*, *118*, 545–555.

244. Wilson, P., Vijayan, S., & Prabhakaran, K. (2018a). Low-density microcellular carbon foams from sucrose by NaCl particle templating using glycerol as a plasticizing additive. *Materials & Design*, *139*, 25–35.https://doi.org/10.1016/j.matdes.2017.10.063

245. Wilson, P., Vijayan, S., & Prabhakaran, K. (2018b). Waste-Fish-Derived Nitrogen Self-Doped Microporous Carbon as Effective Sorbent for CO2 Capture. *ChemistrySelect*, *3*(33), 9555–9563.

246. Wilson, P., Vijayan, S., & Prabhakaran, K. (2019). Thermally Conducting Microcellular Carbon Foams as a Superior Host for Wax-Based Phase Change Materials. *Advanced Engineering Materials*, *21*(4), 1801139.https://doi.org/10.1002/adem.201801139

247. Worsley, M., & Baumann, T. (2016). *Carbon Aerogels*. https://doi.org/10.1007/978-3-319-19454-7_90-1

248. Wu, C., Yang, S., Cai, J., Zhang, Q., Zhu, Y., & Zhang, K. (2016). Activated Microporous Carbon Derived from Almond Shells for High Energy Density Asymmetric Supercapacitors. *ACS Applied Materials and Interfaces*, *8*(24), 15288–15296. https://doi.org/10.1021/acsami.6b02942

249. Wu, W., Du, J., Lin, Y., Chow, L., Bostanci, H., Saarloos, B., & Rini, D. (2011). Evaluation of Compact and Effective Air-Cooled Carbon Foam Heat Sink. *Journal of Heat Transfer*, *133*, 54504.

250. Wu, X., Liu, Y., Fang, M., Mei, L., & Luo, B. (2011). Preparation and characterization of carbon foams derived from aluminosilicate and phenolic resin. *Carbon*, *49*(5), 1782–1786.

251. *www. cfoam/thermalprotection.jpg*. (n.d.). http://www.cfoam.com/wp-content/uploads/thermalprotection.jpg

252. http://www.cfoam.com/wp-content/uploads/tps2.jpg

253. http://www.cfoam.com/wp-content/uploads/emi3.jpg

254. Xiang, M., Wang, Y., Wu, J., Guo, Y., Wu, H., Zhang, Y., & Liu, H.

(2017). Natural Silk Cocoon Derived Nitrogen-doped Porous Carbon Nanosheets for High Performance Lithium-Sulfur Batteries. *Electrochimica Acta*, *227*, 7–16.

255. Xiang, M., Wu, H., Liu, H., Huang, J., Zheng, Y., Yang, L., Jing, P., Zhang, Y., Dou, S., & Liu, H. (2017). A Flexible 3D Multifunctional MgO-Decorated Carbon Foam@CNTs Hybrid as Self-Supported Cathode for High-Performance Lithium-Sulfur Batteries. *Advanced Functional Materials*, *27*(37), 1702573.

256. Xiao, P. W., Meng, Q., Zhao, L., Li, J. J., Wei, Z., & Han, B. H. (2017). Biomass-derived flexible porous carbon materials and their applications in supercapacitor and gas adsorption. *Materials and Design*, *129*(May), 164–172. https://doi.org/10.1016/j.matdes.2017.05.035

257. Xin, W., & Song, Y. (2015). Mesoporous carbons: recent advances in synthesis and typical applications. *RSC Advances*, *5*(101), 83239–83285. https://doi.org/10.1039/C5RA16864C

258. Xue, G., Liu, K., Chen, Q., Yang, P., Li, J., Ding, T., Duan, J., Qi, B., & Zhou, J. (2017). Robust and Low-Cost Flame-Treated Wood for High-Performance Solar Steam Generation. *ACS Applied Materials & Interfaces*, *9*(17), 15052–15057. https://doi.org/10.1021/acsami.7b01992

259. Yam, R. C. M., & Mak, D. M. T. (2014). A cleaner production of rice husk-blended polypropylene eco-composite by gas-assisted injection moulding. *Journal of Cleaner Production*, *67*, 277–284. https://doi.org/10.1016/j.jclepro.2013.12.038

260. Yargic, A. S., & Ozbay, N. (2019). Effect of chemical activation on the cellular structure of biopitch-derived green carbon foam. *Diamond and Related Materials*, *96*, 58–66.

261. Ye, X., Chen, Z., Ai, S., Hou, B., Zhang, J., Zhou, Q., Liu, H., & Cui, S. (2019). Effect of pyrolysis temperature on compression and thermal properties of melamine-derived carbon foam. *Journal of Analytical and Applied Pyrolysis*, *142*. https://doi.org/10.1016/j.jaap.2019.05.008

262. Yi, G.-R., Moon, J. H., & Yang, S.-M. (2001). Ordered Macroporous Particles by Colloidal Templating. *Chemistry of Materials*, *13*(8), 2613–

2618. https://doi.org/10.1021/cm0102584

263. Yin, P., Zhang, L., Wang, J., Feng, X., Dai, J., & Tang, Y. (2021). Facile preparation of cotton-derived carbon fibers loaded with hollow Fe_3O_4 and CoFe NPs for significant low-frequency electromagnetic absorption. *Powder Technology, 380*, 134–142.

264. Yu, L., Feng, Z., Fan, Z., Kong, Q., & Xu, L. (2014). *The preparation and properties of novel structural carbon foams derived from different mesophase pitches*.

265. Yuan, W., Wang, B., Wu, H., Xiang, M., Wang, Q., Liu, H., Zhang, Y., Liu, H., & Dou, S. (2018). A flexible 3D nitrogen-doped carbon foam@CNTs hybrid hosting TiO2 nanoparticles as free-standing electrode for ultra-long cycling lithium-ion batteries. *Journal of Power Sources, 379,* 10–19.

266. Yuan, Y., Ding, Y., Wang, C., Xu, F., Lin, Z., Qin, Y., Li, Y., Yang, M., He, X., Peng, Q., & Li, Y. (2016a). Multifunctional Stiff Carbon Foam Derived from Bread. *ACS Applied Materials and Interfaces, 8*(26), 16852–16861. https://doi.org/10.1021/acsami.6b03985

267. Yuan, Y., Sun, X., Yang, M., Xu, F., Lin, Z., Zhao, X., Ding, Y., Li, J., Yin, W., Peng, Q., He, X., & Li, Y. (2017). Stiff, Thermally Stable and Highly Anisotropic Wood-Derived Carbon Composite Monoliths for Electromagnetic Interference Shielding. *ACS Applied Materials & Interfaces,9*(25), 21371–21381. https://doi.org/10.1021/acsami.7b04523

268. Yue, L., Xia, Q., Wang, L., Wang, L., DaCosta, H., Yang, J., & Hu, X. (2018). CO2 adsorption at nitrogen-doped carbons prepared by K_2CO_3 activation of urea-modified coconut shell. *Journal of Colloid and Interface Science*, *511*, 259–267. https://doi.org/10.1016/j.jcis.2017.09.040

269. Zakhidov AnvarA., H., B. R., Zafar, I., Changxing, C., Ilyas, K., O., D. S., Jordi, M., & G., R. V. (1998). Carbon Structures with Three-Dimensional Periodicity at Optical Wavelengths. *Science, 282*(5390), 897–901.

270. Zareei, S. A., Ameri, F., Dorostkar, F., & Ahmadi, M. (2017). Rice husk ash as a partial replacement of cement in high strength concrete containing micro silica: Evaluating durability and mechanical properties. *Case Studies* *in Construction Materials*, *7*, 73–81.

271. Zeng, Y., Luo, X., Yu, K., & Qian, K. (2019). EMI shielding performance of phenolic-based carbon foam modified with GO/SiO2 hybrid nanomaterials. *Chemical Physics Letters*, *715*, 166–172.

272. Zeng, Z., Zhang, Y., Ma, X. Y. D., Shahabadi, S. I. S., Che, B., Wang, P., & Lu, X. (2018). Biomass-based honeycomb-like architectures for preparation of robust carbon foams with high electromagnetic interference shielding performance. *Carbon*, *140*, 227–236.

273. Zhang, B., Xiao, M., Wang, S., Han, D., Song, S., Chen, G., & Meng, Y. (2014). Novel hierarchically porous carbon materials obtained from natural biopolymer as host matrixes for lithium-sulfur battery applications. *ACS Applied Materials and Interfaces*, *6*(15), 13174–13182.

274. Zhang, Jinhua, Qu, S., Li, L., Wang, P., Li, X., Che, Y., & Li, X. (2018). Preparation of Carbon Molecular Sieves Used for CH4/N2 Separation. *Journal of Chemical & Engineering Data*, *63*(5), 1737–1744. https://doi.org/10.1021/acs.jced.8b00048

275. Zhang, Junping, Li, B., Li, L., & Wang, A. (2016). Ultralight, compressible and multifunctional carbon aerogels based on natural tubular cellulose. *Journal of Materials Chemistry A*, *4*(6), 2069–2074. https://doi.org/10.1039/C5TA10001A

276. Zhang, K., Li, Y., Chen, T., Lin, Q., & Huang, X. (2016). Preparation and properties of graphene nanosheets/carbon foam composites. *Journal of Analytical and Applied Pyrolysis*, *117*, 290–295.

277. Zhang, L., Liu, M., Roy, S., Chu, E. K., See, K. Y., & Hu, X. (2016). Phthalonitrile-Based Carbon Foam with High Specific Mechanical Strength and Superior Electromagnetic Interference Shielding Performance. *ACS Applied Materials & Interfaces*, *8*(11), 7422–7430.

278. Zhang, X., Li, W., & Lu, A. (2015). Designed porous carbon materials for efficient CO_2 adsorption and separation. *New Carbon Materials*, *30*(6), 481–501. https://doi.org/10.1016/S1872-5805(15)60203-7

279. Zhang, Youfang, Zuo, L., Zhang, L., Huang, Y., Lu, H., Fan, W., & Liu, T. (2016). Cotton Wool Derived Carbon Fiber Aerogel Supported Few-

Layered MoSe2 Nanosheets As Efficient Electrocatalysts for Hydrogen Evolution. *ACS Applied Materials & Interfaces*, *8*(11), 7077–7085. https://doi.org/10.1021/acsami.5b12772

280. Zhang, Yuhang, Sun, J., Tan, J., Ma, C., Luo, S., Li, W., & Liu, S. (2021). Hierarchical porous graphene oxide/carbon foam nanocomposites derived from larch for enhanced CO_2 capture and energy storage performance. *Journal of CO_2 Utilization*, *52*, 101666.

281. Zheng, Y., Song, Y., Gao, T., Yan, S., Hu, H., Cao, F., Duan, Y., & Zhang, X. (2020). Lightweight and Hydrophobic Three-Dimensional Wood-Derived Anisotropic Magnetic Porous Carbon for Highly Efficient Electromagnetic Interference Shielding. *ACS Applied Materials & Interfaces*, *12*(36), 40802–40814. https://doi.org/10.1021/acsami.0c11530

282. Zhu, Z. L., Li, M. F., Xia, M. F., Wan, J. N., & Zhang, Q. X. (2008). Preparation and Characterization of Polymer-Based Spherical Activated Carbons. *Chin. J. Polym. Sci.*, *26*, 645.

283. Zhuo, H., Hu, Y., Tong, X., Zhong, L., Peng, X., & Sun, R. (2016). Sustainable hierarchical porous carbon aerogel from cellulose for high-performance supercapacitor and CO2 capture. *Industrial Crops and Products*, *87*, 229–235.

284. Zimmermann, M. V. G., Perondi, D., Lazzari, L. K., Godinho, M., & Zattera, A. J. (2020). Carbon foam production by biomass pyrolysis. *Journal of Porous Materials*, *27*(4), 1119–1125.

LIST OF PUBLICATIONS BASED ON THE THESIS

1. A.Chithra, Praveen Wilson, Sujith Vijayan, R. Rajeev, K. Prabhakaran, Robust thermally insulating carbon-gehlenite composite foams from newspaper waste and sucrose by filter pressin*g*, Materials and Design 160 (2018) 65–73.
2. A. Chithra, Praveen Wilson, Sujith Vijayan, R. Rajeev, K. Prabhakaran, Carbon foams with low thermal conductivity and high EMI shielding from sawdust"- Industrial Crops & Products 145 (2020) 112076.
3. A. Chithra, Praveen Wilson, Sujith Vijayan, R. Rajeev, K. Prabhakaran, Thermally insulating robust carbon composite foams with high EMI shielding from natural cotton, Journal of Material Science and Technology 94 (2021) 113-122.
4. Chithra, A., Rajeev, R., & Prabhakaran, K. C/SiO_2 and C/SiC composite foam monoliths from rice husk for thermal insulation and EMI shielding. Carbon Letters, (2021) 1-13.

LIST OF CONFERENCES ATTENDED

1. Presented paper on *Thermally insulating carbon composite foam from newspaper and sucrose* - International Conference on Material Science and Technology (ICMST-2018), Thiruvananthapuram, India
2. Presented paper on *Natural Cotton Derived Carbon composite foam for thermal insulation* National Conference on Material Science and Technology(NCMST-2019), Thiruvananthapuram, India
3. Presented paper on Sawdust Derived *Carbon Foam Composite for Thermal Insulation* at International Conference on Advanced Thermostructural Materials & Thermal Protection Systems (ADTHERM-20), Thiruvananthapuram, India
4. Presented paper on *Rice husk derived C/SiO_2 and C/SiC composite foams for EMI shielding and thermal insulations* National Conference on Material Science and Technology(NCMST-2021), Thiruvananthapuram, India Thiruvananthapuram, India